

Submit all experiment reports to:
LANSCE User Office, MS H831, Los Alamos National Laboratory, Los Alamos, NM 87545

Experiment was carried out at:	Local Contact	Proposal #	LANSCE Use Only
<input checked="" type="checkbox"/> Manuel Lujan Jr. Neutron Scattering Center	Don W. Brown	2003002	Report Rc'd 1/7/04
<input type="checkbox"/> Weapons Neutron Research Facility	FP/Instrument Used		
<input type="checkbox"/> WNR/Blue Room	SMARTS		

Title: The Development of Intergranular Strains in a Commercial Purity Titanium Alloy Polycrystal Subjected to Compressive Plastic Strains.

Authors and Affiliations

- 1) Kelly T. Conlon, National Research Council of Canada, Chalk River Laboratories, Stn. 18, Chalk River ON. Canada K0J 1J0.
- 2) David Dye, Dept. of Materials, Imperial College London, Exhibition Road, London SW7 2AZ, United Kingdom.

Experiment Report

The elastic response of individual crystallites in a plastically flowing solid is strongly influenced by the intrinsic elastic and plastic anisotropy of the crystal lattice, as deforming polycrystals must satisfy conditions of equilibrium and compatibility. Anisotropy of crystal properties results in the accumulation of elastic microstrains (termed "intergranular" strains) following the onset of yield in metals and alloys owing to local misorientations at grain boundaries. The prediction of magnitude and sign of intergranular strains that develop in common engineering materials following simple deformation experiments represents a powerful new test of advanced computer codes of polycrystalline plasticity.

Slip and twinning are competitive deformation mechanisms in hexagonal metals, a question arises as to whether twinning leads to a pattern of microstrain accumulation in hcp polycrystals that is unique and can be differentiated from the pattern that develops due to slip mechanisms. This question was not clearly resolved in previous experiments conducted on a "near-alpha" titanium alloy IMI-834 as the alpha phase does not appear to twin [1]. A further ambiguity arising from the previous work is the role played by the minority bcc β phase present in IMI-834.

Three twinning mechanisms are available to allow relaxation of strains along the basal pole. Two of the mechanisms (twinning plane {1012} and {1121}) result in extension of the crystal along the "c"-axis and are thus favorable in tension; a third mechanism (twinning plane {1122}) results in contraction along the "c"-axis and is favorable in compression. In-situ tensile testing experiments are currently in progress at Chalk River. We recently undertook experiments on the SMARTS instrument to conduct compression tests on CP titanium to complement the Chalk River experiments. The compression experiments were carried out on cylindrically shaped specimens of nominal dimensions 22 mm long x 10 mm diameter.

Experiment Report (continued)

Some of the results obtained from the SMARTS experiment are shown below in Figure 1. At low plastic strains, significant compressive strains are accumulated in the basal planes at the onset of macroscopic plastic yielding (which is observed to occur at a stress of approximately 400 MPa). Beyond a stress of approximately 475 MPa, the rate of elastic strain accumulation in the basal planes switches sign (i.e. increasingly tensile). This is clear evidence of the activation of a secondary mechanism to relieve stresses in the basal orientation. Texture measurements on the deformed compression specimens appear to confirm twinning on $\{1122\}$ as the operative strain relaxation mechanism.

Work is still in presently in progress at Imperial College London to correlate twinning directly with grain orientation via EBSD. Further work is in progress at Chalk River to compare the microstrains obtained in compression vs. microstrains in tension.

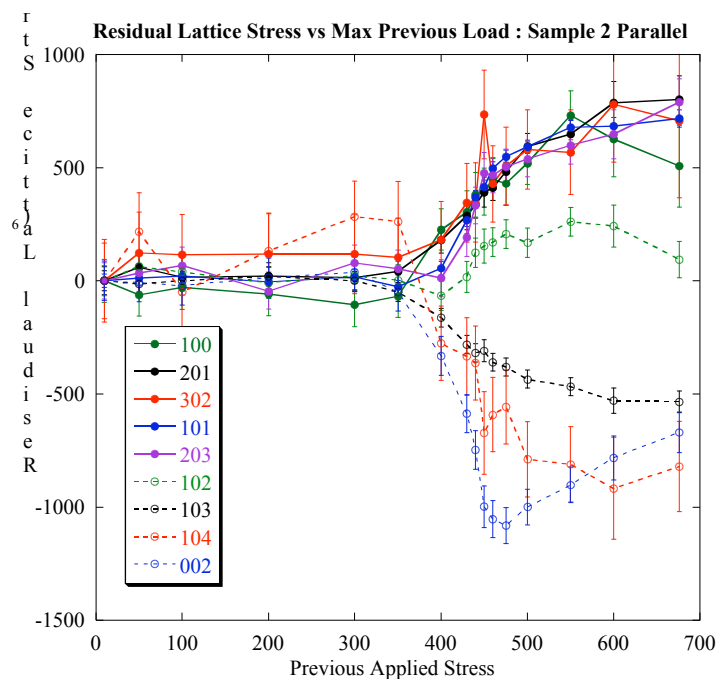


Figure 1. Accumulated microstrains in CP titanium as a function of applied compressive load.

References

J-R. Cho, D. Dye, K.T. Conlon, M.R. Daymond and R.C. Reed (2002), "*Intergranular Strain Accumulation in a Near- α Titanium Alloy During Plastic Deformation*", Acta Mater., 50 (17), pp. 4847-64.

IMPORTANT! List or attach a list of publications resulting from this experiment (published or in press).



REPORT ON EXPERIMENT

(Please Type)

Submit all experiment reports to:
 LANSCE User Office, MS H831, Los Alamos National Laboratory, Los Alamos, NM 87545

Experiment was carried out at:		Local Contact	Proposal #	<i>LANSCE Use Only</i>
<input checked="" type="checkbox"/>	Manuel Lujan Jr. Neutron Scattering Center	Sven C. Vogel	2003009	Report Rc'd 6/3/04
<input type="checkbox"/>	Weapons Neutron Research Facility	FP/Instrument Used		
<input type="checkbox"/>	WNR/Blue Room	FP4 / HIPPO		

Title	Texture Evolution in Ferroelectric Ceramics
Authors and Affiliations	<p>Jacob L. Jones, Thomas S. Key, Sudhanshu Mallick, Elliott B. Slamovich, and Keith J. Bowman Materials Science and Engineering, Purdue University, West Lafayette, Indiana</p> <p>William F. Shelley II. Piezo Technologies, Indianapolis, Indiana</p>

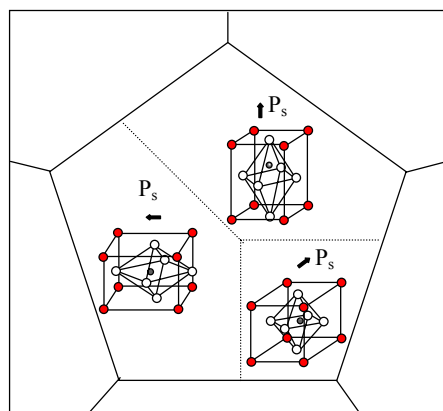
Experiment Report

Ferroelectric ceramics are widely used as sensors and actuators in applications such as sonar, ultrasound, and high-precision positioning and measurement systems. Texture gives rise to the electromechanical response in ferroelectric ceramics because a global spontaneous polarization, apparent from unequal volume fractions of the local polarization domain structures, is preferentially oriented with respect to the driving electric field. Both the polarization domain texture and the crystallographic preferred orientation independently influence the electromechanical response because either can enhance alignment of local polarization vectors. Polarization domain textures can be described using diffraction because the crystallographic axes follow most spontaneous polarization vector reorientations. In contrast, crystallographic preferred orientation is independent of the domain structures, a more classical texture problem. Using the diffractometer HIPPO, this experiment evaluated polarization domain textures induced in tetragonal PZT ($\text{PbZr}_x\text{Ti}_{1-x}\text{O}_3$) ceramics by electrical poling (Fig. 1) and crystallographic preferred orientation induced in templated bismuth titanate ceramics (e.g., $\text{Bi}_4\text{Ti}_3\text{O}_{12}$) by tape casting (Fig. 2). A 4th order spherical harmonics function was used to describe the axisymmetric texture of both ferroelectric structures and the 001 pole figure recalculated from the measured ODF indicates the degree of texture induced by either process.

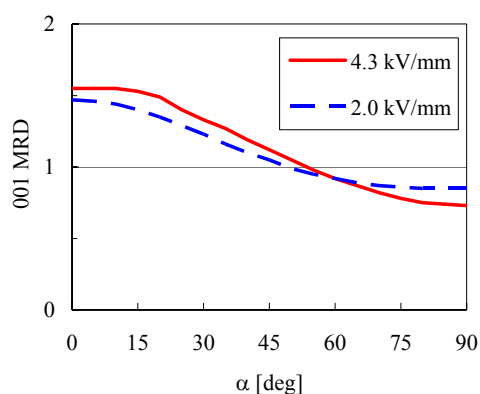
The polarization domain textures (Fig. 1) are limited by crystal symmetry because ferroelectric domains are analogous to crystallographic twinning. These textures, though modest, give rise to the electromechanical response of PZT ceramics. Crystallographic texture in bismuth titanate (Fig. 2) is enhanced through the use of templates, which are anisometrically shaped particles preferentially oriented during tape casting to seed texture evolution. In this experiment, the templates possess a similar structure (Aurivillius oxide) but are unique in a layered ordering sequence from the matrix powder. Texture analysis using HIPPO data permits separation of the textures of these two phases. The texture strength of the matrix phase increases slightly with template but, more importantly, a residual texture is apparent in untemplated ceramics (0% template fraction).

Clearly a complete description of texture in ferroelectric ceramics encompasses both polarization domain texture and crystallographic texture. It was found in bismuth titanate, an ideal candidate for such an analysis, that the polarization domain texture was not measurable using HIPPO because of the very small distortions of the orthorhombic lattice ($a/b \sim 1.0050$). Therefore, the crystallographic texture determined using HIPPO was combined with polarization domain texture measurements from higher resolution synchrotron XRD (performed at beamline X18A, NSLS).

Experiment Report (continued)

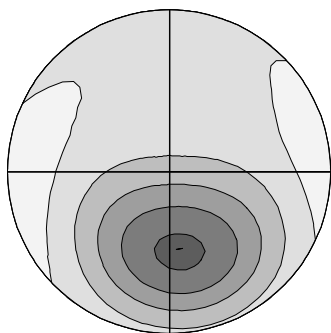


(a.)

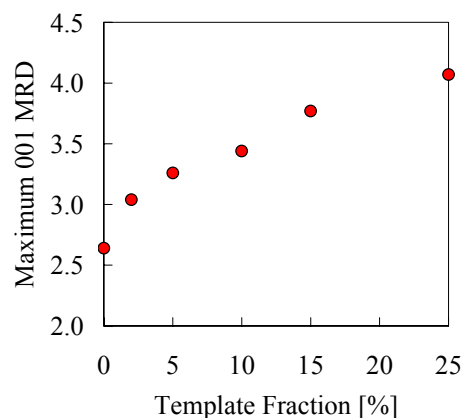


(b.)

Fig. 1. (a.) Idealized schematic of three domains within a single grain showing a random distribution of tetragonal lattice distortions ($c > a$) and polarization vectors. Prior to poling, equal volume fractions of all domains are apparent. (b.) 001 (polarization axis) axial distribution functions of two samples poled using different electric fields. The angle α is to the applied electric field (polar angle).



(a.)



(b.)

Fig. 2. (a.) Recalculated 001 pole figure of untemplated bismuth titanate, shown on an equal area projection in with contour lines spaced at 0.5 MRD intervals and the lowest contour line representing 0.5 MRD. (b.) Maximum 001 pole figure value of the matrix phase as a function of the template phase fraction (vol%).

IMPORTANT! List or attach a list of publications resulting from this experiment (published or in press).

REPORT ON EXPERIMENT (Please Type)

Submit all experiment reports to:

LANSCE User Office, MS H831, Los Alamos National Laboratory, Los Alamos, NM 87545

Experiment was carried out at: Local Contact **Proposal #** *LANSCE Use Only* xManuel Lujan Jr. Neutron Scattering Center Paul Langan **2003016** **Report Rc'd** Weapons Neutron Research Facility **FP/Instrument Used** 6/9/04 WNR/Blue Room PCS

Title

Comparative Hydrogen Position Studies Using X-rays and Neutrons **Authors and Affiliations**

Bryant Leif Hanson, University of Tennessee, Knoxville TN

Amy Katz, Fox Chase Cancer Center, Philadelphia PA

Jenny P. Glusker, Fox Chase Cancer Center, Philadelphia PA

H. L. Carrell, Fox Chase Cancer Center, Philadelphia PA

Gerard J. Bunick, Oak Ridge National Laboratory/ University of Tennessee, Oak Ridge, TN

Experiment Report

The metalloenzyme D-xylose isomerase forms well-ordered crystals that diffract X rays to ultrahigh resolution ($< 1 \text{ \AA}$).

However, structural analysis with X-ray diffraction data has as yet been unable to differentiate between several postulated mechanisms that describe the catalytic activity of this enzyme. Neutrons with their greater scattering sensitivity to hydrogen atoms could help resolve this by determining the protonation states within the active site of the enzyme. Neutron diffraction data were measured to 1.8 \AA from the unliganded protein at the Los Alamos Neutron Science Center Protein Crystallography Station as the first step in the process of investigating the mechanism action of D-xylose isomerase from *S. rubiginosus*. Measurement of these neutron diffraction data represents several milestones: this is one of the largest biological molecules (a tetramer, MW $\sim 160,000$ daltons (Da), with unit-cell lengths around 100 \AA) ever studied at high resolution using neutron diffraction. It is also one of the first proteins to be studied using time-of-flight techniques.

Two data sets have now been collected, one with manganese ions and the most recent with cobalt ions at the active site. The size of the cobalt ion containing xylose isomerase crystal was approximately 4 mm in each dimension. This structure is being fitted and refined. It has been possible to refine the protein backbone and the D/H ratio of the peptide nitrogen atoms. Many of the labile hydrogens have been replaced by deuterium atoms and are observed in serine, tyrosine, tryptophan, lysine, and histidine residues. Many more hundreds of water molecules (DOD) are observed in this data set than in the previous data set. The waters form extensive networks throughout the structure and loops of waters are present along many areas of the backbone. The Rfactor is 23% for strong data as the fitting and refinement continue using the graphics program XtalView and the refinement program Shelx.

The 0.94 \AA resolution X-ray structure of xylose isomerase has been refined to a final Rfactor of 11.6%. This structure will be compared to the neutron structure to differentiate the capabilities of the two methods in revealing the chemistry of the protein structure. Additional neutron studies of the magnesium containing enzyme and of crystals soaked in substrate/ inhibitor analogs are planned in order to elucidate the mechanism xylose isomerase. **List or attach a list of publications resulting from this experiment (published or in press).**

High-Resolution Neutron Diffraction Data Collected on the Protein Crystallography Station at LANSCE Exceed Researchers' Expectations. (2003)

Sweet Success: Protein Crystallography Experiment Points to Emerging Promise of Neutron Analysis. (2003) ORNL Reporter, Oak Ridge National Laboratory, U. S. Department of Energy, Number 47, April, p1.

Neutron Diffraction Overcomes Flux Limits to Resolve a Large Protein Structure. (2003) Physics Today, Search & Discovery, November, p17-19.

Hanson, B. L., Langan, P., Katz, A., Li, X., Harp, J. M., Glusker, J. P., Schoenborn, B. P., and Bunick, G. J. (2004) "Preliminary Time of Flight Neutron Diffraction Study of *S. rubiginosus* D-Xylose Isomerase," Acta Cryst. D60,241-249.

Bunick, G. J., Hanson, B. L., Langan, P., Katz, A., Carrell, H. L., Schoenborn, B. P., and Glusker, J. P. (2004) "Adventures with Neutron Diffraction: Protonation states of D-xylose isomerase." American Crystallographic Association Annual Meeting, July 17-22, Chicago, IL. Abstract P168.

IMPORTANT! List or attach a list of publications resulting from this experiment (published or in press).

REPORT ON EXPERIMENT (Please Type)

Submit all experiment reports to:

LANSCE User Office, MS H831, Los Alamos National Laboratory, Los Alamos, NM 87545

Experiment was carried out at: Local Contact Proposal #LANSCE Use Only X Manuel Lujan Jr. Neutron Scattering Center Sven Vogel
2003024 Report Rc'd Weapons Neutron Research Facility **FP/Instrument Used** 6/9/04 WNR/Blue Room HIPPO
Title: "Investigation of the Magnetization of Wüstite (Fe_{1-x}O) Under High Pressure". Sept. 12-13, 2004.

Authors and Affiliations

J. Xu,¹ Y. Ding,^{1, 2} S.D. Jacobsen,¹ H.K. Mao,¹ R. J. Hemley,¹ J. Zhang,³ J. Qian,³ C. Pantea,³ S.C. Vogel,³ D. J. Williams,³ and Y. Zhao³

¹ Geophysical Laboratory, Carnegie Institution of Washington, 5251 Broad Branch Road, Washington, DC 20015, USA; ² HPCAT, Advanced Photon Source; Argonne National Laboratory, 9700 Cass Ave, Argonne, IL 60439, USA; ³ LANSCE, Los Alamos National Laboratory, Los Alamos, NM 87545, USA.

Experiment Report

High-pressure powder neutron diffraction of wüstite-Fe_{0.93}O has been achieved to 12 GPa using a large gem-moissanite (SiC) anvil cell. The moissanite anvils are weakly absorbing and provide greater neutron fluxes to the sample than is possible with tungsten carbide anvils. There is minimal diffraction overlap from the single-crystal moissanite anvils compared to tungsten carbide or synthetic diamond anvils, providing cleaner background profiles. The required sample volume for high-pressure neutron diffraction is dramatically reduced to several cubic millimeters. High-quality powder diffraction patterns of wüstite were recorded at 90-minute exposure times on the HIPPO diffractometer at LANSCE when the sample volume was in the range of ~10 mm³. This is about two orders of magnitude smaller than the necessary sample volume (~1.0 cm³) for the same kind of experiment with other high-pressure cells and nominal neutron fluxes.

Based on the results we have observed, we have submitted a paper: "Powder neutron diffraction of wüstite (Fe_{0.93}O) to 12 GPa using large moissanite anvils", to High Pressure Research, and it has been accepted, and in pressing.

EXPERIMENTAL DETAILS

The FeO sample was prepared by cold-pressing reagent-grade hematite (Fe₂O₃) into centimeter-sized pellets. The hematite pellets were held for ~24 hours at 1200°C and 10⁻¹¹ atmospheres f_{O₂} in a CO/CO₂ gas-mixing furnace. The formation of magnetite on cooling was avoided by drop-quenching the sample into a separate container with the same gas mixture. The cell parameter of the FeO was measured by X-ray diffraction to be a = 0.4300(2) nm, corresponding to

The gem-moissanite anvil system is used. A Ti/Zr composite gasket measuring initially 3 mm thick and 6 mm in diameter was prepared with a 3 mm diameter hole. The anvil-gasket assembly is fitted with an Al holder for additional support and alignment. Each single-crystal moissanite anvil weighs approximately 30 carats (6 grams). The full diameter is 16 mm, which is coned to reach a full circular culet diameter of 6 mm. In order to help reduce the stresses along the edge of the culets, a 10°-bevel was added such that a smaller culet of ~5 mm is in contact with the sample. This moissanite-anvil system was loaded into the TAP-98 press on the HIPPO beam-line at LANSCE, Los Alamos National Laboratory, USA (Fig 2). The press is capable of producing forces up to ~5 MN. In this feasibility study, we simplified the experiment by not using an internal pressure marker in the sample chamber. The pressure was determined from the d-spacing of the (200) diffraction peak (d_{200}) of FeO. This d_{200} scale was calibrated previously by x-ray diffraction on the same sample, and can be written as a linear relationship, P (GPa) = 2580* (0.21506- d_{200}).

The experimental geometry is similar to that for the Paris-Edinburgh cell. In addition to an initial 8-mm rotating collimator, a hexagonal boron nitride collimator further reduces the incident-beam diameter to about 3 mm before entering the TAP-98 press from the left. The incident thermal neutrons pass into the press and through one of the single-crystal moissanite anvils to the sample along the unique axis of the cell. The diffracted-beam intensities are obtained by integrating the detected intensities from 192 ³He tubes, arranged in 8 panels around the beam direction at a diffraction angle of 90°. Diffracted neutrons collected at a number of other detectors distributed at the 150°, 40°, 20° and 10° panels were not used because they were blocked by the top and bottom parts of the press while in the horizontal position.

RESULTS AND DISCUSSION

Before experiment, the sample volume was ~21 mm³, and the Ti/Zr gasket was 3.0 mm thick. At 12 GPa, the gasket thickness was reduced to ~2 mm, and we calculate the volume of FeO sampled by the 3.0 mm diameter beam to be approximately 14 mm³.

The neutron diffraction patterns collected at 0.1 MPa, 5.2 GPa and 9.7 GPa shown that 90-minute exposure times are OK even though the gasket thickness was only about 1.4 mm (corresponding to about 10 mm³ of FeO sampled by the neutrons). Thus, the necessary sample volume for such powder neutron diffraction experiments can be dramatically reduced with the gem-moissanite anvil cell. We anticipate that with longer exposure times and stronger gasket materials (such as T301 stainless steel) the sample volume in the gem-moissanite cell could be reduced to as little as ~1-5 mm³. The reduced sample volumes could potentially reach pressures as high as ~20 GPa, making accessible many high-pressure phase transitions in materials such as the magnetic phase transition in FeO at around 17 GPa.

In conclusion, the present study demonstrates the potential of the hem-moissanite (SiC) anvil cell for high-pressure neutron diffraction. The technique produces clean background profiles with significantly reduce sample volume for diffraction, as shown by patterns measured for FeO to 12 GPa with sample volumes of ~10mm³. The technique can be extended to higher pressures, including examination of transitions in FeO at higher pressures and variable temperature.

Powder neutron diffraction of wüstite ($\text{Fe}_{0.93}\text{O}$) to 12 GPa using large moissanite anvils,
submitted High Pressure Research,

Submit all experiment reports to:
LANSCE User Office, MS H831, Los Alamos National Laboratory, Los Alamos, NM 87545

Experiment was carried out at:	Local Contact	Proposal #	LANSCE Use Only
<input checked="" type="checkbox"/> Manuel Lujan Jr. Neutron Scattering Center	Jarek Majewski	2003-025	Report Rc'd 7/15/04
<input type="checkbox"/> Weapons Neutron Research Facility	FP/Instrument Used		
<input type="checkbox"/> WNR/Blue Room	FP9 (SPEAR)		

Title Probing Protein Adsorption of Reversible Protein Traps
Authors and Affiliations Bruce C. Bunker, Sandia National Laboratories Dale L. Huber, Sandia National Laboratories Jarek Majewski, Los Alamos National Laboratories

Experiment Report <p>The central focus of this investigation is to determine whether or not the “reversible protein trap” technology developed at Sandia is applicable for creating highly selective surfaces for the capture of specific biological species. The essence of the project is to see if specificity can be achieved by using the protein trap to capture a monolayer of antibodies that can be subsequently used for the highly selective adsorption of whatever bio-species the antibody is designed to target. Our ultimate goal is to integrate the bio-trapping capability into a surface acoustic wave sensor device in which analyte trapping, detection, and release (device regeneration) can be achieved within a single module.</p> <p>Research has involved a range of experiments to study the adsorption and desorption behavior of antibodies and a virus on the protein trap. The experimental approach has involved using ellipsometry as a simple means of detecting the adsorption and desorption of species of interest, but a more sophisticated method for characterizing adsorbed layers involves the use of neutron reflectivity measurements. With neutrons, we can probe the density of adsorbed layers as a function of distance from the substrate surface, which will tell us how species are oriented on the surface (critical for antibody interactions) as well as how much material is present.</p> <p>Ellipsometry Results</p> <p>Initial experiments were done with three species: 1) tobacco mosaic virus (TMV), 2) TMV-IgG (an antibody specific for interacting with IgG), and 3) Rabbit IgG (an antibody that should not exhibit selective binding for TMV). These three species were exposed to control surfaces and surfaces coated with thin films of the active polymer (poly(n-isopropylacrylamide or PNIPAM) used in the protein trap. At 50°C, PNIPAM should be in a collapsed state that adsorbs proteins, while at room temperature, PNIPAM swells to create an anti-fouling surface to which proteins should not stick. Ellipsometry was used to measure the quantities of IgG adsorbed as</p>

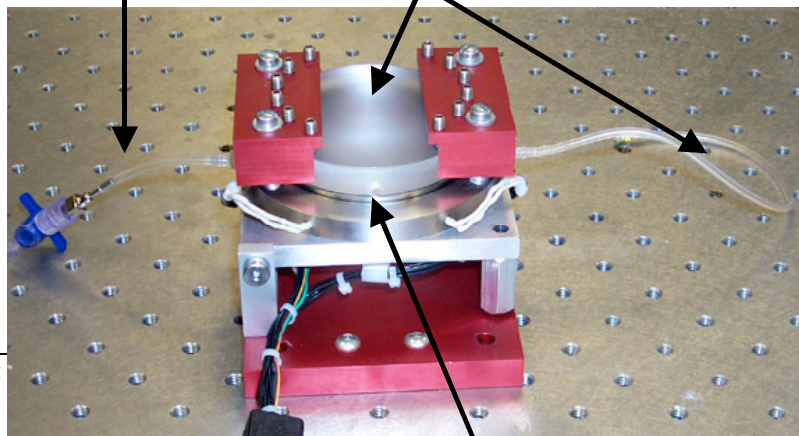
Experiment Report *(continued)*

IgG adsorption was studied on substrates coated with a 4.2 nm thick film of PNIPAM at 50°C. This temperature is well above PNIPAM's transition temperature of 35°C, promoting protein adsorption. Under the same adsorption conditions used for the control, both Rabbit IgG and TMV-IgG are adsorbed by PNIPAM, but the effective thickness of the antibody films is less than that seen on the control (1.2 nm or 30% of a monolayer). The antibody adsorption results are consistent with previous studies performed using simple water-soluble proteins such as myoglobin and albumin which show that proteins tend to have a slightly higher affinity for hydrocarbon SAMs than for PNIPAM. When the PNIPAM film is cooled to room temperature, all of the IgG desorbs as expected, validating that we can achieve completely reversible adsorption of antibodies.

These experiments were performed in preparation for neutron experiments, to make any beam time as efficient as possible. Having prequalified the system to be tested, we were able to prepare four substrates for testing using already established protocols. These protocols were known to create surfaces with excellent adsorption and release properties.

Neutron Experiments

To elucidate the structure of the adsorbed monolayers, we designed and built a cell for performing temperature controlled neutron reflectivity experiments and used that cell to conduct the first series of antibody and TMV adsorption experiments. The neutron reflectivity curves obtained in those experiments confirm that the PNIPAM film is swollen at room temperature and collapses above 35°C, and that IgG sticks to the PNIPAM above its transition temperature. However, the curves do not reflect the level of detail expected regarding antibody orientation. Theoretical fits to the reflectivity curves indicated that the results were compromised by the appearance of unanticipated surface roughness (> 5 nm) during the neutron experiments. Post-mortem analyses of the samples showed that the roughness is the result of the gradual attack by water of the interface between substrate and the SAM onto which the PNIPAM was deposited. SAM fabrication procedures have now been modified to minimize this degradation, and we anticipate that higher quality results will be obtained in the next series of LANSCE experiments.

Fluid entry, exit ports**PNIPAM-coated quartz****IMPORTANT!** List

(or in press).

Heating stage

Submit all experiment reports to:
LANSCE User Office, MS H831, Los Alamos National Laboratory, Los Alamos, NM 87545

Experiment was carried out at:	Local Contact	Proposal #	LANSCE Use Only
<input checked="" type="checkbox"/> Manuel Lujan Jr. Neutron Scattering Center	Sven Vogal	2003029	Report Rc'd
<input type="checkbox"/> Weapons Neutron Research Facility	FP/Instrument Used		7/15/04
<input type="checkbox"/> WNR/Blue Room	HiPPO		

Title "Structural investigation of Ag-doped PLZT 12/70/30 bulk samples"

Authors and Affiliations

Mark A. Rodriguez, Sandia National Laboratories
Bruce A. Tuttle, Sandia National Laboratories

Experiment Report

The perovskite material lead-zirconium-titanium-oxide (PZT) is under investigation for a wide range of applications including non-volatile memories, sensors, electro-optic devices, capacitors, and actuators. We are currently investigating high zirconia content PZT based materials that are being used as high energy density pulse discharge capacitors for both present and next generation integrated micro-firing sets.

Currently we are investigating the effect of Ag-doping on PLZT 12/70/30 compositions (L = lanthanum). We successfully measured undoped and 3% Ag-doped PLZT bulk samples at different temperatures between 25 and 100°C. We have successfully refined data for the room temperature undoped PLZT 12/70/30 sample. The results for this sample are shown in table 1. A total of 98 histograms from four orientations were used to generate pole figures for the sample. Figure 1 shows the resulting observed pole figures from this sample. It shows a weak texture along the (001) direction with and in-plane fiber texture. This is of interest as historically we assumed these samples to have random texture because they are prepared from pressed powders. Our current results suggest that this assumption is not entirely true. What this result suggests is that there may be some slight preferential orientation of the powder during the pressing of the pellet prior to sintering. This will undoubtedly have some effect on the properties of the resulting discharge capacitor.

We are encountering difficulties in the Uiso values for the Ti and Zr sites as they are show negative refined values. More work needs to be done to evaluate why this is happening. Other refined parameters such as lattice parameters and atom positions show reasonable values. The structure refinement procedure is quite involved due to the very large data sets associated with each sample.

Experiment Report (continued)

Table 1. Refined parameters for Undoped PLZT at 25°C.

Temperature	25C
CHISQ (LeBail)	2.62 (2.34)
a [Å]	5.73396(4)
c [Å]	14.0106(2)
z_Pb	0.2780(2)
z_La	0.2061(8)
z_Ti	0.0539(3)
z_Zr	0.0371(2)
x_O	0.1589(1)
y_O	0.3548(2)
z_O	0.0997(2)
Uiso_Pb	4.49(2)
Uiso_La	13.7(6)
Uiso_Ti	-4.45(7)
Uiso_Zr	-0.18(4)
Uiso_O	2.34(1)
Texture Index	1.22

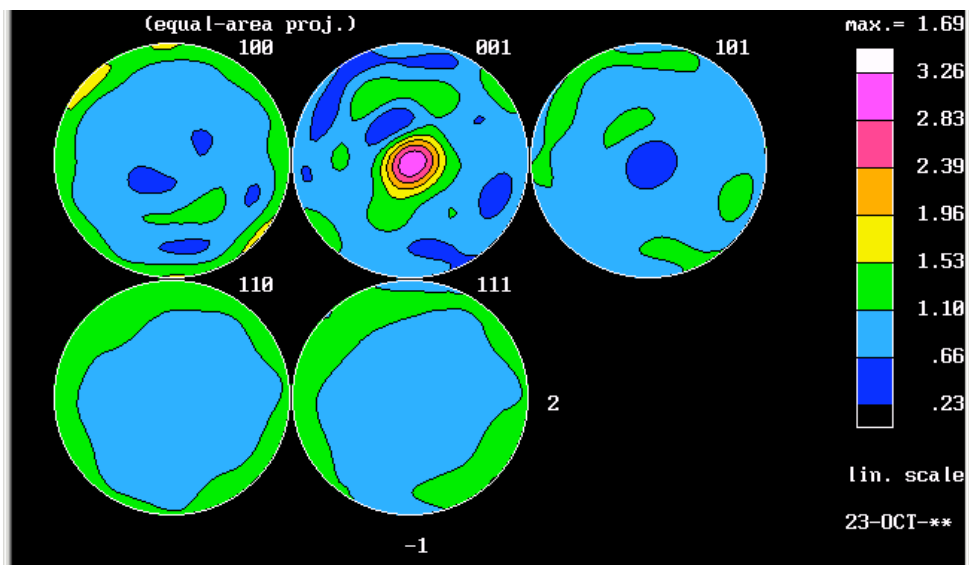


Figure 1. Pole figures for undoped PLZT sample at 25°C.

IMPORTANT! List or attach a list of publications resulting from this experiment (published or in press).

REPORT ON EXPERIMENT (Please Type)

Submit all experiment reports to:

LANSCCE User Office, MS H831, Los Alamos National Laboratory, Los Alamos, NM 87545

Experiment was carried out at: Local Contact Proposal #LANSCCE Use Only XManuel Lujan Jr. Neutron Scattering Center Paul Langan 2003033 Report Rc'd Weapons Neutron Research Facility FP/Instrument Used 1/7/04 WNR/Blue Room PCS

Title

Neutron Diffraction Studies on Blue Copper Proteins Authors and Affiliations

N. Sukumar, NE-CAT, Sector 24, Bldg. 436E, Argonne National Laboratory, Argonne, IL 60439

P. Thyagarajan, IPNS, Argonne National Laboratory, Argonne, IL 60439

V.L. Davidson, Dept. of Biochemistry, The Univ. of Mississippi Medical Center, Jackson, MS 39216 F.S. Mathews, Dept. of Biochemistry and Molecular Biophysics, Washington University School of Medicine, St. Louis, MO 63110

Experiment Report

Both amicyanin and azurin are belong to family of type I blue copper proteins, a subclass of the copper proteins family containing analogous functional, structural and spectroscopic features. The molecular weight of amicyanin and azurin are 11.2KD and 13.9KD respectively. In both the proteins, the Copper binding site is located eccentrically at a distance of ~6Å from the outer surface.

The aim of the project is to study the pH induced conformational transitions involving changes in the coordination sphere of the copper. Especially, we are interested in studying the protonated/ deprotonated states of all the residues that interact with copper by locating all the hydrogen atoms associated with these residues and the role of water molecules during conformational transition.

The crystals of amicyanin were grown by the sitting drop method. The large dimension crystals of ~1mm size were obtained by repeated macroseeding. In the beginning stage, the macroseeding carried out by using the buffer, salts prepared in H₂O. But, when the crystals size were ~0.45mm, all the macroseeding were carried out using solutions prepared with D₂O.

The three best crystals of ~1mm size were mounted separately in each 1.5mm quartz capillary tube and sealed with mother liquor prepared in D₂O. All were mailed to PCS for checking as the user office in consultation with PCS's instrumentation scientist Dr. Paul Langan offered this option.

Dr. Paul Langan tested one of the three crystals during the allotted time (24 hours) and found that the crystal is showing capacity to diffract. According to Dr. Langan, there are spots in the low-resolution region of diffraction pattern.

Currently, amicyanin crystals are growing with solutions made with D₂O from the start. Even the protein stabilizing solution was exchanged with buffer made with D₂O during final stage of purification. Next time, crystals which are growing completely with the solutions made of D₂O will be checked in the neutron beam.

Experiment Report (continued)

IMPORTANT! List or attach a list of publications resulting from this experiment (published or in press).

None

Submit all experiment reports to:
LANSCÉ User Office, MS H831, Los Alamos National Laboratory, Los Alamos, NM 87545

Experiment was carried out at:	Local Contact	Proposal #	LANSCÉ Use Only
<input checked="" type="checkbox"/> Manuel Lujan Jr. Neutron Scattering Center	M. Fitzsimmons	2003035	Report Re'd
<input type="checkbox"/> Weapons Neutron Research Facility	FP/Instrument Used		6/28/04
<input type="checkbox"/> WNR/Blue Room	11A		

Title
Identifying the spatial distribution of thermoremanent magnetization in CoO/MgO superlattices.

Authors and Affiliations
A.E. Berkowitz (UCSD) et al.

Experiment Report

Coupling of a ferromagnetic material to an antiferromagnetic material can give rise to exchange bias, which manifests itself as a shift of the ferromagnetic hysteresis loop away from symmetry about zero magnetic field (this shift is called the exchange bias, H_E). Even though this effect was discovered long ago (1956) and is widely used in technological applications in the magnetic recording and memory industries), a comprehensive understanding of the fundamental origin of exchange bias is still lacking. Recent studies of polycrystalline permalloy (Py)/CoO bilayers showed that the temperature dependencies of H_E and the thermoremanent magnetization (TRM) in the antiferromagnet of a CoO/MgO superlattice were the same; thus, suggesting exchange bias is correlated with the net magnetization in the antiferromagnet.¹ TRM is produced when a magnetic field induces the uncompensated spins to have a component in the forward hemisphere around the field direction (by flipping the Néel axes 180°, when necessary) in the antiferromagnet as the material is cooled through the Néel temperature. In the case of the CoO/MgO superlattice, TRM was attributed to uncompensated moments at the antiferromagnet interface. More recently, significant enhancements (up to 50%) of exchange bias have been achieved through intentional chemical doping (diluting) of the antiferromagnet. By chemical doping, we mean that some of the atoms with magnetic moments are replaced with atoms that do not have any moments, thus, creating uncompensated moments on the antiferromagnetic sublattice. During field cooling, a net magnetization in the antiferromagnet is produced by the alignment of domains (achieved when the exchange field from the ferromagnet interacts with uncompensated spins).² Within this picture, exchange bias arises from a fraction of the uncompensated spins being unchanged (hence pinned) throughout the full hysteresis loop (even in fields sufficiently strong to saturate the ferromagnet). The pinned magnetization was attributed to uncompensated spins that may be at or near interfaces or perhaps distributed throughout the antiferromagnet.

In order to directly observe the magnetization of uncompensated spins in CoO, Takano et al., fabricated superlattices in which the Py layers were replaced with MgO, thus, removing ferromagnetic material from the sample. The superlattices consisted of $[\text{CoO}(300 \text{ \AA})/\text{MgO}(30 \text{ \AA})]_{15}$ grown on silicon substrates. Magnetization measurements of the sample were obtained for a variety of cooling fields and temperatures. The measurements shown in Fig. 1 are those for the neutron scattering sample we studied on Asterix last run-cycle. The TRM is characterized by two features. First, a (fairly) temperature independent region, called the “plateau” region, is observed between 50 and 200 K. Second, a pronounced increase in magnetization occurs below 50 K, called the low freezing temperature region. The intent of our neutron scattering study was to locate the positions of the uncompensated spins.

¹ K. Takano, et al., Phys. Rev. Lett., **79**, 1130 (1997).

² P. Miltényi, et al., Phys. Rev. Lett. **84**, 4224 (2000).

Experiment Report *(continued)*

In order to enhance the neutron scattering signal, we cooled the sample to 4 K in an 11T field. Next, we applied a field of 0.2 T^3 to the sample and measured its reflectivity with polarized neutron beams. In order to make these measurements, we learned how to propagate a beam of polarized neutrons through the equator of a superconducting magnet (operating in symmetric mode) while maintaining good polarization of the neutron beam. Maintaining good polarization of the neutron beam when the magnet is operating at low field is, perhaps counterintuitively, the most difficult situation, since the region through the magnet's equator where the stray field changes polarity is rather extensive and tends to rapidly depolarize the neutron beam.

The reflectivity for the sample is shown in Fig. 2 (upper). The ratio of the difference between the spin-up and spin-down reflectivities to their sum is called the spin asymmetry and is shown for 4 K and 300 K in the lower panel. There are two important points to make about the data in Fig. 2. First, the spin asymmetry at 4 K is much larger than that at 300 K. This difference we believe is evidence for uncompensated magnetization in the sample at low temperature. The disappearance of spin asymmetry at 300 K coincides with the antiferromagnetic transition temperature of CoO; therefore, we believe the uncompensated magnetization is associated with uncompensated spins in antiferromagnetic CoO and not in MgO. The second point concerns the location of the spin asymmetry (at 4 K). The spin asymmetry is peaked *between* superlattice Bragg reflections. We tentatively attribute this result to the presence of uncompensated spins at the CoO/MgO interfaces rather than in the CoO layers.

The lack of spin asymmetry at superlattice reflections was surprising to us. Therefore, we investigated the structure of the neutron sample in detail with cross-section transmission electron microscopy. We learned from this investigation, to our surprise, that the grain size of the CoO increased with subsequent layer deposition (see Fig. 3); thus, our neutron sample contained much less CoO grain boundary material than we had expected (and consequently much less bulk uncompensated magnetization).

We have recently completed a study of the microstructures of CoO/MgO and CoO/SiO₂ superlattices and have found that superlattices of CoO/SiO₂ can be grown with much higher perfection (i.e., much smoother) than CoO/MgO, and, more importantly, the grain size of the CoO layers in the CoO/SiO₂ superlattice does not change with layer deposition. In retrospect, CoO/SiO₂ superlattices would have been a better choice to characterize the uncompensated magnetization in CoO, than was CoO/MgO (though we did succeed in detecting uncompensated magnetization in CoO/MgO).

IMPORTANT! List or attach a list of publications resulting from this experiment

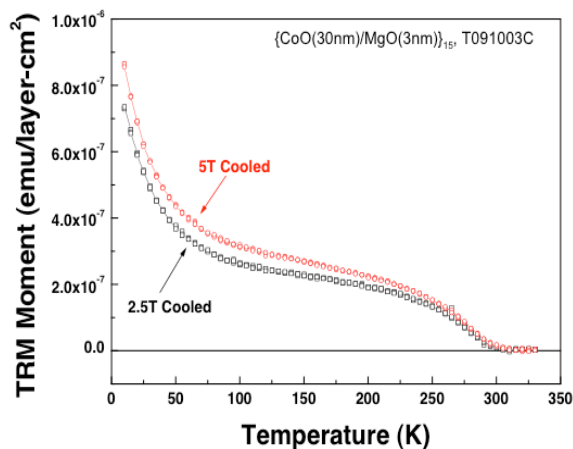


Fig. 1 Field cooled moment densities vs. temperature for the neutron scattering sample.

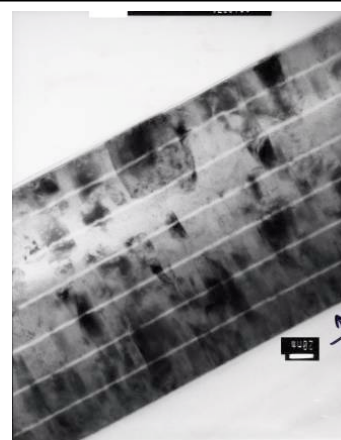


Fig. 3 Cross-sectional TEM image of the CoO/MgO superlattice sample showing a variation in CoO grain size.

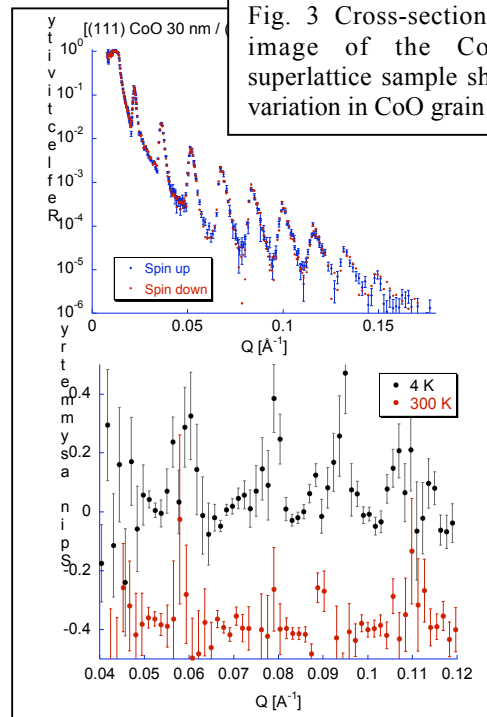


Fig. 2 (upper) Polarized neutron reflectivity of the sample cooled to 4 K in a 11 T (the applied field was 0.2 T). (lower) The spin asymmetry (defined in the text) for the sample at 4 and 300 K.

³ We note a measurement of the thermalremanent magnetization is one taken at zero field. We are not able to make such a measurement with our 11T superconducting magnet on account that even after reducing the current in the magnet to zero there remains trapped flux of unknown magnitude and direction. Therefore, we decided to take our measurements in a condition (0.2 T) such that we would know the magnitude and direction of the field applied to the sample.

Submit all experiment reports to:
 LANSCE User Office, MS H831, Los Alamos National Laboratory, Los Alamos, NM 87545

Experiment was carried out at:		Local Contact	Proposal #	LANSCE Use Only
<input checked="" type="checkbox"/>	Manuel Lujan Jr. Neutron Scattering Center	Rex P. Hjelm	2003036	Report Rc'd
<input type="checkbox"/>	Weapons Neutron Research Facility	FP/Instrument Used	10/LQD	10/04/04
<input type="checkbox"/>	WNR/Blue Room			

Title	SANS Studies of Nano-Energetic Materials
--------------	--

Authors and Affiliations

Joseph T. Mang, LANL/DX-2
Rex P. Hjelm, LANL/L-12

Experiment Report

Introduction

Nano-sized particles have found wide application. Recent interest in the use of nano-particles in energetic materials (e.g., a thermitic mixture of aluminum and iron oxide) has shown a need for more quantitative characterization of the individual components, with particular emphasis on determination of particle sizes and distributions.

Small-angle neutron scattering (SANS) techniques, are widely used for microstructural investigation. They have been applied to a variety of systems, including polymers, high explosives, and particulate systems. SANS probes a statistically significant number of particles and can provide a quantitative measure of particle morphology, size distribution and aggregation properties. The unique sensitivity of SANS, to regions of differing chemical composition allows for accurate measurement of the passivation (oxide, organic, inorganic) layer which surrounds the Al particles.

For the current studies, we have used SANS techniques to characterize nano-particles composed of aluminum and tungsten trioxide (WO₃). With the aid of microscopy techniques, physical models were developed to describe the measured scattering data, allowing for a quantitative determination of particle morphology, mean particle size, particle size distribution (PSD) and surface layer thickness.

Results

During the 2003-2004 run cycle we performed SANS measurements on ~ 30 different nano-powders. SANS were performed on dry powders as well as powders dispersed in mixtures of deuterated and non-deuterated toluene. SEM images revealed that the Al nano-particles studied are spherically shaped, having a thin outer layer of aluminum oxide (Al_2O_3), whereas the WO_3 particles were found to have a sheet-like structure. The results of several powders are discussed below.

Fig. 1a shows the SANS line shape measured for a nano-Al powder (Nano-Al-Son-6) measured in air. The solid line in the figure is the result of analysis according to a model of polydispersed spheres, having a core-shell structure. Details of the model can be found in the beam time proposal (LQD2003036). The core was modeled as pure Al and the shell as Al_2O_3 . Good agreement was found between the model and data, enabling a particle size distribution (Fig. 1b) to be extracted and a measurement of the oxide layer thickness.

Experiment Report (continued)

Fig. 1c shows the SANS data obtained from nano-Al particles dispersed in toluene and deuterated toluene. By employing the method of contrast variation, we were able to confirm the particle structure and provide a measurement of the average density of the Al_2O_3 layer. The density of the Al_2O_3 layer is important in understanding the structure of the oxide layer as well as aging properties of the Al. The density of the oxide layer as measured by SANS was 3.53 g/cc, compared to 3.51 g/cc as measured by helium pycnometry.

The SANS data obtained for the WO_3 data (Fig. 2a) were modeled as infinite sheet-like structures. The data shows an initial power-law ($I \propto Q^{-\square}$) region, with $\square = 2$, suggesting an infinite sheet-like structure. The final slope of the data is monotonic, indicating a high degree of polydispersity in the sheet thickness, and falls-off as Q^{-4} . This behavior indicates a uniform structure with smooth interfaces. The results of the analysis are shown as solid lines in Fig. 2a and the resulting size distribution is shown in Fig. 2b.

SUMMARY

Small-angle neutron scattering methods have been used to characterize nano-powders being used in the development of nano-energetics. Detailed structural models were developed, based upon SEM images, to analyze the SANS data. The combination of these techniques makes a powerful tool for the characterization of nano-particle systems. Our models describe the data very well and enabled details of the particle microstructure to be quantified.

SANS provides a unique sensitivity to regions of differing chemical composition and can elucidate fine structural details such as the passivation layer thickness. This sensitivity is highly advantageous for the characterization of new coated aluminum systems.

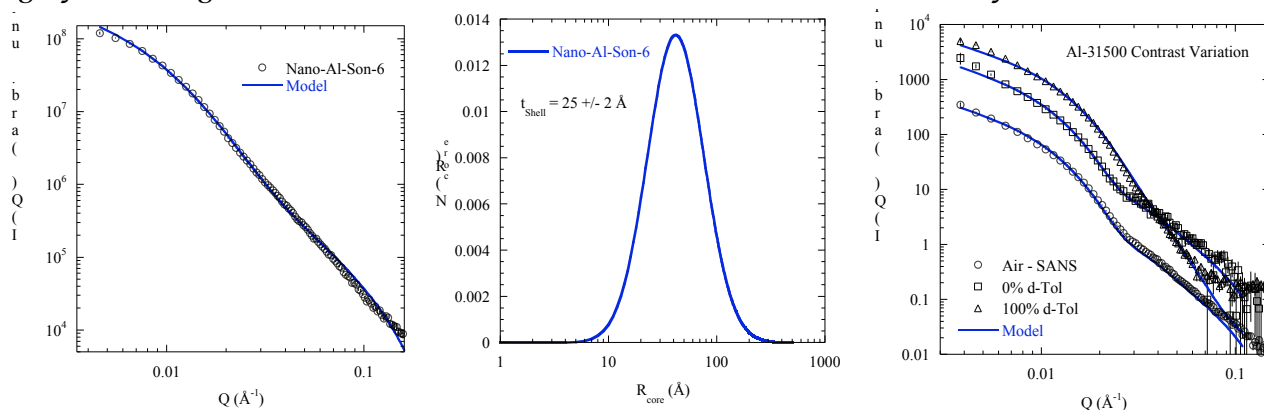
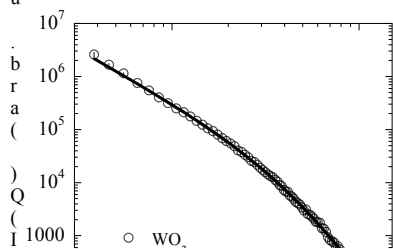


Figure 1: (a) SANS data for a nano-Al powder showing fit to model (b) PSD obtained from analysis (c) Contrast variation measurements of a nano-Al powder. A simultaneous fit to the model allows a measurement of the density of the Al_2O_3 layer surrounding the Al core.



IMPORTANT! List or attach a list of publications resulting from this experiment (published or in press).



REPORT ON EXPERIMENT

(Please Type)

Submit all experiment reports to:

LANSCCE User Office, MS H831, Los Alamos National Laboratory, Los Alamos, NM 87545

Experiment was carried out at:		Local Contact	Proposal #	<i>LANSCE Use Only</i>
<input checked="" type="checkbox"/>	Manuel Lujan Jr. Neutron Scattering Center	Frans Trouw	2003-040	Report Rc'd 6/16/04
<input type="checkbox"/>	Weapons Neutron Research Facility	FP/Instrument Used		
<input type="checkbox"/>	WNR/Blue Room	PHAROS		

Title

The Phonon Entropy of Mo-Fe Alloys

Authors and Affiliations

Olivier Delaire, Max Kresch, Tabitha Swan-Wood, Michael McKerns, Tim Kelly, Brent Fultz
California Institute of Technology
Materials Science Department
1200 California blvd, MC 138-78
Pasadena CA 91125

Experiment Report

The goal of this experiment was to investigate the phonon entropy contribution to the Mo rich end of the Mo-Fe phase diagram. The Mo-rich side of the Mo-Fe phase diagram is essentially similar to that of the Mo-Co system and the Mo-Fe samples proved much easier to prepare. Besides, Fe has better neutron scattering properties than Co, since it does not absorb neutrons as strongly.

Mo-5%Fe samples were prepared by arc-melting under an inert Ar atmosphere from high-purity materials. The ingots were subsequently ball-milled to ensure a homogeneous distribution of Fe impurities in a solid-solution on the BCC host Mo lattice. X-ray diffraction was performed to check that the Fe solutes were not segregated and that the material was indeed in the BCC phase. From the solid-solution material, a material with separated Mo(Fe) and sigma phase was prepared by annealing under vacuum. Roughly 50grams of each sample were prepared. Reference samples of pure Mo powder and pure Fe powders were also measured in the experiment.

The inelastic neutron scattering spectra from all samples were measured on the Pharos time-of-flight spectrometer at LANSCE. The samples were encased in thin-wall Al sample holders, and mounted on the spectrometer. All spectra were collected at room temperature. Typical acquisition times were about 12 hours for each sample. A sample S(Phi,E) scattering intensity map for the Mo-Fe solid-solution sample is presented in Figure 2. The phonon scattering on either side of the elastic line is strong, with fainter dispersions visible. The recorded spectra are currently under analysis to produce phonon densities of states from which the phonon entropy is easily calculated. We expect that with the good quality of the data acquired, clear phonon densities of states will be produced and the entropy of dilute alloying for Fe in Mo will be unambiguously established.

Submit all experiment reports to:
LANSCE User Office, MS H831, Los Alamos National Laboratory, Los Alamos, NM 87545

Experiment was carried out at:	Local Contact	Proposal #	LANSCE Use Only
<input checked="" type="checkbox"/> Manuel Lujan Jr. Neutron Scattering Center	Sven Vogel	2003041	Report Rc'd
<input type="checkbox"/> Weapons Neutron Research Facility	FP/Instrument Used		7/14/04
<input type="checkbox"/> WNR/Blue Room	HIPPO		

Title "Neutron
Diffraction Study of Erbium Dideuteride Thin Films"

Authors and Affiliations
Michael A. Mangan, Sandia National Laboratories
James F. Browning, Sandia National Laboratories
Mark A. Rodriguez, Sandia National Laboratories

Experiment Report

This proposal is part of a larger, existing program to develop a scientific understanding of helium evolution in tritide thin films. The importance of this problem stems from the fact that tritide thin films are used in neutron tubes, a component of nuclear weapon systems that must be periodically replaced due to its limited lifetime.

In this experiment, the question we are trying to answer is "Can neutron diffraction be used as an analytical technique for investigations of tritide thin films?" More specifically, in the erbium hydride system, hydrogen isotopes are known to preferentially reside in tetrahedral (and possibly octahedral sites) of an FCC lattice having the fluorite structure. This raises the questions: "Does tritium site occupation strongly affect the dynamics of helium evolution in the film? Also, do octahedral site vacancies affect helium evolution?" We are trying to develop a technique that will allow these questions to be answered.

In our experiment outlined in the proposal we hoped to improve signal of the ErD_2 films sufficiently to bring it into the range of detectability. Our idea was to increase sample volume by depositing ErD_2 films on very thin Mo sheets. By using both sides of the Mo substrate we could substantially increase the sample volume over the initial experiment (see experimental report for 2002123). This idea worked. Figure 1 shows diffraction data for 80 ErD_2 films on 40 thin Mo substrates. Although the signal is weak, we can clearly see the ErD_2 (220) peak in the diffraction data; calculated patterns of the ErD_2 fluorite-type structure indicate that the ErD_2 (220) peak is the 100% peak in the diffraction pattern. Refinement results indicated an ErD_2 lattice parameter of $a = 5.126$ Angstroms and a phase fraction of ErD_2 of 2.1 wt%. These numbers are very reasonable; the theoretical ErD_2 phase-fraction based on the film and substrate volumes was 2.6 wt%. Other ErD_2 peaks were also observed but had a low degree to be

Experiment Report (continued)

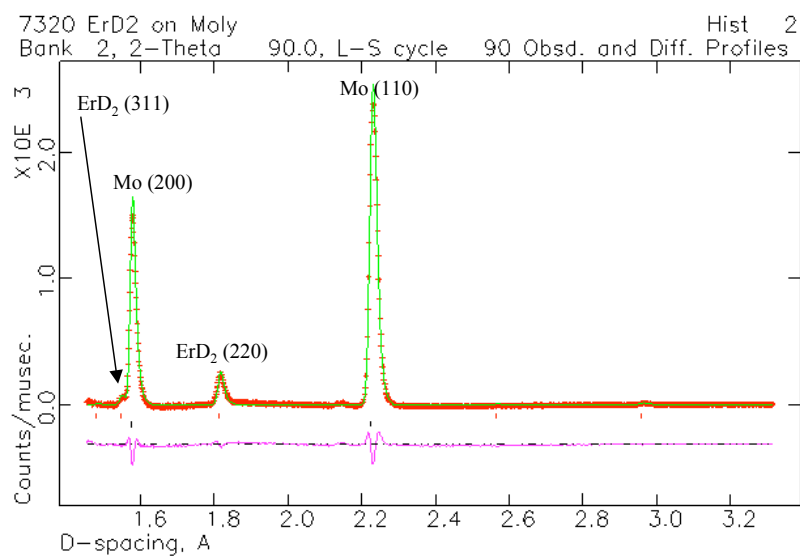


Figure 1. Diffraction pattern for summed 90° banks showing clear detection of ErD₂.

We consider this experiment a success in that we have now been able to detect and refine ErD₂ as a film. This is significant step forward for the investigation of ErT₂ thin films as the neutron scattering lengths for D (6.671 fm) and T (4.792 fm) are similar. Our refinements on the ErD₂ did verify D on the tetrahedral (_ _ _) site and also indicated the possibility of some small site-occupancy of D on the (_ _ _) octahedral site in difference-Fourier maps. Figure 2 shows a model of ErD₂ with a difference-Fourier map superimposed. There is still some uncertainty about the validity of the D on the octahedral site as it is hard to refine stably. This could result from the weak signal and lack of good modeling of the texture effects. Regardless, the result gives us some hope that we can be sensitive to octahedral site occupancy in future experiments.

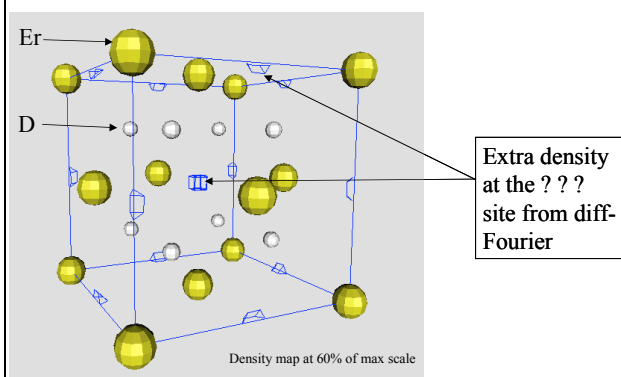


Figure 2. Refined ErD₂ structure with superimposed difference-Fourier map showing possible density on (_ _ _) site.

IMPORTANT! List or attach a list of publications resulting from this experiment (published or in press).

Submit all experiment reports to:
LANSCCE User Office, MS H831, Los Alamos National Laboratory, Los Alamos, NM 87545

Experiment was carried out at:	Local Contact	Proposal #	LANSCCE Use Only
<input checked="" type="checkbox"/> Manuel Lujan Jr. Neutron Scattering Center	Frans trouw	2003-042	Report Rc'd 6/15/04
<input type="checkbox"/> Weapons Neutron Research Facility	FP/Instrument Used		
<input type="checkbox"/> WNR/Blue Room	PHAROS		

Title

Measurement of phonons in Ni at high temperature in Hippo furnace

Authors and Affiliations

Olivier Delaire, Max Kresch, Tabitha Swan-Wood, Tim Kelley, Michael McKerns, Brent Fultz
California Institute of Technology
Materials Science Department
1200 E. California blvd , MC 138-78
Pasadena, CA, 91125

Experiment Report

The goal of this experiment was to measure phonons in pure Ni at high temperatures in-situ using the neutron-scattering dedicated Hippo furnace. Partial measurements with a Ni sample in the furnace at high temperatures had been made by our group on Pharos in a previous run cycle, but the background from the furnace could not be measured at the time due to technical difficulties. This had impeded analysis of our previous data although interesting effects were hinted at by this previous partial data set. The new measurements carried during the allocated beam time allowed to realistically determine the background signal due to the furnace at room temperature and high temperatures (700C and 1050C), which permitted a full correction and analysis of the high-temperature Ni measurements.

The background from the Hippo furnace was found to be significant, with a clear contribution to the inelastic scattering on either side of the elastic line at zero energy transfer, as can be seen in Figure 1. The signal measured at high temperatures was similar in magnitude, although it showed some slight softening. These $S(Q,E)$ spectra were normalized and subtracted from the original data on Ni at high temperatures to produce the Ni-only scattering spectra shown in Figure 2.

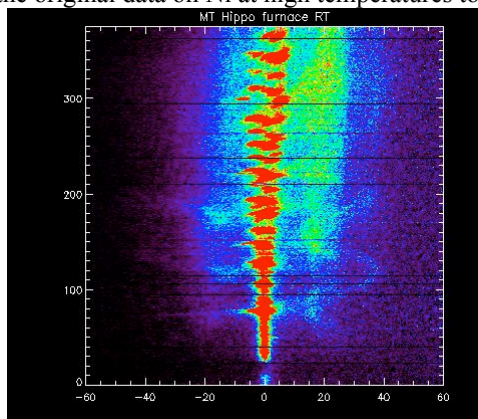


Figure 1: $S(Q,E)$ signal from Hippo furnace at room temperature.

Experiment Report (continued)

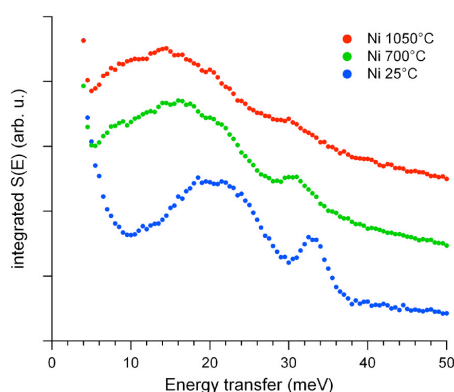


Figure 2: Furnace corrected inelastic neutron scattering $S(E)$ for pure Ni at ambient and high temperatures.

After applying corrections to the data for multiphonon scattering and thermal effects, we were able to extract the phonon density of states (DOS) of Ni at the different temperatures measured. The resulting curves are shown in Figure 3. Note the good agreement between our result for the ambient Ni DOS and that of Brockhouse et al [1]. On the other hand, the phonon DOS of Ni has never been measured at such high temperatures previously. The DOS curves are currently under analysis. Of particular interest is the relatively weak softening of the Ni DOS between 700C and 1050C, compared to the change between 25C and 700C. This effect could be related to some anharmonicity of the inter-atomic potential binding Ni atoms in the crystal, and it is being investigated further. An article presenting our current findings was submitted to the LANSCE research highlight 2003 [2].

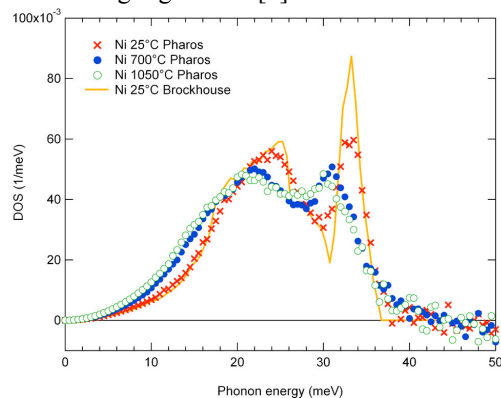


Figure 3: Phonon density of states curves for Ni at ambient and elevated temperatures.

Besides the work on pure Ni, in situ spectra were measured on stoichiometric FeAl at 700C and 1050C. The data are still undergoing analysis, however, preliminary results indicate a negligible softening of phonons from 700C to 1050C. This is interesting as the entropy needed to balance the energy required for the crystal to expand against the bulk modulus, is larger than the anharmonic entropy due to softening. This would mean that entropy must come from another source at high temperatures to balance this energy change. This entropy may be attained by the unusually large vacancy concentration seen in this alloy. This work is expected to be published within the next year.

[1] E.D. Hallman and B.N. Brockhouse, "Crystal dynamics of nickel-iron and copper-zinc alloys," *Canadian Journal of Physics* **47**, 1117–1131 (1969).

[2] O. Delaire, T. Kelley, T. Swan-Wood, M. Kresch and B. Fultz, "Phonon thermodynamics of transition metals and alloys", LANSCE research highlights 2003 (to be published).

IMPORTANT! List or attach a list of publications resulting from this experiment (published or in press).

Submit all experiment reports to:
LANSCE User Office, MS H831, Los Alamos National Laboratory, Los Alamos, NM 87545

Experiment was carried out at:	Local Contact	Proposal #	LANSCE Use Only
<input checked="" type="checkbox"/> Manuel Lujan Jr. Neutron Scattering Center	Jarek Majewski	2003044	Report Rc'd 11/4/03
<input type="checkbox"/> Weapons Neutron Research Facility	FP/Instrument Used		
<input type="checkbox"/> WNR/Blue Room	SPEAR		

Title	Tethered Lipid Bilayers on Silicon for Evaluating Protein-Membrane Interactions
Authors and Affiliations	
Mike Kent, Hyun Yim, Darryl Sasaki Sandia National Labs	

<p>Experiment Report</p> <p>We decided to study protein/lipid interactions with monolayers at the liquid-air interface rather than with supported bilayers at the solid-liquid interface as in the proposal. This is because we had very exciting results in previous work and discovered that one very important aspect needed to be completed. We are using neutron and X-ray reflection to study protein adsorption to Langmuir monolayers of metal-ion-chelating lipids. The use of metal ion coordination to target the adsorption of proteins to lipid membranes has been studied extensively by others [1]. This method utilizes coordination interactions between divalent metal ions and naturally occurring histidine units, genetically engineered metal-ion binding sites, or polyhistidine units inserted at either the N or C terminus of proteins. Particularly useful is the fact that the interaction energy between histidine and the chelated metal ion varies greatly depending upon the nature of the metal ion. For example, the interaction energy for Cu²⁺/IDA with histidine is 15 times greater than that for Ni²⁺/IDA with histidine. Our goals are to understand how to target adsorption of specific proteins, manipulate the orientation and density of adsorbed proteins, determine the time scale of adsorption, determine conditions for which proteins penetrate into the lipid membranes, and understand the conditions for denaturation. In previous work we examined the characteristics of the protein layer adsorbed to a lipid with chelated Cu²⁺ ions. The work focused on repeating this for lipids with chelated Ni²⁺ ions.</p> <p>In this study we prepared Langmuir monolayers of 100% DSIDA (metal ion - chelating synthetic lipid) spread onto the surface of H₂O subphases. With the surface area held constant, we obtained the reflectivity of the lipid monolayer with adsorbed Ni²⁺ ions and then after injection of myoglobin (dimensions: 44 Å x 44 Å x 20 Å). Data were obtained as a function of time at 50 minute intervals until no further variation was detected (after ~ 14 hrs). Reflectivity data are shown in Figure 1. Data were obtained as a function of time for two bulk myoglobin concentrations. The data reveal detailed structural characteristics of a protein layer as a function of time during the adsorption process. Structural characteristics extracted from these data are shown in Figures 2 and 3. Both the thickness and the average segment volume fraction are consistent with a nearly end-on orientation throughout the adsorption process for Ni²⁺, but a transition from side-on to an end-on orientation with increasing protein surface density in the case of Cu²⁺ ions.</p>

Experiment Report *(continued)*

These results suggest that it may be possible to design systems for which certain useful activities, such as enzymatic reactions, could be regulated by controlling the orientation of the adsorbed protein through the bulk protein concentration or the nature of the chelated metal-ion.

[1] Maloney, K. M.; Shnek, D. R.; Sasaki, D. Y.; Arnold, F. H. *Chemistry & Biology*, 1996, 3, 185.

[2] Kent, M.; Yim, H.; Sasaki, D.; Satija, S.; Majewski, J.; Gog, T. *JACS*, under review

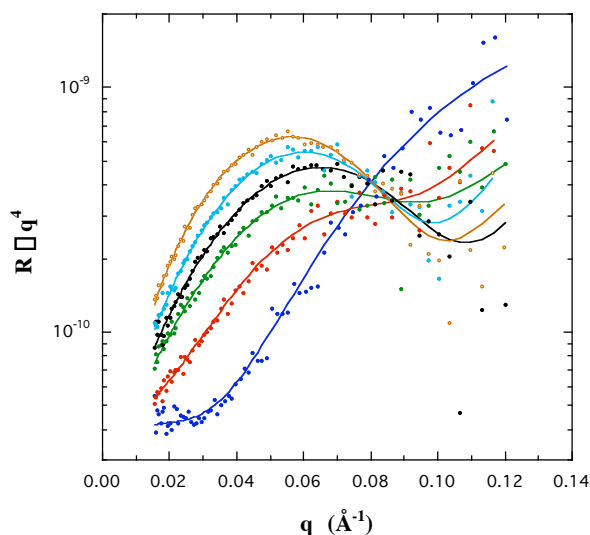


Figure 1. Reflectivity as a function of time during the adsorption process for Ni-loaded DSIDA. The bulk concentration of myoglobin was 50 microM. Curves were obtained at 50 minute intervals.

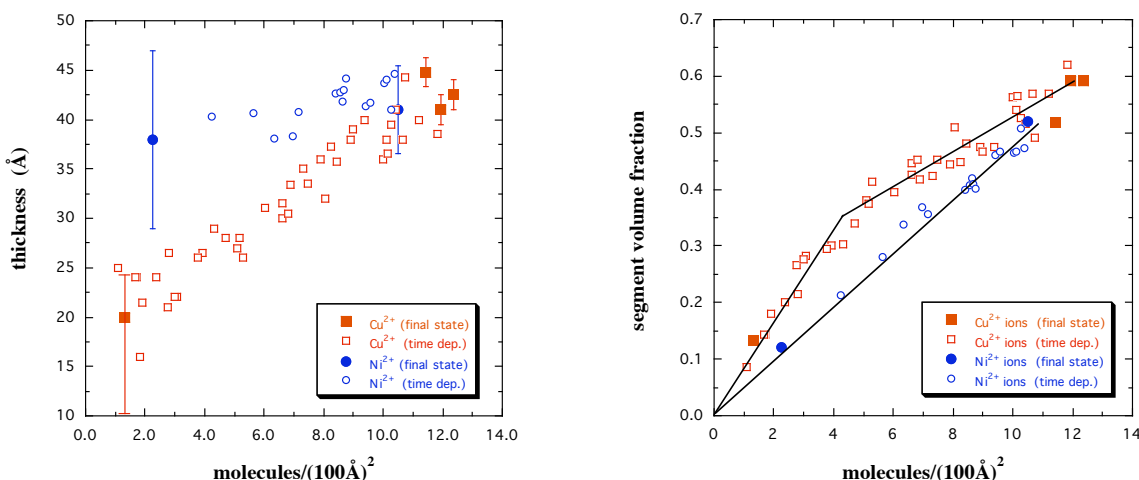


Figure 2. Evolution of the thickness of the adsorbed protein layer as a function of time during the adsorption process for Cu-loaded and Ni-loaded DSIDA. The filled symbols represent the final state for bulk myoglobin concentrations of 10 and 0.1 mM in the case of Cu-loaded DSIDA and 50 and 10 mM in the case of Ni-loaded DSIDA. The open symbols represent the time dependent values for bulk myoglobin concentrations of 10 mM in the case of Cu-loaded DSIDA and 50 mM in the case of Ni-loaded DSIDA.

IMPORTANT! List or attach a list of publications resulting from this experiment (published or in press).

Kent, M.; Yim, H.; Sasaki, D.; Satija, S.; Majewski, J.; Gog, T. *JACS*, under review



REPORT ON EXPERIMENT

(Please Type)

Submit all experiment reports to:
 LANSCE User Office, MS H831, Los Alamos National Laboratory, Los Alamos, NM 87545

Experiment was carried out at:		Local Contact	Proposal #	<i>LANSCE Use Only</i>
<input checked="" type="checkbox"/>	Manuel Lujan Jr. Neutron Scattering Center	Dr Don Brown	2003046	Report Rc'd 7/1/04
<input type="checkbox"/>	Weapons Neutron Research Facility	FP/Instrument Used		
<input type="checkbox"/>	WNR/Blue Room	SMARTS		

Title	Residual Stresses in Zircaloy-4 Weldments
--------------	---

Authors and Affiliations
Dr. M. I. Ripley ANSTO, Australia
D. G. Carr ANSTO, Australia
Dr. T. M. Holden LANL, Canada

Experiment Report

The Australian Replacement Research Reactor (RRR) at Lucas Heights, NSW will have a number of welded Zircaloy-4 components within the core region. It is of great technological importance to measure the texture changes and the residual stresses associated with the welds in order to be able to estimate the lifetime of these components.

There have only been a few reported experiments, by the Chalk River group, on Zircaloy-2 welds and none, prior to our previous work, on Zircaloy-4 welds. We made measurements at SMARTS on an as-welded Zircaloy-4 plate and have reported these results [1,2]. Those experiments confirmed that the crystallographic texture departs rapidly from the texture characteristic of rolled plate as the heat affected zone (HAZ) is traversed and changes again in the melt zone. The residual strains are high and different for different reflections, characteristic of the superposition of type-1 and type-2 stresses. The advantage of neutron diffraction at a spallation source such as SMARTS is that all reflections, corresponding to the grain orientations allowed by the texture at the location, are obtained. This is very important in the heat-affected zone (HAZ) and melt zone where the texture is different from the base metal.

The experiments in the current work were made on the same butt-welded Zircaloy-4 plate (8.6 mm thickness prepared by the TIG welding method) except that it was given a stress relaxation heat treatment the same as that specified for the Zircaloy-4 components of the RRR. The experiments largely repeated the previous measurements, ie. residual stress measurements were made on a locus transverse to the weld in the longitudinal, transverse and normal directions at mid-thickness. The small (2 mm cube) coupons used previously to provide stress-free reference lattice spacings were also heat treated and again measured. This time fewer measurements of the stress free lattice spacing were made in the light of the negligible differences found previously [1].

Progress to date on the analysis of the data is as follows:

- Data collection was not completed during the allocated instrument time due to various experimental problems, mainly with the accelerator and low power. Eventually the final runs were completed by Lujan staff and forwarded to us in March 04.
- Calculation of the strains is still in progress. Preliminary results indicate that the bulk residual strains have decreased but that there is a larger variation in the d zero strains than previously

Experiment Report (*continued*)

Further work is in progress to complete the analysis:

- Residual stresses will be calculated from the strains
- The strains will be modeled as previously using the EPSC model of Tome *et al.*

- [1] Carr, D. G., Ripley, M. I., Holden, T. M., Brown, D. W. and Vogel, S. C. "Residual stress measurements in a Zircaloy-4 weld by neutron diffraction" submitted to *Acta Materialia* (accepted May 04)
- [2] Carr, D. G., Ripley, M. I., Brown, D. W. Vogel, S. C. and Holden, T. M. "Residual stresses in a Zircaloy-4 weld" Presented at 2nd International Conference on Stress Evaluation by Neutron and Synchrotron Radiation (Mecasens II), Manchester, UK, 8-9th September, 2003

IMPORTANT! List or attach a list of publications resulting from this experiment (published or in press).

REPORT ON EXPERIMENT (Please Type)

Submit all experiment reports to:

LANSCE User Office, MS H831, Los Alamos National Laboratory, Los Alamos, NM 87545

Experiment was carried out at: Local Contact Proposal # ~~LANSCE Use Only~~ X Manuel Lujan Jr. Neutron Scattering Center
Rex Hjelm 2003048 Report Rec'd Weapons Neutron Research Facility
FP/Instrument Used 20030497/15/04 WNR/Blue Room LQD

Title

Investigation of Radiogenically Produced ^3He in Erbium Dihydride Systems: Bubble Nucleation and Formation. Authors and Affiliations

JF Browning, Sandia National Laboratories

GS Smith, Oak Ridge National Laboratory

RP Hjelm, Los Alamos national Laboratory

GM Bond, New Mexico Institute of Mining and Technology

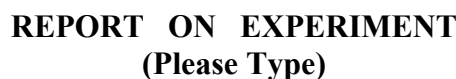
Experiment Report

Experiments carried out under proposal numbers 2003048 and 2003049 are part of a larger study intended to develop a scientific understanding of helium evolution and its resulting affects on the structure of metal tritide thin films. This work represents a continuation of a multi-year project (3–4 years) to study the helium bubble formation and evolution. The importance of this problem stems from the fact that metal tritide thin films are incorporated into neutron generators, a component of nuclear weapon systems.

Observed changes in the helium bubble structure for an erbium tritide sample set as well as changes in scattered intensity are presented below. The resulting change in bubble spacing while maintaining the observed symmetry is of interest. Data analysis and interpretation are ongoing. We are continuing efforts to gain an understanding of the physical mechanism responsible for the observed behavior and have engaged the help of a solid state theorist in those efforts.

Experiment Report (continued)

IMPORTANT! List or attach a list of publications resulting from this experiment (published or in press).



LANSCCE User Office, MS H831, Los Alamos National Laboratory, Los Alamos, NM 87545

Experiment Report

Turbine blades used in both land-based gas turbines and in aircraft engines are made up of single-crystal nickel-base superalloys. Technology for making and usage of these alloys for high-temperature applications is a mature field. The high-temperature strength of these alloys is related to the presence of coherent, hard $L1_2$ ordered γ' precipitates within the γ (face-centered cubic crystal structure) matrix. The important microstructural parameters are volume fraction, size, shape, and composition of γ' phase, as well as lattice mismatch between γ' and γ phases. The above parameters are affected by the bulk composition, heat-treatment conditions, stress, and time. Previous research suggests that on application of stress at high temperature, the hard γ' phase does not take part in the plastic deformation, and plastic deformation is concentrated in the soft γ phase. A critical requirement is to describe the above phenomenon under *in situ* thermomechanical conditions—more importantly in different crystallographic directions. In this research, the lattice parameters of γ' and γ phases in a single-crystal nickel-base superalloy were investigated with a time-of-flight (TOF) neutron-diffraction technique. The unique capability of two detector banks at perpendicular directions in the Spectrometer for Materials Research at Temperature and Stress (SMARTS) facility allowed us to describe the dynamics of lattice strains during the application of tensile stress at different crystallographic directions.

In this research, we used a commercial PWA1480 single-crystal alloy obtained after a standard heat treatment. The focus of this high-temperature experiment was to measure interplanar spacing of γ' and γ phases at two different crystallographic directions [001] and [010] while the single-crystal sample was subjected to a tensile stress of 100 MPa [see Fig. 1]. The samples were heated to 1473 K at a rate of $2.7 \text{ K}\cdot\text{s}^{-1}$ and cooled at the same rate to room temperature. One of the samples was loaded to ~ 100 MPa of tensile stress before cooling to room at high temperature. The TOF positions and intensity of diffraction peaks of both γ' [$\{001\}$, $\{002\}$, and $\{004\}$] and γ [$\{002\}$ and $\{004\}$] phases were measured *in situ* at a time resolution of 3 minutes.

Experiment Report (continued)

An overview of the measured superlattice interplanar spacing from γ' phase $a\{001\}_{+90}$ from +90 detector, $a\{001\}_{-90}$ from -90 detector and area of the peaks showed that the volume fraction of γ' decreases with an increase in temperature and increases with a decrease in temperature. This variation is nearly identical for both detectors at two different directions and there was no difference between conditions with and without the application of stress. In contrast, on application of stress at high temperature, an increase in $a\{001\}_{-90}$ observed while $a\{001\}_{+90}$ decreased as expected from Poisson's effect. Detailed analysis of the thermal and mechanical lattice strains showed interesting observations. The ratio of $\varepsilon\{001\}_{-90}$ to $\varepsilon\{001\}_{+90}$, as expected, on heating the ratio remains closer to a value of one [see Fig. 2]. The results also show that there is no asymmetry between $\varepsilon\{001\}_{-90}$ and $\varepsilon\{001\}_{+90}$. This indicates that the strains are purely thermal in nature. In contrast, while cooling with a stress of 105 MPa, the ratio was found to increase in a nonlinear fashion with a reduction in temperature. This effect may be due to difference in lattice stability in different crystallographic directions and also a change in the modulus with temperature. The reasons for such variations are being evaluated with theoretical models.

The implication of this research is that the computational models that assume hard γ' phase and complete strain partitioning to γ phase may be simplistic. The results indicate that the strain partitioning is much more complex under continuous cooling conditions and will have large impact on describing the performance of these single-crystal alloys. We have also proved that this continuous-cooling technique allows separating thermal strains and mechanical strains in a two-phase material. Further detailed analysis of lattice misfit and stability of γ phase are also being pursued in addition to analysis of isothermal data. The above measurements will be compared with thermodynamic calculations.

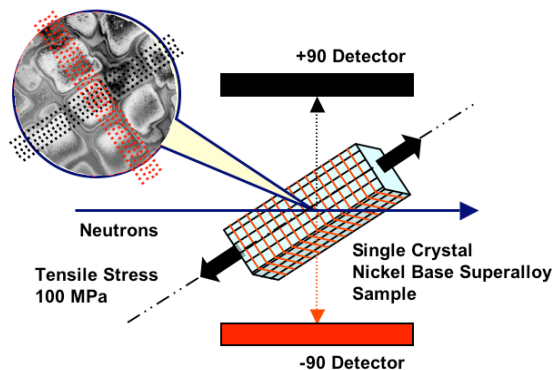


Figure 1. Schematic illustration of the experimental geometry for the present test. The +90° detectors detect the changes in inter planar spacing of one set of $\{001\}$ (black colored), while the -90° detectors detect the changes in inter planar spacing of $\{010\}$ planes (red colored) at 90° degrees to $\{001\}$ planes.

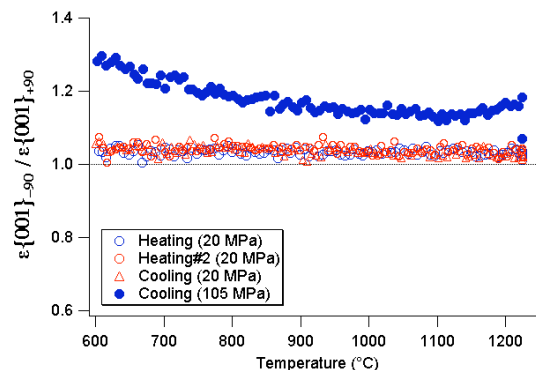


Figure 2. Ratio of measured γ' lattice strains based on $\{001\}$ superlattice reflection in -90 and +90 detector banks as a function of temperature during continuous heating and cooling with and without imposed load of 105 MPa.

IMPORTANT! List or attach a list of publications resulting from this experiment (published or in press).

Submit all experiment reports to:

LANSCCE User Office, MS H831, Los Alamos National Laboratory, Los Alamos, NM 87545

Experiment was carried out at:		Local Contact	Proposal #	<i>LANSCE Use Only</i>
<input checked="" type="checkbox"/>	Manuel Lujan Jr. Neutron Scattering Center	M. Hehlen, F. Trouw	2003054	Report Rc'd 6/8/04
<input type="checkbox"/>	Weapons Neutron Research Facility	FP/Instrument Used		
<input type="checkbox"/>	WNR/Blue Room	PHAROS		

Title

Lattice Dynamics of Relaxor Ferroelectrics

Authors and Affiliations

W. Dmowski, T. Egami, Department of Materials Science & Eng., University of Tennessee

I.-K. Jeong, R. H. Heffner, Los Alamos National Laboratory

J.-S. Park, K.-S. Hong, Seoul National University

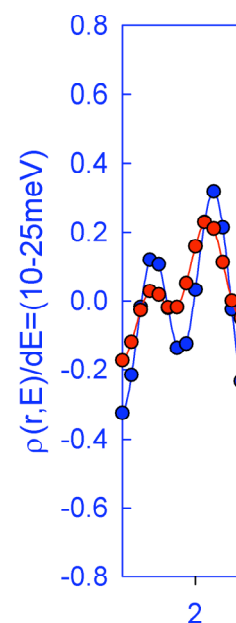
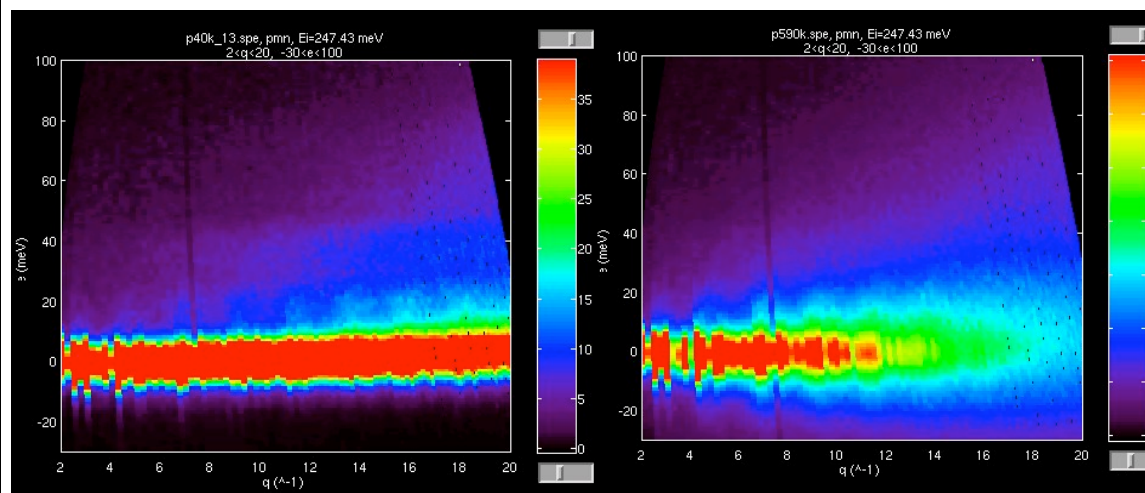
Experiment Report

Typical ferroelectric material exhibits sharp transition temperature (T_c) from the ferro-electric phase having spontaneous polarization to para-electric state upon heating¹. So called relaxor ferroelectrics are characterized by an extended transition range in temperature, on the order of 100 degrees, making peak in a dielectric susceptibility very diffuse. Susceptibility peak is frequency dependent with a broad relaxation spectrum. This diffuse transition is ascribed to the presence of local polar domains above formal T_c . Ceramic relaxor ferroelectrics are a class of lead based perovskite type compounds with the general formula $Pb(B_1, B_2)O_3$ where B are mixed valence cations such as n (like Mg^{2+} , Zn^{2+} , Ni^{2+} , Sc^{3+} , Fe^{3+}) and B_2 is a higher valence cation (like Nb^{5+} , Ta^{5+} , W^{6+}). Pure lead magnesium niobate (PMN or $Pb(Mg_{1/3}Nb_{2/3})O_3$) is a representative of this class of materials with a Curie point at $-10^\circ C$. The origin of the relaxor behavior is generally attributed to the structural frustration and heterogeneity due to the presence of mixed valence cations in the octahedral B site, but the detailed microscopic origin is yet to be fully understood.

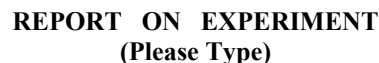
We have measured dynamic structure factor $S(Q, \omega)$ for PMN at three temperatures, close to the so called Burns's temperature, at room temperature and at 40K. The figures present images of the $S(Q, \omega)$ at low and high temperature. It is observed that in the energy range 10-35 meV that dynamic structure factor exhibits much more "structure" at high temperature than at the low one. This observation we ascribe to the "motion narrowing" when oxygen dynamics becomes decoupled from the lead and the local symmetry of Pb atoms become cubic. Furthermore we analyze data by performing Fourier transformation for several energy slices to obtain dynamic pair correlation functions. This dynamic PDF can be compared to the static one, which is obtained from the diffraction experiment to reveal important differences in the structure at different temperatures. Figure 2 shows example of a dynamic PDF obtained for spectra taken at high and low temperature. The most obvious changes appear in the range of 2.4-3.2 Å. Most of the changes involve short and long bonds between Pb and oxygen atoms and indicate that

Experiment Report *(continued)*

Dynamic off-centering of Pb disappears at the Burn temperature.



IMPORTANT! List or attach a list of publications resulting from this experiment (published or in press).



Experiment was carried out at:		Local Contact	Proposal #	<i>LANSCE Use Only</i>
<input checked="" type="checkbox"/>	Manuel Lujan Jr. Neutron Scattering Center	Rex P. Hjelm	2003055	Report Rc'd
<input type="checkbox"/>	Weapons Neutron Research Facility	FP/Instrument Used	10/LQD	10/06/04
<input type="checkbox"/>	WNR/Blue Room			

Authors and Affiliations

Experiment Report

Introduction

The high explosive (HE) material, PBX 9501, is a composite, consisting of a crystalline high explosive (95 wt %) and a polymeric binder (5wt %, Estane + nitroplasticizer). PBX 9501, like other HE materials, possesses both naturally occurring and process-related defects (cracks, voids, etc.). It is well known that microstructural features such as these, can dramatically affect the ignition sensitivity and performance of energetic materials. While these features can be characterized in the raw material, little is known about how they are affected during processing.

Our objective is to explore the effect of pressing intensity on the high explosive microstructure. In the preparation of PBX 9501, variables such as pressing intensity, number of pressing cycles, dwell time, or rest time (between cycles) are often varied in order to achieve nominal density. Although bulk density is met, differences in pressing conditions can lead to variations in microstructure between samples.

We have used SANS in conjunction with the method of *contrast variation* to distinguish scattering arising from the different interfaces (HMX-binder (HB), HMX-voids (HV) and binder-voids (BV)) in the PBX 9501 microstructure. These three interfaces are of interest because they influence the transmission of microstresses through the materials under shock conditions. Quantification of the surface area at these interfaces and how it evolves with different pressing conditions will aid in the development of full-scale constitutive models for both pristine and damaged materials.

Experiment and Results

Experiment Report (continued)

$$I(Q) = \frac{2\Delta\rho}{Q^4} [\Delta\rho_{HB}^2 S_{HB} + \Delta\rho_{HV}^2 S_{HV} + \Delta\rho_{BV}^2 S_{BV}] = \frac{2\Delta\rho}{Q^4} I_p, \quad (1)$$

where, $\Delta\rho_{ij}$ and S_{ij} are the scattering length density contrast and surface area, respectively, between phases i and j . The use of the contrast variation technique enables the scattering arising from the different interfaces to be separated. From Eq. 1, we see that I_p shows a quadratic dependence on the scattering length density of the binder:

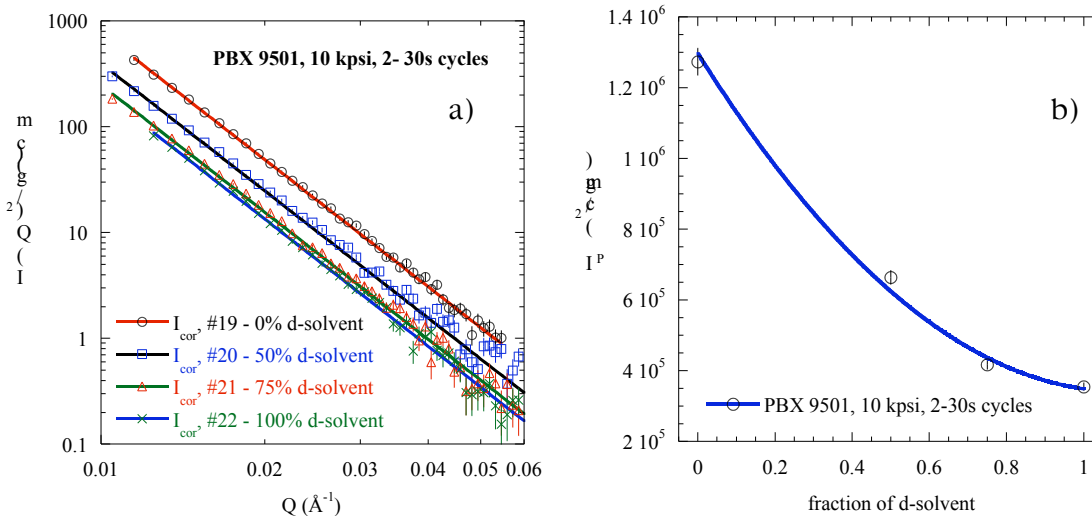
$$I_p(\Delta\rho_B) = [\Delta\rho_{HB}^2 S_{HB} + \Delta\rho_{HV}^2 S_{HV} + \Delta\rho_{BV}^2 S_{BV}] = A\Delta\rho_B^2 + B\Delta\rho_B + C. \quad (2)$$

The parameters A , B and C are related to the different surface areas; the solution of Eq. 2 will yield the individual surface areas.

SANS lineshapes (corrected for solvent and empty cell scattering), measured at different contrasts, for samples prepared with an applied pressure of 10 kpsi, are shown in Fig 1a. The solid lines in the figure are the result of fits to Eq. 1. The values of I_p obtained from these fits are plotted in Fig. 1b as a function of the fraction of deuterated solvent (scattering length density contrast) used to swell the binder. The solid line in Fig. 1b is the result of a fit to Eq. 2. The surfaces areas determined from the fit are $S_{HB} = 1.19 \pm 0.04 \text{ m}^2/\text{g}$, $S_{HV} = 0.20 \pm 0.04 \text{ m}^2/\text{g}$ and $S_{BV} = 0.04 \pm 0.02 \text{ m}^2/\text{g}$. Analysis of the remaining data is underway.

Summary

SANS and contrast variation measurements were made on samples of PBX 9501 that were prepared with applied pressures ranging from 5–29 kpsi. Analysis of the data for samples pressed as 10 kpsi has confirmed that we can separate the scattering signal arising from the three interfaces of interest. The associated surface areas (S_{HB} , S_{HV} , and S_{BV}) were measured. The results of our study will help determine how differences in pressing conditions can lead to variations in the microstructure of high explosive systems. The ability to measure S_{HB} , S_{HV} , and S_{BV} in a pressed sample is novel for these systems and may aid in the understanding of how microstresses are propagated through HE samples under shock.



IMPORTANT! List or attach a list of publications resulting from this experiment (published or in press).

Submit all experiment reports to:
 LANSCE User Office, MS H831, Los Alamos National Laboratory, Los Alamos, NM 87545

Experiment was carried out at:	Local Contact	Proposal #	<i>LANSCE Use Only</i>
<input checked="" type="checkbox"/> Manuel Lujan Jr. Neutron Scattering Center	Daemen, Luc	2003064	Report Re'd 12/12/03
<input type="checkbox"/> Weapons Neutron Research Facility	FP/Instrument Used		
<input type="checkbox"/> WNR/Blue Room	4 / HIPPO		

Title

2003064 "Neutron Powder Diffraction in Highly Absorbing Materials"

Authors and Affiliations

LANL Contributors: Heather Volz (LANSCE-12/NMT-16), Joyce Roberts (LANSCE-DO), Angus Lawson (MST-8), Luke Daemen (LANSCE-12), Sven Vogel (LANSCE-12), Darrick Williams (LANSCE-12), Tim Medina (LANSCE-12), Mike Geelan (LANSCE-12), Kathy Lovell (LANSCE-12), Ross Sanchez (LANSCE-12), Dave Teter (MST-6), Luis Morales (NMT-16), Heather Hawkins (NMT-16).

Experiment Report

- Experiments were performed on the High-Pressure Preferred Orientation diffractometer (HIPPO) to investigate the effects of absorption on neutron diffraction data analysis, and to optimize sample geometry and experimental parameters for strong neutron absorbers. Surrogate materials (dysprosium and erbium) possessing absorption characteristics similar to those of ^{239}Pu have been used to facilitate these preliminary investigations.

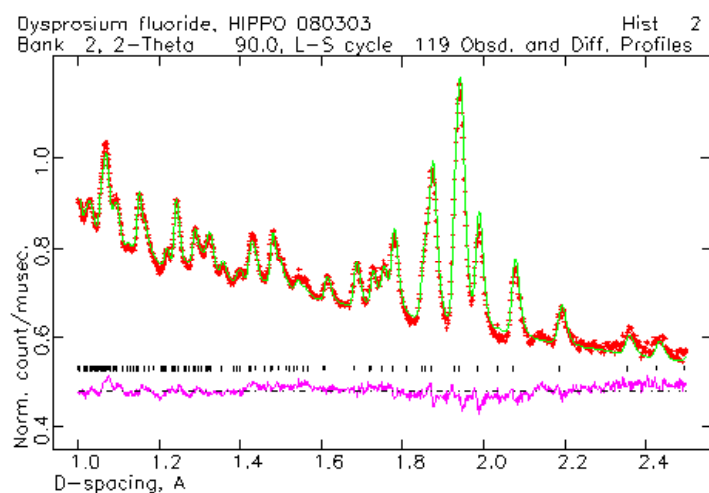


Figure 1: Data (symbols) and preliminary analysis (line fit) of a sample with strong absorption. Based on knowledge gained from experiments with these surrogate materials, Pu experiments will be designed to maximize information gathered from minimal material.

- More specifically, samples investigated on HIPPO thus far include the following: ErF_3 and DyF_3 to study the reliability of the structure factor (and atom positions) in the presence of absorption; flat foils of Dy and Er of varying thicknesses placed perpendicularly to the incident beam; and foils wrapped in an annular (double-walled) cylindrical vanadium sample can that has shown favorable results with absorbing materials at other

Experiment Report (continued)

institutions. With the help of the HIPPO team, we have succeeded in collecting data for our full allotted three days. Early difficulties with noise have been investigated and mitigated. Data collection time on HIPPO of one to one-and-a-half hours per sample was found to be sufficient.

- To date, the time-of-flight data have been collected and analyzed using the Rietveld method with a Debye-Scherrer absorption correction (i.e., Figure 1). However, there are questions as to the applicability of this model to a very strong neutron absorber. Future work will be done on examining the assumptions of standard absorption corrections in software programs such as GSAS, and will possibly lead to enhancements of data analysis techniques. Based on our initial results, we requested additional beam time in the Spring of 2004 to more thoroughly investigate aspects of absorption, and have recently learned that we were granted 4 days (#2003190).
- Attempts have been made to collect a neutron diffraction pattern from elemental dysprosium and erbium powders in an annular geometry. To date, all powders were unintentionally in hydride form. The supplier has been contacted and will be sending a replacement shipment of dehydried powders. Concurrently, staff in MST-6 have generously helped in dehydriding the original shipment of rare-earths on their vacuum furnace. We anticipate re-collecting these data with our Spring 2004 beam time.
- By using parameters obtained by refining neutron diffraction data of the strong absorber dysprosium and similar scattering length erbium, simulated diffraction patterns of ^{239}Pu have been calculated. Values for the histogram scale factor and background functions make the simulations more realistic, and will assist with planning upcoming experiments.
- The texture of Dy and Er foils (two different thicknesses of each element) have been measured on HIPPO in order to correctly account for these effects. Preliminary analysis of the data shows a strong texture consistent with the foil normal and rolling direction for a hexagonal close packed metal, as described in the literature. An example is shown in Figure 2.

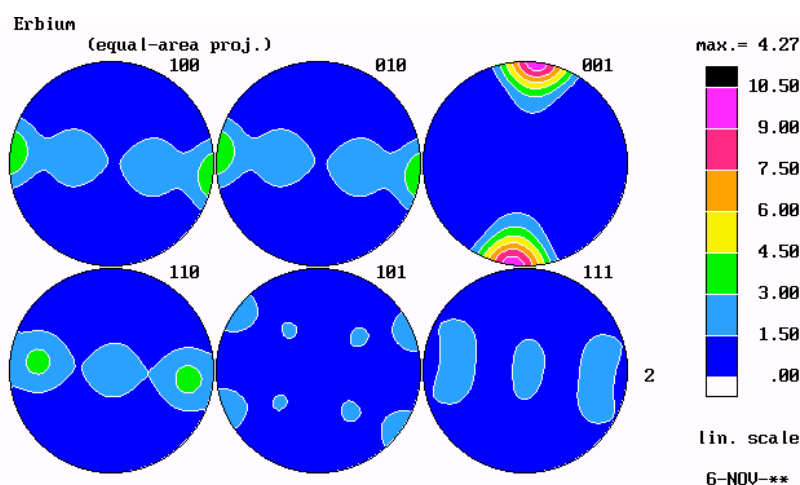


Figure 2: Texture map of erbium foil, 225 microns thickness, analyzed with Debye-Scherrer corrections for absorption. Converged chi-squared equals 1.12. Texture index of roughly 3. Courtesy of Sven Vogel, LANSCE-12.

IMPORTANT! List or attach a list of publications resulting from this experiment (published or in press).

Submit all experiment reports to:
LANSCE User Office, MS H831, Los Alamos National Laboratory, Los Alamos, NM 87545

Experiment was carried out at:	Local Contact	Proposal #	LANSCE Use Only
<input checked="" type="checkbox"/> Manuel Lujan Jr. Neutron Scattering Center	Hjelm, Rex	2003068	Report Rc'd <div style="border: 1px solid black; padding: 2px;">6/30/04</div>
<input type="checkbox"/> Weapons Neutron Research Facility	FP/Instrument Used		
<input type="checkbox"/> WNR/Blue Room	10 / LQD		

Title

2003068 “Low-Q Diffractometer Investigation into Highly Absorbing Materials”

Authors and Affiliations

LANL Contributors: Heather Volz (LANSCE-12/NMT-16), Joyce Roberts (LANSCE-DO), Rex Hjelm (LANSCE-12), Angus Lawson (MST-8), Luke Daemen (LANSCE-12), Robert Hanrahan (MST-6), Luis Morales (NMT-16), Kevin Kupcho (LANSCE-12)

Experiment Report

- The goal of this experiment was to investigate the small-angle neutron scattering behavior of strong neutron absorbers. Surrogate materials (dysprosium and erbium) possessing absorption characteristics similar to those of ²³⁹Pu have been used to facilitate these preliminary investigations.
- Dysprosium and erbium foils with known defects (see list of samples below) were studied with LQD (flightpath 10) in order to verify a model for highly absorbing materials. This FORTRAN code accounts for non-uniformities in the samples by fitting the raw transmission data with three parameters (mean thickness of the sample, variations from that mean thickness, and “pinholes,” or defects that allow additional beam to be transmitted through the foil), and correcting the transmission data for these effects. We thank MST-6 for electrochemically preparing systematically defective foils for this study.
- Once our transmission model is validated for these defective strong neutron absorbers, it can be used to analyze previously collected ²³⁹Pu data, which will lead to efficient, directed future experiments on Pu to explain microstructural properties, such as helium bubble formation.
- Data were collected from the following sets of samples on 11/12/03-11/16/03 and 11/22/03 using an 8mm collimator.
 - o Instrument standards: empty cell, silica, silver behenate, etc.
 - o Sample standards: various thicknesses of dysprosium foils (4 sizes) and erbium foils (3 sizes), as-received from the manufacturer
 - o Dysprosium and erbium wedge-shaped samples (an electrochemically tapered sample of each)

Experiment Report *(continued)*

- o Electrochemically pitted dysprosium and erbium samples (4 samples total)
 - o Three of the same pitted Dy foils with an additional piece of as-received 0.006" Dy stacked in the beam to reduce transmission through the pinholes
 - o A sample each of dysprosium and erbium foil with roughly sinusoidally varying thickness variations, created by a mask during etching
 - o The same instrument standards with an additional piece of as-received 0.006" Dy stacked in the beam to examine the effects of a strong neutron absorber on the standards' data appearance
 - o A dark current measurement
- There was a lower than normal beam current on those days (roughly 70 micro-amps), but the lower current may actually be desirable for our LQD data.
 - At the writing of this report, the data from the above samples have been collected and are awaiting analysis. Now that the code is complete to analyze LQD data collected with the new and improved detector, the transmission data can be properly reduced and entered into the new model. However, preliminary results with this model are confusing. Unrealistic results for thickness variations and extremely large errors necessitate further examination of the code to eliminate the possibility of faults in the program.
 - Work to be carried out in the near future will focus on debugging of the code to correct the transmission data for sample non-uniformities. Then, the neutron scattering from the varieties of dysprosium and erbium samples can be confirmed, which will lead to proper interpretation of the previous ^{239}Pu data.

IMPORTANT! List or attach a list of publications resulting from this experiment (published or in press).

Submit all experiment reports to:
LANSCCE User Office, MS H831, Los Alamos National Laboratory, Los Alamos, NM 87545

Experiment was carried out at:	Local Contact	Proposal #	LANSCCE Use Only
<input type="checkbox"/> Manuel Lujan Jr. Neutron Scattering Center	J. Majewski	2003075	Report Rc'd
<input type="checkbox"/> Weapons Neutron Research Facility	FP/Instrument Used		7/14/04
<input type="checkbox"/> WNR/Blue Room	SPEAR		

Title Morphology of Toughened Anti-Corrosion Films
Authors and Affiliations Guirong Pan, University of Cincinnati Dale W. Schaefer, University of Cincinnati Michael S. Kent, Sandia National Labs Hyun Yim, Sandia National Labs

In the practice of silane surface treatment for corrosion protection, bridged silanes with six hydrolyzable alkoxy groups show superior performance compared to monosilanes.¹⁻² Since the silanes are believed to act as water barriers, understanding of water-silane interaction is essential for further optimizing films for anticorrosion application. So far, we studied the water barrier properties of Bis-[triethoxysilylpropyl]-tetrasulfide (bis-sulfur) and Bis-[trimethoxysilylpropyl]amine (bis-amino) and their mixture using neutron reflectivity (NR). Performance tests show that a Bis-sulfur/bis-amino (3/1) mixture shows greatly enhanced corrosion resistance compared to the two individual silanes.² We attempt to clarify the mechanism underlying these performance results by investigating the structure of films and the response to water.

During previous beam time, we completed a study of bis-amino silane film.³ We have now completed the study of bis-sulfur silane and mixed sulfur-amino silane films. We use NR to study morphology of pristine and water conditioned films. To track water penetration, heavy water (D₂O) is used. NR data were obtained for the films as-prepared, after exposure of the film to saturated D₂O vapors at both room temperature and 80°C, and again after re-drying. The test in the re-dried state determines if there is chemical degradation of the film.

Figure 1a shows the reflectivity of bis-sulfur film as-prepared, after exposure to D₂O at room temperature for 15h and after re-drying. After conditioning, the only obvious change in R(q) is that the first minimum is lower and the tail of the curve is slightly higher relative to the as-prepared state. This behavior indicates minimal swelling and contrasts with the behavior of bis-amino silane, which shows a substantial increase relative to the as-prepared state after water conditioning. The best-fit SLD profiles corresponding to the curves through the data lines are shown in figure 1b. For the as-prepared state, the film thickness is 222Å, which is in

Based on these values, we conclude that, at least for silicon wafer substrate, the water barrier ability of mixture silane is not special but roughly that of both components weighted by their volume fraction. Since no synergistic effect is detected in the mixed film, it is reasonable to speculate that substrate might be the key factor to induce the superior anticorrosion properties of mixed silane. We will use Al-coated silicon as substrate to further investigate the interface issues.

For all three silanes, reflectivity is reversible at room temperature; therefore, water is physically absorbed. At 80°C, however, the reflectivity after redried remains elevated relative to the as-prepared film due to formation of Si-OD in bis-sulfur silane and the exchange of the amine proton with a deuteron in bis-amino silane.

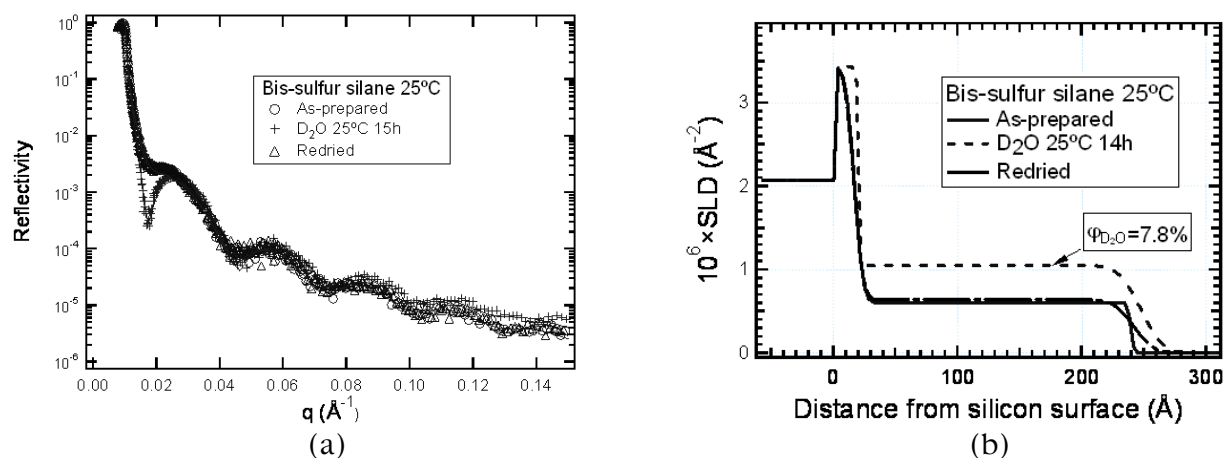
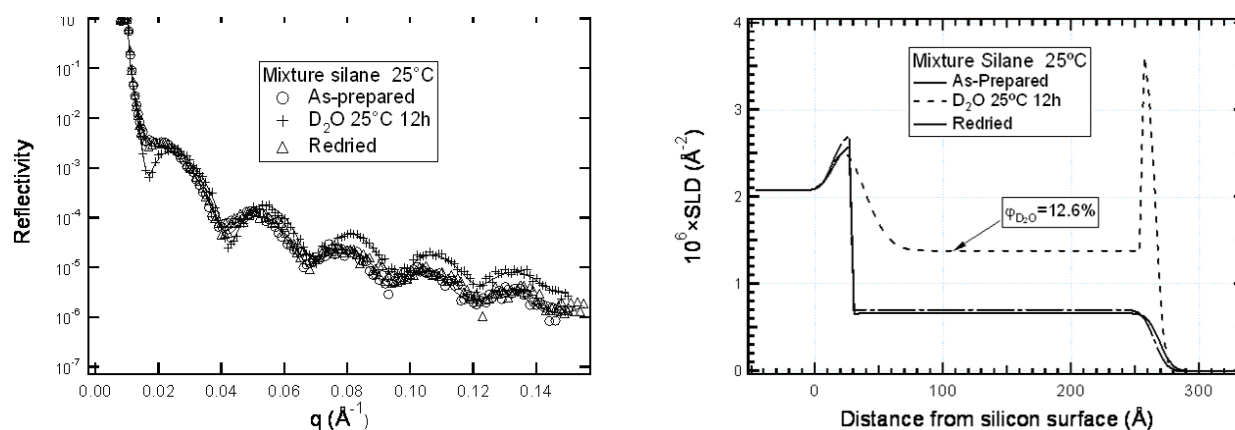


Figure 1 (a): Neutron reflectivity data from bis-amino film as-prepared, after exposure to D₂O at room temperature for 15 h and after re-drying . The curves through the data correspond to best fits using model SLD profile. (b) Best-fit scattering length density profiles corresponding to the curves through the data in (a)



IMPORTANT! List or attach a list of publications resulting from this experiment (published or in press).

(1) Pan, G.; Yim, H.; Kent, M.; Majewski, J.; Schaefer, D. W. *J. Adhesion Sci. Technol.* **2003**, *17*, 2175-2189.

(2) Pan, G.; Yim, H.; Kent, M.; Majewski, J.; Schaefer, D. W. In *Silane and Other*

Submit all experiment reports to:
LANSCE User Office, MS H831, Los Alamos National Laboratory, Los Alamos, NM 87545

Experiment was carried out at:	Local Contact	Proposal #	LANSCE Use Only
<input checked="" type="checkbox"/> Manuel Lujan Jr. Neutron Scattering Center	J. Majewski	2003084	Report Rc'd
<input type="checkbox"/> Weapons Neutron Research Facility	FP/Instrument Used		9/13/04
<input type="checkbox"/> WNR/Blue Room	FP9/SPEAR		

Title

DENSITY AND MOLECULAR CONFIGURATION OF POLYMERS AT SURFACES

Authors and Affiliations

Jacob N. Israelachvili, Nobuo Maeda, Nianhuan Chen, University of California, Santa Barbara
Jarek Majewski, Erik Watkins, Dhaval Doshi, Los Alamos National Laboratory

Experiment Report

The surface state of polymers is an important factor that determines the adhesion, adhesion hysteresis and friction between polymer surfaces. The surface state of polymers can be effectively altered by UV radiation under appropriate atmospheres. UV radiation of polystyrene (PS) in air, for example, is known to result in scission of the polymer chains at the surfaces. UV radiation of poly-vinylbenzylchloride (PVBC) in air, on the other hand, may crosslink the polymer surface. Although UV radiation in air is a convenient way to modify the surface state of the polymers, it is also expected to oxidize the polymer surfaces. Such oxidization due to UV radiation in air was confirmed by a series of contact angle measurements. However, the chemical structure of oxidized groups or the thickness of the oxidized layer is yet to be characterized.

We tried to investigate the thickness of the oxidized surface layer on these polymers that were exposed to UV radiation for different times using the small angle neutron reflectometry. The PS or PVBC was spun-coat on a silicon wafer at 2000 RPM for 30 seconds from either 1 or 2 weight % solution of toluene. After the sample was measured by SPEAR, the polymer film was subsequently subjected to UV light.

Below we summarize the results for PVBC, which is known to crosslink upon UV radiation.

The data prior to UV radiation showed a PVBC layer of 72nm thick. After 5 minutes of UV radiation in air, the thickness shrunk to about 58nm. At the same time, a thin (about 3nm thick) layer appeared at the top of the PVBC layer. The shrinkage of the thickness of the PVBC layer is most likely a result of the crosslinking of the polymer and the new thin layer at the top is most likely an oxidized layer. After 10 minutes of UV radiation, the total thickness of the PVBC layer shrunk further, to about 40nm. The entire layer now appears to have the same properties as the thin top layer observed after 5 minutes of UV radiation.

Our result is consistent with the scenario that the oxidized layer initially forms at the top of the polymer layer, then grows toward inside the polymer layer, ultimately oxidize the entire polymer layer. The timescale of full oxidization of the polymer layer of tens of nanometers appears to be of the order of 10 minutes.

Submit all experiment reports to:
LANSCE User Office, MS H831, Los Alamos National Laboratory, Los Alamos, NM 87545

Experiment was carried out at:	Local Contact	Proposal #	LANSCE Use Only
<input checked="" type="checkbox"/> Manuel Lujan Jr. Neutron Scattering Center		2003089	Report RcId
<input type="checkbox"/> Weapons Neutron Research Facility	FP/Instrument Used		
<input type="checkbox"/> WNR/Blue Room	NPDF		

Title
Local structure measurements in selected quantum paraelectrics

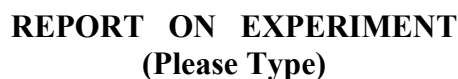
Authors and Affiliations
I.-K. Jeong, R. H. Heffner, T. Darling, T. Park, L.-C. Tung, J. Sarroa, and J. D. Thompson, LANL

Experiment Report

SrTiO₃ and KTaO₃ are quantum paraelectrics, polarizable materials which do not undergo ferroelectric transitions at finite temperature, presumably due to quantum fluctuations [1]. Ferroelectricity can be induced in these systems by the application of external electric fields, mechanical stress or introducing substitutional impurities into the lattice. For example, Bednorz and Müller observed a crossover from an XY quantum ferroelectric state to a *diffusive* state in Sr_{1-x}Ca_xTiO₃ [1]. Since then, it has been established that these doped systems remain paraelectric when the impurity concentration x is low, undergoing a paraelectric-to-ferroelectric transition when $x > x_c$. With increasing x the Curie temperature T_C is $(x-x_c)^{1/2}$. When $x > x_r > x_c$ the system can exhibit *relaxor* behavior, where the permittivity peak broadens and the temperature of the peak maximum is frequency dependent, much as in the analogous magnetic spin glass systems.

In Sr_{1-x}Ca_xTiO₃, two scenarios were proposed for the origin of local polarization: (i) off-center displacements of Ca²⁺ ions, (ii) Ca²⁺ substitution for Ti⁴⁺. Since Ca²⁺ ionic size (0.99 Å) is smaller compared to Sr²⁺ (1.12 Å), Ca²⁺ substitution for Sr²⁺ sets up random strains which couple to the polarization. Alternatively, some of the Ca²⁺ ions may substitute Ti⁴⁺. In this case, to make a charge balance, oxygen vacancy, V_o, can be created in an oxygen octahedron, forming a Ca²⁺-V_o neutral center. Such Ca²⁺-V_o centers form dipoles. These scenarios have never been tested experimentally. We have performed local structural studies of Sr_{1-x}Ca_xTiO₃ using neutron pair distribution function (PDF) to find evidence for Ca off-center displacements and Ca²⁺ substitution for Ti⁴⁺.

Figure 1 shows the PDF spectra of Sr_{1-x}Ca_xTiO₃ ($x=0, 0.011, 0.06, 0.1$) at T=15K. We observe small but noticeable changes in the PDF spectra with increasing Ca concentration. In particular, Sr/Ca/O-O



Experiment was carried out at:		Local Contact	Proposal #	LANSCE Use Only
<input checked="" type="checkbox"/>	Manuel Lujan Jr. Neutron Scattering Center	Dr. Don Brown	2003098	Report Rc'd 7/16/04
<input type="checkbox"/>	Weapons Neutron Research Facility	FP/Instrument Used	2003235	
<input type="checkbox"/>	WNR/Blue Room	SMARTS		

Influence of Fatigue Damage on the Deformation Behavior of Haynes 230 Nickel Based Superalloys

Tarik A. Saleh, P.K. Liaw, H. Choo
Department of Materials Science, University of Tennessee, Knoxville

D. L. Klarstrom
Haynes International, Inc.

Haynes 230 is a nickel based superalloy that is used in many fatigue intensive applications such as turbine engines. This experiment was designed to explore the evolution of lattice and internal strains under high-cycle fatigue conditions. These results are a part of a comprehensive study of the fatigue behavior of this alloy, also including low-cycle fatigue and high temperature conditions.

Three separate experiments were performed. The first was a typical in situ loading experiment. The sample was loaded slowly from 20 MPa to 700 MPa and then unloaded to 20 MPa. The loading was paused periodically for diffraction experiments to be performed. Diffraction patterns were taken at 22 points during loading and 3 during unloading.. This experiment served as the one cycle fatigue test and was our baseline for comparison.

The second experiment was a 110 cycle fatigue test. The testing conditions were at a R ratio of 0.1 ($\sigma_{\min}/\sigma_{\max}$, where σ_{\min} and σ_{\max} are the applied minimum and maximum stresses, respectively) and a σ_{\max} of 700 MPa. Diffraction patterns were taken at 20 MPa before the test began and after the 110 cycles were completed. Additionally, a diffraction pattern was taken at σ_{\max} for each cycle.

The third experiment was a complete fatigue test under the same conditions as the second ($R = 0.1$, $\sigma_{\max} = 700$ MPa). Testing was paused approximately every half order of magnitude to take a diffraction pattern at σ_{\min} and σ_{\max} . Cycling occurred at a frequency of 10 Hz between diffraction patterns. Due to experimental constraints, diffraction patterns were taken for 45 minutes, instead of the 15 minute patterns taken during the first two experiments.

Experiment Report (continued)

Discussion

Figure one shows the internal strain versus stress loading curve for the one cycle test and the 110 cycle test. The 111 and 200 axial reflections are shown. There are very few differences between the internal and residual strains between the two tests. However if we consider the complete test, shown in Figure 2, there is a subtle relaxation of internal strains over the first 100-1000 cycles. Previous work done on low cycle fatigue have shown large increases in internal strains over the initial cycles of fatigue, followed by a subtle relaxation of strain. It is possible that the large macroscopic strain developed over the first cycle of this test saturated the generation of internal strains that were seen in previous tests. Further experiments will be conducted at smaller macroscopic strains to test this hypothesis.

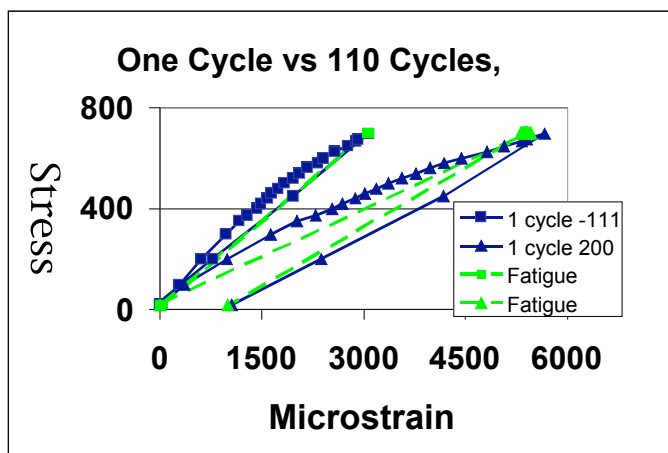


Figure 1: Comparison Between One Cycle of Fatigue and 110 Cycles, 111 and 200, Axial Direction

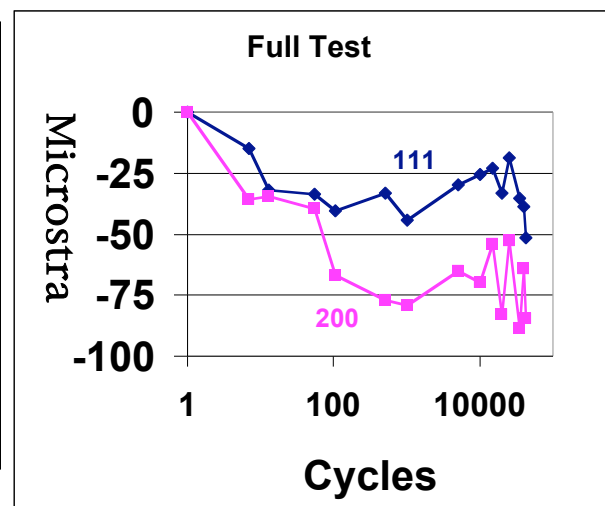


Figure 2: Relaxation of Strains in the Axial Direction During the Full Test

Conclusions

In tension-tension fatigue, at high loads, the internal strains saturate in the first few cycles. Under the conditions tested, the residual strain after a uniaxial tension test, 110 cycles of fatigue and 45,000 cycles of fatigue is very similar. There are slight trends in relaxing residual strains over the first 100-1000 cycles. We are currently exploring the differences between the internal strain development during low-cycle and high-cycle fatigue testing and plan on expanding these experiments to lower stress range.

IMPORTANT! List or attach a list of publications resulting from this experiment (published or in press).

T.A. Saleh et al.: "In Situ Loading Studies of Haynes® 230®" 2004 TMS Annual Meeting, March 2004, Charlotte, North Carolina. Oral Presentation.

T.A. Saleh et. al. "In situ Neutron Studies of Haynes® 230® Nickel Based Superalloy", ANSWER workshop, Knoxville TN 11/03. Poster Presentation (first prize)

T.A. Saleh et. al. "In situ Neutron Studies of Haynes® 230® Nickel Based Superalloy", OakRidge Chapter ASM Student Poster Competitions, Knoxville TN 11/03. Poster Presentation (first prize)

T.A. Saleh et. al. "In situ Studies on the Cyclical Deformation of Haynes® 230® Nickel Based Superalloy" American Conference on Neutron Scattering, College Park, MD 6/04. Poster Presentation

Submit all experiment reports to:
LANSCE User Office, MS H831, Los Alamos National Laboratory, Los Alamos, NM 87545

Experiment was carried out at:	Local Contact	Proposal #	LANSCE Use Only
<input checked="" type="checkbox"/> Manuel Lujan Jr. Neutron Scattering Center	Jarek Majewski	2003116	Report Rc'd 1/29/04
<input type="checkbox"/> Weapons Neutron Research Facility	FP/Instrument Used		
<input type="checkbox"/> WNR/Blue Room	SPEAR		

Title Structure of Synthesized Non-Linear Optical Films
Authors and Affiliations Jeanne Robinson, Hsing-Lin Wang, Jarek Majewski,, Erik Watkins; Los Alamos National Laboratory

Experiment Report	Experiment
<p>When light is transmitted through non-linear optical materials its frequency is changed. By exploiting this property, non-linear optical films can be created for use as second harmonic generators. A variety of such films containing optically active S-AZO molecules were synthesized. Using neutron reflectometry, we examined the structure of these layered, non-linear optical films.</p> <p>S-AZO-C18/d-Stearic acid Bilayers: An octadecyltrichlorosilane (OTS) layer was attached to a quartz or silicon substrate to provide a hydrophobic surface. Then, using the Langmuir Blodgett technique, alternating layers of deuterated stearic acid and S-AZO-C18 molecules were deposited. Samples were prepared both by depositing d-stearic acid first and by depositing S-AZO-C18 molecules first. Additionally, two samples were prepared at different subphase temperatures.</p> <p>The following samples were prepared and measured:</p> <ul style="list-style-type: none"> • Silicon / d-stearic / S-AZO-C18 @ 10°C • Silicon / d-stearic / S-AZO-C18/ d-stearic / S-AZO-C18 @ 10°C • Silicon / S-AZO-C18 / d-stearic @ 10°C • Silicon / S-AZO-C18 / d-stearic / S-AZO-C18 / d-stearic @ 10°C • Silicon / d-stearic / S-AZO-C18 @ 25°C • Quartz / d-stearic / S-AZO-C18 @ 10°C <p>Box models have been used to fit the bilayer reflectivity measurements. In addition, the quartz bilayer was measured using x-ray reflectometry to better pin down the thickness and roughness parameters.</p>	

Experiment Report (continued)

Figure 1 compares the X-Ray and Neutron SLD profiles for a single bilayer

Figure 2 compares the SLD profiles of single bilayers with different layer orderings. The first peak represents the SiO₂ layer, followed by a dip representing the OTS layer. After these features, the higher peak represents the d-Stearic layer and the broader, lower scattering layer represents the S-AZO molecules.

Several interesting conclusions can be drawn from these profiles.

Concerning single bilayers:

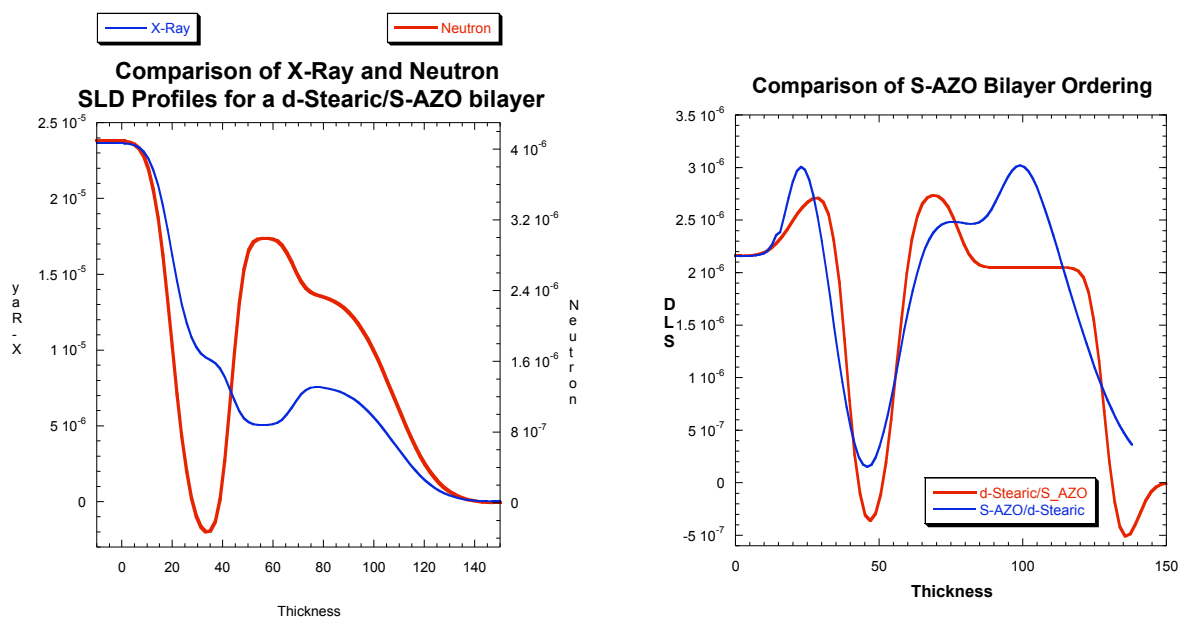
- For S-AZO/d-Stearic ordering the reflectivity data indicates a 50-60 Å length scale
- For d-Stearic/ S-AZO ordering the reflectivity data indicates a 30-30 Å length scale
 - These length scales are larger than any molecule length which indicates more complex packing for these systems than hypothesized
- Deposition order effects packing and layer thickness

Comparing single and multiple bilayers we see that:

- Scattering length density of deuterated peaks decreases as the bilayer number increases
 - Indicates sparsely packed layers
- Decreasing order within layers as the bilayer number increases
 - Indicates intermixing of molecules between adjacent layers
- Model corresponds to the observed decrease in the SHG signal with increasing bilayer number

Fig. 1:

Fig.2 :



IMPORTANT! List or attach a list of publications resulting from this experiment (published or in press).

IMPORT

Submit all experiment reports to:

LANSCCE User Office, MS H831, Los Alamos National Laboratory, Los Alamos, NM 87545

Experiment was carried out at:		Local Contact	Proposal #	<i>LANSCE Use Only</i>
<input checked="" type="checkbox"/>	Manuel Lujan Jr. Neutron Scattering Center	Rex P. Hjelm	2003117	Report Rc'd 6/9/04
<input type="checkbox"/>	Weapons Neutron Research Facility	FP/Instrument Used		
<input type="checkbox"/>	WNR/Blue Room	LQD		

Title: Volume Transition and Internal Structures of Small Poly(*N*-isopropylacrylamide) Microgels and Their Derivatives

Authors and Affiliations: Lise Arleth, Rex P. Hjelm, Los Alamos National Laboratory; Xiaohu Xia, Zhibing Hu, University of North Texas; Jianzhong Wu, University of California at Riverside

Poly(*N*-isopropylacrylamide) (PNIPA) gel is thermally sensitive to the external temperature changes. It absorbs a lot of water at room temperature but exhibits abrupt volume changes and shows a phase separation as the temperature is increased above its lower critical solution temperature (LCST, ~33°C). There are a variety of applications for PNIPA gel, such as artificial muscle, on-off switches, and controlled drug delivery.

In this work, monodispersed, small PNIPA microgel particles were synthesized. The average radius of these particles is less than 50 nm at room temperature, about two orders of magnitude smaller than those reported previously. **Figure 1** shows the PNIPA microgel size distributions below and above the LCST, measured by dynamic light scattering (Data: \circ , 25° C; \bullet , 40° C). Such small microgel particles are advantageous for potential applications in the fields of nanocatalyst, synthetic templating and controlled drug release. Small angle neutron scattering (SANS) and laser light scattering (LLS) were used to give a clear picture of the structural transformation of small PNIPA microgel particles below and above the LCST. We used the high contrast of the particles in D₂O to amplify the SANS signal to provide more detailed, shorter length scale information on the particle size, internal structure, particle-particle and particle-solvent interactions below and above the LCST without radiation damage. All of these aspects are accessible for particles of the size studied here and smaller using the SANS technique.

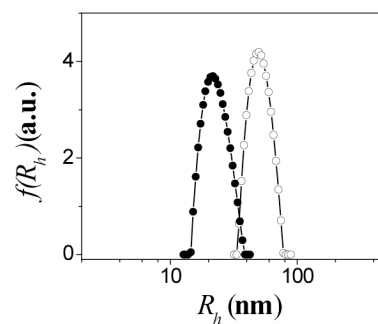


Figure 1

The experiment so far was a success: The neutron scattering data for the

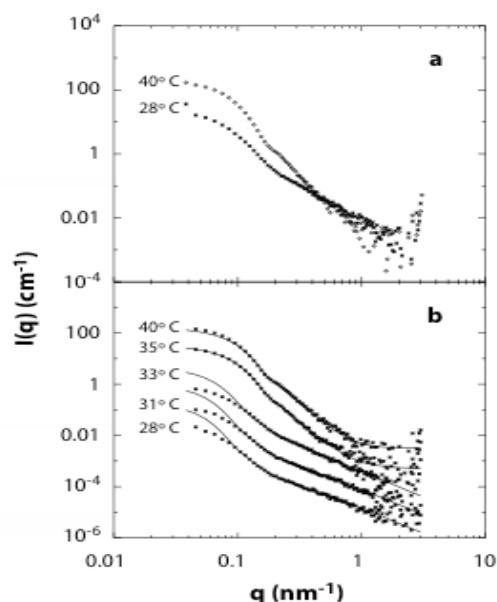


Figure 2

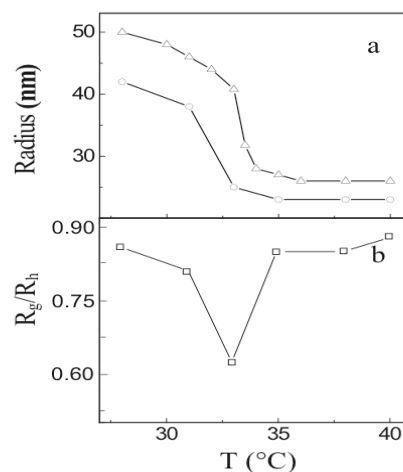


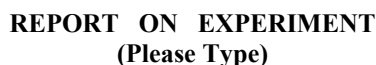
Figure 3

Future study will be focused on a novel microgel possessing the structure of PNIPA-poly(acrylic acid) (PAAc) interpenetrating network (IPN). SANS is the technique we intend to pursue to unveil the IPN microgel internal structure, particle-solvent and particle-particle interactions as a function of temperature and polymer concentration. The mechanism of the IPN colloid inverse thermogelation is likely to be solved through understanding the IPN particle morphology change under different conditions, in contrast to its precursor PNIPA nanoparticles.

Reference:

1. L. Arleth, X. Xia, R. Hjelm, J. Wu, Z. Hu "Volume Transition and Internal Structures of Small Poly(N-isopropylacrylamide) Microgels" *Macromolecules*, (Submitted).

IMPORTANT! List or attach a list of publications resulting from this experiment (published or in press).



Experiment was carried out at:		Local Contact	Proposal #	<i>LANSCE Use Only</i>
<input checked="" type="checkbox"/>	Manuel Lujan Jr. Neutron Scattering Center	Paul Langan	2003118	Report Rc'd 2/24/04
<input type="checkbox"/>	Weapons Neutron Research Facility	FP/Instrument Used		
<input type="checkbox"/>	WNR/Blue Room	PCS		

Neutron Diffraction Study of Rubredoxin from *Pyrococcus furiosus*

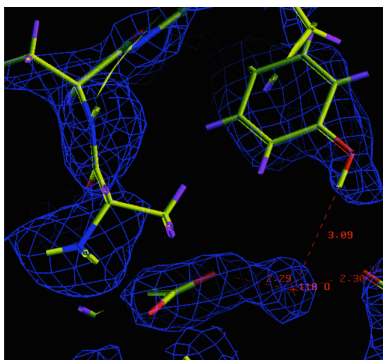
Professor Benno Schoenborn Los Alamos National Laboratory, Manuel Lujan Jr. Neutron Scattering Center
Dr. Paul Langan
Dr. Xinmin Li

In recent years we have been actively engaged in diffraction work on the small (54 amino acid) iron-sulfur redox protein rubredoxin (Rd) from *Pyrococcus furiosus* (Pf), a microorganism found in deep undersea superheated vents. Our original intent was to rationalize why this particular form of rubredoxin is stable for days in boiling water, whereas most other rubredoxins (from bacteria that grow at normal temperatures) are readily denatured within minutes at 100°C. In other words, we were curious to see if the structure of PfRd might be stabilized by an unusually large number of hydrogen bonds and/or salt bridges as compared to other (normal) rubredoxins. In a high-resolution (0.95Å) low-temperature X-ray study we published several years ago,¹ we reported that, contrary to expectations, we did not find an unusually large number of H-bonds in PfRd, and hence the question we were asking remains unresolved to date.

For the present Los Alamos collaboration, the ultimate aim of the project is different, and the rubredoxin samples under investigation are also slightly different. The primary purpose of the present investigation is to study the pro-

Experiment Report (*continued*)

(one in which the tryptophan in the #3 position is replaced by tyrosine). Three different samples of this W3Y mutant have been prepared, in which the protein was boiled in D₂O for 0, 30, and 60 minutes prior to crystallization. We have recently collected a room temperature data set for one of the samples at the PCS at medium resolution (2.1 Å). Data were measured from nine crystal settings, each of approximately 12 h duration. The strategy used was to collect data from an octant of reciprocal space by scanning the crystal (longest dimension of 1.5 mm) around its spindle axis in three steps of 30° in ω . The data over the wavelength range 0.6-0.7 Å were processed using a version of *d*TREK* (Pflugrath, 1999) modified for wavelength-resolved neutron Laue protein crystallography (Langan & Green, 2004). The processed intensities from all crystal settings were scaled and wavelength-normalized using *LAUENORM* (Campbell *et al.*, 1986; Helliwell *et al.*, 1989). In order to obtain reasonable values for R_{merge} , the wavelength range was narrowed to 0.8-4.5 Å and only reflections with $I > 3\sigma$ were used in determining the wavelength-scaling normalization curve. The values of R_{merge} calculated using the program *LAUENORM* for the data measured at all crystal settings are 0.131 for all measurements of a reflection (2920 reflections), 0.110 for measurements of a reflection of the same sign (2029 reflections) and 0.096 for all measurements of a reflection of the same sign within $\Delta = 0.1$ Å (277 reflections). The results were good enough to clearly show, for example, that a labile H atom from a tyrosine group had been replaced by a D atom (Figure 1). Full analysis of this data reveals a wealth of information on hydration and backbone-chain dynamics and has been reported elsewhere.² Room temperature data collection of the “30-minute D₂O-exchanged ” crystal has just been completed and the analysis of that data set is currently underway. We hope to continue this investigation with the final sample sometime in the near future.



IMPORTANT! List or attach a list of publications resulting from this experiment (published or in press).

(1) Li, X.; Langan, P.; Bau, R.; Tsyba, I.; Jenney, F.; Adams, M.; and Schoenborn, B. *Acta Cryst.* (2004), D60, 200-202

Submit all experiment reports to:
 LANSCE User Office, MS H831, Los Alamos National Laboratory, Los Alamos, NM 87545

Experiment was carried out at:		Local Contact	Proposal #	<i>LANSCE Use Only</i>
<input checked="" type="checkbox"/>	Manuel Lujan Jr. Neutron Scattering Center	Don Brown	2003120	1/29/04
<input type="checkbox"/>	Weapons Neutron Research Facility	FP/Instrument Used		
<input type="checkbox"/>	WNR/Blue Room	FP2/SMARTS		

Title

Investigation of Stress-Strain During the Elastic and Plastic Deformation of Marble, Limestone, and Sandstone

Authors and Affiliations

J. A. TenCate LANL EES-11,
T. W. Darling LANL MST-10,
D. Brown LANL LANSCE-12,
B. Clausen LANL LANSCE-12

Experiment Report

This reports on work to continue and improve measurements performed during the 2002 run cycle as project #2002161. The experiment report for that project contains much of the background for these results.

The noise levels for both stress and strain measurements in these experiments were reduced by using a smaller load cell for the low stress levels we apply and a larger jaw on the strain extensometer. We also improved our temperature measuring capability to confirm that the gradient across the sample remained small. (Figures 1 and 2)

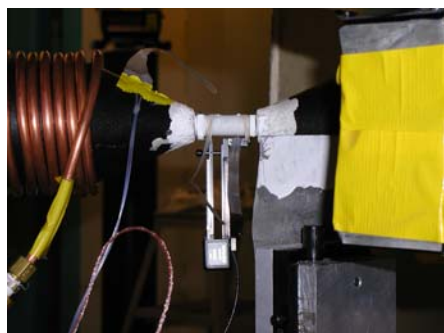


Figure 1. Extensometer and thermocouples on marble sample. The cooling coil on left removes heat from the hydraulics.

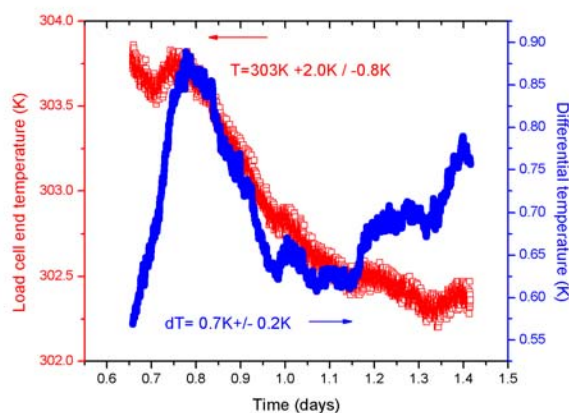


Figure 2. There is an overall downward temperature drift of $\sim 2\text{K}$ over 1 day, but the differential across the ends is constant to $\pm 0.2\text{K}$

Experiment Report (continued)

We measured several cylindrical specimens of single-phase, fine-grained rocks for measurement under axial loading in the SMARTS load frame. Our samples are Carrara Marble, Lavoux Limestone, Meule Sandstone and Arkansas Novaculite (in 2002 we completed measurements on two other sandstones) to distinguish effects due to composition and microscopic bond types. Our procedure was to apply incremental compressive stress to the sample at room temperatures in air, while measuring the stress-strain behavior from the load rig and also the coherent scattering to determine the lattice parameters. We use the standard SMARTS measurement with the sample axis at 45 degrees to the beam to resolve axial and radial responses.

The aim is to explore the differences between the macroscopic mechanical behavior and the internal response of the crystallites. This is relevant because the source of any differences can be localized to either the crystallite volumes or the much smaller bond volumes.

Figures 3 and 4 below plot strain-stress curves for three of our quartz-based rock samples. Figure 3 shows the macroscopic response and figure 4 shows the simultaneously measured response of the strain in the crystalline components from the neutron scattering measurements.

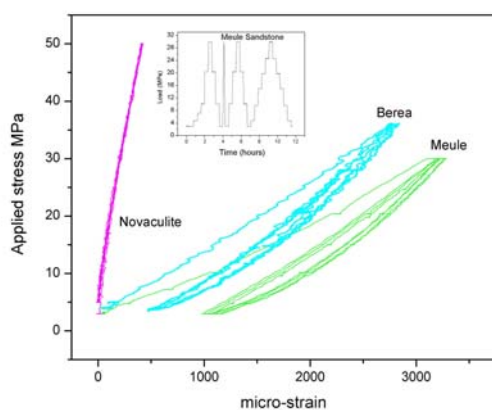


Figure 3. Curves, loops and offsets in the macro stress-strain response of sandstones, but not in the Novaculite.

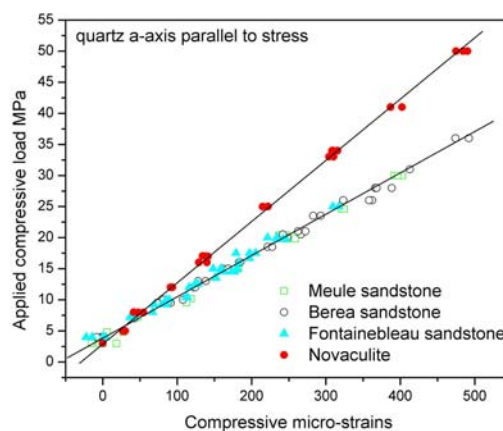


Figure 4. Lattice parameter strain from the neutron data: no loops, curves or offsets.

The large difference we observe in the behavior of the macro- and micro-scale strains confirms our previous results but now we have sufficient high quality data for publication. The data excludes the bulk of the crystalline material from being responsible for nonlinear behavior and indicates that the form of the contacts between grains is critical for the observation of nonlinear effects.

IMPORTANT! List or attach a list of publications resulting from this experiment (published or in press).

See previous report #2002161, Darling, TenCate et al. in preparation to be submitted to Geophys. Res. Lett. '04

Submit all experiment reports to:
LANSCÉ User Office, MS H831, Los Alamos National Laboratory, Los Alamos, NM 87545

Experiment was carried out at:	Local Contact	Proposal #	LANSCÉ Use Only
<input checked="" type="checkbox"/> Manuel Lujan Jr. Neutron Scattering Center	Don Brown	2003138	Report Re'd
<input type="checkbox"/> Weapons Neutron Research Facility	FP/Instrument Used		
<input type="checkbox"/> WNR/Blue Room	FP2 / SMARTS		7/16/04

Title In-Situ Creep Deformation of a FCC Polycrystalline Stainless Steel
Authors and Affiliations <p>Hahn Choo^{1,2}, Donald W. Brown³, and Mark A. M. Bourke³</p> <p>1. Department of Materials Science and Engineering, University of Tennessee, Knoxville, TN 37996 2. Metals and Ceramics Division, Oak Ridge National Laboratory, Oak Ridge, TN 37831 3. Materials Science and Technology Division, Los Alamos National Laboratory, Los Alamos, NM 87505</p>

Experiment Report <p>The evolution of texture and strain was studied using in-situ time-of-flight neutron diffraction during creep deformation of an austenitic 316FR stainless steel at 180, 240, and 300MPa at 873K (a power-law creep regime) with time resolutions ranging from 120s to 900s.</p> <p>The macroscopic (global) and mesoscopic (lattice) strains were measured simultaneously during creep using extensometer and neutron diffraction, respectively, at the SMARTS beamline at the Los Alamos Neutron Science Center.</p> <p>The hkl-specific lattice strains were measured to gain insights into the plastic anisotropy at various stages of creep deformation (i.e., primary, secondary, and tertiary regimes). Furthermore, the creep-induced lattice strain behavior was compared to the result obtained from a quasi-static tension test at 873K to understand the implications of the different deformation mechanisms (slip, dislocation creep, or grain-boundary sliding) on the mesoscopic behavior.</p> <p>The preliminary result (Fig. 1) shows that the lattice strain evolution during the primary and secondary creep (dislocation creep) is quite similar to the quasi-static case (slip). However, in the tertiary creep regime, the creep-induced lattice strain accumulation is smaller than the quasi-static case at a given total strain, except in the (111) reflection. This could be attributed to the grain-boundary sliding facilitated by the grain rotation and the relatively slower strain rate during the creep compared to the quasi-static testing.</p>

Experiment Report (continued)

The plastic anisotropy at various stages of creep and its comparison to the quasi-static tensile behavior is currently under investigation to gain further insights to the implications of the various deformation mechanisms (slip, dislocation creep, or grain boundary sliding) on lattice strain behavior.

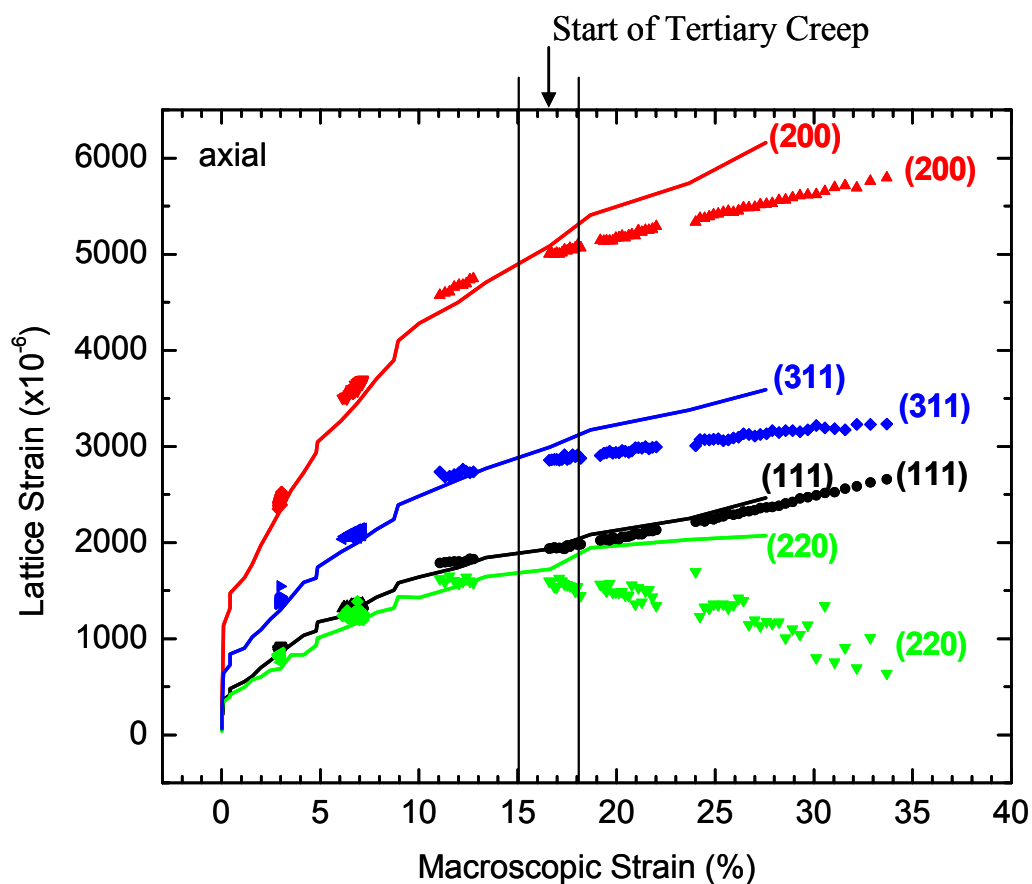


Fig. 1. Comparison of the lattice strain evolutions between the quasi-static tensile deformation (lines) and the creep deformation (symbols) as a function of macroscopic applied strain.

This work is supported by the NSF International Materials Institutes Program under DMR-0231320. Authors are grateful to Dr. B. Clausen and Mr. T. Sisneros at LANSCE for their help during the neutron diffraction measurements; and to Dr. B. Swindeman at Oak Ridge National Laboratory for the 316FR ingots.

IMPORTANT! List or attach a list of publications resulting from this experiment (published or in press).

A Neutron-Diffraction Study of Phase Transformations by Tracking Texture Evolution with Temperature in Ti-6Al-4V

D. Bhattacharyya¹, G.B. Viswanathan¹, S.C. Vogel², D.J. Williams², V. Venkatesh³ and H.L. Fraser¹

¹*The Ohio State University, Columbus, OH 43210*

²*Los Alamos National Laboratory, Los Alamos, NM 87545*

³*TIMET- R&D, 8000 W. Lake Mead Drive, Henderson, NV 89015*

Introduction

Titanium alloys are widely used in various industrial, domestic, and medical applications such as turbine blades, bicycle frames, knee implants, etc. The two-phase ($\alpha + \beta$) titanium alloy Ti-6Al-4V is considered to be a workhorse alloy for many applications in these diverse fields. One of the major aspects of this alloy, which is not yet well understood, is the way in which the phase transformation occurs from the β to the α phase on heating from room temperature (RT) to above the β transus (i.e., the temperature above which all of the hexagonal closed-packed [hcp, β] phase is transformed to the body-centered cubic [bcc, α] phase). It has not yet been clearly resolved whether the α crystals that form at high temperatures are nucleated freshly from the β phase or whether they grow from the α grains that are preexisting at RT. Another important, and as yet unresolved, question is whether the α phase maintains the Burgers orientation relationship (OR) with the β phase even after being cold worked and recrystallized. The Burgers orientation relationship predicts that the $\{0001\}$ crystal direction in a grain of the β phase becomes a $\{110\}$ crystal direction in a grain of the α phase after the transformation.

These unresolved issues are extremely critical for the understanding and modeling of the evolution of microstructure. The microstructure, in turn, influences mechanical properties in titanium alloys. A unique way to address these issues is to monitor the development of texture as a function of temperature. Our present study attempts to do this by carrying out, for the first time, high-temperature *in situ* texture measurements using the High-Pressure Preferred Orientation (HIPPO) diffractometer at LANSCE. This instrument enables texture measurements by neutron diffraction at various temperatures with the sample located inside a vacuum furnace. Based on the textures of the α and the β phases measured at RT and 800 °C, these experiments establish that the Burgers orientation relationship between the equiaxed (or globular) grains of the α phase and the matrix β phase is largely destroyed during the recrystallization of the α phase. Also, when the texture of the α phase at 1020 °C was compared with the α and β textures at the lower temperatures, it is conclusively proven that the α phase could only have formed at high temperature by the growth of pre-existing α grains and not by fresh nucleation within β grains.

Background

The bimodal microstructure at RT in an α/β titanium alloy such as Ti-6Al-4V consists of a mixture of equiaxed α phase and a lath-structure consisting of alternating plates of α and β phases as shown in Figure 1. The black regions in this scanning electron microscope (SEM) micrograph represent the β phase, which can be seen in two forms—one which is of a globular nature, and the other having a lath-like morphology. The white regions in this micrograph represent the α phase. This bimodal microstructure forms when the alloy is thermomechanically processed in the ($\alpha + \beta$) two-phase region. A strong texture in the alloy develops during this exposure—depending on the temperature and the type of processing. In the lath part of the bimodal microstructure, the α and β phases exhibit a Burgers orientation relationship defined by $\{0001\}\alpha \parallel \{110\}\beta$ and $\langle 11\bar{2}0 \rangle\alpha \parallel \langle 111 \rangle\beta$ ¹. However, whether or not such an orientation relationship is maintained for the equiaxed α with the β phase, after the alloy undergoes thermomechanical processing, remains an open question. Secondly, whether recrystallization alone can change the texture of the globular α (apart from the question of the Burgers orientation relationship with

the β phase) also remained the subject of research in recent years. These issues are very important because they are fundamental to understanding and prediction of the textures of both phases which in turn is extremely critical to the understanding and prediction of the mechanical properties of the alloy. The literature contains conflicting views concerning texture development: Whereas Gey *et al.*² in their paper state that recrystallization modifies the orientation of β grains and destroys the Burgers orientation relationship, Lütjering³ reports that the β texture after recrystallization remains essentially unchanged.

The main difficulty in testing the validity of the Burgers orientation relationship of the globular β with the α phase lies in obtaining the texture of the β phase which has only a low-volume fraction of typically less than 8 vol.% at RT. Measurements by methods such as X-ray or electron back-scattered diffraction mostly represent textures of material in the vicinity of the surface. In contrast, neutron scattering is capable of probing a bulk sample, which is best suited for obtaining the texture from a minor phase constituent such as the β phase in the titanium alloy in this study. Understanding the development of β -phase texture is also critical to understanding the mode of transformation of the β to the α phase. As noted above, the transformation of β to the α can either occur by the growth of the α phase pre-existing at RT, or by the fresh nucleation of α within β grains. This issue has not yet been resolved due to the difficulty in obtaining the β -phase texture at higher temperatures. Gey *et al.*² attempted the back-calculation of the β phase texture from the α texture obtained after cooling from the β phase, which needs experimental verification. If the texture development in this alloy can be monitored *in situ* (i.e., as a function of temperature), the development of the β texture and its relation to the α phase in the microstructure can be captured. When cooled down below the β transus, an inverse transformation from β to α occurs in which only laths of α are formed within the β grains. In this case the Burgers orientation relationship is obeyed. .

It is the intention of this study to attempt to answer the questions discussed above by measuring the β and the α textures directly, using the time-of-flight neutron diffractometer HIPPO at LANSCE that has the following unparalleled advantages over other methods: (a) Neutron diffraction gives a true evaluation of the texture in the bulk material especially when the second phase (i.e., the β phase in this study) is present in small amounts (but greater than ~2-4 volume percent), (b) HIPPO, with its large detector coverage, provides the opportunity to measure the three dimensional orientation distribution of the crystals with rotation of the sample limited to one rotation axis, allowing to use special sample environments like the furnace used in this study, and (c) HIPPO provides the unique opportunity, with its high-temperature capability, to measure the texture of the materials in-situ as a function of temperature.

Experiments

The neutron-diffraction texture measurements were done on cold-worked specimens of Ti-6Al-4V, an α/β alloy (T_β transus ≈ 980 °C) with about 95% α and 5% β at RT. The samples were α/β forged at ~ 930 °C followed by annealing at ~ 805 °C for 3 hr and then water quenched. The final test pieces were machined to cuboids of about 20 mm \times 20 mm \times 15 mm. Texture measurements were performed on the HIPPO⁴ diffractometer (Figure 2) at the pulsed-neutron source of LANSCE⁵. HIPPO views a decoupled high-intensity/low-resolution water moderator of 2.5 cm thickness. For the present experiments, the beam was collimated to 10 mm in diameter at the sample position approximately 9 m from the moderator. An ILL-type vacuum furnace modified with vanadium instead of the standard niobium heating elements and heat shields was used to heat the sample. The vanadium setup prevents any contamination of the diffraction patterns with diffraction peaks from the furnace itself. Due to HIPPO's large detector coverage, rotation around the vertical axis only is sufficient to obtain an orientation distribution function (ODF), allowing the use of equipment such as an ILL-type furnace to perform texture measurements at

non-ambient conditions. Total neutron beam time was about 60 minutes per sample orientation at an average proton current of 100 μA . In all, 98 histograms obtained from four different sample orientations for diffraction angles of 150°, 90° and 40° were refined simultaneously using the general-structure analysis system GSAS⁶ to obtain the orientation distribution function (ODF). The ODF was represented by a spherical harmonics approximation⁷. From the ODF, individual pole figures were recalculated. For the RT measurement, an 8th-order spherical harmonics description of the ODF was sufficient to describe the data—whereas for all other measurements terms up to order 10 were required, indicating stronger textures than at RT. No sample-symmetry constraints were imposed on the analysis. Pole figures were plotted using the popLA package⁸. The microstructure of the cold-rolled sample was characterized using scanning electron microscopy (SEM) (XL 30 ESEM FEG) and Transmission Electron Microscopy (TEM) (CM200).

To simulate the conditions inside the furnace of the HIPPO diffractometer at 800 °C, another specimen from the same sample sheet was heat-treated to 800 °C and held for 4 hr in a vacuum furnace and then furnace cooled to RT. The microstructure of this sample was characterized using SEM and TEM.

Results and discussion

The microstructure of the cold-rolled sample as received from TIMET \square is shown in Figure 3. In this TEM micrograph, taken with the central globular \square grain on a $\{11\bar{2}0\}$ zone axis, a large number of fine precipitates, probably secondary \square or martensite, populating the \square regions is observed. Thus, the fraction of \square in the microstructure is less than what is seen in the SEM, and may actually be less than 5%. Moreover, the \square shows a very high density of dislocations and some subgrain boundaries, indicating a large amount of deformation. No peaks of the \square phase were observed by the neutron-diffraction measurements at RT. The detection limit for minority phases for this technique is about 2%. The TEM measurements showed large strains in the \square phase, resulting in a further broadening of the very weak peaks. Hence, a volume fraction of 2%–5% for the \square phase is still in agreement with the neutron-diffraction measurements.

The pole figures from the neutron-diffraction experiments at RT are shown in Figure 4. The \square phase shows a moderate to strong hcp rolling texture with a typical preferred orientation of the $\{0001\}$ poles to the normal direction (ND). The maximum pole density was found to be 4 times random. The \square pole figure also exhibited a spread of the $\{0001\}$ poles away from the ND towards the transverse direction (TD). This is in agreement with previously published results by other authors for rolling of titanium alloys^{9,10}.

The *in situ* neutron-diffraction experiments at 800 °C showed that the texture of the \square phase was sharpened and the intensity of the $\{0001\}$ preferred orientation along the ND became stronger (Figure 6a), with the maximum of about 6 times random. This strengthening of the \square texture is likely to be due to the recrystallization of the \square . To confirm this observation, as-received samples were separately heat-treated at 800 °C for 4 hr, furnace cooled in a vacuum, and then examined in the TEM. The TEM micrograph in Fig. 5 shows that the primary \square grains are relatively free of dislocations that are indicative of the recrystallization of the \square grains. The \square phase was also detected in the HIPPO diffractometer at this temperature and the volume fraction was estimated to be about 15 \pm 1%. The \square texture, derived from these measurements by Rietveld analysis, was found to be very weak, with a slight concentration of $\{111\}$ peaks towards the ND, as shown in the pole figures of Fig. 6b. This is a very interesting observation—indicating that the Burgers orientation relationship is destroyed, at least at the recrystallization stage, if not at the deformation stage, because otherwise one would observe a

concentration of $\{110\}$ β poles near the ND, which had a high concentration of $\{0001\}$ β poles near it at RT.

The pole figures measured at 1020 °C are shown in Fig. 7. As the alloy is transformed completely to β at 1020 °C, only the β texture is evaluated at this temperature. No peaks from the α phase were visible in the histograms (not shown here). As is evident from Fig. 7, the β grains show a strong $\{111\}$ texture parallel to the ND. It is interesting to note that there appears to be a distinctive strengthening of the β texture when compared with that at 800 °C. This is evident when the strengths of the $\{111\}$ poles near the ND from the results at 800 °C and 1020 °C are compared. The $\{100\}$ poles seem to show a tendency to concentrate towards one orientation, though the texture is very weak. The strengthening of the β texture when the sample is heated from 800 °C to 1020 °C gives conclusive evidence that the α phase transforms to the β phase by the growth of the preexisting α and not by the fresh nucleation of β in the α as otherwise there would have been a high concentration of $\{0001\}$ poles near the ND, as dictated by the Burgers orientation relationship.

After the sample was cooled down, the β texture was again measured at RT. The results of these measurements are shown in Fig. 8. Again, the α phase was below the detection limit for the ND measurement. It should be noted that we observed $\{0001\}$ pole concentrations at mutual angles, which are very similar to those between $\{110\}$ poles of a single α crystal. Moreover, we observed a high concentration of $\{11\bar{2}0\}$ poles parallel to the direction of the strongly textured $\{111\}$ poles of the β observed at 1020 °C. This is an indication of the Burgers orientation relationship being followed for the retransformation from β to α when the sample is cooled from above the β transus, which is expected if the α forms by nucleation and growth from the β matrix.

Conclusions

The results indicated a definite departure from the Burgers orientation relationship either during deformation or during recrystallization of the α phase. More work is required to shed light on the extent to which the Burgers orientation relationship is destroyed during the deformation stage or the recrystallization stage. The α phase shows a strengthening of the initial rolling texture after the heat treatment at 800 °C. It may be concluded that this is due to the recrystallization of the α grains and the growth of some α grains at the expense of others. The $\{111\}$ texture in the β phase starts to develop at 800 °C and progressively strengthens while it is heated up to 1020 °C when the alloy fully transforms to the β phase. The presence of a high concentration of $\{111\}$ poles at 1020 °C, near the $\{0001\}$ poles of the α phase at 800 °C, indicates that the Burgers orientation relationship was not followed in the transformation of α to β . Thus, it is concluded that the β phase grew from the preexisting α phase, rather than by fresh nucleation from the β phase.

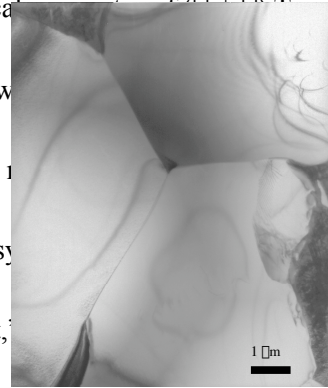
Acknowledgements

The work has benefited from the use of the Los Alamos Neutron Science Center at Los Alamos National Laboratory. LANSCE is funded by US Department of Energy under Contract W-7405-ENG-36. The authors are grateful to TIMET® for providing the samples for the experiments.

References

- ¹ W.G. Burgers, "The process of transition of the cubic body centered modification into the hexagonal close packed modification of zirconium," *Physica* **1**, 561 (1934).
- ² N. Gey, M. Humbert, and H. Moustahfid, "Study of the α/β phase-transformations of a $\text{Ti}_6\text{Al}_4\text{V}$ sheet by means of texture change," *Scripta Materialia* **42**, 525–530 (2000).

- ³ G. Lutjering, "Influence of processing on microstructure and mechanical alloys," *Materials Science and Engineering A* **243**, 32–45 (1998).
- ⁴ H.-R. Wenk, L. Lutterotti, and S. Vogel, "Texture analysis with the new *Nuclear Instruments and Methods A* **515**, 575–588 (2003).
- ⁵ P.W. Lisowski *et al.*, "The Los Alamos National Laboratory spallation *Science and Engineering A* **106**, 208–218 (1990).
- ⁶ A.C. Larson and R.B. von Dreele, "GSAS - general structure analysis system Laboratory report LA-UR-94-748 (1994).
- ⁷ R.B. von Dreele, "Quantitative texture analysis by Rietveld refinement," *Crystallography* **30**, 517–525 (1997).
- ⁸ J.S. Kallend *et al.*, "Operational texture analysis," *Materials Science and Engineering A* **132**, 1–11 (1991).
- ⁹ A.J. Hatch, "Texture strengthening of titanium alloys," *Transactions of The Metallurgical Society of AIME* **233**, 44–50 (1965).
- ¹⁰ U.F. Kocks, C.N. Tome, and H.-R. Wenk, *Texture and Anisotropy: Preferred Orientation in Polycrystals and Their Effect on Materials Properties*, (Cambridge University Press, Boston, 1998).



Figures and Captions

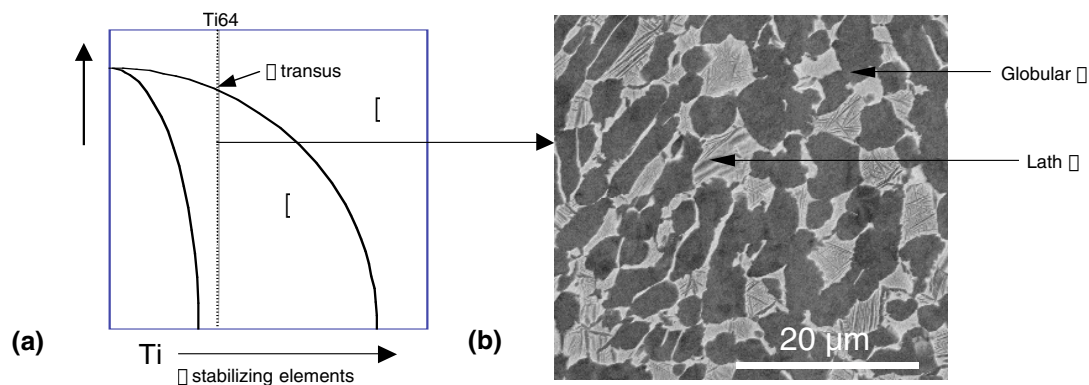


Figure 1. (a) Schematic phase diagram of titanium and (b) typical microstructure of Ti-6Al-4V processed alloy

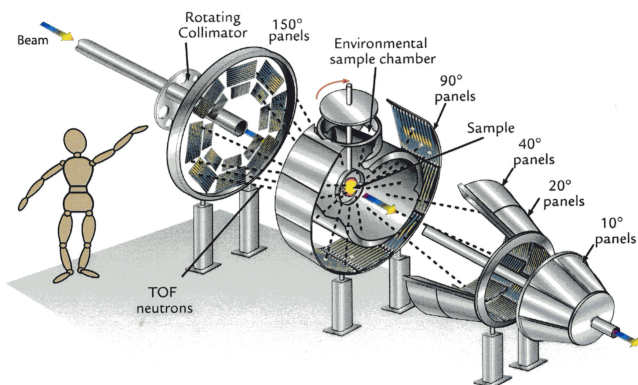


Figure 2. Schematic of HIPPO instrument at LANSCE.



Figure 3. TEM micrograph of the as rolled Ti64 sample.

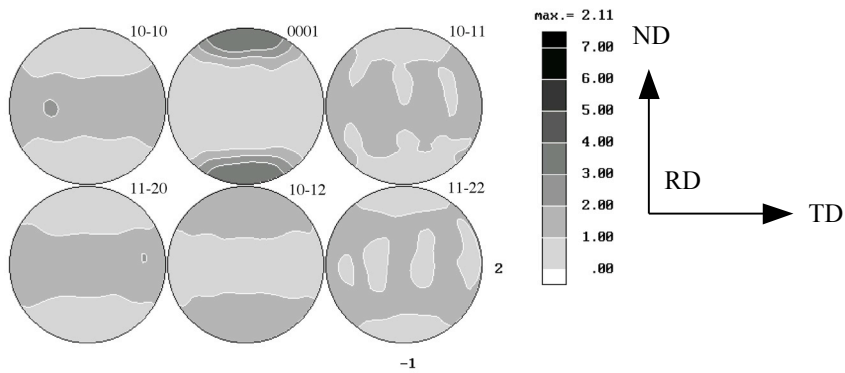


Figure 4. Pole figures of α at room temperature

Figure 5. TEM micrograph of annealed sample

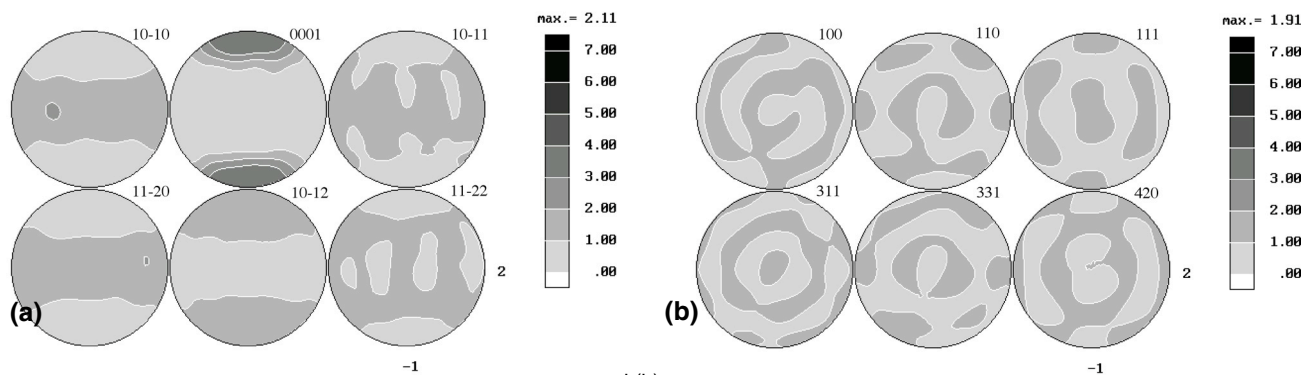
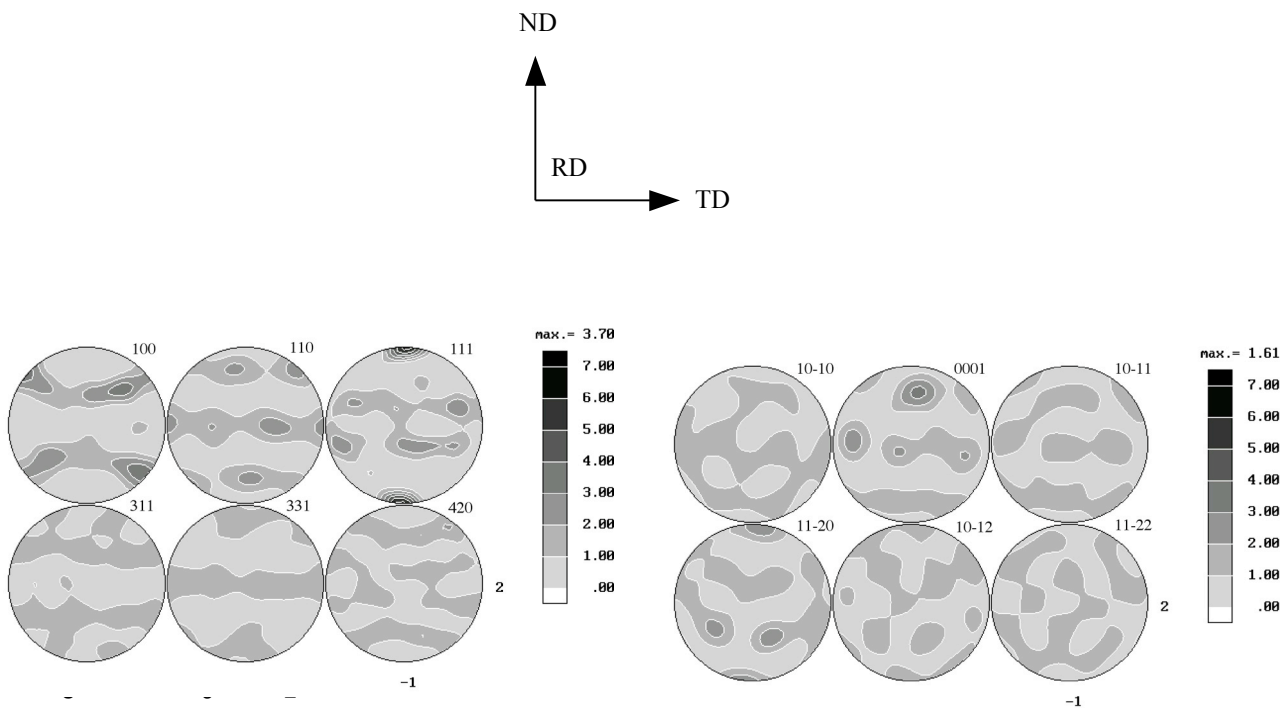


Figure 6. (a) Pole figures of β at 600 °C and (b) pole figures of β at 600 °C



Submit all experiment reports to:

LANSCE User Office, MS H831, Los Alamos National Laboratory, Los Alamos, NM 87545

Experiment was carried out at:	Local Contact	Proposal #	LANSCE Use Only
<input checked="" type="checkbox"/> Manuel Lujan Jr. Neutron Scattering Center	Thomas Proffen	2003167	<div>Report Re'd</div> <div>6/2/04</div>
<input type="checkbox"/> Weapons Neutron Research Facility	FP/Instrument Used		
<input type="checkbox"/> WNR/Blue Room	NPDF		

Title

Local structure of gold nanoparticles

Authors and Affiliations

Thomas Proffen, LANSCE-12
Katharine Page, LANSCE-12
Ram Seshadri, UC Santa Barbara
Anthony Cheetham, UC Santa Barbara

Experiment Report

Nanoparticles of FCC gold, with a mean diameter of approximately 5 nm, have been studied by total scattering powder neutron diffraction at 15 K and 295 K on the NPDF diffractometer at the Manuel Lujan Jr. Neutron Scattering Center. The results compared with a sample of bulk gold powder. The Pair Distribution Functions (PDFs) reveal several interesting features. The PDF patterns for the nanoparticles are significantly attenuated compared with the bulk gold due to the finite size of the particles; the attenuation is consistent with the 5 nm size of the particles. The nanoparticles have smaller lattice parameters at both temperatures but the nearest neighbor Au-Au vectors are entirely symmetrical and there is no evidence for structural relaxation associated with the atoms near the surface. However, the vector between the surface atoms and the sulfur of the thiol layer can be observed at ~2.4 Å.

Experiment Report (continued)

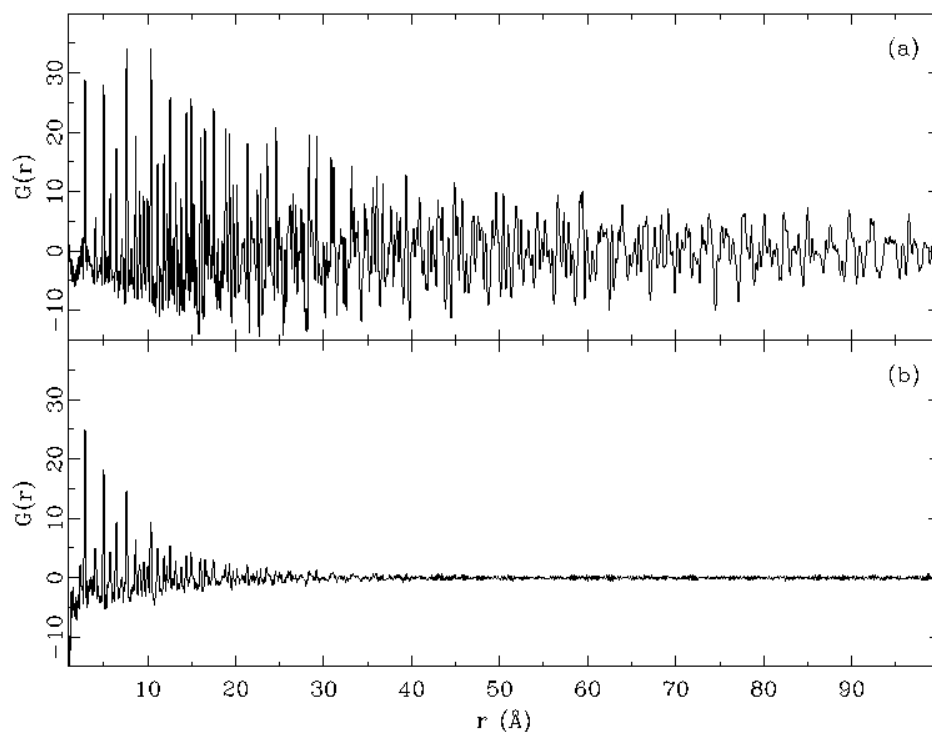


Figure 1: $G(r)$ of bulk gold (a) and gold nanoparticles (b) measured on NPDF at $T=15\text{K}$. In both cases the maximum momentum transfer used to obtain $G(r)$ was $Q_{\text{max}}=30\text{\AA}^{-1}$.

IMPORTANT! List or attach a list of publications resulting from this experiment (published or in press).

K.L. Page, Th. Proffen, H. Terrones, M. Terrones, L. Lee, Y. Yang, S. Stemmer, R. Seshadri and A.K. Cheetham, *Chem. Phys. Lett.*, in press (2004).

Submit all experiment reports to:
 LANSCE User Office, MS H831, Los Alamos National Laboratory, Los Alamos, NM 87545

Experiment was carried out at:		Local Contact	Proposal #	<i>LANSCE Use Only</i>
<input checked="" type="checkbox"/>	Manuel Lujan Jr. Neutron Scattering Center	Thomas Proffen	2003168	Report Rc'd <div>6/2/04</div>
<input type="checkbox"/>	Weapons Neutron Research Facility	FP/Instrument Used		
<input type="checkbox"/>	WNR/Blue Room	NPfDF		

Title

Local structure of carbon black

Authors and Affiliations

Thomas Proffen, LANSCE-12

Michael Gerspacher, Sid Richardson Carbon Company

Experiment Report

Carbon black is an important ingredient in many products, most notably tires. In this study we investigated the local atomic structure of several samples made via different processing conditions. Figure 1 shows a comparison of three samples extracted after different times in the reactor. Local structural differences are clearly visible. The detailed analysis of these data is still in progress.

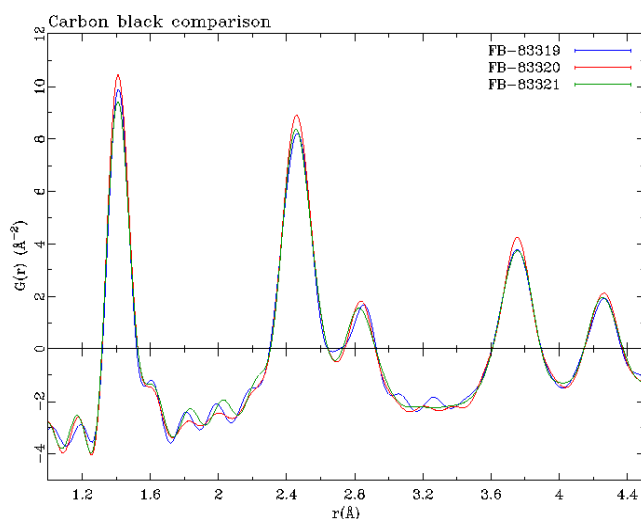


Figure 1: Pair distribution function (PDF) of three different carbon black samples measured on NPDF.



REPORT ON EXPERIMENT

(Please Type)

Submit all experiment reports to:
 LANSCE User Office, MS H831, Los Alamos National Laboratory, Los Alamos, NM 87545

Experiment was carried out at:		Local Contact	Proposal #	<i>LANSCE Use Only</i>
<input checked="" type="checkbox"/>	Manuel Lujan Jr. Neutron Scattering Center	Paul Langan	2003175	Report Rc'd 6/18/04
<input type="checkbox"/>	Weapons Neutron Research Facility	FP/Instrument Used		
<input type="checkbox"/>	WNR/Blue Room	PCS		

Title

Structure and Mechanism of Protocatechuate 3,4-Dioxygenase

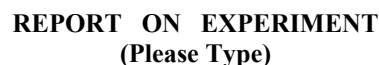
Authors and Affiliations

Douglas H. Ohlendorf, C. Kent Brown, Dept. of Biochemistry, Mol. Biol. & Biophysics,
University of Minnesota

Experiment Report

Data on this project was collected January 28-29 and April 6-9. The initial experiment on a wild-type protocatechuate 3,4-dioxygenase (PCD) crystal of volume $\sim 10 \text{ mm}^3$. Crystal had been soaked in deuterated mother liquor for 3 months. Crystal displayed diffraction to $\sim 2.4 \text{ \AA}$ upon initial data frames ($\sim 20 \text{ hr}$ exposures). Subsequent 36 hr exposures displayed diffraction to $\sim 2 \text{ \AA}$ with x-rays. Data processing using these initial frames provided intensities for 1.9% of the unique data to 2 \AA , i.e., 4372 reflections. The R_{sym} for these data was 0.195 (only 1.2 multiplicity).

PCD crystallizes as a 587 kDa dodecamer in a C2 unit cell ($V_{\text{AU}} = 830,000 \text{ \AA}^3$). It is remarkable that a problem of this size is now possible using the PCS. Since perdeuteration can yield a significant improvement in the neutron diffraction signal, we are investigating the production of perdeuterated crystals. In addition similarly sized crystals of a mutant PCD were left at Los Alamos for potential further testing as time might become available.



Experiment was carried out at:		Local Contact	Proposal #	LANSCE Use Only
<input checked="" type="checkbox"/>	Manuel Lujan Jr. Neutron Scattering Center	J. Majewski	2003176	Report Rc'd 9/10/04
<input type="checkbox"/>	Weapons Neutron Research Facility	FP/Instrument Used		
<input type="checkbox"/>	WNR/Blue Room	SPEAR		

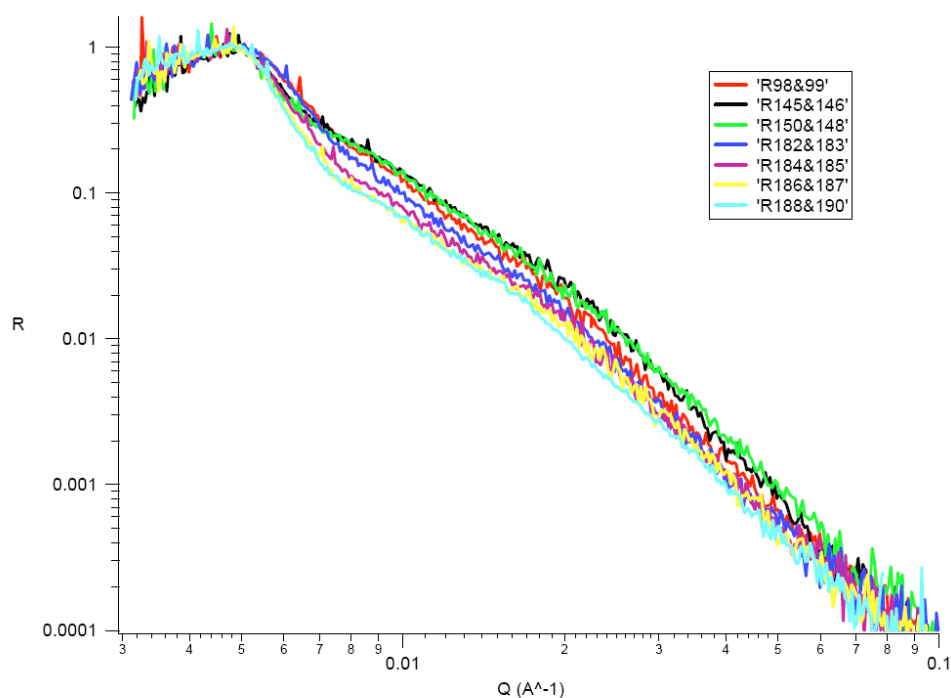
Authors and Affiliations
Matthew D. Brown, Kansas State University Physics Department
Bruce M. Law, Kansas State University
William Hamilton, Oak Ridge National Lab
Serif Uran, Pittsburg State University

The purpose of our experiment was to study the composition structure at a solid-liquid interface of a critical binary liquid mixture near, and above the de-mixing phase transition critical temperature. The mixture we used was deuterated cyclohexane + methanol, at a bulk volume fraction $V_C = 0.285$ methanol. The solid substrate was a quartz crystal. At the interface we expected an adsorbed layer of pure methanol, with a profile decaying to the bulk volume fraction over a length scale on the order of $\xi = \xi_0 t^{\varpi}$, where ξ is the composition fluctuation correlation length, which here ranges from $\sim 10^2$ angstroms to $\sim 10^3$ angstroms. $t \equiv \left| \frac{T - T_C}{T_C} \right|$ is the reduced temperature (a measure of how far the system is from the demixing critical temperature), and ϖ is a universal (system independent) critical exponent. We expect that the profile should be universal, and scale as

$$V_a(z) = M_{\square} t^{\square} P_+(z/\square_+) + V_C \quad (1),$$

Where $P_{\pm}(x)$ is a universal (system independent) composition scaling function. $P_{\pm}(x)$ was measured in [1] at a liquid vapor interface via ellipsometry, but these results disagreed with an x-ray reflectometry done at Argonne National Labs[2]. While the results of our neutron reflectometry experiment agree qualitatively with [2], problems with our sample cell render the data suspect. The critical temperature of the sample was measured after the experiment, and was found to have shifted by over 1 C from the value before the experiment. This was likely due to leaking from the sample cell, which incorporated Teflon in a large part of the structural design. While previous tests had shown no leaking, apparently the frequent changes in temperature necessary for the experiment combined with the thermal expansion hysteresis of Teflon lead to leaking. Our cell has since been redesigned, and remade. All structural parts now consist of stainless steel and quartz.

Experiment Report (continued)



Run #s	T(C)	$t = (T - T_c) / T_c$	$\xi = \xi_0 t^{-\nu}$ (Å)
95,96	49.904	2.00e-2	39.2
98,99	44.922	4.22e-3	103.4
145,146	49.898	2.00e-2	39.2
147-151	54.868	3.56e-2	27.0
182,183	44.413	2.61e-3	140.0
184,185	44.018	1.37e-3	210.4
186,187	43.820	7.42e-4	309.2
188,189,190	43.723	4.36e-4	432.3

Note:

- (i) The two high temperature runs (50 and 55C) more or less agree (runs 145&146 (black) and 150&148 (green)).
- (ii) The two low temperature runs (43.8 and 43.7C) more or less agree (runs 186&187 (yellow) and 188&190 (light blue)).
- (iii) There is a systematic variation in R versus Q between these two extremes for the in between temperatures – a similar trend was also found for the x-ray data at the liquid/vapor surface of tetrabromoethane + dodecane.

IMPORTANT! List or attach a list of publications resulting from this experiment (published or in press).

No publications at this time

Submit all experiment reports to:
LANSCÉ User Office, MS H831, Los Alamos National Laboratory, Los Alamos, NM 87545

Experiment was carried out at:	Local Contact	Proposal #	LANSCÉ Use Only
<input checked="" type="checkbox"/> Manuel Lujan Jr. Neutron Scattering Center	Sven Vogel	2003181	Report Re'd 5/21/04
<input type="checkbox"/> Weapons Neutron Research Facility	FP/Instrument Used		
<input type="checkbox"/> WNR/Blue Room	HIPPO		

Title
Investigation of the Texture Evolution during Secondary Recrystallization of Mg Alloys
Authors and Affiliations
María Teresa Pérez-Prado, Centro Nacional de Investigaciones Metalúrgicas (CENIM), CSIC, Madrid, Spain Sven Vogel, Los Alamos National Laboratory

<p>Experiment Report</p> <p>The evolution of the texture of two commercial Mg alloys, namely AZ31 and AZ61, during in-situ annealing at high temperatures was investigated. Previous thermomechanical processing of these alloys included a final hot rolling step, and thus both materials had a strong initial basal texture, i.e., the c-axes lay preferentially parallel to the normal to the rolling plane (ND). Squares of 2x2x0.3cm³ were cut out of the original sheets, grinded to about 1/3 of their original thickness to avoid the presence of texture gradients, and then piled-up in order to increase the volume in the beam.</p> <p>Figure 1 shows the evolution of the texture of the AZ31 Mg alloy during in-situ annealing at 520°C. The (0001) pole figures, corresponding to annealing times as long as 131 min., are plotted in sequence. Unfortunately it was not possible to acquire texture measurements after longer times due to unexpected sample melting. As anticipated, a strong basal texture is observed at the beginning of the experiment. Little texture changes can be appreciated during the short annealing times available. In fact, previous X-ray diffraction experiments involving quenching of the material suggested that major changes in crystallite orientations would only be apparent after heat treatments lasting about 2 to 3 h, even at the relatively high temperature employed in this experiment. The same experiment was performed with the AZ61 alloy, resulting also in sample melting after a few minutes of annealing.</p> <p>The causes that provoked the unexpected sample melting are still not fully understood. The solidus temperatures for the AZ31 and AZ61 alloys are, respectively, 605°C and 525°C. Both of them are higher than the annealing temperature used (520°C). Furthermore, static annealing treatments at this temperature were previously performed in air in these alloys in a conventional furnace and, although surface oxidation was pronounced, no signs of incipient melting were detected. In HIPPO, all in-situ annealings are performed in vacuum, and therefore sample oxidation can be completely avoided. We believe that the way the samples were held in the HIPPO furnace caused the failure: We used a standard Vanadium can with slits cut into it to clamp the sample. At the annealing temperatures the force resulting from the clamping and the gravity together with the soft sample at this temperature might have caused the samples to fall apart, followed by evaporation on the hot surface of the heating elements (the sample material was found on the upper heat shields of the furnace, above the original position). During heat treatment of the same material in our lab, with the sample</p>

3. A faster DAQ saving time would also be beneficial in order to reduce the blind time and therefore to minimize temperature-related problems such as the ones encountered. With count times of 1 minutes per pattern and 4 patterns required for a texture analysis, the time resolution is closer to 8 minutes than the 4 minutes during which neutron data is actually taken. Depending on the kinetics of the recrystallization, the sample texture might change considerably during these 8 minutes and 4 minutes time resolution would improve the quality of the data.

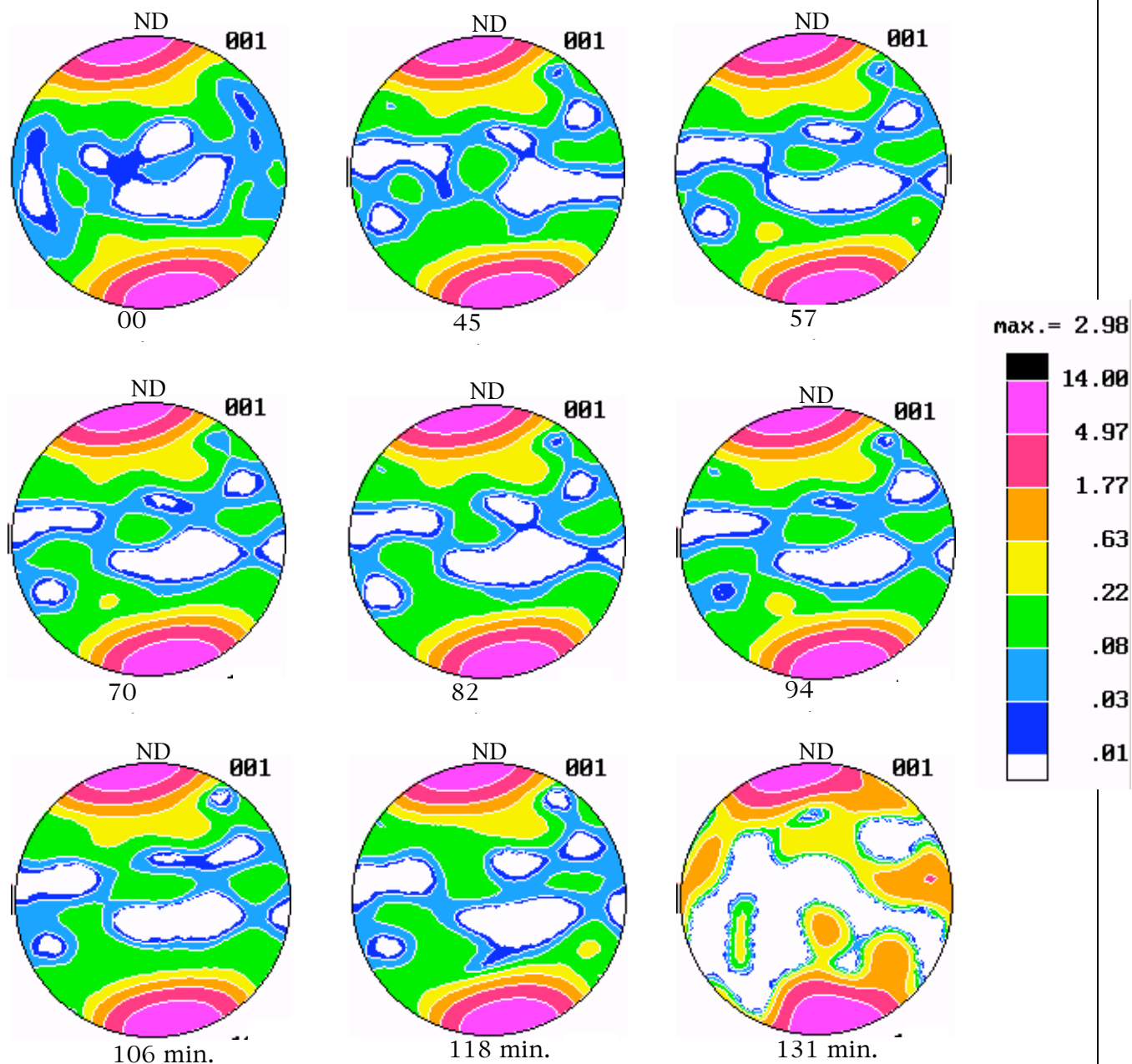


Figure 1. Evolution of the texture of the AZ31 Mg alloy during in-situ annealing at 520°C. The texture is represented by means of the (001) pole figures.

IMPORTANT! List or attach a list of publications resulting from this experiment (published or in press).

Submit all experiment reports to:
 LANSCE User Office, MS H831, Los Alamos National Laboratory, Los Alamos, NM 87545

Experiment was carried out at:		Local Contact	Proposal #	<i>LANSCE Use Only</i>
<input checked="" type="checkbox"/>	Manuel Lujan Jr. Neutron Scattering Center	Jarek Majewski	2003187	Report Rc'd 7/8/04
<input type="checkbox"/>	Weapons Neutron Research Facility	FP/Instrument Used		
<input type="checkbox"/>	WNR/Blue Room	SPEAR		

Title

A peptide-based membrane system to study membrane-protein interactions

Authors and Affiliations

Ingo Koeper, Max Planck Institute for Polymer Research, Mainz, Germany
Fatma Nese Koek, Max Planck Institute for Polymer Research, Mainz, Germany
Eva Sinner, Max Planck Institute for Biochemistry, Martinsried, Germany

Experiment Report

The study of membrane proteins in artificially created lipid bilayer membrane systems is an upcoming scientific issue. Building an artificial model membrane is an important step towards the biomimesis of the natural bilayer lipid membrane. It offers the possibility for investigation of membrane-related processes like cell adhesion, photosynthesis, respiration, toxin-membrane and drug-protein interactions. In living yeast cells, ergosterol is present in biological membranes, particularly in the plasma membrane. Thus, we intended to mimic a native environment for the hydrophobic molecule by the setup of an artificial phospholipid bilayer. The possibility to create stable systems by tethering a lipid bilayer to a solid support opens the way to use all kind of different surface analytic methods, as for example neutron reflectivity experiments.

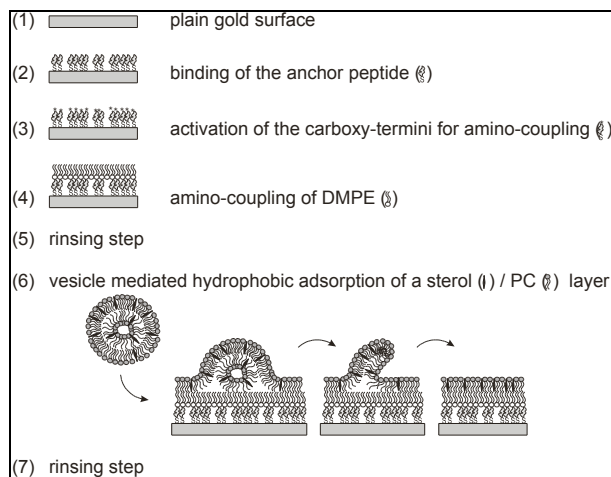


Fig. 1

Based on a peptide tether (laminin peptide P19, Sigma) we are able to create artificial lipid bilayers that have been characterised so far by AFM, QCM, Surface Plasmon (SPR) and Impedance measurements. This basis is used in the study of the oxysterol binding protein Osh5p. Using sterols we introduce rafts into the system in order to mimic properties of a natural cell.

We followed by neutron reflectivity the sequential building up of the system as depicted in figure 1.

Experiment Report (continued)

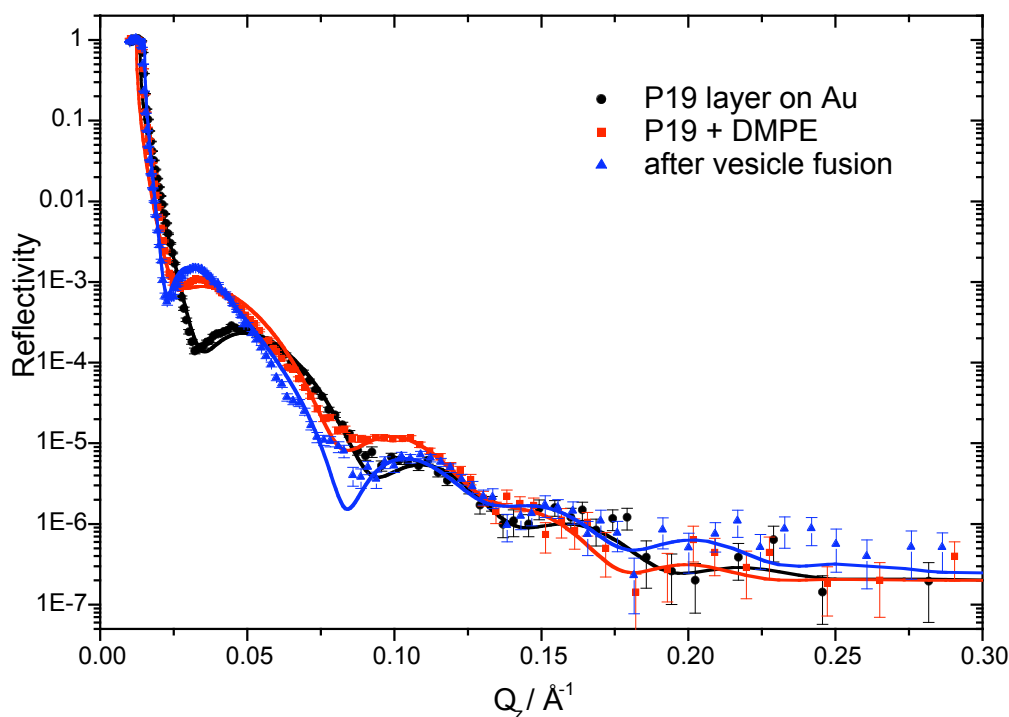


Fig. 2

Figure 2 shows the reflectivity curves after the different steps.

Data are fitted with box models using the PARRAT 32 software. Thicknesses for the substrate (Si, SiO₂, Cr, Au) were derived from measurement of the bare gold surface against air. The obtained parameters are in good agreement with literature values for the scattering length densities and with expected values from the evaporation process for the thickness.

The peptide layer can be modeled with a thickness of 5-7 Å and a scattering length density of $2.9 \times 10^{-6} \text{\AA}^{-2}$. The thickness is lower as one would expect from SPR measurements (10-13 Å) but can be explained with a rather high roughness of about 24 Å. The overall picture is that of a more or less loosely packed peptide layer.

In the second step, a lipid (DMPE) is coupled to this layer. It is impossible to introduce a separate box in the fitting routine. Instead we fitted the overall layer (peptide+DMPE) using one box. We get a thickness of about 14 Å, $\rho = 1.1 \times 10^{-6} \text{\AA}^{-2}$ and a roughness of about 16 Å. This shows, that the lipid layer is covering the peptide layer by formation of a smoother surface. The thickness-increase is in good agreement with SPR data.

The vesicle fusion experiment did not lead to a complete coverage. Parameters of the fit (thickness : 8 Å, roughness 55 Å) suggest an incomplete film plus addition non-fused vesicles on the surface.

Submit all experiment reports to:
LANSCCE User Office, MS H831, Los Alamos National Laboratory, Los Alamos, NM 87545

Experiment was carried out at:	Local Contact	Proposal #	LANSCCE Use Only
<input checked="" type="checkbox"/> Manuel Lujan Jr. Neutron Scattering Center	Rex Hjelm	2003188	Report Rc'd
<input type="checkbox"/> Weapons Neutron Research Facility	FP/Instrument Used		8/9/04
<input type="checkbox"/> WNR/Blue Room	LQD		

Title

SANS of DMPC/DOPE-N-Lactone in Ionic Liquid [CH₃O(CH₂)₂-mim][Tf₂N]

Authors and Affiliations

Sheila N. Baker; Chemistry Division; Los Alamos National Laboratory

Gary A. Baker; Bioscience Division; Los Alamos National Laboratory

William T. Heller; Condensed Matter Sciences Division and Center for Structural Molecular Biology; Oak Ridge National Laboratory

Experiment Report

Small-angle neutron scattering was used to study solutions of a 4:1 molar ratio mixture of the lipid dimyristoyl phosphatidylcholine (DMPC) and the glycosylated lipid dioleoyl phosphatidylethanolamine-N-lactone (DOPE-N-Lactone) in the ether-based ionic liquid 1-ethylmethylether-3-methylimidazolium bis(trifluoromethylsulfonyl)imide ([CH₃O(CH₂)₂-mim][Tf₂N]). The DMPC for the study was deuterated. Our goal was to determine if the DMPC/DOPE-N-Lactone/[CH₃O(CH₂)₂-mim][Tf₂N] mixture forms a uniform solution, phase separates or self assembles, thereby determining the suitability of the system for use as a solvent for membrane-based biocatalysis. The mixture was studied as a function of the lipid concentration and temperature. This work complements previous experiments studying mixtures of DMPC and the commonly used ionic liquid 1-butyl-3-methylimidazolium-PF₆ ([bmim][PF₆]) by small-angle neutron scattering, which suggests that the lipid forms a temperature-dependent mass-fractal aggregate.

The samples, containing three concentrations of the lipid mixture (stock concentration = 4.5 mg/ml. 50% and 20% of the stock concentration were also studied), were measured at four temperatures: 6 °C, 10 °C, 25 °C and 40 °C. Due to difficulties with the data reduction, only data from 6 °C, 10 °C and 25 °C have been reduced to date. The difficulties with the data reduction are also why this report is being submitted late. The scattering intensity profile of the neat ionic liquid is shown as a function of temperature in Figure 1. Of interest is the peak near $q = 0.30/\text{\AA}$, which corresponds to distances of ~21 Å. The data suggests that the ionic liquid has formed an ordered structure, but without higher order diffraction patterns, we cannot say what that structure might be. The precise position of the peak is uncertain because the data does not extend further in q . When the sample temperature is increased to 25 °C, there is little indication of the diffraction peak, suggesting that ionic liquid has adopted a disordered state. The intensity at low- q ($q < 0.01/\text{\AA}$) exists in the empty cell data.

When lipid is added to the ([CH₃O(CH₂)₂-mim][Tf₂N]), the signal changes slightly with increasing lipid concentration. The data collected for the three lipid concentrations and the neat ionic liquid at 10 °C are shown in Figure 2. The low- q region of the data changes less than the diffraction peak, but this trend is not as clear in the data collected at 6 °C (not shown). The data collected at 6 °C were collected after the data at 10 °C, so it is possible that the sample relaxed during the collection of the data at 10 °C. The difference intensity profile for the stock lipid concentration, minus the neat ionic liquid, is shown in Figure 3. Clearly, the lipid has not formed a large-scale structure independent of the ionic liquid, which would result in a clear intensity profile starting at low q . While it is true that there are still indications of the diffraction peak at high- q , the signal suffers from noise. The addition of lipid made the peak slightly wider or caused the position to slightly change, as can be seen in Figure 2, which is reflected in the difference profile. Additional experiments using a powder diffractometer or similar instrument with a broader q -range are required to understand the behavior of the system.

Experiment Report (continued)

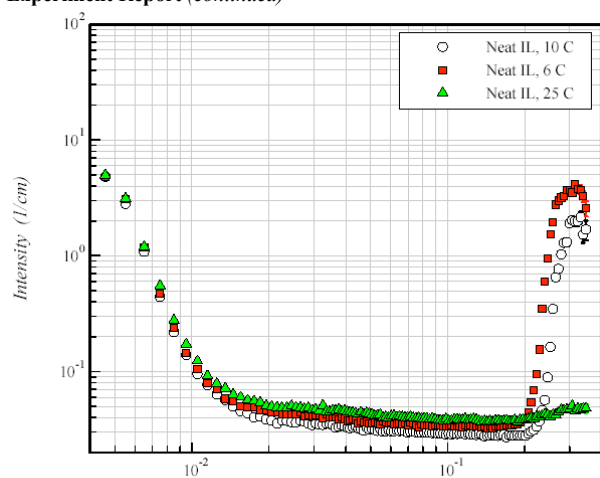


Figure 1

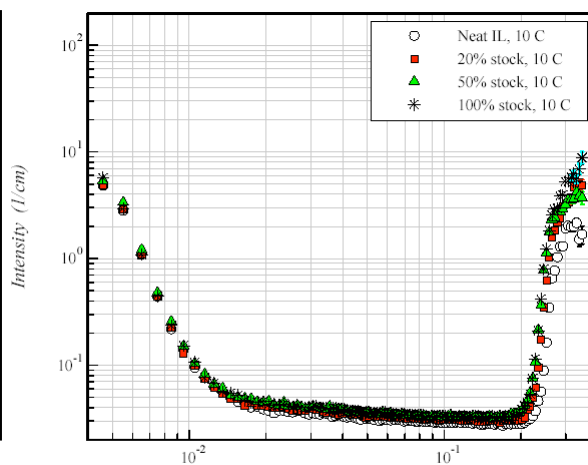


Figure 2

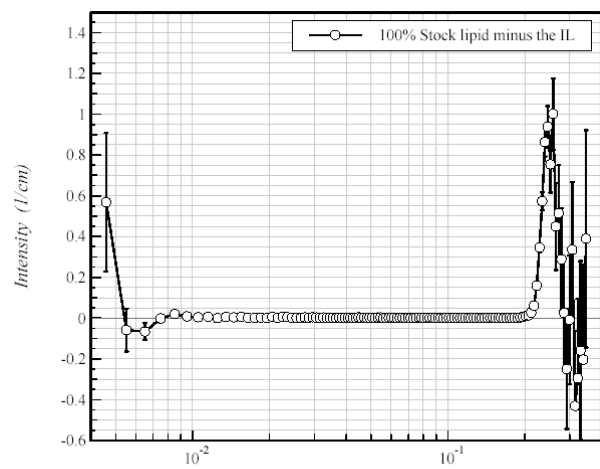


Figure 3

IMPORTANT! List or attach a list of publications resulting from this experiment (published or in press).

Submit all experiment reports to:
LANSCCE User Office, MS H831, Los Alamos National Laboratory, Los Alamos, NM 87545

Experiment was carried out at:	Local Contact	Proposal #	LANSCCE Use Only
<input checked="" type="checkbox"/> Manuel Lujan Jr. Neutron Scattering Center	Dr. Yusheng Zhao	2003189	Report Rc'd 6/3/04
<input type="checkbox"/> Weapons Neutron Research Facility	FP/Instrument Used		
<input type="checkbox"/> WNR/Blue Room	NPDF		

Title

Surface Reconstruction in Nano-Size Diamond

Authors and Affiliations

Cristian Pantea, Yusheng Zhao, Jiang Qian, Jianzhong Zhang, Luke Daemen, Thomas Proffen, Los Alamos National Laboratory
T. Waldek Zerda, Texas Christian University
Bogdan Palosz, UNIPRESS, Poland

Experiment Report

The nano-size diamond crystals are of increasing experimental and theoretical interest. The unique physical, chemical and mechanical properties of nanocrystalline solids can be understood in terms of their nanoscale structure and special features of the grain boundary phase. The surface of nano-size diamond crystallites can undergo sublimation, desorption, adsorption, chemical reaction, surface reconstruction, or phase transition to graphite. These effects are very significant in nanocrystalline solids, since the surface area-to-volume ratio is much larger than in bulk materials. The number of the atoms on the surface is comparable with those on the volume in nano-size crystals. When heated at high temperatures in an inert gas, different molecular species adsorbed on the diamond surface will be released, the surface undergoing a reconstruction.

We studied the surface reconstruction of nano-size diamond crystals, function of different gases desorbed from the diamond surface at different temperatures, up to the phase transition of surface diamond layers to curved graphite-like structures.

Diamond surface reconstruction was previously observed in bulk diamond, only π -bonded chain structures described by Pandey fit all the experimental data satisfactorily. In these structures (see Fig. 1 below) the whole outer puckered-hexagon layer of the ideal (111) surface is distorted. The connectivity to the next layer of underlying atoms is affected, with the formation of alternative five- and seven-membered rings.

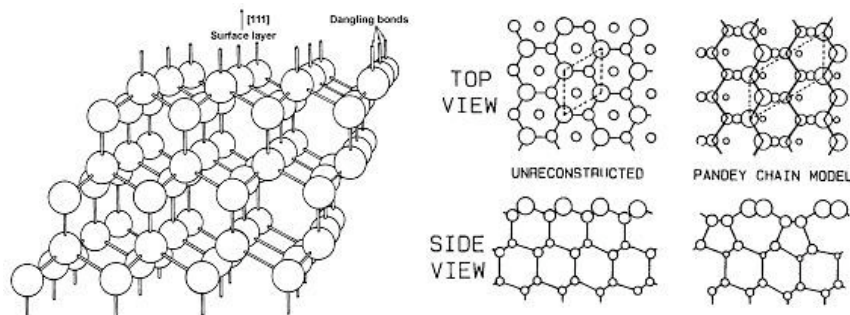


Fig. 1. Diamond surface reconstruction

Experiment Report *(continued)*

The nano-size diamond used in our experiments is obtained by explosive detonation and has a narrow particle size distribution, 2-10 nm, with an average value of 5nm. The nano-diamond crystals contain: carbon, up to 88%; hydrogen, 1.0%; nitrogen, 2.5%; oxygen, up to 10%. Desorption of different species present on the nano-diamond surface were done ex-situ, in inert atmosphere. The temperatures used are: 673 K (water desorption), 873 K (oxygen), 1073 K, 1273 K (hydrogen), and 1473 K (graphitization).

In Fig 2 and 3 the scattering pattern of nano-diamond sample before and after treatment at 1200 C for 2 hours in inert atmosphere are shown. The peak corresponding to the (002) reflection of graphite can be easily observed at about 1.84 \AA^{-1} .

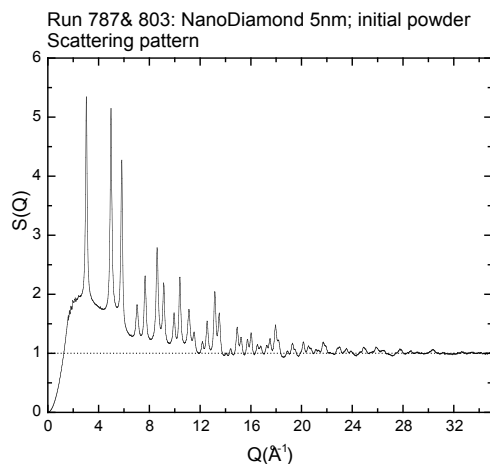


Fig. 2. Scattering pattern of nano-diamond, initial powder.

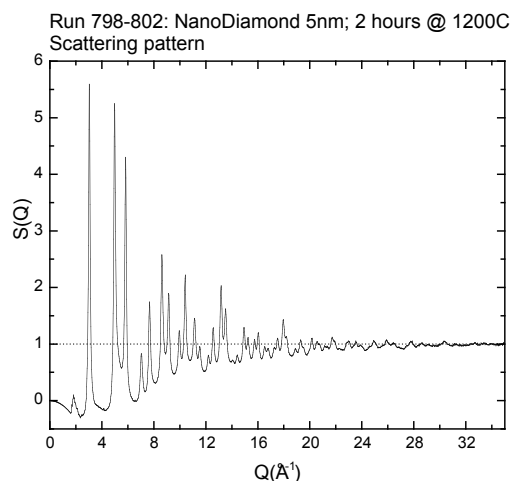


Fig. 3. Scattering pattern of nano-diamond, treated for 2 hours at 1200 C.

The relative changes in inter-atomic distances distribution in diamond can easily be observed in the Fig. 4 and 5, where the pair distribution function is plotted vs the distance between carbon atoms, indicating the rearrangement of C-C bonds.

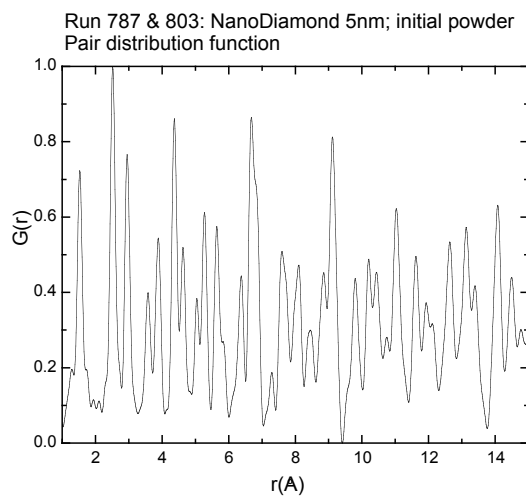


Fig. 4. G(r) of nano-diamond, initial powder.

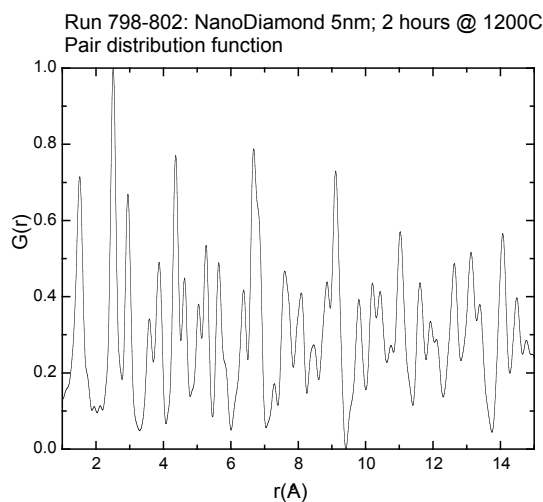


Fig. 5. G(r) of nano-diamond, treated for 2 hours at 1200 C.

IMPORTANT! List or attach a list of publications resulting from this experiment (published or in press).

None. The data analysis is still in progress.

Submit all experiment reports to:
LANSCE User Office, MS H831, Los Alamos National Laboratory, Los Alamos, NM 87545

Experiment was carried out at:	Local Contact	Proposal #	LANSCE Use Only
<input checked="" type="checkbox"/> Manuel Lujan Jr. Neutron Scattering Center	Daemen, Luc	2003190	Report Rc'd
<input type="checkbox"/> Weapons Neutron Research Facility	FP/Instrument Used		
<input type="checkbox"/> WNR/Blue Room	4 / HIPPO		<div style="border: 1px solid black; padding: 2px;">6/3/04</div>

Title

2003190 “Neutron Powder Diffraction in Highly Absorbing Materials, continued”

Authors and Affiliations

LANL Contributors: Heather Volz (LANSCE-12/NMT-16), Joyce Roberts (LANSCE-DO), Angus Lawson (MST-8), Luke Daemen (LANSCE-12), Sven Vogel (LANSCE-12), Darrick Williams (LANSCE-12), Tim Medina (LANSCE-12), Mike Geelan (LANSCE-12), Kathy Lovell (LANSCE-12), Ross Sanchez (LANSCE-12), Mike Ramos (NMT-16), Luis Morales (NMT-16), Heather Hawkins (NMT-16), Franz Freibert (NMT-16), Don Brown (MST-8), Thomas Sisneros (MST-8), Frans Trouw (LANSCE-12)

Experiment Report

- This was a continuation of proposal #2003064. Experiments were performed on the High-Pressure Preferred Orientation diffractometer (HIPPO) to investigate the effects of absorption on neutron diffraction data analysis, and to optimize sample geometry and experimental parameters for strong neutron absorbers. Surrogate materials (dysprosium and erbium) possessing absorption characteristics similar to those of ²³⁹Pu have been used to facilitate these preliminary investigations.

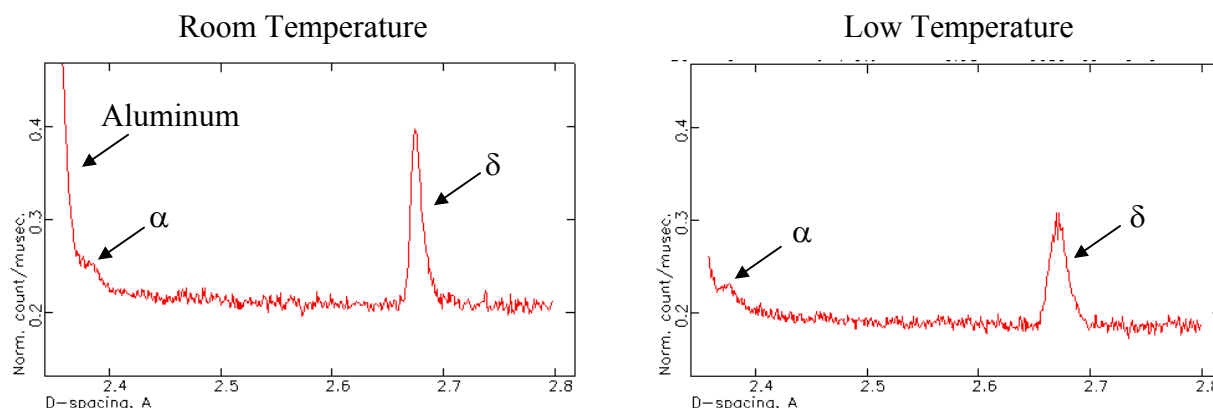
- On 1/26/04, several foil samples were measured on HIPPO's automatic sample changer at several orientations in order to study the texture of these strong neutron absorbers. These samples included: a thick stack of Dy foil (nine foils of thickness 0.003"); a single 0.003" thick copper foil; a Dy – Cu – Dy sandwich; and a thick stack (0.024") of Dy blocking a single copper foil. These last two stacks of samples with two very different materials were studied in order to understand the effect a strong neutron absorber might have on data analysis when multiple phases are present.

- Data analysis of the textured foils (including the previous work, #2003064) has been ongoing, and has started to yield trends (see submitted work to conferences, listed on page 2). So far, the focus has been on GSAS using spherical harmonics for the texture with two of the built-in absorption correction models, Debye-Scherrer and Linear absorption. Future work will continue on understanding the implications of absorption corrections on refined parameters, such as the thermal motion parameter, weight fraction, and texture index, particularly when an absorbing and non-absorbing phase are present. Also, the program MAUD will be investigated for its suitability for absorption corrections and its alternative texture model WIMV.

- On 3/21/04 to 3/22/04, data from a 2g sample of ²³⁹Pu (MT-52) was recorded on HIPPO. The sample was doubly encapsulated in aluminum, attached to the displer unit, and cooled to roughly 50K. The goal of the experiment was to look for the martensitic phase transformation from cubic (δ) to monoclinic (α').

Experiment Report (continued)

- Data analysis on the plutonium sample was inconclusive: the error is too great to definitively state whether the transformation did or did not occur. One reason for problems with data analysis is that the most intense monoclinic peak was on the shoulder of an intense aluminum peak from the sample holder, which was more of a problem than we expected. It is difficult to say if the amount of monoclinic phase actually increased, or if the cold temperature narrowed the aluminum peak, revealing more of the monoclinic phase (data shown on equal scale).



- Changes in integrated intensity (calculated from RAWPLOT) between ratios of aluminum and delta peaks were not significant between room temperature and 60K. Refinement with GSAS proved difficult, with the results for weight fraction of the different phases having errors much larger than the values themselves. The reason for this difficulty probably has several contributing factors. The large aluminum sample holder had several nested pieces, each one separately machined and not necessarily aligned, making convergence of the Al texture refinement elusive. Without a good refinement of the aluminum pattern, the plutonium was made even more difficult to converge and correctly refine, resulting in large statistical errors. The low overall fraction of monoclinic phase compared with aluminum pushed the monoclinic peaks into the noise.
- Ideas for future experiments will focus on improvements to the sample holder. This includes changes to the sample holder design, such as switching from aluminum to vanadium. Decreasing the thickness of the walls to reduce the sample container phase fraction would also help. Also, more work could be done to reduce the background instrument noise, and we could count for longer times (the above data were collected for approximately 4 hours each).
- Future Conferences / Publications
 - “Quantitative Texture Analysis of Highly Absorbing Materials from Neutron TOF Data”, H.Volz, S.Vogel, J.Roberts, D.Williams, A.Lawson, L.Daemen, T.Medina, M.Geelan. Poster presentation at the ACNS Conference, College Park, MD, June 6-10, 2004.
 - “Analysis of Texture From Strong Neutron Absorbers,” H.Volz, S.Vogel, J.Roberts, D.Williams, A.Lawson, L.Daemen, C.Necker. Oral presentation at the 53rd Denver X-Ray Conference, Steamboat Springs, CO, August 2-6, 2004.

IMPORTANT! List or attach a list of publications resulting from this experiment (published or in press).

Submit all experiment reports to:
LANSCCE User Office, MS H831, Los Alamos National Laboratory, Los Alamos, NM 87545

Experiment was carried out at:	Local Contact	Proposal #	LANSCCE Use Only
<input checked="" type="checkbox"/> Manuel Lujan Jr. Neutron Scattering Center	Dr. Yusheng Zhao	2003193	Report Rc'd 6/3/04
<input type="checkbox"/> Weapons Neutron Research Facility	FP/Instrument Used		
<input type="checkbox"/> WNR/Blue Room	FDS		

Title

Adsorption of Hydrogen, Water, and Hydrogen Peroxide on Diamond

Authors and Affiliations

Cristian Pantea, Luke Daemen, Yusheng Zhao, Jiang Qian, Jianzhong Zhang, Thomas Proffen, Los Alamos National Laboratory
T. Waldek Zerda, Texas Christian University
Bogdan Palosz, UNIPRESS, Poland

Experiment Report

Nano-size diamond crystals are of increasing experimental and theoretical interest. The unique physical, chemical and mechanical properties of nanocrystalline solids can be understood in terms of their large surface-to-volume ratio. The surface of nano-size diamond crystallites can undergo sublimation, surface reconstruction, physisorption, chemisorption, or phase transition to graphite. These effects are very significant in nanocrystalline solids because the surface area-to-volume ratio is much larger than in bulk materials. (The number of the atoms on the surface is roughly comparable to that of bulk atoms in the smaller nano-size crystals.)

Diamond surface reconstruction was previously observed in bulk diamond, and only π -bonded chain structures described by Pandey fit all the experimental data satisfactorily. In these structures (see figure below) the whole outer puckered-hexagon layer of the ideal (111) surface is distorted. The connectivity to the next layer of underlying atoms is affected, with the formation of alternative five- and seven-membered rings

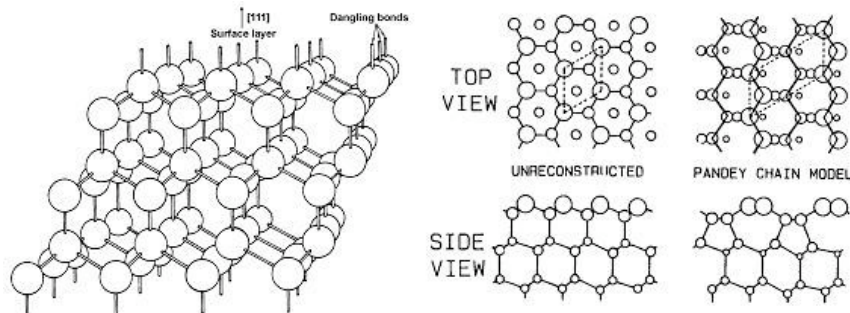


Fig. 1. Diamond surface reconstruction.

Exposed to air, the nano-size diamond crystals will adsorb different species present in the atmosphere, forming functional groups such as methyl, nitrile, hydroxy, oxycarboxylic at the surface. The hypothetical 'dangling bonds' present at the terminated surface of nano-crystals will be compensated by these functional groups. By treatment of the nano-diamond sample at different temperatures, the species from the outer layer will be desorbed from the surface at different temperatures, leading to a sequential reconstruction of the outer layer of the diamond nano-crystals. In the case of 5 nm diamond crystals the outer layer can contain as much as 40-50 % of the total number of atoms.

Experiment Report *(continued)*

After desorption at high temperature, we exposed the surface of the nano-diamonds to known quantities of hydrogen and water. Incoherent inelastic vibrational spectroscopy on FDS allows us to examine the dynamics and chemical nature of the species adsorbed on the surface of nano-diamonds.

To the best of our knowledge no attempts to characterize the nature of chemisorbed species on nano-size diamond crystals have been made. Such information, however, is very important not only because of its scientific value but also due to possible practical applications.

The nano-size diamond used in our experiments is obtained by explosive detonation and has a narrow particle size distribution, 2-10 nm, with an average value of 5nm. The nano-diamond crystals contain: carbon, up to 88%; hydrogen, 1.0%; nitrogen, 2.5%; oxygen, up to 10%. Desorption of different species present on the nano-diamond surface was done ex-situ, in inert atmosphere at 1273 K. The quantity of the sample used was in the range of 1.5-2 grams. After desorption we adsorbed a monolayer of the relevant hydrogenous substance and cooled the sample to low temperature and measured a vibrational spectrum on FDS.

The vibrational spectra obtained for the samples used in the present experiment are shown in Fig. 2. The data are still under investigation, and the interpretation of the vibrational information for different adsorbed species is still in progress.

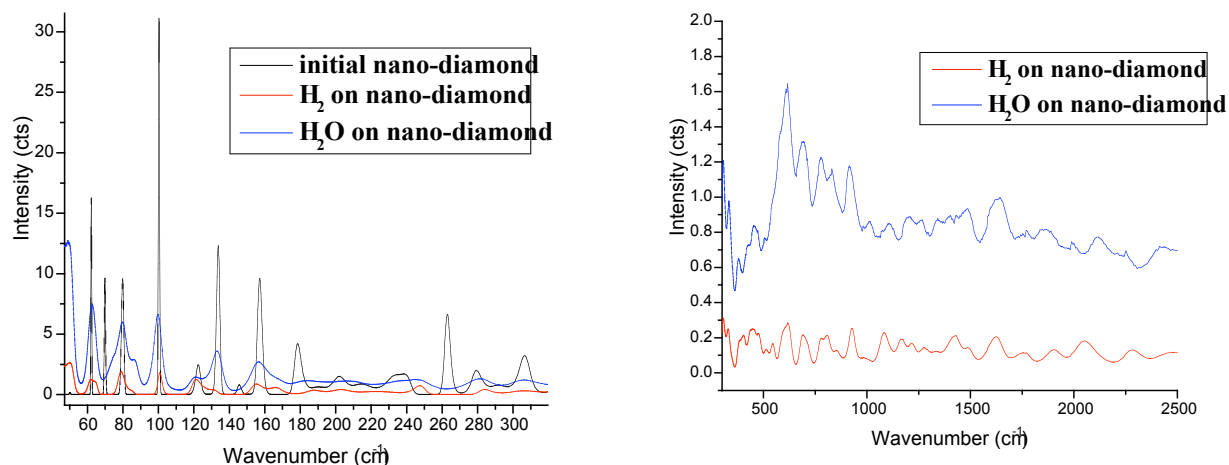


Fig. 2. Vibrational pattern of nano-diamond, as is, and with different adsorbed species on the surface (H₂ and H₂O)

IMPORTANT! List or attach a list of publications resulting from this experiment (published or in press).

None. The data analysis is still in progress.

Submit all experiment reports to:
LANSCE User Office, MS H831, Los Alamos National Laboratory, Los Alamos, NM 87545

Experiment was carried out at:	Local Contact	Proposal #	LANSCE Use Only
<input checked="" type="checkbox"/> Manuel Lujan Jr. Neutron Scattering Center	Anna Llobet	2003197	Report Rc'd
<input type="checkbox"/> Weapons Neutron Research Facility	FP/Instrument Used		7/15/04
<input type="checkbox"/> WNR/Blue Room	HIPD		

Title
Magnetic Structure of NiO nanoparticles

Authors and Affiliations
C.Cheng (UCSD); S.K.Sinha (UCSD/LANL); A.Berkowitz (UCSD); A.Llobet (LANL); F.Hellman (UCSD)

Experiment Report

We have had initial problems in preparing sufficient quantities of the NiO nanoparticles, so we decided instead to do some preliminary experiments on an available sample (0.5g) of CoO which Prof. Hellman was studying. The powder diffraction scans were run at 350K and at 15K , below the T_N of CoO (291 K). The scans are shown in Fig.1 and show that even with the small amount of sample, several nuclear and (at low temperatures) magnetic diffraction peaks could be observed in a reasonable amount of time (~ 15 hours/scan). A profile refinement of the room temperature data, however, revealed an extra phase identifiable as Co₃O₄, which amounted to ~ 5% of the total sample. Since Co₃O₄ also has its own antiferromagnetic structure, no attempt was made to refine the low temperature diffraction pattern. We are now making in our laboratory at UCSD, significantly larger quantities of pure phase CoO nanoparticles, which we are also characterizing with x-ray diffraction and with electron microscopy (to check the size distribution of the particles). These samples will be used in the next run to get better powder diffraction patterns of pure phase monodisperse nanoparticles of CoO in order to study their magnetic structure.

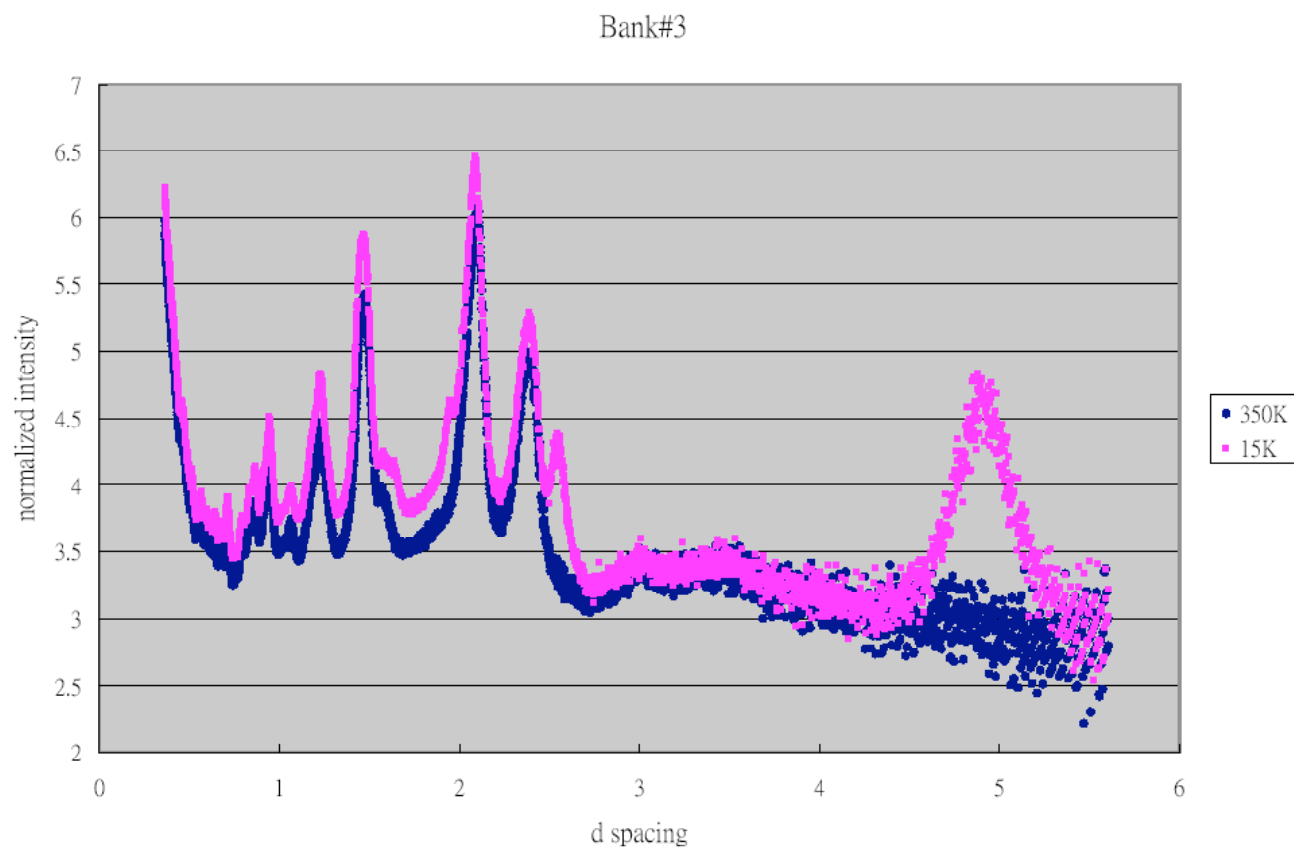
Experiment Report
(continued)

Fig.1 Diffraction Patterns in a single detector bank from the CoO sample at 2 different temperatures.

IMPORTANT! List or attach a list of publications resulting from this experiment (published or in press).

Submit all experiment reports to:
LANSCE User Office, MS H831, Los Alamos National Laboratory, Los Alamos, NM 87545

Experiment was carried out at:	Local Contact	Proposal #	LANSCE Use Only
<input checked="" type="checkbox"/> Manuel Lujan Jr. Neutron Scattering Center	M. Fitzsimmons	2003198	Report Rc'd
<input type="checkbox"/> Weapons Neutron Research Facility	FP/Instrument Used		6/28/04
<input type="checkbox"/> WNR/Blue Room	11A		

Title Origin of anomalous exchange bias in Fe/FeF ₂ bilayers
Authors and Affiliations I.K. Schuller (USCD) et al.

<p>Experiment Report</p> <p>A comprehensive theoretical explanation of exchange bias, the shift of the ferromagnetic hysteresis loop with respect to applied field of zero due to exchange coupling across the interface between an antiferromagnet with a ferromagnet, has proven to be elusive.^{1,2} Understanding exchange bias is important for the physics and engineering communities. In particular, it is not understood what factors are crucial in determining the magnitude (and even the sign) of the exchange bias. Fitzsimmons et al.^{3,4,5} have recently conducted extensive studies of exchange coupled bilayers of Fe and FeF₂ to understand the influence of crystalline quality of the antiferromagnet on bias. We found in our study that samples with single crystal FeF₂ layers had much smaller bias than samples having twinned FeF₂ layers.</p> <p>Recently, a sample of Co on untwinned (110) single crystal FeF₂ was grown on a single crystal MgF₂ substrate (our work had used MgO or FeF₂ substrates) and exhibited exchange bias comparable to samples with twinned antiferromagnetic layers.⁶ Our research group has more recently determined that indeed Co, Ni and Fe films on untwinned FeF₂ grown on MgF₂ substrates all exhibit very large exchange bias.</p> <p>The question of immediate importance is why is the exchange bias of samples grown on MgF₂ substrates so much larger than those of samples grown on FeF₂ substrates? We hypothesize that untwinned FeF₂ films grown on MgF₂ substrates contain many more uncompensated moments that tend to promote large exchange bias, than those grown on FeF₂ substrates. During field cooling, uncompensated moments (particularly those located at or near the ferromagnetic/antiferromagnetic interface) preferentially align opposite to the cooling field (for cooling fields typically less than 1 T) in the Fe/FeF₂ system.⁷ Domain walls in the antiferromagnet, which occur more frequently in defective films compared to more perfect films, pin the net magnetization of uncompensated moments in the antiferromagnet.⁸ So, we expect an enhancement of magnetization at the Fe/FeF₂ interface, one that is large in a sample of Fe/FeF₂ grown on an MgF₂ substrate, since this sample exhibits anomalously large bias.</p>
--

¹ W.H. Meiklejohn and C.P. Bean, Phys. Rev., **105** 904 (1957).

² J. Nogués and I.K. Schuller, J. Mag. Mag. Mat., **192** 203 (1998).

³ M.R. Fitzsimmons, P. Yashar, C. Leighton, Ivan K. Schuller, J. Nogués, C.F. Majkrzak and J.A. Dura, Phys. Rev. Lett., **84**, 3986 (2000).

⁴ M.R. Fitzsimmons, C. Leighton, A. Hoffmann, P.C. Yashar, J. Nogués, Ivan K. Schuller, C.F. Majkrzak, J.A. Dura and H. Fritzsche, Phys. Rev. B, **64**10, 4415 (2001).

⁵ M.R. Fitzsimmons, C. Leighton, J. Nogués, A. Hoffmann, K. Liu, C.F. Majkrzak, J.A. Dura, J.R. Groves, R.W. Springer, P.N. Arendt, Phys. Rev. B, **65**, 4436 (2002).

⁶ M. Grimsditch, A. Hoffmann, P. Vavassoi, H. Shi and D. Lederman, Phys. Rev. Lett., **90**, 257201-1 (2003).

⁷ C. Leighton, J. Nogués, B.J. Jonsson-Akerman, I.K. Schuller, Phys. Rev. Lett., **84**, 3466 (2000).

⁸ A.P. Malozemoff, Phys. Rev. B, **35**, 3679 (1987).

Experiment Report *(continued)*

Indeed, FeF_2 single crystals grown on MgF_2 are highly effective films. In the high-resolution transmission electron micrograph shown in Fig. 1, dislocations at the FeF_2 - MgF_2 interface are observed with ~ 40 nm spacing.

Last year, we used an ingenious neutron scattering technique to identify uncompensated magnetization in the FeF_2 and to show that much of this magnetization was pinned to a direction parallel to the cooling field. The technique involves rotating the sample (after it had been field cooled) along a direction perpendicular to its surface normal in a large (5 kOe) magnetic field (see schematic in Fig. 2). In this configuration, magnetization that can respond to the applied field appeared in

the non-spin-flip channels [blue and red data, Fig. 2(c)], while pinned magnetization (i.e., the magnetization that is pinned to the FeF_2 crystal, which was rotated) appeared in the spin-flip channel [green data, Fig. 2(c)]. We have fitted a simple model that consists of a domain wall parallel and centered at the Co/FeF_2 interface. The domain wall is a 106° wall⁹ and extends about 2 μm on either side of the interface. From these characteristics, we infer an interface anisotropy of 10^6 erg/ cm^3 (rather typical of bulk Fe and Co, but an order of magnitude smaller than the anisotropy of FeF_2). The root mean square magnetization of the uncompensated spins in the FeF_2 layer is ~ 67 emu/ cm^3 , and, very importantly, the uncompensated magnetization extends at least 16 μm into the FeF_2 layer and perhaps throughout its entire 33 nm thickness.

The experimental case for uncompensated and pinned magnetization in the FeF_2 layer is convincing. However, while we know that this magnetization [as evidenced by the spin-flip scattering in Fig. 2(c)] disappears (the green data in Fig. 2(a) is nearly zero for all measurements of Q) when the sample temperature is raised to 108 K, i.e., about 30 K greater than the Neel point of FeF_2 , we do not know whether the uncompensated magnetization in the FeF_2 is the source of exchange bias or whether bias and the magnitude of the uncompensated magnetization are correlated. For example, exchange bias and uncompensated magnetization in an antiferromagnet both naturally disappear when the antiferromagnet is no longer ordered.

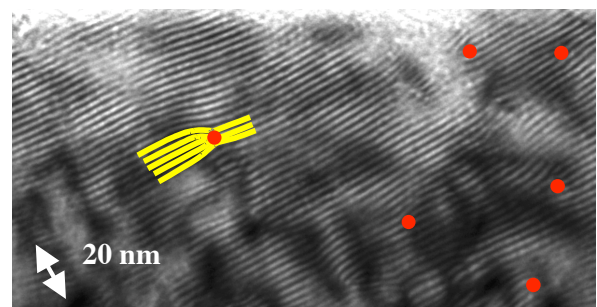


Figure 1 Plan view TEM image showing dislocations (marked by the red circles) at the interface between FeF_2 and MgF_2

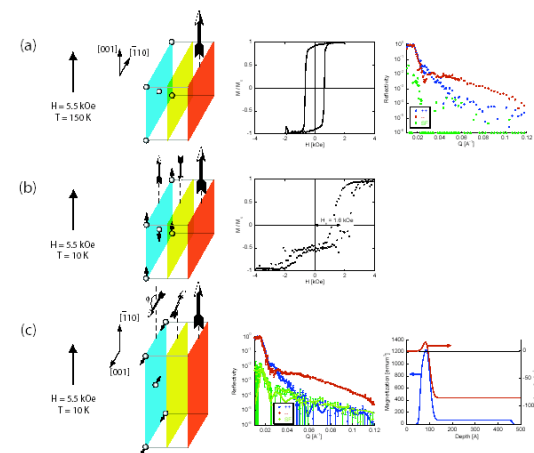


Fig. 2 The orientation of the cooling field relative to the crystallographic axes of the FeF_2 film are shown at the right of the figure for the temperatures of (a) 108 K, (b) 10 K before rotation, and (c) 10 K after rotation. The neutron reflectivities for cases (a) and (c) are shown plotted vs. momentum transfer Q . The orientation of the spins in the FeF_2 , interface and Co film are qualitative representations of a fitted model (discussed in the text).

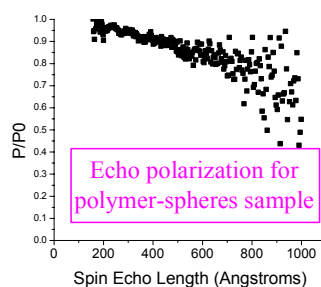
IMPORTANT! List or attach a list of publications resulting from this experiment (published or in press).

Experiment Report (continued)

First Neutron Spin Echo Achieved at a Spallation Source

- **Motivation** – study structure with neutrons on length scales between 1 nm & 500 nm for nanoscience & biology
- **Issue** – samples have small volumes (e.g. films, membranes) or are dilute (e.g. proteins in solution)
 - Neutron spin echo scattering angle measurement (SESAME) can help

SESAME apparatus on ASTERIX at LANSCE

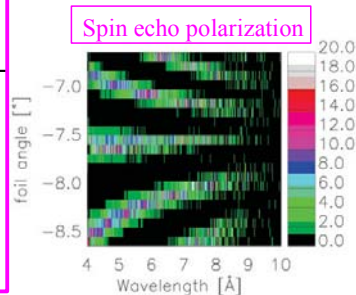


Conclusions

Spin echo polarization shows expected dependence on precession foil angle & neutron wavelength →

← We can access length scales to about 100 nm with this simple apparatus

Precession Foil



IMPORTANT! List or attach a list of publications resulting from this experiment (published or in press).

Data from this experiment were presented in an invited talk at the *Polarized Neutrons in Condensed Matter Research* conference recently held in Washington DC (June 1-4, 2004)

High-Pressure High-temperature Studies of Nanocrystalline SiC and Diamond

Proposal #2003207: Preliminary report

Purpose

Determination of the atomic structure of the nanograin core and surface by diffraction methods and examination of the grain-size dependencies of physical properties of nanocrystals in order to understand and control the formation of nanocompacts and nanocomposites. Examination of different structural and elastic properties of the grain cores and surface (grain boundaries) of nanocrystallites based on the analysis of strains generated under high pressures.

Experiments

In a series of experiments proposed for this study we planned to perform the following measurements:

Under High Hydrostatic Pressure conditions:

- (1) diffraction data for micron- and nano-sized powders under different (increasing) pressures (4-6 pressures).

Under High Isostatic-Pressure High-Temperature conditions:

- (2) samples annealed at a given temperature (2-3 different temperatures) under increasing pressure (5-8 pressure points) until the yield strength of the material decreases (this would lead to a disappearance of both surface- and bulk-related *micro*-strains attained under different p-T conditions);
- (3) samples subjected to a high pressure (2-3 different pressures) at different temperatures (4-6 temperatures) to examine the response of the material to the temperature change (to distinguish the surface and core contributions through the analysis of relaxation of *micro*-strains located at the surface and in the bulk).

Under ambient conditions:

- (4) reference diffraction data for micron- and nano-sized powders (a), before and, (b), after high-pressure high-temperature processings.

Due to the required long exposure time for nanopowder samples, the measurements were limited to room temperature conditions. We did measurements on differently pre-processed five nano-size (2, 5, 7, 9 and 11 nm in diameter) and one micron-size SiC powders in vanadium containers (reference measurements, p. 4 above). We selected three samples (7, 11 nm and micron size) for high pressure measurements (pp.2 & 3 above). The high pressure data were obtained in the Q-range of up to 20 - 25 \AA^{-1} .

Results

The results of the measurements, for one of the nano-sized and the micron-sized samples is shown in Fig. 1 (The data were elaborated based only on the positions of the maxima of the diffraction peaks.)

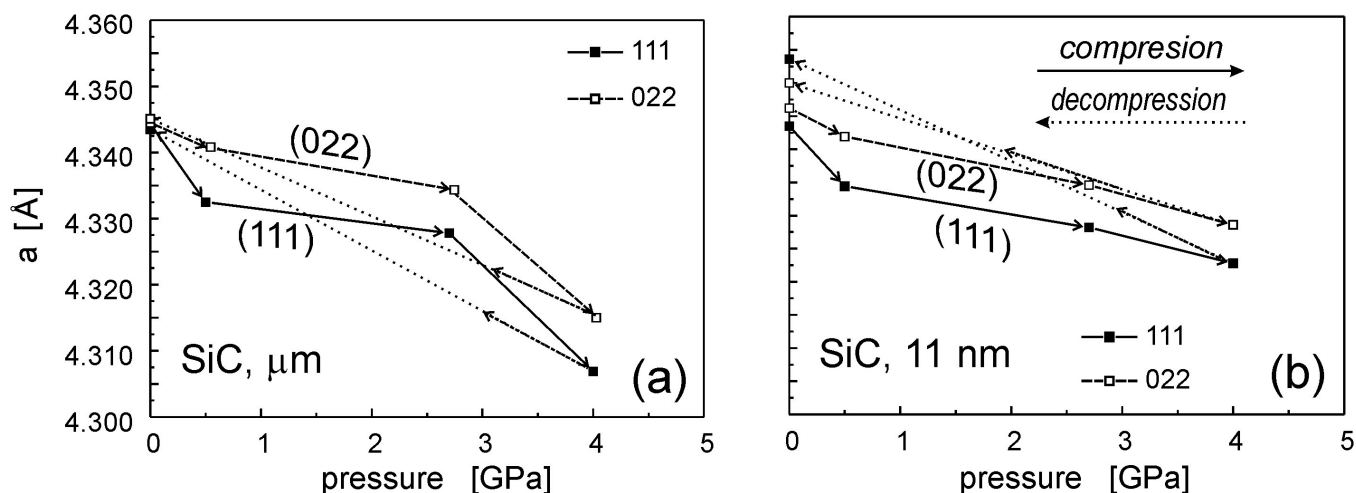


Fig. 1 Dependence of the lattice parameters on pressure determined from the reflections (111) and (022) of SiC powders. Grain diameter: (a), 1-2 μm ; (b), 11 nm.

The results lead to the following conclusions:

1. The difference in the slope between the curves for (111) and (022) reflections for lower pressures (< 1 GPa) suggests a presence of a strong compression anisotropy of the SiC lattice.
2. Relatively small compression exhibited by micro-powder between 0.5 and 2.5 GPa is apparently due to accumulation of micro-strains at the grain boundaries. Those strains get relaxed, dissipated into the grain bulk, when the pressure grows from 2.5 GPa up, Fig. 1a [1].
3. Compression of SiC lattice in the nanopowder in the pressure range of up to 4 GPa is much smaller than that for the micropowder, Fig. 1b. That difference is apparently again due to a presence of micro-strains at the surface of the grains, but the effect is much stronger since the fraction of the surface-related atoms in nanopowder is much larger than that for micron-sized material. We conclude that the strongly strained surface leads to an increase in the "overall" (as measured from the Bragg lines) hardness of the material.
4. After decompression the lattice of micro-grains returns to its starting point, Fig. 1a. It is different for nanograins: under stress the lattice apparently undergoes a substantial reconstruction which is demonstrated as an increase in the lattice parameter after sample decompression, Fig. 1b. This may be related to generation of defects, but it might also be a result of changes of the structure at the surface of the grains.

In general, a clear difference between the properties of micron- and nano-sized powders is observed. The specific conclusions are preliminary only. A more complete analysis (now in progress) will account for changes in the specific inter-atomic distances and in the width of peaks of the $G(r)$ function, what requires performing the PDF analysis (compare our preliminary results in ref. [2]). Some of the results will be presented during the upcoming IPDIC-9 conference [10].

The following data elaboration is in progress:

- (a) Structure modeling and simulation of the diffraction patterns combined with the analysis of the experimental results using the Apparent Lattice Parameters vs. Q relation [3 - 5]. (The current results provide much better statistics than the previous ones obtained with HIPD instrumentation.)
- (b) Analysis of *macro*- and *micro*-strains based on the Bragg peak positions, broadening, and asymmetry (examination of deviatoric stress [6 - 8]).
- (c) PDF analysis [4, 5].

The analysis will also account for thermal vibrations in the lattice. Preliminary studies of the temperature factors in SiC nanocrystals were done use of x-ray diffractograms [9]. The present data should allow for a similar but much more accurate analysis of the overall temperature factors and, what is particularly important, extend the previous study to examination of vibrations of the atomic pairs to those based on the PDF analysis. So far we did calculations/simulations of diffractograms and PDF spectra assuming harmonic vibrations.

The next, logical step in this research project is studying the powders under different temperatures. That topic will be a subject of our future application for HIPPO beam time. After the present data are elaborated, and after examination of thermal vibrations in powders and sintered SiC nanocrystals at elevated temperatures under ambient conditions is done, we plan to complete the remaining objectives of this project.

Note: The elaboration of the data measured in the present experiment is due to the first time use of HIPPO data for PDF analysis. This instrument is not yet optimized for such type of experiments. That concerns particularly the analysis of the diffraction data collected under high-pressures, where calibration has to account for a presence of anvils and shieldings. In our next application for the beam-time we will ask for 2 days dedicated to calibration runs alone.

References:

1. B. Palosz et al., *Journal of Physics. Condensed Matter*, 16 (5) (2004) S353 - S377.
2. B. Palosz et al., *Mat. Res. Soc. Symp. Proc.* 778 (2003) U1.11.1 - 6.
3. B. Palosz et al., *Acta Phys. Polonica A*, 102 (1), (2002), 57-82.
4. B. Palosz et al., *Zeitschrift für Kristallographie*, 217 (2002) 497 - 509.

5. B. Palosz et al., *Solid State Phenomena*, 94, (2003), 203-216.
6. Y.H. Zhao et al., *Phys.Rev. B* 56, (1997), 14,322-14,329.
7. D.J. Weidner et al., *High Pressure Research: Application to Terra and Planetary Sciences*, (1992),13-17.
8. D.J. Weidner et al., *Geophys.Res.Lett.* 21, (1994), 753-756.
9. S. Stel'makh et al., *J. Alloys and Compounds (Proc. E-MRS Meeting, 2003)*, in the press.
10. S. Stel'makh et al., *IX European Powder Diffraction Conference, Prague, Czech Republic, 2-5 September 2004*.

Submitted by: B. Palosz, W. Palosz, S. Vogel, T.W. Zerda, and J. Zhang.

Enclosure

File "Prague 04", Abstract of the presentation at the EPDIC-9.



LANSCe User Office, MS H831, Los Alamos National Laboratory, Los Alamos, NM 87545

Experiment Report

The $\text{Ge}_2\text{Sb}_2\text{Te}_5$ compound has been widely used as a high-speed phase-change material such as DVD-RAMs. The study of these crystal structures becomes an important subject for the improvement of commercial performance such as the effective energy conversion from light to heat in a limited area. We have found the significant displacement of germanium atoms even in this crystalline cubic phase. Usually, such a large lattice distortion has disadvantage for the electronic conductivity. Our result, however, implies that this distortion in addition to the lattice defect reduces only the thermal conductivity, resulting in the effective conversion of light energy to lattice heat in a limited area.

Within the average structure analysis, the space group of $Fm\bar{3}m$ gives us the best results. If the average crystal structure was intrinsic, the first nearest neighbor peak in the $G(r)$ should be a broad simple Gaussian. Figure 1 shows observed, calculated, and difference of $G(r)$ for the average and the local crystal structures. The position and width of a peak in $G(r)$ reflect the value and distribution of distances between different atomic correlations, and the peak area provides a measure of the corresponding coordination number. As shown in Fig. 1, the observed first nearest neighbor peak had a complex structure. It cannot be described by one broad peak expected from the average structure. Since the peak widths were much wider than the expected r -resolution of 0.11 Å, many peaks are involved in the first peak. Since 4(a) site is entirely occupied by tellurium atom, only Ge-Te and Sb-Te atomic correlations appear in the first peak. The obtained $G(r)$ pattern in the real space range of 2.0 < r < 12.0 Å was fitted under the following restriction ($R_{\text{wp}} = 10.8\%$ and $R_e = 4.0\%$). We set a periodic non-symmetric cubic unit cell with 8 sites, where one tellurium atom was fixed at the origin. All tellurium occupation factors were fixed to be unity, while the summation of occupation factors of germanium and antimony atoms at all the similar positions of 4(b) site was fixed to be an average value of 0.8. Isotropic thermal factors were assumed to depend only on the elements. Otherwise, all atoms were freely displaced. The obtained distorted crystal structure is shown in Fig. 1.

Experiment Report (continued)

There was some correlation between germanium and antimony occupancies in (111) plane. It suggests that same atoms prefer in the same (111) plane, which is characteristic for a hexagonal layered phase of $\text{Ge}_2\text{Sb}_2\text{Te}_5$.

As shown in Fig. 1(c), Ge-Te bond lengths ($3.03(0.22)$ Å) have much wider distribution than Sb-Te bond lengths ($3.02(0.10)$ Å). The wide and split Ge-Te bond lengths would be due to the narrower radius of germanium $4p$ orbital than antimony $5p$ orbital. As a whole, large displacement of germanium atoms are characteristic in the crystal structure.

In conclusion, we have found large displacement of germanium atoms in a crystalline cubic phase of $c\text{-Ge}_2\text{Sb}_2\text{Te}_5$, a commercial high-speed phase-change memory material, by using PDF method. In addition to the heavy elements in $c\text{-Ge}_2\text{Sb}_2\text{Te}_5$, the lattice distortion and the lattice defect reduce the thermal conductivity, limiting the heat diffusion under laser irradiation, while they little affect the electronic conduction that has mainly $5p$ orbital character of tellurium anions. Because of this low thermal conductivity, the memory mark can be recorded in a limited area. So, even in the future sophisticated crystalline memory materials, phonon should be scattered strongly by local lattice distortion, lattice defect, or impurity, in order to reduce the heat diffusion.

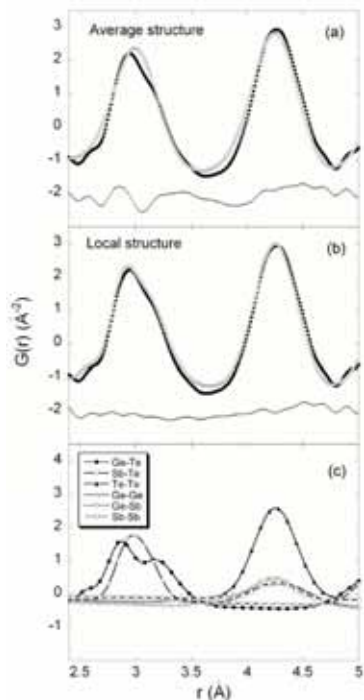


Figure 1. Observed (closed circle), calculated (open circle), and difference (small closed circle) pair distribution function profiles for average (a) and local (b) structures in a short r -range. Fitted $G(r)$ components for local structure in (b) are shown in (c), indicating large displacement of germanium atoms.

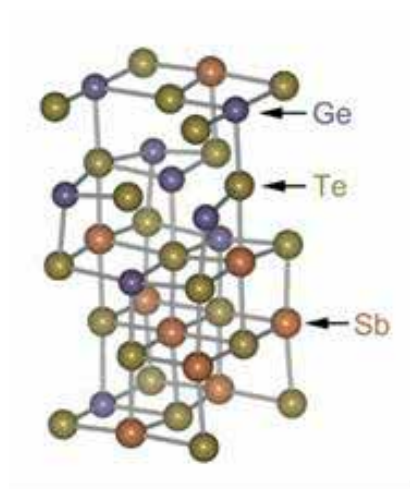


Figure 2. Local crystal structure of $c\text{-Ge}_2\text{Sb}_2\text{Te}_5$. Only bonds shorter than 3.2 Å are shown.

IMPORTANT! List or attach a list of publications resulting from this experiment (published or in press).

Submit all experiment reports to:
LANSCE User Office, MS H831, Los Alamos National Laboratory, Los Alamos, NM 87545

Experiment was carried out at:	Local Contact	Proposal #	LANSCE Use Only
<input checked="" type="checkbox"/> Manuel Lujan Jr. Neutron Scattering Center	Jarek Majewski	2003214	Report Rc'd
<input type="checkbox"/> Weapons Neutron Research Facility	FP/Instrument Used		9/16/04
<input type="checkbox"/> WNR/Blue Room	SPEAR		

Title

Hydrophobic Interactions between LB-deposited Surfactant Monolayer Surfaces: Density Depletion Effects Near the Interface?

Authors and Affiliations

Jacob Israelachvili (UCSB), Jarek Majewski (LANL), Emily Meyer (UCSB), Qi Lin (UCSB)

Experiment Report

The hydrophobic interaction is important in biological self-organizing processes such as protein folding, ligand binding to hydrophobic receptor sites, and membrane and micelle formation as well as in many technological applications such as mineral flotation, wetting of surfaces, and colloid stability ^{1,2}. Understanding the factors underlying the nature and molecular origin of this effect will be important for fully understanding these phenomena. The important role of the hydrophobic interaction has led to a great deal of study yet, over 20 years since the first direct measurement of the long-range attraction between two hydrophobic surfaces ^{3,4}, no single theory is able to account for all observed experimental behavior and understanding of the origin of this interaction remains elusive. While some proposed models such as those invoking electrostatic effects ⁵, correlated dipole-dipole interactions ⁶, and water structural effects have proven unlikely to fully explain the hydrophobic interaction, models involving nanobubbles ⁷⁻⁹, lateral enhancement of subcritical density fluctuations in the film ¹⁰, and the metastability of the confined fluid ^{11,12} continue to be the focus of much discussion.

The effects of such parameters as electrolytes ^{9,13} and temperature ¹⁴ on the hydrophobic interaction remains unclear, but the absence of dissolved gas has been shown to decrease the range of the hydrophobic attraction as well as the magnitude at long range (e.g. ^{15,16} and our own unpublished results), and has also been shown to increase emulsion stability ¹⁷. One would expect the presence of dissolved gas to play a significant role in models based on the presence of nanobubbles or the metastability of the liquid film. In these cases the density of the solvent medium can also be expected to deviate from its bulk value ¹⁸. It cannot be seen from the data currently available whether the effect of removing dissolved gas is a bulk effect, a surface effect, or both. Studies to determine the behavior of water density near hydrophobic walls may play an important role in validating or refuting current theories of the hydrophobic interaction.

Our goal was to obtain information to clarify and resolve some issues concerning the origin of the hydrophobic interaction

Experiment Report (continued)

During our time at Los Alamos, we were unable to obtain conclusive data about density depletion near an LB-deposited hydrophobic surface. The thickness of our monolayer (~3 nm) was at the edge of the resolution of the technique, resulting in large errors in the most critical area of the resulting neutron reflectivity curves, making accurate analysis impossible. In an attempt to resolve hydrophobic chains from a possible air layer, deaerated D₂O was used, but the results of this study were also inconclusive.

References

1. Christenson, H. K. & Claesson, P. M. Direct measurements of the force between hydrophobic surfaces in water. *Advances in Colloid and Interfaces Science* **91**, 391-436 (2001).
2. Southall, N. T., Dill, K. A. & Haymet, A. D. J. A view of the hydrophobic effect. *Journal of Physical Chemistry B* **106**, 521-533 (2002).
3. Israelachvili, J. N. & Pashley, R. The Hydrophobic Interaction Is Long-Range, Decaying Exponentially with Distance. *Nature* **300**, 341-342 (1982).
4. Israelachvili, J. N. & Pashley, R. M. Measurement of the hydrophobic force between two hydrophobic surfaces in aqueous electrolyte solutions. *Journal of Colloid and Interface Science* **98**, 500-514 (1984).
5. Attard, P. Long-range attraction between hydrophobic surfaces. *Journal of Physical Chemistry* **93**, 6441-6444 (1989).
6. Yoon, R. H. & Ravishanker, S. A. Long-range hydrophobic forces between mica surfaces in dodecylammonium chloride solutions in the presence of dodecanol. *Journal of Colloid and Interface Science* **179**, 391-402 (1996).
7. Tyrrell, J. W. G. & Attard, P. Atomic force microscope images of nanobubbles on a hydrophobic surface and corresponding force-separation data. *Langmuir* **18**, 160-167 (2002).
8. Attard, P., Moody, M. P. & Tyrrell, J. W. G. Nanobubbles: the big picture. *Physica A-Statistical Mechanics and Its Applications* **314**, 696-705 (2002).
9. Parker, J. L., Claesson, P. M. & Attard, P. Bubbles, Cavities, and the Long-Ranged Attraction between Hydrophobic Surfaces. *Journal of Physical Chemistry* **98**, 8468-8480 (1994).
10. Yaminsky, V. V. & Ninham, B. W. Hydrophobic force: Lateral enhancement of subcritical fluctuations. *Langmuir* **9**, 3618-3624 (1993).
11. Christenson, H. K. & Claesson, P. M. Cavitation and the interaction between macroscopic hydrophobic surfaces. *Science* **239**, 390-392 (1988).
12. Bernard, D. Cavitation of a Lennard-Jones fluid between hard walls, and the possible relevance to the attraction measured between hydrophobic surfaces. *Journal of Chemical Physics* **98**, 7236-7244 (1993).
13. Christenson, H. K., Claesson, P. M. & Parker, J. L. Hydrophobic Attraction - a Reexamination of Electrolyte Effects. *Journal of Physical Chemistry* **96**, 6725-6728 (1992).
14. Christenson, H. K., Parker, J. L. & Yaminsky, V. V. Comment on "Interactions between hydrophobic surfaces. Dependence on Temperature and alkyl chain length." *Langmuir* **8**, 2080 (1992).
15. Sakamoto, M. K., Miyahara, M.; Higashitani, K. Origin of the long-range attractive force between surfaces hydrophobized by surfactant adsorption. *Langmuir* **18**, 5713-5719 (2002).
16. Craig, V. S. J., Ninham, B. W. & Pashley, R. M. Direct measurement of hydrophobic forces: A study of dissolved gas, approach rate, and neutron irradiation. *Langmuir* **15**, 1562-1569 (1999).
17. Craig, V. S. J., Ninham, B. W. & Pashley, R. M. The Effect of Electrolytes on Bubble Coalescence in Water. *Journal of Physical Chemistry* **97**, 10192-10197 (1993).
18. Kekicheff, P. & Spalla, O. Refractive-Index of Thin Aqueous Films Confined between 2 Hydrophobic Surfaces. *Langmuir* **10**, 1584-1591 (1994).

IMPORTANT! List or attach a list of publications resulting from this experiment (published or in press).

Submit all experiment reports to:
LANSCCE User Office, MS H831, Los Alamos National Laboratory, Los Alamos, NM 87545

Experiment was carried out at:	Local Contact	Proposal #	LANSCCE Use Only
<input checked="" type="checkbox"/> Manuel Lujan Jr. Neutron Scattering Center	J. Majewski	2003216	Report Re'd
<input type="checkbox"/> Weapons Neutron Research Facility	FP/Instrument Used		9/16/04
<input type="checkbox"/> WNR/Blue Room	SPEAR		

Title

Construction and Characterization of the Selectin Ligand-Receptor System

Authors and Affiliations

Jacob N Israelachvili, Qi Lin, Emily E Meyer, University of California, Santa Barbara
Jarek Majewski, Los Alamos National Laboratory
Scott I Simon, University of California, Davis

Experiment Report

The migration of leukocytes from blood vessels into inflamed tissue is a key step in the process of inflammation. The initial tethering of leukocytes to the endothelial cell surface is mediated by selectins. Special mechanisms enable selectins to trap leukocytes as they flow rapidly in the bloodstream. Understanding this fast and specific targeting mechanism is essential for predicting and controlling these systems: it could enhance our ability to develop better drug delivery processes, create new types of drugs and biomaterials, and develop powerful new treatments for various diseases.

We used the Surface Forces Apparatus (SFA) to directly measure the selectin-ligand interaction forces, the binding dynamics and strength, the effect of ligand affinity, ligand density, and other environmental factors. Our aim is to combine the techniques of Neutron Reflectometry (SANS) and Surface Forces Apparatus (SFA) to achieve a better understanding of the conformations of selectins and their ligands at surfaces.

The selectin/ligand surface was prepared in a similar way as in our SFA experiments. Since mica is not proper for neutron scattering, Si wafer and quartz were used instead. The first and second layers were DPPE and DLPE/DPPE-biotin and constructed by LB deposition. Then the substrate was transferred to a flow cell that filled with buffer (made with D₂O). The rest of the surface construction was done layer by layer by incubation with streptavidin and biotinylated IgG antibody respectively. (See Figure 1)

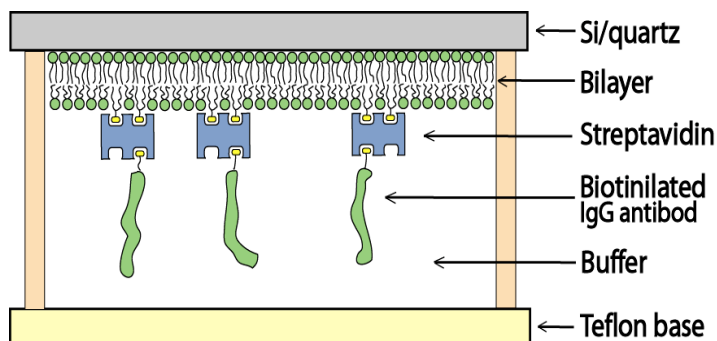


Figure 1. Schematic drawing of the

Experiment Report *(continued)*

Ideally, we would like to use selectins or their ligands as the materials for the last layer. But to cover up the whole substrate (about 40cm²) with those expensive molecules, it is not very practical simply because of the cost. Instead, we used biotinilated IgG, which has similar structure and molecular weight as the selectins, and the price is much more affordable.

During the beam time, we tried to determine the thickness for the surfaces at three stages: bilayer only, bilayer with streptavidin, and finally, bilayer with streptavidin and IgG antibody. However, the results showed that we were only able to identify the bilayer no matter how many things we put on the substrate. It might due to the fact that the last two layers are formed by macromolecules that are miscible in D₂O and not as close packed as the bilayer. In the absence of sharp interfaces in the system, the sensitivity it requires is beyond the limit of neutron scattering technique.

IMPORTANT! List or attach a list of publications resulting from this experiment (published or in press).



REPORT ON EXPERIMENT

(Please Type)

Submit all experiment reports to:
 LANSCE User Office, MS H831, Los Alamos National Laboratory, Los Alamos, NM 87545

Experiment was carried out at:		Local Contact	Proposal #	<i>LANSCE Use Only</i>
<input checked="" type="checkbox"/>	Manuel Lujan Jr. Neutron Scattering Center	Rex Hjelm	2003219	Report Rc'd 7/9/04
<input type="checkbox"/>	Weapons Neutron Research Facility	FP/Instrument Used		
<input type="checkbox"/>	WNR/Blue Room	LQD		

Title

SANS Study of Magnetic Correlations in Ferromagnetic GaMnAs

Authors and Affiliations

Brian Kirby, Univ. of Missouri
Jim Rhyne, LANL

Experiment Report

This experiment was to examine the critical scattering accompanying the paramagnetic/ferromagnetic phase transition in the ferromagnetic semiconductor GaMnAs. The concentration of the Mn is limited to values less than 9%, and our particular sample had 7% Mn. The total active film thickness was 7 microns. At this very dilute concentration and thin film thickness, expecting to see the magnetic critical scattering was a very high-risk endeavor, especially considering the small Q scattering from the GaAs substrate.

Small Q data were taken at three temperatures above and at the 45K Curie temperature. Unfortunately, with the available counting time (also possibly true with much longer counts) the statistics were such that the magnetic signal obtained after subtraction of the non-magnetic background obtained at high temperature was not statistically significant. Thus it was not possible to draw any quantitative conclusions about the nature of the phase transition in the GaMnAs or to obtain the critical scattering exponents, which was the original objective of the experiment.

It is intended to repeat the experiment at a later date if deposition procedures are developed to produce a much thicker sample that exhibits the same bulk magnetic properties as found in these films.

REPORT ON EXPERIMENT
(Please Type)

Submit all experiment reports to:

LANSCE User Office, MS H831, Los Alamos National Laboratory, Los Alamos, NM 87545

Experiment was carried out at: Local Contact Proposal #LANSCE Use OnlyxManuel Lujan Jr. Neutron Scattering CenterSven Vogel2003223Report Rc'dWeapons Neutron Research FacilityFP/Instrument Used7/14/04WNR/Blue RoomHIPPO

Title

Texture as a potential biosignature**Authors and Affiliations**

Jenny Pehl University of California, Berkeley Department of Earth and Planetary Science

Curtis Pehl University of California, Berkeley Department of Integrative Biology

Experiment Report

The experiment was conducted by using the HIPPO system to examine for a consistent texture of stromatolitic fossil material. Previous work on the texture had indicated the possibility of a weak texture that existed in the fossils as a result, most likely, of the style of formation. This could be the result of either the direct precipitation of calcium carbonate from the cyanobacteria that compose a stromatolite, or it would be the result of orientation of mineral grains that fall into the matrix composed of filamentous bacteria. We collected a suite of samples from the University of California Museum of Paleontology and Yale University collections. These samples represented a wide range of ages and types of stromatolites. The detection of a texture in these rocks could have served as a biosignature to help detect differences between biologically formed stromatolites, and layers of inorganic precipitates.

Texture analysis was performed with MAUD and no significant texture was found in any of the samples. Any texture seen was simply stochastic noise and was quite weak. This leads us to reject the idea that the formation of stromatolite fossils imparts any detectible texture, nor can texture be used as a biomarker for stromatolites.

The lack of texture may still be important in establishing a constraint upon the formation of the stromatolites, but that question has yet to be fully examined.

Experiment Report (continued)

IMPORTANT! List or attach a list of publications resulting from this experiment (published or in press).

None.

REPORT ON EXPERIMENT (Please Type)

Submit all experiment reports to:

LANSCe User Office, MS H831, Los Alamos National Laboratory, Los Alamos, NM 87545
Experiment was carried out at: Local Contact Proposal #LANSCe Use Only X
Manuel Lujan Jr. Neutron Scattering Center
Don Brown
2003224
Report Rc'd
Weapons Neutron Research Facility
FP/Instrument Used7/16/04
WNR/Blue Room
SMARTS

Title

Deformation Behavior of a Co-based Superalloy **Authors and Affiliations**

M. L. Benson, P.K. Liaw, T. A. Saleh, H. Choo – Department of Materials Science and Engineering,
The University of Tennessee

D. W. Brown – Los Alamos Neutron Science Center, Los Alamos National Laboratory

D. L. Klarstrom – Haynes International, Inc.

Experiment Report

Introduction

The ULTIMET[®] superalloy (54Co-26Cr, wt%) consists of a single-phase, face-centered-cubic (fcc) microstructure. The fcc phase, however, is thermodynamically stable only at high temperatures (i.e., above ~900°C) and is held in a metastable state upon fast quenching to room-temperature after solid-solution heat treatment. Upon applying a load to the material, it will undergo a strain-induced martensitic phase transformation to a hexagonal-close-packed (hcp) phase, which is the stable room temperature structure. We hypothesize that the development of this new phase significantly affects the mechanical properties of the alloy. Specifically, the hcp phase could contribute to the load-partitioning mechanisms upon deformation. Neutron diffraction offers an excellent tool to study this phenomenon. This report summarizes preliminary results of in-situ loading neutron-diffraction experiments on this alloy.

Experimental Procedure

Two room-temperature experiments were performed on the Spectrometer for Materials Research at Temperature and Stress (SMARTS): 1) a tensile monotonic-loading experiment and 2) a tension-tension cyclic-loading experiment. The monotonic-loading experiment was performed to a maximum tensile load of 890 MPa. Diffraction patterns were obtained at 23 points along the macroscopic stress-strain curve and upon unloading. The cyclic-loading experiment was conducted under load control with a stress ratio, $R = 0.1$ [R is the ratio of minimum stress (σ_{\min}) to maximum stress (σ_{\max})]. A maximum tensile stress of 840 MPa was applied to the specimen during the in-situ fatigue investigation. Diffraction patterns were obtained at the maximum and minimum stresses at 16 different cycles during the experiment. For both studies, a diffraction pattern was obtained at a stress of 20 MPa before the experiment initiated so that reference d-spacings were available for calculating strain. The development of the hcp martensitic phase and internal strain evolution was observed for these experiments.

Experiment Report (continued)

Results

Figure 1 shows the evolution of the hcp peak in the diffraction patterns normalized with respect to background from the axial detector bank as a function of stress. The hexagonal phase was not observed until a stress of 720 MPa was reached during the tensile experiment. Figure 2 displays the development of hkl-dependent internal strains as measured from the axial detector bank in the alloy during tension. These

curves demonstrate that the elastic and plastic anisotropies exist in the alloy among grains of differing crystallographic orientations. In addition, load partitioning among the fcc grains is observed in that the 200 orientation accommodates more strain than the other orientations. Similar behavior has been quantified before for fcc alloys in the literature [1].

Results of the tension-tension fatigue experiment are not included in a graphic format here. However, the hcp phase formed upon the first cycle, as would be expected, given the results of the monotonic- loading study. As fatigue proceeded, the intensity of the hcp peak did not change from what was observed at the first cycle. The calculation of the internal strains at the maximum tensile load during fatigue suggests that they quickly saturate within the early stages of fatigue.

Future Work

Quantifying the role that the hcp phase plays in load partitioning during monotonic and cyclic loading still remains incomplete. Also, a clear understanding of the texture development in the alloy during deformation has not yet been developed.

Reference

[1] B. Clausen, T. Lorentzen, and T. Leffers, *Acta Mater.*, 9 (1998) 3087-3098.

Submit all experiment reports to:
 LANSCE User Office, MS H831, Los Alamos National Laboratory, Los Alamos, NM 87545

Experiment was carried out at:		Local Contact	Proposal #	<i>LANSCE Use Only</i>
<input checked="" type="checkbox"/>	Manuel Lujan Jr. Neutron Scattering Center	Dhaval Doshi	2003226	Report Rc'd
<input type="checkbox"/>	Weapons Neutron Research Facility	FP/Instrument Used		7/21/04
<input type="checkbox"/>	WNR/Blue Room	FP9/SPEAR		

Title

Neutron Reflectivity on Super-Hydrophobic Films

Authors and Affiliations

Pratik Shah, Eric Branson, Seema Singh, Ralf Koehn, (University of New Mexico)
Frank van Swol, Jeff Brinker (UNM/Sandia National Laboratories)
Dhaval A. Doshi (LANSCE-12, Los Alamos National Laboratory)

Experiment Report

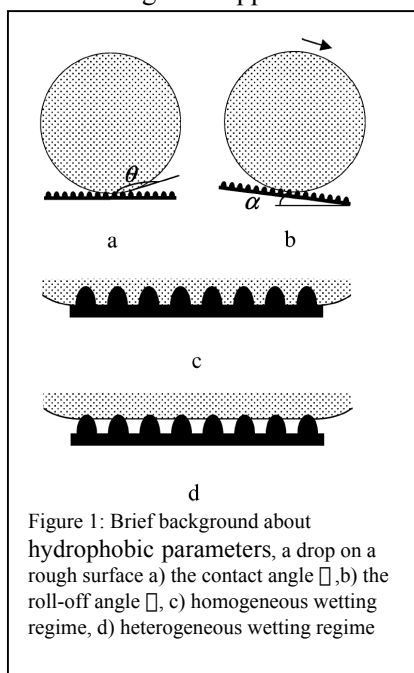
Super-hydrophobic (SH) surfaces have considerable technological potential for various applications due to their extreme water repellent properties. The contact angle of water droplets on low energy surfaces increases strongly with growing surface roughness and porosity. Apparently, the air trapped at the interface would play a crucial role because it reduces the effective contact area between solid and liquid. We were interested in characterizing the trapped air or water vapor in super-hydrophobic material while it was in contact with water.

Figure 1 gives the brief description of the hydrophobic parameters.

The goals of the experiment were to:

- (i) To understand the superhydrophobic-water interface i.e. the presence of an air/vapor layer.
- (ii) Further characterize the efficacy of the SH film in terms of water infiltration into the pores

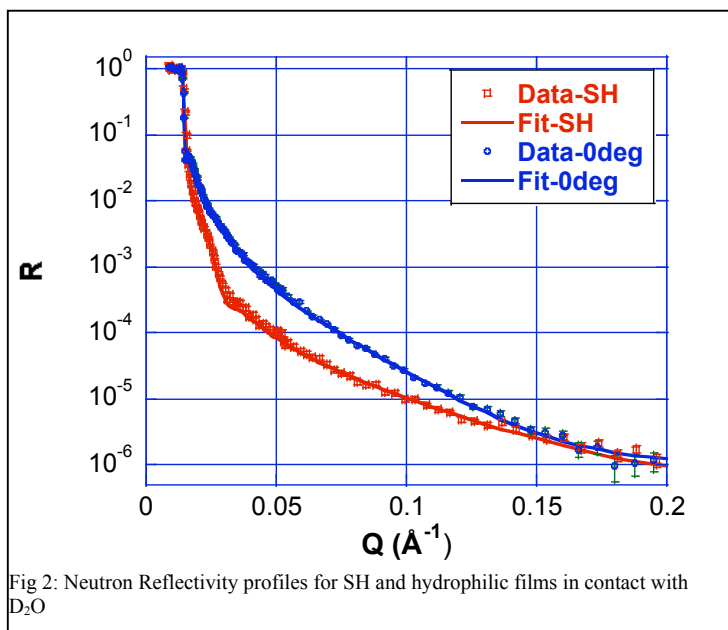
We conducted neutron reflectivity experiments on these SH films against different sub-phases. Since the surface coverage of hydrophobic organics can be controlled with UV/ozone treatment SH films that were made hydrophilic via such a treatment were also studied as a control to understand the film roughness. Further, oil was used to infiltrate the pores of the porous SH film to provide another contrast. Due to the low density of the porous SH film about 90% porosity and scattering length density (SLD) of $0.6 \times 10^{-6} \text{ \AA}^{-2}$ insufficient contrasts was available to characterize the films in air. Filling the 90% pores with a fluorocarbon oil increased the films total SLD such that the exact film thickness could be determined. The data were analyzed by a box model using the Parratt formalism. The roughness is currently treated to be gaussian in nature.



Experiment Report *(continued)*

Traditionally micron thick SH films are created for various applications, however in order to study them with NR we spin coated thin films about 50nm in thickness and found these to retain their SH nature. The films were exposed to saturated D₂O vapor environment and also in contact with D₂O liquid. SH films in a saturated D₂O vapor environment showed minimal water infiltration, the enhanced SLD of the SH-Film layer could be explained by presence of D₂O vapor instead on air in the pores.

Figure 2 shows the NR data and fits for (i) SH film and (ii) a similar film that was made hydrophilic by UV/ozone treatment, in contact with D₂O. NR results, have unequivocally shown the absence water penetration into the SH films over the surface areas (10cm²) probed.



Contrast matching experiments (D₂O/H₂O mixtures) were conducted to probe the nature of the SH film and water interface. Significant off-specular scattering was observed for the SH films as compared to hydrophilic films with the same structure. Data analysis of the off-specular scattering is under progress and might help elucidate the nature of the roughness at the SH film-water interface.

We could also study a sample where the surface coverage of organics was controlled to yield a contact angle of 100 degrees. Due to beam time limitations this film was studied in a saturated D₂O vapor atmosphere, the fitting results indicate minimal water infiltration into the pores. Visual analysis of this film when dipped in water exhibits an optical contrast different from the SH-film. This suggests that there are different cut-offs in terms of water infiltration when a SH-film is exposed to vapor and to liquid.

Conclusion

We have been able to unequivocally show the absence of water penetration into porous SH films over large surface areas. Data analysis of off-specular scattering is in progress to understand the film-water interface. Future experiments using amphiphilic colloidal particles to decorate the SH film-water interface might be another method to study this interface. We were also able to demonstrate the SH phenomena to occur in thin films of the order of 50nm in thickness with about 10nm of roughness. This observation does challenge the conventional choice of higher roughness (order of microns for lithographically patterned SH surfaces) for better SH behavior

IMPORTANT! List or attach a list of publications resulting from this experiment (published or in press).

REPORT ON EXPERIMENT (Please Type)

Submit all experiment reports to:

LANSCE User Office, MS H831, Los Alamos National Laboratory, Los Alamos, NM 87545

Experiment was carried out at: Local Contact **Proposal #** *LANSCE Use Only* X Manuel Lujan Jr. Neutron Scattering Center Jarek Majewski **2003230** **Report Rec'd** Weapons Neutron Research Facility **FP/Instrument Used** **2003236** **7/15/04** WNR/Blue Room **FP9/SPEAR**

Title

Investigation of Radiogenically Produced ^3He in Erbium Dihydride Systems: Depth Profiling using Neutron Reflectivity. **Authors and Affiliations**

JF Browning, Sandia National Laboratories

GS Smith, Oak Ridge National Laboratory

GM Bond, New Mexico Institute of Mining and Technology

Experiment Report

Experiments carried out under proposal numbers 2003230 and 2003236 are part of a larger study intended to develop a scientific understanding of helium evolution and its resulting affects on the structure of metal tritide thin films. This work represents a continuation of a multi-year project (3–4 years) to study the helium depth distribution and evolution in thin films of erbium tritide. The importance of this problem stems from the fact that metal tritide thin films are incorporated into neutron generators, a component of nuclear weapon systems.

The presence of an intermixed layer at the erbium/molybdenum interface was unexpected. Theoretical calculations based on the thermodynamic properties of erbium and molybdenum suggests the two are insoluble at the temperatures used during film deposition for this experiment. It is believed that the intermixing of erbium and molybdenum may be aided by the presence of oxygen at the surface of the molybdenum during the deposition of erbium. A separate study is needed in order to gain an understanding of this interface and its implication to the analysis of helium in the erbium tritide layer of the film. Another complicating factor associated with the sample is the high concentration of hydrogen in the hydride layer. Additional samples with much lower hydrogen contamination concentrations will be introduced into a follow-on experimental proposal.

Experiment Report (continued)

IMPORTANT! List or attach a list of publications resulting from this experiment (published or in press).

Submit all experiment reports to:
LANSCE User Office, MS H831, Los Alamos National Laboratory, Los Alamos, NM 87545

Experiment was carried out at:	Local Contact	Proposal #	LANSCE Use Only
<input checked="" type="checkbox"/> Manuel Lujan Jr. Neutron Scattering Center	Jianzhong Zhang	2003233	Report Rc'd 5/11/04
<input type="checkbox"/> Weapons Neutron Research Facility	FP/Instrument Used		
<input type="checkbox"/> WNR/Blue Room	HIPPO		

Title

Neutron powder diffraction of methane at high pressure

Authors and Affiliations

Jae-Hyun Park, Magnus Lipp and Choong-Shik Yoo, Lawrence Livermore National Laboratory; Yusheng Zhao, Jianzhong Zhang, Jiang Qian, Los Alamos National Laboratory; Christian Pantea, Texas Christian University, Los Alamos National Laboratory

Experiment Report

Methane is one of the major constituents in the "ice" layer of Jovian planets. The phase diagram and structures of methane at high pressures and temperatures are crucial to understanding and/or developing the planetary models. For this reason, there have been an extended amount of high-pressure studies on methane using optical spectroscopic and x-ray diffraction techniques [1-5]. Among seven reported phases, the crystal structures are available only for three phases: I (Fm-3m) [2], II (Fm-3c) [3] and III (Cmca) [4], mostly at relatively low pressures.

Recently, we have reinvestigated the phase diagram of methane by using x-ray diffraction and Raman spectroscopy. In this study, we have learned that the phase stability of methane is strongly dependent on the purity of sample and/or the presence of lattice strain and that there are considerable uncertainties regarding the presence and structures of the previously proposed phases at high pressures. Therefore, the objective of this study is to address these uncertainties and to obtain the fully characterized structural information of high-pressure phases of methane and water, by using high-pressure neutron diffraction experiments at the LANSCE.

The progress in this first experimental run has been made toward two key experimental areas in (i) cryogenic loading of methane into the TAP-98 and in (ii) high temperature-high pressure experiment of water using a graphite heater built for the TAP-98. Both of these developments are critical to the proposed diffraction experiments, which has been applied to the TAP-98 at the LANSCE for the first time.

[1] R. Bini et al., Phys. Rev. B 55, 14800 (1997) and J. Chem. Phys. 103, 1353 (1995).

[2] R.M. Hazen et al, Appl. Phys. Lett., 37, 289 (1980).

[3] W. Press, J. Chem. Phys. 56, 2597 (1972).

[4] M.A. Neumann et al., J. Chem. Phys. 119, 1586 (2003).

[5] S. Umemoto et al., J. Phys.: Condens. Matter 14, 10675 (2002).

Submit all experiment reports to:
LANSCCE User Office, MS H831, Los Alamos National Laboratory, Los Alamos, NM 87545

Experiment was carried out at:	Local Contact	Proposal #	LANSCCE Use Only
<input checked="" type="checkbox"/> Manuel Lujan Jr. Neutron Scattering Center	Mike Fitzsimmons	2003234	Report Rc'd
<input type="checkbox"/> Weapons Neutron Research Facility	FP/Instrument Used		7/26/04
<input type="checkbox"/> WNR/Blue Room	Asterix		

Title

Magnetization depth profiling in superconducting/ferromagnetic superlattices

Authors and Affiliations

Axel Hoffmann, Suzanne te Velthuis, Argonne National Laboratory
Jacobo Santamaria, Universidad Complutense de Madrid

Experiment Report

The interplay between ferromagnetism and superconductivity has generated lots of research interest, since the competition between these generally mutually exclusive types of long-range order gives rise to a rich variety of phenomena. While superconducting/ferromagnetic proximity effects have been studied in the past mostly in systems based on simple metallic alloy, there have recently been many experiments performed on complex oxides based systems, such as high- T_c superconductors [i.e., $\text{YBa}_2\text{Cu}_3\text{O}_{7-\delta}$ (YBCO)] and colossal magnetoresistive manganites [i.e., $\text{La}_{0.7}\text{Ca}_{0.3}\text{MnO}_3$ (LCMO)]. In both of these types of materials their superconducting and magnetic properties depend very sensitively on the charge carrier density and thus one may expect that the interface properties may deviate significantly from bulk behavior.

LCMO/YBCO superlattices were grown on (100) SrTiO_3 by high pressure sputtering with a fixed LCMO thickness of 15 unit cells (corresponding to 60 Å) and varying thicknesses of YBCO intralayers ranging from 1 to 12 unit cells. Subsequently we characterized the structural and magnetic properties of these superlattices with SQUID magnetometry and X-ray and polarized neutron reflectivity. The magnetometry shows that the saturation magnetization of the LCMO layers depends on the YBCO interlayer thickness. Furthermore for all samples the LCMO saturation magnetization is significantly below the expected bulk magnetization of 400 emu/cm³. It should be noted that single layers of LCMO grown under the same conditions as the superlattices do show the full bulk magnetization.

In order to identify the origin of the reduced magnetization we determined the magnetization depth profile with polarized neutron reflectometry using ASTERIX. This allows us to distinguish between a homogeneous depression of the magnetization or magnetically dead regions at the interface with YBCO. The polarized neutron reflectometry is shown in Fig. 1 for a sample with YBCO interlayers of 3 unit cell thickness. In order to saturate the sample we applied a field of 5.4 kOe during the measurements. The first and second order Bragg peaks due to the superlattice structure are clearly visible. The information about the magnetization depth profile is contained in the difference between the reflectivity for neutrons with spin up (R^+) or down (R^-).

Experiment Report *(continued)*

In order to analyze this data further we first determine the chemical structure with X-ray reflectivity, which was obtained with the X-ray facility at the Lujan center. The refined model structure is then used for fitting the polarized neutron reflectivities by only varying parameters for the magnetization in the LCMO layers using either a homogeneous or an inhomogeneous magnetization distribution in each LCMO layer. For a comparison between the two cases we show in Fig. 2 the measured neutron polarization ($R^+ - R^-$)/($R^+ + R^-$) together with the best fits for both the homogeneous and the inhomogeneous model. It is noteworthy that the sign of the polarization is opposite for the two model calculations at the position of the second superlattice Bragg peak (at 0.15 1/\AA); namely, it is positive for the inhomogeneous case, while it is negative for the homogeneous case. Since the experimentally observed polarization at the second superlattice peak is clearly positive, this shows unambiguously that the magnetization in the LCMO is inhomogeneous with a region of reduced magnetization close to the interface with YBCO. Therefore the ferromagnetic/superconductive proximity effects in high- T_c /Manganite heterostructures are much more complex than in their analogous transition metal structures.

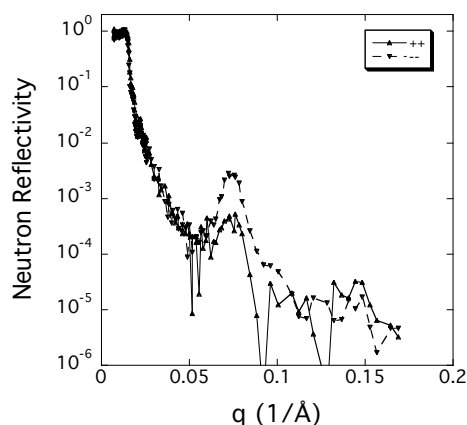


Figure 1: Polarized neutron reflectometry on a LCMO/YBCO superlattice with 3 unit cell thick YBCO layers. Shown are the spin-up (solid line) and spin-down (dashed line) reflectivities.

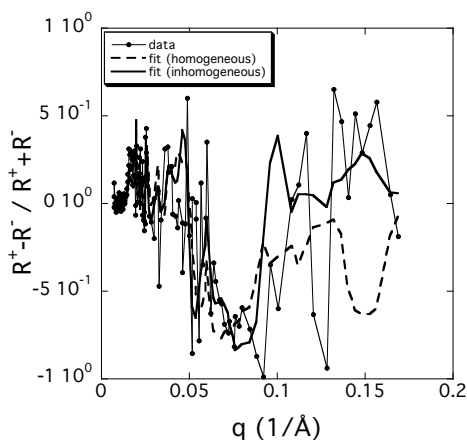


Figure 2: Neutron polarization for a LCMO/YBCO superlattice with 3 unit cell thick YBCO layers. Experimental data is shown in red. Also shown are fits to models with either homogeneous (dashed line) or inhomogeneous (solid line) magnetization distribution in each LCMO layer.

IMPORTANT! List or attach a list of publications resulting from this experiment (published or in press).

REPORT ON EXPERIMENT (Please Type)

Submit all experiment reports to:

LANSCE User Office, MS H831, Los Alamos National Laboratory, Los Alamos, NM 87545

Experiment was carried out at: Local Contact Proposal #LANSCE Use Only X Manuel Lujan Jr. Neutron Scattering Center D. W. Brown 2003237 Report Rec'd Weapons Neutron Research Facility FP/Instrument Used 7/17/04 WNR/Blue Room SMARTS
Title: In-Situ Neutron-Diffraction Measurements of Damage Processes around a Growing Crack

Authors and Affiliations:

Y. Sun¹, H. Choo^{1,2}, P. K. Liaw¹, Y. L. Lu¹, B. Yang¹, and D. W. Brown³

1.

Materials Science and Engineering Department, The University of Tennessee, Knoxville, TN 37996

2.

Metals and Ceramics Division, Oak Ridge National Laboratory, Oak Ridge, TN 37831

3.

Materials Science and Technology Division, Los Alamos National Laboratory, Los Alamos, NM 87545

Experiment Report

Fracture mechanics is a science that relates the globe-loading configuration to the stress and strain state around the crack tip. It views the crack-tip region as a black box and doesn't take into account of the damage mechanism around the crack tip. From a material perspective, only after a better understanding of this damage mechanism, new materials with better crack resistances could be designed. Neutron diffraction, with its powerful penetration, provides a tool for us to probe the detailed damage process around the crack tip. The changes in the elastic- lattice-strain profiles and plastic zone around the fatigue crack in a compact-tension (CT) specimen were investigated during monotonic tensile-loading and unloading cycle using neutron diffraction.

The CT specimen, made of an austenitic 316 stainless steel, was fatigue pre-cracked under a load control with a maximum applied load of 6,667 N. Spatially-resolved strain measurements were performed to determine the in-plane (IP, parallel to the loading direction) and through-thickness (TT, perpendicular to the loading direction) lattice-strain profiles ahead of the crack tip under a constant tensile load, using the SMARTS instrument at the Los Alamos Neutron Science Center. The strain scanning was repeated under various applied loads ranging from 667 to 8,889 N (shown in Figure 1). In each measurement, 32 points had been scanned in front of the crack tip. The scan positions are shown in the Figure 2.

Experiment Report (continued)

In Figure. 3, as the load went up, the peak strain became larger, and the widths of the profiles were wider. In Figure 4, there are two peaks in each profile. One could be due to in-situ loading, where the peak decreased significantly as the load decreased. The other one could be due to bending and the residual stress left by overloading, which did not change very much as the load decreased. After the overload, in front of the crack tip, there were compressive lattice strains occurring at 667 N loading, which would prevent the crack tip to grow. There might be an indication of crack closure after overloading.

The peak-width change indicates the plastic deformation, which corresponds to the plastic zone. In Figure 5, we can measure the plastic-zone size, which is approximately 6 mm. According to Equation (1), the plastic-zone size is about 5.8 mm, which is very close to what we measured for the peak-width change, resulting from the neutron experiments.

IMPORTANT! List or attach a list of publications resulting from this experiment (published or in press).

CHANGES IN ELASTIC STRAIN PROFILES AROUND A CRACK TIP DURING TENSILE LOADING AND UNLOADING CYCLES (in preparation for the Denver X-ray Conference in August 2004).

REPORT ON EXPERIMENT (Please Type)

Submit all experiment reports to:

LANSCCE User Office, MS H831, Los Alamos National Laboratory, Los Alamos, NM 87545

Experiment was carried out at: Local Contact Proposal # *LANSCCE Use Only* X Manuel Lujan Jr. Neutron Scattering Center Jarek Majewski
Report Rc'd Weapons Neutron Research Facility **FP/Instrument Used** 20032387/15/04 WNR/Blue Room SPEAR
Title

Oxygen solubility in PFC monolayer **Authors and Affiliations**

Frank Huang, New Mexico Tech

Jim Browning, Sandia National Laboratories

Experiment Report

Results for the two different samples are presented in Table 1. The scattering length density (ρ), as well as layer thickness, of the self-assembled layer for each sample was determined from a fit of a proposed profile to the reflectivity versus Q data. The physical density (ρ) of the layer was then calculated from the relationship,

where N_A is Avogadro's number, A the molecular weight and b_i the scattering lengths of the individual components making up the PFC molecule. The areal density (Σ) was calculated from the relationship,

where d is the layer thickness.

Figures 1 show the reflectivity versus Q data and fit for the DIP coated layer while the associated scattering length density profile is presented in Figure 2. Data from the Langmuir-Blodgett sample are presented in Figures 3 and 4.

Experiment Report (contued)

In both cases the packing fraction is found to be too great to allow for the migration of oxygen into the PFC layer. **IMPORTANT!** List or attach a list of publications resulting from this experiment (published or in press).

REPORT ON EXPERIMENT (Please Type)

Submit all experiment reports to:

LANSCE User Office, MS H831, Los Alamos National Laboratory, Los Alamos, NM 87545

Experiment was carried out at: Local Contact Proposal # LANSCE Use Only x Manuel Lujan Jr. Neutron Scattering Center Frans
Trouw Report Rc'd Weapons Neutron Research Facility FP/Instrument Used 20032396/18/04 WNR/Blue Room Pharos
Title

Effect of the metal-insulator transition on oxygen phonons in Ca-doped
 $\text{YBa}_2\text{Cu}_3\text{O}_6$

Authors and Affiliations

Rob McQueeney, Iowa State University and Ames Laboratory

Sung Chang, Ames Laboratory

Pengcheng Dai, University of Tennessee and Oak Ridge National Laboratory

Fatih Dogan, University of Missouri-Rolla

Experiment Report

High-temperature superconductors are based on antiferromagnetic insulating materials caused by strong electronic correlations. Doping charge carriers (holes) into this system creates a two-dimensional correlated metallic state in the CuO_2 plane that becomes superconducting at low temperatures. The development of the metallic state with hole doping and the metallic state itself still remain poorly understood. A study of the evolution of the lattice dynamics could shed light on the nature of the metal-insulator transition (MIT) and the normal state properties. Studying the doping dependence in YBCO is problematic because the primary way to dope holes and create the metallic state is by increasing the oxygen content (MIT at $y \sim 0.2$). However, this process introduces additional oxygen phonon states making it difficult to isolate any electron-phonon coupling effects. We used the Pharos spectrometer to obtain the phonon density-of-states as a function of hole doping in $\text{YBa}_2\text{Cu}_3\text{O}_{6+y}$ via the systematic replacement of Y by Ca. Calcium concentrations were chosen to straddle the metal-insulator transition at $x \sim 0.2$. We obtained ~ 60 grams each of several compounds of $\text{Y}_{1-x}\text{Ca}_x\text{Ba}_2\text{Cu}_3\text{O}_{6+y}$ ($x=0, 0.075, 0.15, 0.2, 0.25$) in powder form and ran each sample (in annular geometry) and an empty can at the base temperature of the 2-stage displacer (~ 15 K) with an incident energy of 120 meV. The angle averaged inelastic scattering functions are shown in the figure. The results shown in the figure indicate that doping dependent effects occur in the 30, 55, 70, and 85 meV energy regions, the doping dependence in the higher energy regions may be due to electron-phonon coupling. However, after completion of the experiment, we discovered that the oxygen stoichiometry parameter (y) was not properly characterized and the samples likely have an inhomogeneous oxygen composition. We are now attempting a thorough re-characterization to determine the extent of the problem. Experiment Report (continued)

IMPORTANT! List or attach a list of publications resulting from this experiment (published or in press).

Submit all experiment reports to:
LANSCCE User Office, MS H831, Los Alamos National Laboratory, Los Alamos, NM 87545

Experiment was carried out at:	Local Contact	Proposal #	LANSCCE Use Only
<input checked="" type="checkbox"/> Manuel Lujan Jr. Neutron Scattering Center	Don Brown / Sven Vogel	2003245	Report Rc'd 6/3/04
<input type="checkbox"/> Weapons Neutron Research Facility	FP/Instrument Used		
<input type="checkbox"/> WNR/Blue Room	SMARTS, HIPPO		

Title

Residual Strain Measurement in Limestone Using High-Resolution Neutron Diffraction

Authors and Affiliations

Kurt T. Nihei, Lawrence Berkeley National Laboratory [ktnihei@lbl.gov; 510-486-5349]
Hans-Rudolf Wenk, University of California at Berkeley [wenk@seismo.berkeley.edu]
Seiji Nakagawa, Lawrence Berkeley National Laboratory [snakagawa@lbl.gov]

Experiment Report

The objective of this research was to carry out residual stress measurements on an Austin Chalk sample (SMARTS) and texture measurements on a kaolinite clay sample (HIPPO). The purpose of the chalk test was to determine if plastic deformation processes in a carbonate sample subjected to moderate stresses (e.g., twinning) would produce measurable residual strains. The purpose of the clay test was to determine if a deformed, high porosity clay sample would exhibit resolvable texture. These measurements, as stated in the LANSCCE proposal, were intended for use as supporting material for a full proposal to the DOE Office of Basic Energy Sciences (DOE-OBES) to continue this line of investigation. Using the results of our LANSCCE measurements, a proposal was completed and sent to DOE-OBES in April 2004. A brief summary of the measurements and analysis resulting from the measurements at LANSCCE in Feb. 2004 are provided below.

Austin Chalk measurements:

Neutron diffraction tests were conducted using SMARTS. It is emphasized that these were pilot experiments, simply to test feasibility. Of the 3 days of beamtime we could only use 12 hours because of problems with the accelerator. Nevertheless results were very revealing and encouraging.

One test sample of Austin Chalk (AC4) was loaded up to multiple predetermined stress levels (Fig. 1a), and the evolution of residual strains were measured upon unloading for each loading cycle (Fig. 1b). The changes in the residual strains due to the relaxation (time-delayed) deformation of rock are small, yet systematic. After the SMARTS experiment the texture of the stressed sample was measured with HIPPO. A weak texture could be documented with c-axes concentrated near the compression direction (Fig. 2). This is consistent with crystal reorientations due to mechanical {01-18} twinning (e.g. Wenk et al. 1972). Thus both elastic and plastic deformation in limestone was produced and could be documented.

Experiment Report *(continued)*

taken parallel to the bedding direction. Neutron diffraction measurements were carried out in HIPPO with the automatic sample changer. Data collection was 30 minutes for a spectrum. Fig. 3a shows a raw spectrum for one detector. Clearly counting statistics are not optimal and longer data collection would be desirable in the future. A relatively high background can be attributed to incoherent scattering from crystalline water. However clearly defined diffraction peaks are present and compare well with a calculated spectrum based on the ideal kaolinite structure (Fig. 3b).

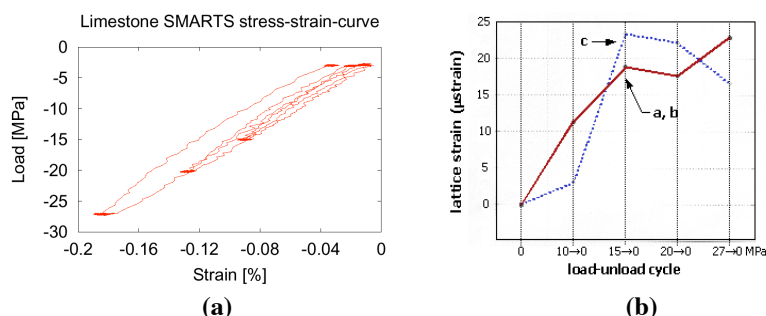


Figure 1. SMARTS experiment on Austin chalk in uniaxial stress load frame. (a) Stress-strain curve showing 4 load-unload cycles up to 27 MPa. (b) Residual compressive lattice strains measured after unloading to 0 MPa from a peak stress of 10 MPa, 15 MPa, 20 MPa, and 27 MPa.

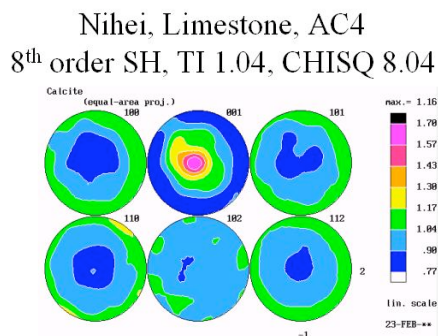


Figure 2. Calcite pole figures from preliminary HIPPO measurements on Austin Chalk (sample AC4 tested after loading to 27 MPa on SMARTS). The compression direction is in the center. The maximum of (0001) poles parallel to the compression direction is consistent with orientation changes due to mechanical twinning.

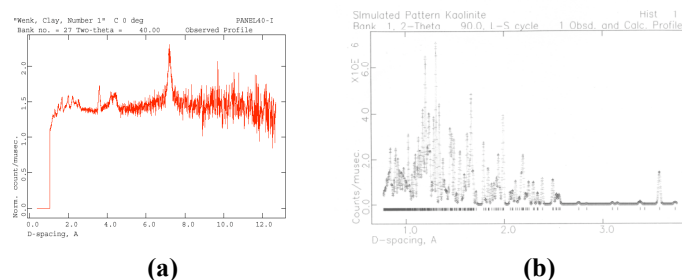


Figure 3. (a) TOF neutron diffraction spectrum for kaolinite compacted to 2 MPa axial stress under uniaxial strain conditions. (b) simulated spectrum based on the ideal kaolinite crystal structure.

IMPORTANT! List or attach a list of publications resulting from this experiment (published or in press).

No publications currently. Experiments were used to generate supporting material for a full proposal to DOE-OBES.

Submit all experiment reports to:
 LANSCE User Office, MS H831, Los Alamos National Laboratory, Los Alamos, NM 87545

Experiment was carried out at:		Local Contact	Proposal #	<i>LANSCE Use Only</i>
<input checked="" type="checkbox"/>	Manuel Lujan Jr. Neutron Scattering Center	Thomas Proffen	2003248	Report Rc'd
<input type="checkbox"/>	Weapons Neutron Research Facility	FP/Instrument Used		
<input type="checkbox"/>	WNR/Blue Room			

Title

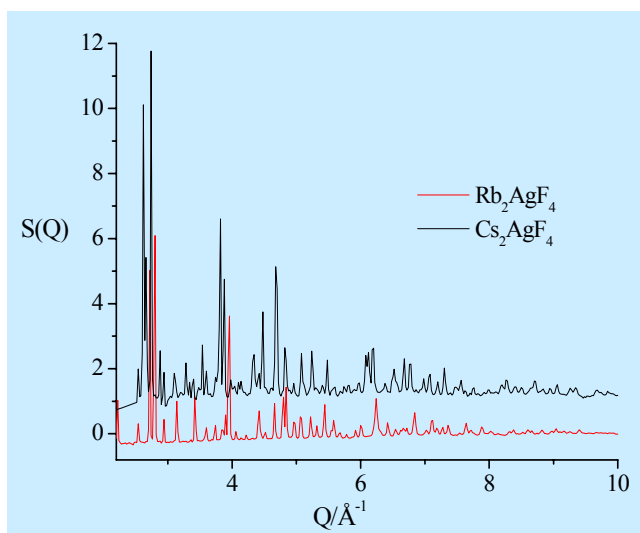
The Structure of Potentially Superconducting Silver Fluorides

Authors and Affiliations

Sylvia E. McLain, Department of Chemistry, University of Tennessee, Knoxville, Tennessee, USA
John F. C. Turner, Department of Chemistry, University of Tennessee, Knoxville, Tennessee, USA
Ted E. Barnes, Department of Physics and Astronomy, University of Tennessee, Knoxville, Tennessee, USA
Thomas Proffen, Los Alamos National Laboratory, LANSCE division, Los Alamos, New Mexico, USA

Experiment Report

Silver difluoride containing compounds may give rise to a new class of superconducting materials. The compounds Cs_2AgF_4 and Rb_2AgF_4 are structurally similar to La_2CuO_4 . High temperature superconducting cuprates have been investigated extensively in recent years. Understanding of these materials obviously requires a detailed understanding of the atomic structure, and analysis based on Bragg intensities alone gives an incomplete picture by completely ignoring disorder or the local structure of these materials. In order to understand the average total structure as well as the local



structural information provided the total scattering pattern data has been collected on both Cs_2AgF_4 and Rb_2AgF_4 using the NPDF instrument in order to obtain the local structure via the Pair Distribution Function (PDF) method in addition to determining the average total structure by Rietveld analysis. The instrument NPDF is specifically designed for such total scattering studies. The figure on shows the diffraction patterns from both Cs_2AgF_4 and Rb_2AgF_4 collected on the NPDF instrument. PDF analysis in addition to Rietveld analysis methods are currently in progress. **IMPORTANT! List or attach a list of publications resulting from this experiment (published or in press).** None to date.

Submit all experiment reports to:
LANSCÉ User Office, MS H831, Los Alamos National Laboratory, Los Alamos, NM 87545

Experiment was carried out at:	Local Contact	Proposal #	LANSCÉ Use Only
<input checked="" type="checkbox"/> Manuel Lujan Jr. Neutron Scattering Center	J. Majewski	2003251	Report Rc'd 7/8/04
<input type="checkbox"/> Weapons Neutron Research Facility	FP/Instrument Used		
<input type="checkbox"/> WNR/Blue Room	SPEAR		

Title

Swelling of Asymmetric Block Copolymer Thin Films

Authors and Affiliations

Ryan C. Hayward, Edward J. Kramer; University of California, Santa Barbara
Roger Pynn, Los Alamos National Labs

Experiment Report

We are developing strategies to convert the structures formed in block copolymer thin films into porous inorganic or hybrid organic/inorganic materials with well-controlled nanostructures. Such materials are expected to find applications such as membranes, catalysts, sensors, and solar cells. As one route, we are studying the selective incorporation of inorganic precursors from solution into swelled films of cross-linked block copolymers. For this strategy to be effective, it is important that we understand the morphological changes that occur when block copolymer thin films are swelled by solvents.

The block polymer currently under investigation forms cylinders of perdeuterated polystyrene (dPS) in a poly(2-vinylpyridine) (P2VP) matrix. In thin films the lower vacuum surface energy of dPS and preferential wetting of P2VP at the substrate cause the cylinders to orient with their long axes parallel to the film plane, as shown schematically in Figure 1. This leads to a layering of the block copolymer microstructure, and hence of the neutron scattering length density, normal to the film plane. We measured specular neutron reflectivity from films in air and under liquid solvents that are selective for P2VP (methanol and 0.1 M aqueous HCl) to see the extent to which the cylinder layers move apart and broaden during swelling.

Detailed fitting of the reflectivity data to model scattering length density profiles is still underway, but the initial analysis is promising. For example, Figure 2 shows the methanol-swelling behavior of a moderately cross-linked film (7% of the P2VP units were reacted with the cross-linking agent) consisting of two layers of dPS cylinders. Under methanol, the specular reflectivity curve shows a nearly featureless decay, suggesting that the layering of the block copolymer structure was mostly lost upon swelling. After removal of the methanol, oscillations due to the total film thickness ($\sim 500 \text{ \AA}$) can once again be seen, but the "Bragg" peak associated with the block copolymer structure (at $\sim 0.032 \text{ \AA}^{-1}$) is greatly diminished in intensity, indicating that layering of the block copolymer structure has not been recovered upon removing the solvent. In contrast, for a heavily cross-linked sample (23% functionalization), the Bragg peak persists upon swelling in methanol and shifts to smaller q_z , indicating that the block copolymer structure has swelled by roughly a factor of two relative to its initial size. Upon removal of methanol, the Bragg peak persists, although it is somewhat diminished in intensity, suggesting that the structure has partially disordered upon swelling.

Figure 3 shows the swelling behavior of a moderately cross-linked (7%) 4-layer thick film under 0.1 M aqueous HCl. The observed swelling is strikingly different from that under methanol at the same degree of cross-linking. For the measurement under liquid, a series of Bragg peaks ($\sim 0.1, 0.22, 0.34 \text{ \AA}^{-1}$) is observed, indicating that the layering of the block copolymer structure is preserved, and that the cylinder layers swell to nearly three times their initial spacing. The similarity of the reflectivity curves before and after swelling suggests that the process is nearly reversible, most likely with an increase in the roughness of the film after swelling.

Experiment Report *(continued)*

Subsequent experiments involving AFM imaging of swelled block copolymer films and X-ray scattering from swelled bulk samples have shown that the osmotic stresses induced upon swelling with methanol are sufficient to cause rearrangement of the dPS cylinders into spheres. In contrast, when samples are swelled with acidic water, the cylinders of dPS do not break up. Presumably the methanol plasticizes the polystyrene sufficiently to allow microstructural rearrangement of the polymer. Apparently this rearrangement also leads to a loss of layering in thin films of moderately cross-linked block copolymer.

Already the results of these experiments have provided some useful input for the design of block copolymer films as templates for nanostructured inorganic materials. Further analysis of the data and fitting to model scattering length density profiles is currently underway to provide a quantitative picture of how the film morphology changes upon swelling.

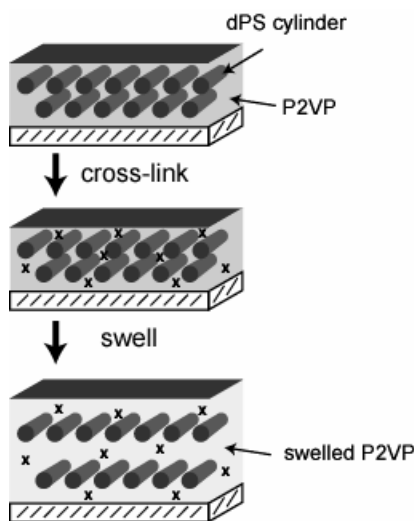


Fig. 1: schematic illustration of film structure

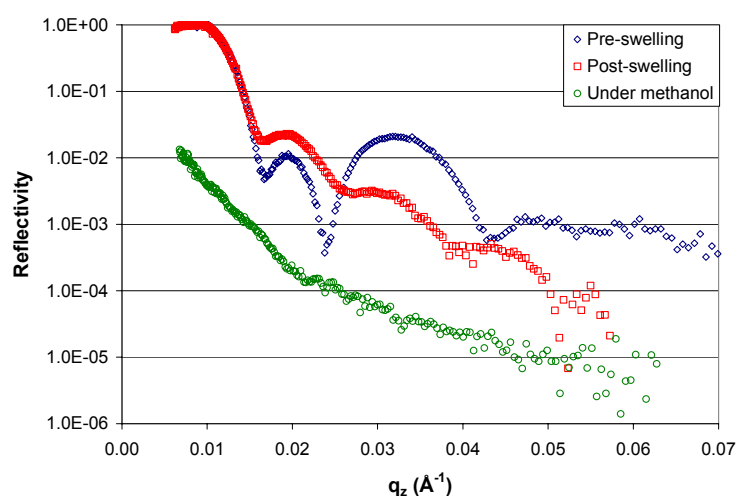


Fig. 2: Specular reflectivity curves for a moderately cross-linked 2-layer sample swelled in methanol

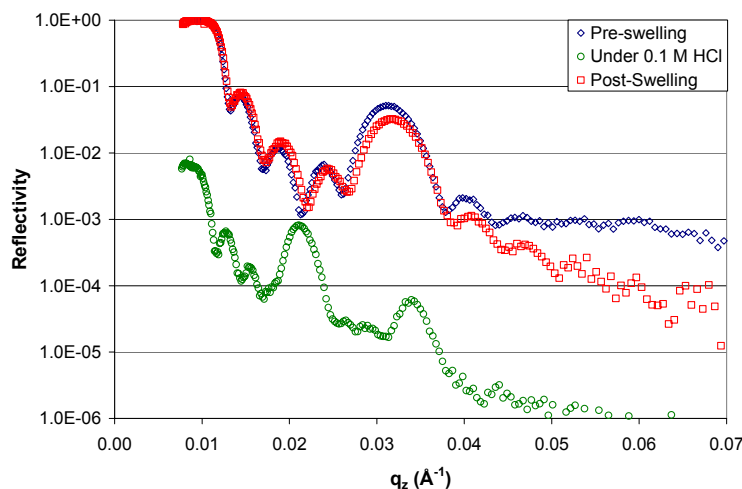


Fig.3 Specular reflectivity curves for a moderately cross-linked 4-layer sample swelled in 0.1 M HCl

IMPORTANT! List or attach a list of publications resulting from this experiment (published or in press).

No publications have been submitted yet, but a communication is anticipated.

Submit all experiment reports to:
 LANSCE User Office, MS H831, Los Alamos National Laboratory, Los Alamos, NM 87545

Experiment was carried out at:		Local Contact	Proposal #	LANSCE Use Only
<input checked="" type="checkbox"/>	Manuel Lujan Jr. Neutron Scattering Center	Don Brown	2003254	Report Rc'd 6/24/03
<input type="checkbox"/>	Weapons Neutron Research Facility	FP/Instrument Used		
<input type="checkbox"/>	WNR/Blue Room	SMARTS		

Title

In-Situ Lattice Dilation, Hydride Formation, and Damage Evolution in a Hydrogen-Charged Zirconium Alloy

Authors and Affiliations

E. Hornoii-Garlea, H. Choo, B. Yang, M. L. Morrison, R.A. Buchanan, P. K. Liaw, Materials Science and Engineering Department, The University of Tennessee, Knoxville, TN 37996.

D. W. Brown, MST-8, Los Alamos National Laboratory, Los Alamos, NM 87545.

S. Park, L. L. Daemen, LANSCE-12, Los Alamos National Laboratory, Los Alamos, NM 87545.

A. Ionita, C. R. Hubbard, Metals and Ceramics Division, Oak Ridge National Laboratory, Oak Ridge, TN 37831.

H. F. Letzring, Pretreatment and Specialty Products, PPG Industries, Troy, MI 48083.

Experiment Report

Hydrogen embrittlement (HE) results from the combined action of hydrogen and residual or applied tensile stress. Hydrogen damage to specific alloys manifests itself in many ways, and accordingly, there are numerous theories for the various forms of degradation. Hydride formation is one of the main degradation sources of Group Vb metals (Nb, V, and Ta) and Zr, Ti, and Mg in hydrogen environments. When sufficient hydrogen is available in these alloys, a brittle metal hydride precipitates at the crack tip. Cracking of the hydrides occurs, followed by crack arrest in the more ductile matrix or continued crack growth between hydrides by ductile rupture. The hydride formation is believed to be enhanced by application of stress. Therefore the increase in stress field ahead of the crack tip may induce precipitation of additional hydrides that cleave.

The objective of the proposed experiment was to investigate the effect of hydrogen charging on the lattice dilation near the crack tip, and on mechanical behavior of zircaloy-4 (Zry-4) alloy, using neutron diffraction. Zry-4, which is a high-performing alloy with respect to severe pressure and temperature conditions, is technologically important as a nuclear-reactor material. Moreover, zirconium is a favorable element for this study because it forms hydride and its neutron absorption coefficient and incoherent scattering cross-sections are very weak. All specimens were compact tension (CT) specimens fatigue pre-crack to a crack length of 22.86 mm. Using neutron diffraction technique, spatially-resolved strain measurements were performed on two different sets of Zry-4 specimens: sample in as received condition, which was only fatigue pre-cracked; and pre-cracked sample, which was electrochemically charged with hydrogen for 4 hours.

Measurements were made at the crack tip region for in-plane (IP) and through-thickness (TT) strain components at about 1 mm intervals under *in-situ* tensile load of 667 N and 4,444 N.

The effect of applied stresses on as-received specimen as a function of the distance from the crack tip is shown in Figure 1. Strain profile along a axis significantly increases with the increase in stress. The experimental results are in good agreement with the theoretical prediction of the FEM modeling results (Figure 2).

Experiment Report (continued)

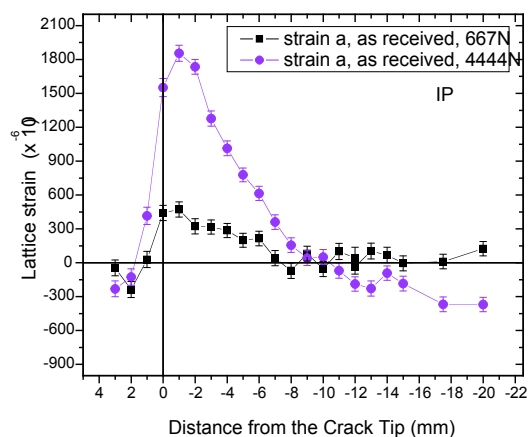


Fig. 1. Lattice strain profiles measured in the as-received, fatigue pre-cracked specimen under 667 N and 4,444 N loads. Only the in-plane (IP) strain components are shown.

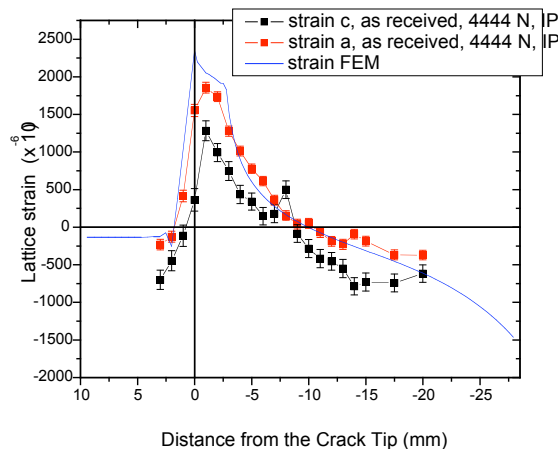


Fig. 2. Comparison between measured and predicted strain profile for the as-received specimen under a 4,444 N applied load.

The effect of hydrogen charging on the lattice strain profile under a 4,444 N load, as a function of the distance from the crack tip is plotted in Figure 3. We observed changes in the strain profile, for the H-charged sample and a shift of the peak to the right, ahead the crack tip, by approximately 2 mm.

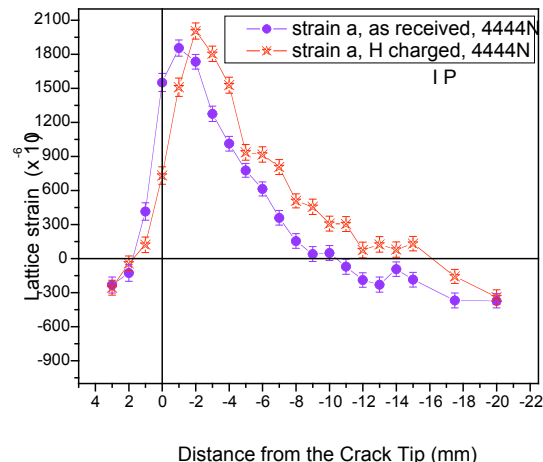


Fig. 3. Comparisons of lattice strain profiles in a hydrogen charged specimen and as-received specimen under a 4,444 N load. Only the in-plane (IP) strain components are shown.

We identified few potential reasons of the changes in lattice strain profile of the H-charged specimen: the presence of the hydrogen in the bulk, the presence of the hydrides in bulk and/or on the surface of the sample, and a crack growth. The presence of a γ -ZrH₂ layer on the surface was identified using XRD at LANSCE.

Measurement of the crack length, after neutron experiment, showed no change in length. Therefore, the formation of a γ -ZrH₂ layer on the surface or the presence of H in bulk is most likely to be the explanation for the observed behavior. Theoretical calculations of the strain profile for the H-charged sample are presently in progress.

IMPORTANT! List or attach a list of publications resulting from this experiment (published or in press).

Garlea E., Choo H., Brown D. W., Park S., Daemen L. L., B. Yang B., Ionita A., Morrison M. L., Buchanan R. A., Liaw P. K., Letzring H. F., and Hubbard C. R., *Interplay Between Internal Strain and Hydride Formation Around the Crack Tip in Zircaloy-4*, presented at American Conference on Neutron Scattering, Collage Park, June 6-10, 2004.

Submit all experiment reports to:
LANSCE User Office, MS H831, Los Alamos National Laboratory, Los Alamos, NM 87545

Experiment was carried out at:	Local Contact	Proposal #	LANSCE Use Only
<input checked="" type="checkbox"/> Manuel Lujan Jr. Neutron Scattering Center	Don Brown	2003255	Report Rc'd
<input type="checkbox"/> Weapons Neutron Research Facility	FP/Instrument Used		7/16/04
<input type="checkbox"/> WNR/Blue Room	SMARTS		

Title De-Convoluting the Influences of Heat and Plastic Deformation on the Residual Stresses in the Friction Stir Welds of 6061-T6 Aluminum Alloy
Authors and Affiliations W. Woo ^a , H. Choo ^{a, b} , D. W. Brown ^c , Z. Feng ^b , P. K. Liaw ^a , S. A. David ^b , and C. R. Hubbard ^b ^a Material Science and Engineering Department, University of Tennessee, Knoxville, TN 37996, USA ^b Metal and Ceramics Division, Oak Ridge National Laboratory, Oak Ridge, TN 37830, USA ^c Materials Science and Technology Division, Los Alamos National Laboratory, Los Alamos, NM 87545, USA

Experiment Report

Abstract

Friction stir welding (FSW) is a solid-state joining process that produces relatively enhanced mechanical properties in welded products. The plastic deformation and heat is necessary for the joining. However, it generates residual stresses (RS) in the welds, which are detrimental to the integrity of the joined components. Three different welded specimens were prepared from 6061-T6 aluminum alloy: (Case 1) a plate processed with both the stirring pin and pressing shoulder, i.e., a regular FSW, (Case 2) a plate processed only with the pressing shoulder, and (Case 3) a plate processed only with the pin. The strain components of longitudinal, transverse, and through-thickness were measured across the weld line using neutron diffraction. The comparison among the three cases shows distinctly different profiles revealing de-convoluted effects based on the different sources of the residual stress, i.e., plastic deformation, friction heat, or their combination.

1. Introduction

FSW can produce a strong metallurgical bonding by both a severe plastic deformation from the rotation of the pin and a friction heat from the compression of the shoulder. It has many advantages compared to the fusion welding process such as minimized cracking, compositional variation and lower manufacturing cost. However, FSW exhibits significant level of the RS that can degrade the mechanical properties of components. For example, recent publications indicate that the RS in the longitudinal direction of the welds can amount to 70~85% of yield stress of the base materials in the case of aluminum alloys. Even though, it is known that the heat and the plastic deformation are the major sources of RS in the welds, quantitative relationship among the sources of the RS are not available to date. Thus, the purpose of this experimental is to investigate the relationship among the RS to reveal the relative influences of plastic deformation and heat on RS during FSW.

2. Experimental Details

The used material was 6061-T6 aluminum alloy plate with a dimension of 306 x 306 x 6.5 mm³. FSW was proceed under 28 cm/min of the traveling speed, 1250 rpm of the clockwise rotating speed and 1800 lb/in² of the pressure on the 19.05mm and 6.35mm diameters of the shoulder and the pin, respectively.

Table 1. Summary of the sample preparation.

	Source of the RS		Effective part of the tool	
	Heat	Deformation	Shoulder	Pin
Case 1	Maximize	Maximize	O	O
Case 2	Maximize	Minimize	O	X
Case 3	Minimize	Maximize	X	O

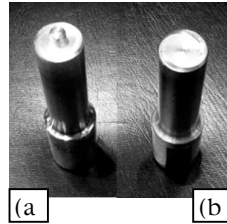


Figure 1. A photograph of the tool shape (a) case 1 and 3, (b) case 2

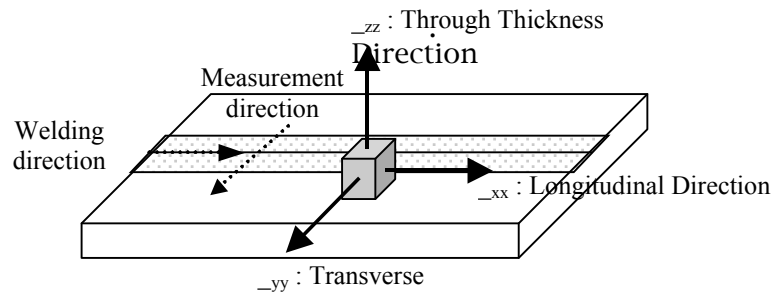


Figure 2. Three directions and components of residual stresses along the transverse measurements

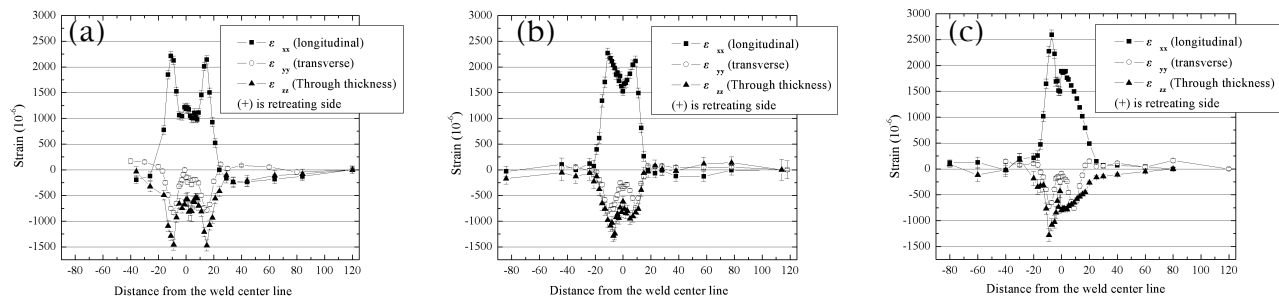


Fig. 3. Residual strains measured along y-direction
(a) a normal FSW (case 1), (b) the shoulder only (case 2), and (c) the pin only (case 3)

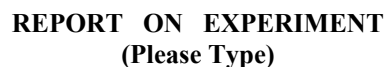
3. Preliminary Results

Using SMARTS, the longitudinal (ϵ_{xx}), transverse (ϵ_{yy}) and through-thickness (ϵ_{zz}) strain components were measured along y-direction.

1) Three kinds of specially designed FSW specimens were prepared from the 6061-T6 aluminum alloy and the residual strain components were measured using the neutron diffraction. 2) The three cases, the pin only, the shoulder only and their combined system, show distinctively different profiles, which can be attributed to the effects of the individual part of the tool on the residual stresses. 3) The friction of the shoulder largely produces the heat and the stirring of the pin typically causes the plastic deformation as sources of the residual stresses. 4) The comparison of the longitudinal strains among the cases shows

IMPORTANT! List or attach a list of publications resulting from this experiment (published or in press).

- 1) "De-Convoluting the Influences of Heat and Plastic Deformation on the Residual Stresses in the Friction Stir Welds of 6061-T6 Aluminum Alloy", W. Woo et al., The American Conference on Neutron Scattering place, June, 2004.
- 2) "Two-dimensional mapping of residual stresses in Al 6061-T6 friction stir welds", W. Woo et al., to be presented at the Denver X-ray conference place, August, 2004.



Experiment was carried out at:	Local Contact	Proposal #	LANSCE Use Only
<input checked="" type="checkbox"/> Manuel Lujan Jr. Neutron Scattering Center	Donald Brown	2003256	Report Rc'd
<input type="checkbox"/> Weapons Neutron Research Facility	FP/Instrument Used		<input type="text" value="7/16/04"/>
<input type="checkbox"/> WNR/Blue Room	SMARTS		

Authors and Affiliations

Department of Materials Science and Engineering
University of Tennessee, Knoxville, TN 37996

Strain-induced martensitic transformation is one of the unique features of austenitic stainless steels. Carbon and nitrogen have a very strong effect on austenite stability and the extra-low carbon grades such as 304L are quite sensitive to strain-induced martensite transformation. Deformation-induced martensite significantly enhances strength generated by cold work. The extent of strain-induced transformation of austenite to martensite is dependent on temperature, strain rate, and strain in addition to composition.

The objective of this experiment is to investigate the strain-induced martensite formation and its deformation behavior in 304L stainless steel at cryogenic temperature using the newly developed cryogenic in-situ loading capability at the SMARTS instrument. Three specimens of single-phase austenitic 304L stainless steel were used to perform compression tests at 296K, 268K and 203K; and neutron diffraction spectra were recorded in-situ during uniaxial compressive loading.

Using the phase and *hkl* selectivity of neutron diffraction, we can determine the partitioning of stress between phases and grain families. In addition to the determination of internal stress, the neutron method can also give the information about the texture evolution and the phase volume fractions by Rietveld refinement of the diffraction spectra.

This report presents preliminary results of neutron diffraction studies of strain-induced martensitic transformation in 304L stainless steel.

Fig. 1. is the macroscopic stress-strain curves acquired during the in-situ loading measurements. Stronger work hardening observed at 203K can be attributed to two factors, temperature and martensite formation. Further analysis is needed to identify the effect of martensite formation.

Experiment Report (continued)

Fig. 2. shows the diffraction patterns after compression tests at RT, 268K, and 203K. No martensite formation was observed at RT and 268K, while a number of martensite peaks formed at 203K. The peak indexing shows that the martensitic transformation is from face-centred cubic to body-centred tetragonal. The relative comparison of peak intensities in the axial and transverse diffraction spectra (not presented here) indicates that the austenite grains with $\langle 100 \rangle$ parallel to the loading axis are preferred for transformation.

Fig. 3. is the lattice strain evolution of bct and fcc phase in axial direction at 203K. Although the initial lattice parameter of martensite phase is a subject of on-going analysis, the relative changes in strain still give an insight into the interaction of the matrix phase and the martensite phase.

The results will provide us a quantitative micromechanical understanding of the strain-hardening behavior of the alloy undergoing strain-induced martensitic phase transformation.

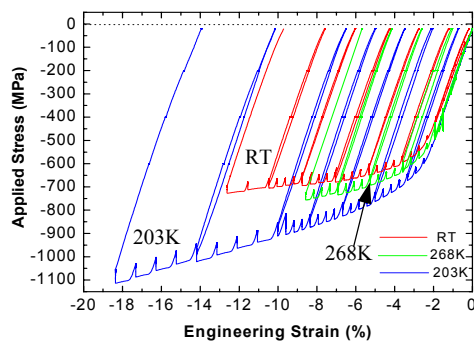


Fig. 1. Macroscopic stress-strain curves measured at RT, 268K, and 203K.

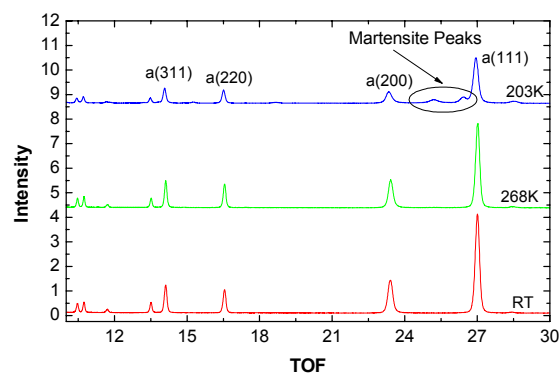


Fig. 2. Axial diffraction patterns after compression tests at RT, 268K and 203K; a – austenite.

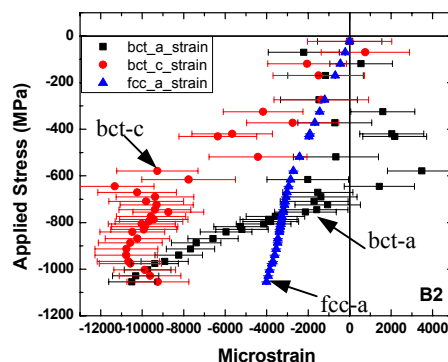
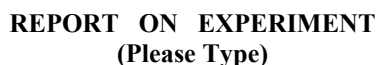


Fig. 3. Lattice strains of austenite (fcc) and martensite (bct) phases in axial direction

IMPORTANT! List or attach a list of publications resulting from this experiment (published or in press).

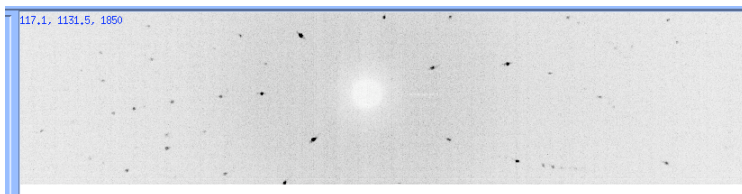
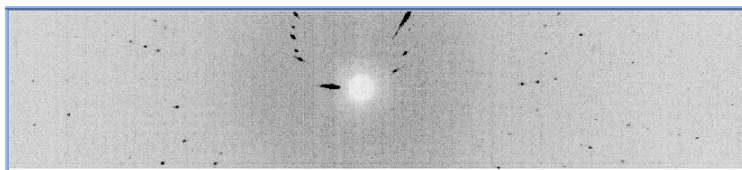
“In-Situ Neutron Diffraction Study of Strain-Induced Martensite Formation and Its Deformation Behavior at a Cryogenic Temperature”, K. Tao et al., to be presented at MRS Fall Meeting, Boston, MA, Nov. 29 – Dec. 3, 2004.



Experiment was carried out at:		Local Contact	Proposal #	<i>LANSCE Use Only</i>
<input checked="" type="checkbox"/>	Manuel Lujan Jr. Neutron Scattering Center	Paul Langan	2003264	Report Rc'd 6/24/03
<input type="checkbox"/>	Weapons Neutron Research Facility	FP/Instrument Used		
<input type="checkbox"/>	WNR/Blue Room	PCS		

N. Sukumar, NE-CAT, Sector 24, Bldg 436E, Argonne National Laboratory, Argonne, IL 60439
V.L. Davidson, Department of Biochemistry, University of Mississippi Medical Center, Jackson, MS 39216
P. Thiagarajan, IPNS, Argonne National Laboratory, Argonne, IL 60439
F.S. Mathews, Department of Biochemistry, Washington University School of Medicine, St. Louis, MO 63110

Subsequently, in April 2004, Dr. Paul Langan, Instrumentation Scientist at PCS collected entire data of 2 θ resolution, by keeping the crystal in the beam for nearly 17 days. The final data contain total observed reflections of 15,119 in the wavelength range of 0.6-7 \AA .

Experiment Report *(continued)*

The above figures show neutron diffraction data from two different settings for the amicyanin. Further analysis of the data is in progress.

IMPORTANT! List or attach a list of publications resulting from this experiment (published or in press).
None

REPORT ON EXPERIMENT (Please Type)

Submit all experiment reports to:

LANSCe User Office, MS H831, Los Alamos National Laboratory, Los Alamos, NM 87545

Experiment was carried out at: Local Contact **Proposal #** LANSCe Use Only X **Manuel Lujan Jr. Neutron Scattering Center** Paul Langan **2003266** **Report Rec'd** Weapons Neutron Research Facility **FP/Instrument Used** 6/3/04 WNR/Blue Room PCS

Title

Global Orientational Tuning of Water in Aquaporins **Authors and Affiliations**

David Savage, Pascal Egea, and Robert Stroud

Department of Biochemistry and Biophysics, University of California at San Francisco, 600 16th St., San Francisco, CA, 94153

Experiment Report

Aquaporins are a physiologically important class of channel membrane proteins necessary for the rapid conduction of water across the cellular membrane. Our experiment, entitled Global Orientational Tuning of Water in Aquaporins, seeks to determine the molecular mechanisms whereby aquaporins are able to conduct water at near diffusion rates, while excluding protons. It is our hypothesis, based on x-ray diffraction data and computer simulation, that aquaporins achieve this by “tuning” the orientation of water in the channel through hydrogen bonding and helix dipole effects. To further test this hypothesis, we sought to collect neutron diffraction data suitable to resolve the channel water orientation.

This experiment is highly non-trivial, as only a handful of atomic resolution neutron diffraction protein structures have been solved and none are membrane proteins, which are historically difficult to work with. We were awarded one day of data collection time for our proposal, and we therefore sought to screen the diffraction quality of our current crystals. Due to the length of collection time necessary to verify diffraction, we were able to screen two crystals.

The first crystal, .03mm³ in size (Fig 1), was exposed for 12 hours to polychromatic neutrons. The detector readout suggested the possibility of diffraction to low resolution, but poor signal to noise ratio prohibited any data analysis. A second crystal (Fig 2), grown in deuterated solutions and roughly .05mm³ in size, was then exposed for 12 hours. Once again, poor data quality prohibited integration and analysis of the diffraction pattern.

Upon completion of the experiment, we discussed future directions of the experiment with our local

Experiment Report (continued)

contact, Paul Langan. The relative low flux of neutrons in comparison with x-rays requires large sample size, and we are currently optimizing crystallization conditions in the hopes of increasing crystal size to 1mm³. Size limitations can also be partially overcome with the use of perdeuterated samples, and we are investigating this as well. Finally, the Stroud laboratory has several other crystal forms of different aquaporins, which diffract x-rays to high resolution. These proteins belong to the same family, meaning their study is pertinent to our hypothesis, and perhaps could yield higher quality samples. Upon

obtaining high quality samples (namely larger crystals), we are to contact Paul, in the hopes of screening more crystals and obtaining useful diffraction data.

Fig 1. 0.3mm³ Crystal of AqpZ

Fig 2. 0.05mm³ Deuterated crystal of AqpZ **IMPORTANT!** List or attach a list of publications resulting from this experiment (published or in press).

REPORT ON EXPERIMENT

(Please Type)

2003268 "Crystal Field Excitations and Anisotropy in Heavy Fermion and Intermediate Valence Systems"

Submit all experiment reports to:

LANSCE User Office, MS H831, Los Alamos National Laboratory, Los Alamos, NM 87545

Experiment was carried out at: Local Contact Proposal #LANSCE Use Only x Manuel Lujan Jr. Neutron Scattering Center
Frans Trouw 2003268 Report Rc'd Weapons Neutron Research Facility FP/Instrument Used 6/3/04 WNR/Blue Room PHAROS

Title Crystal Field Effects in Anisotropic Intermediate Valence $\text{Yb}_2\text{Rh}_3\text{Ga}_9$ Authors and Affiliations

A. D. Christianson, University of California Irvine

J. M. Lawrence, University of California Irvine

Experiment Report

Previous studies of intermediate valence (IV) systems have found that the Kondo scattering is so strong that crystal field levels are not observed [1]. On the other hand, in heavy fermion materials the crystal field splitting is much larger than the Kondo temperature, indicating that the interesting physics is occurring within the crystal field ground state. $\text{Yb}_2\text{Rh}_3\text{Ga}_9$ appears to lie in the middle of these two extremes and thus provides a unique opportunity to explore the effect of strong crystal field splitting in an intermediate valence (IV) system [2]. Consequently we have initiated inelastic neutron scattering measurements to characterize the magnetic response of polycrystalline samples of $\text{Yb}_2\text{Rh}_3\text{Ga}_9$.

$\text{Yb}_2\text{Rh}_3\text{Ga}_9$ crystallizes in a hexagonal structure (space group $P6_3cm$) [3]. Upon first examination, the magnetic susceptibility appears to be typical of an IV material. However, a closer inspection reveals that a broad maximum occurs at different temperatures depending whether the magnetic field is applied along the c axis (~100 K) or the magnetic field is applied in the basal plane (~150 K) [2].

Our results indicate that at low temperature a large region of magnetic scattering exists from ~10 meV – 100 meV with the maximum intensity found at 40 meV (figure 1). This appears to be consistent with crystal field model where each crystal field level hybridizes to a different degree with the conduction electrons [2]. Detailed theoretical calculations are underway to verify this point. At higher temperatures we find a significant increase in the quasielastic intensity consistent with the expectation for an IV material.

Experiment Report (continued)

Figure 1. Magnetic contribution to the inelastic neutron scattering spectrum of $\text{Yb}_2\text{Rh}_3\text{Ga}_9$ at 18 K. Data has been collected at two incident energies 70 and 120 meV. The 70 meV data has been scaled to the 120 meV data.

References

- [1] For example see J. M. Lawrence, P. S. Riseborough, C. H. Booth, J. L. Sarrao, J. D. Thompson, R. Osborn, Phys. Rev. B **63**, 54427 (2001).
- [2] N. O. Moreno, A. Lobos, A. A. Aligia, J. L. Sarrao, P. G. Pagliuso, J. D. Thompson, C. D. Batista, C. H. Booth, and Z. Fisk, unpublished.
- [3] S. Bobev, N. O. Moreno, J. L. Sarrao, Z. Fisk, unpublished. **IMPORTANT! List or attach a list of**

REPORT ON EXPERIMENT (Please Type)

Submit all experiment reports to:

LANSCE User Office, MS H831, Los Alamos National Laboratory, Los Alamos, NM 87545

Experiment was carried out at: Local Contact Proposal #LANSCE Use Only X Manuel Lujan Jr. Neutron Scattering
Center Thomas Proffen Report Rc'd Weapons Neutron Research Facility FP/Instrument Used 20032738/5/04 WNR/Blue
Room NPDF

Title

Atomic Pair Distribution Analysis of High Resolution Neutron Powder Diffraction Data on Disordered Materials

Authors and Affiliations

Simon Billinge, Michigan State University

Hyunjeong Kim, Michigan State University

John Mitchell, Argonne National Laboratory

Thomas Proffen, Los Alamos National Laboratory

Experiment Report

Manganites have been studied to a great extent due to their interesting intrinsic property, colossal magnetoresistance (CMR), which has been understood by the existence of phase inhomogeneities in the material.¹ Currently, quite a number of physicists have looked for a crossover temperature, T^* , at which ferromagnetic metallic clusters start forming in the paramagnetic insulating state of the manganite upon cooling from high temperature. Since the PDF is sensitive to the local structure of a material, using high real-space resolution neutron PDFs, we are planning to search for a local structural response to T^* indicating metallic drop formation for $\text{La}_{0.72}\text{Ca}_{0.28}\text{MnO}_3$ and furthermore those for other compositions.

The neutron experiments were conducted on 8.09g of $\text{La}_{0.72}\text{Ca}_{0.28}\text{MnO}_3$ powder sample at the NPDF at the Lujan center at Los Alamos National Laboratory. Neutron powder diffraction data were collected at 670 K first and then at several temperatures while the temperature was decreased (555, 443, 415, 387, 360, 333, 302 K). Each data set was measured for 2 hours. The PDF, which gives the probability of finding an atom at a distance r away from another atom, was obtained by a Fourier transformation of the total scattering structure function, $S(Q)$ using the program PDFgetN.² $S(Q)$ was truncated at Q_{max} of 30 \AA^{-1} before the PDF was calculated.

Because the difference between ferromagnetic metallic (FM) and paramagnetic insulating (PI) states in $\text{La}_{0.72}\text{Ca}_{0.28}\text{MnO}_3$ may be seen through the PDF peaks corresponding to the Mn-O bonds, we have concentrated on studying low- r regions of the PDFs. Since we are looking for the temperature T^* where FM clusters start forming while decreasing temperature from a very high one, as a first step, differences between two PDFs at different temperatures are obtained and compared each other. The T^* for the $\text{La}_{1-x}\text{Ca}_x\text{MnO}_3$, $x=0.3$ has been reported around 400 K using other experimental techniques and the Experiment

values of T^* for $x < 0.3$ are expected higher than that for $x=0.3$, so roughly assuming $415 \text{ K} < T^* < 555 \text{ K}$ for $\text{La}_{0.72}\text{Ca}_{0.28}\text{MnO}_3$, the PDFs at 333, 415, 555 and 670 K are chosen to be compared. Those temperatures are selected so that temperature dependent changes in the PDF in the mixed state (333 and 415 K where FM and PI states are expected to coexist) and in the pure PI state (555 and 670 K where FM clusters completely vanish) can be compared. Because problems with the temperature controller, and some beam loss, during the experiment we couldn't obtain enough data sets at the temperatures we initially planned (more measurements are necessary). This limits the temperature range for comparison. The Figure (a) shows the low- r region of two PDFs measured at 333 K (a blue line) and 415 K (a red line) and their difference (a dark cyan line). Two vertical lines placed at 1.94 and 2.16 Å show the positions of the short and long Mn-O bonds in the insulating state due to the Jahn-Teller distortions. The Figure (c) shows the PDFs at 555 K (a blue line) and at 670 K (a red line) and their difference (a dark cyan line). Finally, the Figure (b) shows PDFs obtained at 415 K where the FM clusters are presumed to exist (a blue line) and at 555 K where they do not (a red line) and their difference (a dark cyan). In all data, long and short Mn-O bonds due to the Jahn-Teller distorted MnO_6 octahedron are observed clearly. One interesting feature found in this figure is the abrupt change of the low- r side slope of the 1st peak of two PDFs in the Figure (b) whereas in (a) and (c) changes of the slopes look more gradual. It is hard to say whether we can distinguish the pure PI state from the PI state mixed with FM clusters from the PDF at this stage. Further analysis and more data sets between 415 K and 555 K and above 670 K are necessary for solid conclusions.

References :

- 1 E. Dagotto, Nanoscale Phase Separation and Colossal Magnetoresistance, Springer, Berlin, 2002
- 2 P. F. Peterson, M. Gutmann, Th. Proffen, and S. J. L. Billinge, J. Appl. Crystallogr. **33**, 1192 (2000)

IMPORTANT! List or attach a list of publications resulting from this experiment (published or in press).

Submit all experiment reports to:
 LANSCE User Office, MS H831, Los Alamos National Laboratory, Los Alamos, NM 87545

Experiment was carried out at:		Local Contact	Proposal #	<i>LANSCE Use Only</i>
<input checked="" type="checkbox"/>	Manuel Lujan Jr. Neutron Scattering Center	Thomas Proffen	2003274	Report Rc'd <div style="border: 1px solid black; padding: 5px; width: fit-content;">6/18/04</div>
<input type="checkbox"/>	Weapons Neutron Research Facility	FP/Instrument Used		
<input type="checkbox"/>	WNR/Blue Room	NPfDF		

Title

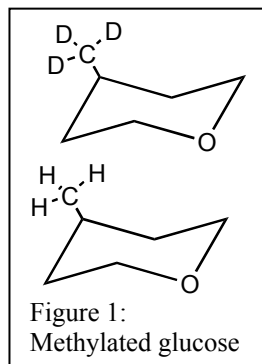
Local Structure of Dissolved Sugar

Authors and Affiliations

Sylvia E. McLain, Department of Chemistry, University of Tennessee, Knoxville, Tennessee
John. F. C. Turner, Department of Chemistry, University of Tennessee, Knoxville, Tennessee
David. C. Baker, Department of Chemistry, University of Tennessee, Knoxville, Tennessee
Thomas Proffen, Los Alamos National Laboratory, LANSCE division, Los Alamos, New Mexico

Experiment Report

Data was collected on D₂O and on two samples of methylated glucose dissolved in D₂O, where in one of the samples the methyl group was hydrogen labeled and in the analogous sample the methyl group was deuterium labeled. The structure of methylated glucose is shown in figure 1. The data was collected using the NPDF instrument at the LANSCE facility in order to ascertain if neutron diffraction with isotopic substitution of a liquid could be performed.



The data collected are shown in figure 2, where the blue line represents pure D₂O, the green line represents the

hydrogenated methylated glucose and the red line represents the deuterated methylated glucose. As can be seen clearly from Figure 2, there are some subtle difference in the data sets and analysis to extract the distances about the methyl position in the glucose is currently in progress.

IMPORTANT! List or attach a list of publications resulting from this experiment (published or in press).

None at this time

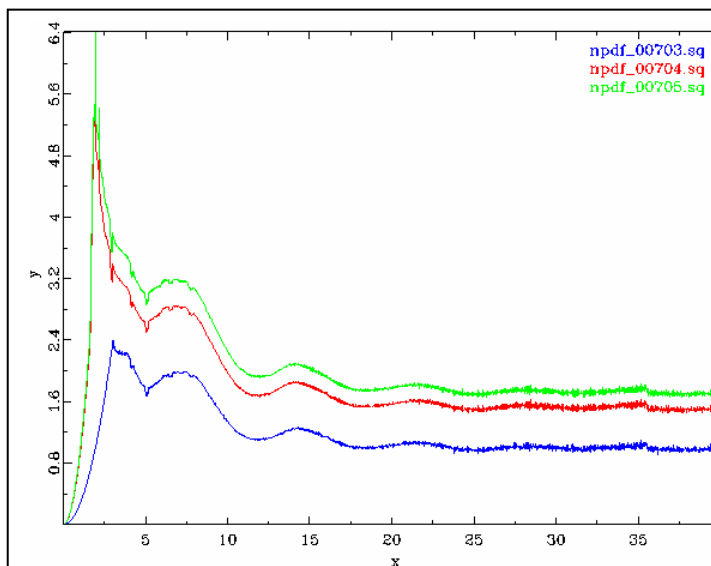


Figure 2: NPDF data for D_2O and methylated glucose samples dissolved in D_2O .

REPORT ON EXPERIMENT (Please Type)

Submit all experiment reports to:

LANSCCE User Office, MS H831, Los Alamos National Laboratory, Los Alamos, NM 87545

Experiment was carried out at: Local Contact Proposal #LANSCCE Use Only X Manuel Lujan Jr. Neutron Scattering Center Th.
Proffen Report Rc'd Weapons Neutron Research Facility FP/Instrument Used 20032826/22/04 WNR/Blue Room NPDF

Title

PDF study of superconducting cuprates and cobaltates Authors and Affiliations

Jin Nakamura, Wojtek Dmowski, Takeshi Egami

University of Tennessee

Experiment Report

Three systems were measured using Neutron Powder Diffractometer (NPDF).

1. $\text{La}_{2-x}\text{Sr}_x\text{CuO}_4$ ($x = 0.0 - 0.3$) at 15 K

2. $\text{Na}_{0.35}\text{CoO}_2 \cdot 1.4\text{D}_2\text{O}$ at 15 K

3. $\text{Pr}_{0.89}\text{LaCe}_{0.11}\text{CuO}_4$ (super- and nonsuperconducting phase) at room temperature

1. $\text{La}_{2-x}\text{Sr}_x\text{CuO}_4$ ($x = 0.0 - 0.3$)

There is great interest in the possibility that the charge distribution in the CuO_2 planes of the high- T_c superconductors is microscopically inhomogeneous and that this is related to the high- T_c superconductivity itself. If the holes in the CuO_2 plane are inhomogeneously distributed, a distribution of Cu-O bond lengths in the CuO_2 plane would exist.

The 16 $\text{La}_{2-x}\text{Sr}_x\text{CuO}_4$ samples which had different composition in x between 0.0 and 0.3 were measured.

We are carrying out the PDF analysis to examine the evidence of charge inhomogeneity directly using the peak due to the Cu-O bond in the CuO_2 plane (about 1.9 Å) and the indirectly using peaks above 1.9 Å that involve correlations of Cu- and O- pairs.

2. $\text{Na}_{0.35}\text{CoO}_2 \cdot 1.4\text{D}_2\text{O}$

Recently an interesting kind of new superconductor has been discovered in the hydrated sodium cobalt oxide. This peculiar superconductivity occurs when Na-deficient Na_xCoO_2 is intercalated with water (H_2O) or heavy water (D_2O), and understanding a role of this intercalated block is important. Experiment Report (continued)

So far several structural models are reported, and the differences between those models are mainly based on the structure of the intercalated block composed of Na, O and H (D). Furthermore, it is also reported that several percents of hydrogen is at Na site.

We measured $\text{Na}_{0.35}\text{CoO}_2 \cdot 1.4\text{D}_2\text{O}$ sample synthesized using 99.99 % D_2O . We had known that this sample has several percents of H which seems to be inevitably taken in the synthesis process, but the position of H in the sample has been unclear. First we used a model suggested by Jorgensen *et al.* for Rietveld refinement, however some peaks could not be explained. We are modeling data in real space to clarify the origin of those peaks and determine the position of H.

3. $\text{Pr}_{0.89}\text{LaCe}_{0.11}\text{CuO}_4$ (super- and non- super-conducting phase)

High- T_c superconductivity appears when holes or electrons are doped to the suitable copper oxides.

$\text{Pr}_{0.89}\text{LaCe}_{0.11}\text{CuO}_4$ (PLCCO) is one of the few electron doped oxide superconductors. The oxidized sample shows superconductivity, while the reduced sample does not. This behavior has been explained by the amount of excess oxygen or the existence of Pr_6O_{11} in the sample, but it has been clearly demonstrated by the structural data.

Both super and nonsuperconducting phase of PLCCO were measured. We are performing the Rietveld and PDF analysis, and relating local atomic structure to the superconductivity in these materials.

IMPORTANT! List or attach a list of publications resulting from this experiment (published or in press).

Submit all experiment reports to:
LANSCÉ User Office, MS H831, Los Alamos National Laboratory, Los Alamos, NM 87545

Experiment was carried out at:	Local Contact	Proposal #	LANSCÉ Use Only
<input checked="" type="checkbox"/> Manuel Lujan Jr. Neutron Scattering Center			Report Re'd
<input type="checkbox"/> Weapons Neutron Research Facility	FP/Instrument Used	2003287	1/20/04
<input type="checkbox"/> WNR/Blue Room			

Title
Study of the unusual dielectric properties in $\text{CaCu}_3\text{Ti}_4\text{O}_{12}$ using dynamic structure function

Authors and Affiliations

I.-K. Jeong,, R. H. Heffner, M. Hehlen, and F. Trouw, LANL
J. S. Park, K. S. Hong, Seoul National University, South Korea

Experiment Report

In recent, an exceptionally large room temperature dielectric constant, $\epsilon \sim 10^4$ was observed in a perovskite compound $\text{CaCu}_3\text{Ti}_4\text{O}_{12}$ (CCTO) [1-3]. The dielectric constant of CCTO also exhibits very interesting temperature dependence, i.e. its low frequency dielectric constant is almost constant in the temperature range 100K-300K. Below $T \sim 100\text{K}$, however, the dielectric constant drops by factor of 100. Despite the huge change in dielectric constant around 100 K, the Rietveld analysis of neutron powder diffraction of CCTO at 100K and 35K shows no indication of a phase transition; the material remains cubic from room temperature down to 10K [1]. In addition, recent local structural studies by Bozin *et al.* [4] using neutron and x-ray pair distribution function (PDF) have found no evidence for the local disorder. This is a quite remarkable since high dielectric constants ($\epsilon > 1000$) in most perovskite oxide ceramics like BaTiO_3 and $\text{Pb}(\text{Mg}_{1/3}\text{Nb}_{2/3})\text{O}_3$, are usually related to ferroelectric phase transitions or relaxor properties, thus the dielectric constant ϵ shows strong temperature dependence.[5]

Numerous scenarios have been proposed for the origin of the dielectric properties of CCTO. The first-principle calculation by He *et al.* found no direct evidence for intrinsic lattice or electronic mechanism of large dielectric response of ideal structure CCTO [6]. He *et al.*, therefore, suggested that the dielectric property of CCTO might be due to extrinsic effects such as blocking interface mechanism. Lunkenheimer *et al.* [7] also proposed contact or grain boundary effects for the giant dielectric constant of CCTO. Another explanation was proposed by Ramirez *et al.* [8]. They proposed dilute concentration of defect in the perovskite structure as an origin for the unusual dielectric constant. However, the origin of the giant dielectric constant and its temperature dependence of CCTO remain unsettled and controversial.

From our studies [9] on dynamic atomic correlation of the CCTO as a function of temperature using the joint neutron powder diffraction and x-ray absorption fine structure (XAFS) measurements, we

Experiment Report (continued)

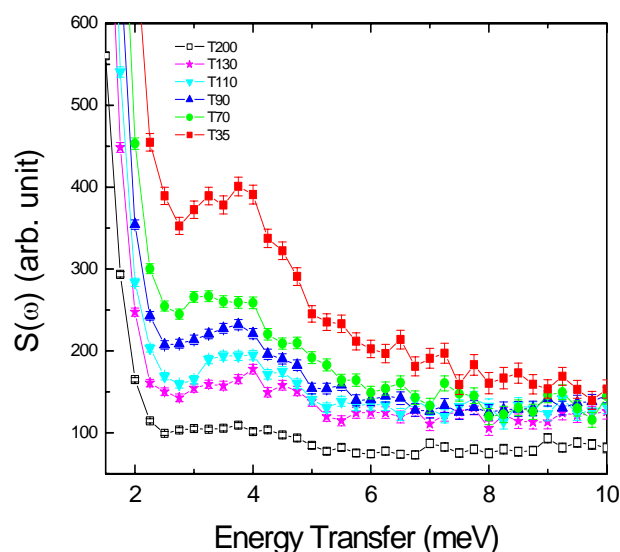


Fig. 1. Dynamic structure function, $S(\omega)$ of CCTO as a function of temperature from 200K to 35K.

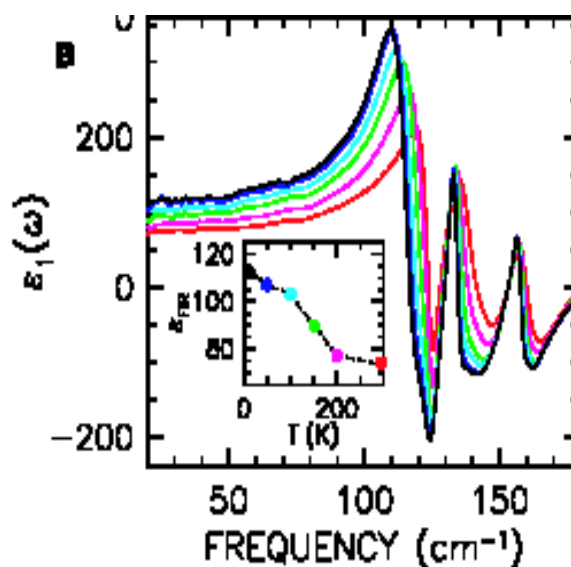


Fig. 2. The real part of the dielectric function of CCTO in the infrared region for various temperatures [3]. Inset shows T-dependence of ϵ_{FIR} .

observed very interesting dynamic motional correlation of atom pairs in CCTO that the Ca-(Cu+O) pair motion switches from strong anti-correlated to almost uncorrelated thermal motion around 100K where the dielectric constant shows sudden drop. This crossover in thermal atomic motion of Ca-(Cu+O) pair around 100K suggests that dynamics of lattice might be responsible for the dielectric properties of CCTO. In order to better understand dynamic correlation and its role in the anomalous dielectric properties of CCTO, we measured dynamic structure function, $S(\omega)$ as a function of temperature. As shown in Fig. 1 we observed very low energy excitation around 3.5 meV and the intensity of this mode increases as the temperature decreases from 200K to 35K. We expect that this low energy excitation is related to the dynamic atomic correlation between Ca-(Cu+O) atoms. In addition, the increasing intensity of the low energy mode with decreasing temperature is connected to the increase in ϵ_{FIR} (Fig. 2 inset) due to a violation of f -sum rule [3].

[1] M. A. Subramanian et al., J. Solid State Chem. **151**, 323 (2000).

[2] A. P. Ramirez et al., Solid State Comm. **115**, 217 (2000).

[3] C. C. Homes et al., Science **293**, 673 (2001).

[4] E. S. Bozin et al., arXiv:cond-mat/0303189 (2003).

[5] F. Jona and G. Shirane, *Ferroelectric Crystals* (Dover, New York, 1993).

[6] L. He et al., Phys. Rev. B **65**, 214112 (2002).

[7] P. Lunkenheimer et al., Phys. Rev. B **66**, 052105 (2002).

[8] A. P. Ramirez et al., unpublished.

[9] I.-K. Jeong et al., unpublished.

IMPORTANT! List or attach a list of publications resulting from this experiment (published or in press).

REPORT ON EXPERIMENT (Please Type)

Submit all experiment reports to:

LANSCe User Office, MS H831, Los Alamos National Laboratory, Los Alamos, NM 87545

Experiment was carried out at: Local Contact Proposal #LANSCe Use Only X Manuel Lujan Jr. Neutron Scattering

Center Markus P. Hehlen Report Rc'd Weapons Neutron Research Facility FP/Instrument Used 20032886/22/04 WNR/Blue Room PHAROS

Title

Spin and Lattice Dynamics in Watery Cobaltate Authors and Affiliations

Jin Nakamura, Wojtek Dmowski, Takeshi Egami

University of Tennessee

Experiment Report

Recently, an interesting kind of new superconductor has been discovered in the hydrated sodium cobalt oxide. This peculiar superconductivity occurs when Na-deficient Na_xCoO_2 is intercalated with water (H_2O) or heavy water (D_2O), and the maximum T_c of ~ 5 K is found near the composition $\text{Na}_{0.3}\text{CoO}_2 \cdot 1.4\text{H}_2\text{O}$. There are opinions that this superconductor is analogous to the copper oxides. Since the superconductivity appears only when water is intercalated, it is of a prime interest to understand the role the water layer is playing in metallicity and/or superconductivity. We have examined the $\text{Na}_{0.3}\text{CoO}_2 \cdot 1.4\text{D}_2\text{O}$ sample. We found that small amount of H is present in the sample, and was most likely introduced during the synthesized process. Therefore, to examine precisely the role of water layer, it is necessary to know how much H is in the sample, and how it is bonded.

Inelastic neutron scattering for about 35 g of polycrystalline $\text{Na}_{0.35}\text{CoO}_2 \cdot 1.4\text{D}_2\text{O}$ sample synthesized using 99.9 % D_2O was measured by High Resolution Chopper Spectrometer (PHAROS) at 15 K, incident energy $E_i = 99.7$ meV and 247.4 meV, respectively.

In Fig. 1, which shows the result from $E_i = 247.4$ meV measurement, the previously unknown peak appears around 180 meV. It has been reported that the bending mode frequency is found to be at ~ 200 meV for both crystalline ice and liquid water. It has also been reported that a peak appears, or shifts to, above 200 meV, when H_3O exist in the sample. We think that this peak in our data originates in H-D bending mode. Therefore, H does not enter as H_2O or H_3O , but must be in other form in the sample.

Experiment Report (continued)

Submit all experiment reports to:
LANSCE User Office, MS H831, Los Alamos National Laboratory, Los Alamos, NM 87545

Experiment was carried out at:	Local Contact	Proposal #	LANSCE Use Only
<input checked="" type="checkbox"/> Manuel Lujan Jr. Neutron Scattering Center	Fitzsimmons, Michael	2003293	Report Re'd 7/15/04
<input type="checkbox"/> Weapons Neutron Research Facility	FP/Instrument Used		
<input type="checkbox"/> WNR/Blue Room	FP 11		

Title
Reflectivity study of buried interfaces in feco/gaas

Authors and Affiliations
Sungkyun Park and Mike Fitzsimmons – LANSCE 12
X.Y. Dong, B.D. Schultz and C.J. Palmstrøm – University of Minnesota

Experiment Report

Polarized neutron reflectometry was used to measure the magnetization depth profile of an epitaxial FeCo single crystal film grown on GaAs(100) (2x4)/c(2x8) at 95°C—a prototypical example of a ferromagnetic/semiconductor heterostructure. From a quantitative analysis of the neutron scattering data, we find the magnetic thickness of the FeCo layer to be 6 Å thinner than its chemical thickness. Further, we show the chemical and magnetic structures of the FeCo film are incommensurate at the FeCo/GaAs interface, suggesting that the FeCo/GaAs interface region does not possess the magnetization of the FeCo film.

Los Alamos Laboratories (LANSCE)

Cosmic Ray latch up and Soft Error Rate Test results

Objective:

The objective of this experiment was to determine the effects of accelerated cosmic ray bombardment at the system level, on Extreme Networks next generation and current generation products. This will help determine an accelerated cosmic ray soft error rate, and cosmic ray latch-up susceptibility. A special evaluation of one SRAM vendor's device (NEC) will include a comparison test of a device where the BPSG layer in the chip has been replaced with a Boron 11 material, as opposed to a Boron 10 material. The Boron 11 material is supposed to improve the neutron soft error rate and cosmic ray latch up susceptibility. Another SRAM vendor with the same type of device (Samsung) was evaluated at the same time to determine a soft error rate and cosmic ray latch up exposure, and an A/B comparison of the two devices. The Netlogic CAM and select ASIC devices will also be tested in the same manner..

Purpose:

The purpose of this test is to evaluate the effects of cosmic ray soft error rates and latch up effects on current and future product lines. The primary focus of the test will be to evaluate CMOS SRAM and ASIC devices, and the effects of cosmic ray events with various vendors. The purpose of this test on next generation product is to evaluate specific vendor performance, the effects of long term system reliability, and calculate accelerated Cosmic Ray Soft Error FIT rate. A special consideration will be given to one vendor that offers a Boron 11 BPSG layer to help combat cosmic ray effect. It is hoped to establish the benefits of this enhancement when comparing the performance to the same device the vendor manufactures with a Boron 10 BPSG material. This information may be used to convince other vendors to establish this process change, or to migrate away from Boron based BPSG layers altogether.

The purpose of this test for current generation products, is to determine what our current cosmic ray exposure might be on two of our most popular product lines. The reason for this is two fold: to establish a current risk assessment, and to establish a base line comparison between current generation and future generation product lines. Data collected from both current and future product lines, will be used to compare against current and future vendor device level cosmic ray test data.

Extreme Network's current concern on cosmic ray exposure has been developed from various white papers on the subject, and discussions with SRAM vendors Micron, Sony, Samsung, and NEC that have or will be performing cosmic ray testing at Los Alamos Labs. Some of the presented material was from a presentation given at the 2001 International Reliability Physics Symposium by Robert Baumann. Supporting evidence gathered from mainframe industry field data for soft error rates, also shows a correlation of soft error rates and the effects of altitudes on RAM devices. LANL staff personnel have also recommended this testing, to determine the effects of these phenomena on Extreme Networks equipment used at LANL.

Section I-Test Setup

The test setup and procedure will follow the guidelines of JEDEC specification JESD89 for Cosmic Ray-Induced Soft Error testing. Since the QDR device can not be voltage margined at the system level due to internal voltage regulators, section 5.4.2.2 of JESD89 will be performed at nominal voltage. The physical orientation of all units and devices are listed below:

Section I-Test Setup cont.

- All CPU and I/O blades were positioned vertically in the chassis/test fixture so the neutron beam strikes at a 90 degree angle in reference to device under test. (DUT) The area under test was fit within the 8.5 cm Neutron beam. The systems were positioned about 2 meters from beam source.
- An adjustable table provided by the LANSCE ICE house allowed the chassis/test fixture to be positioned to strike various ASIC/QDR/CAM/SRAM locations on the CPU and I/O blades.
- Initial test setup information (beam flux, beam fluence, incidence angle, exposure time, ect...) were collected from Netlogic and NEC from their experiments at LANL. These parameters were considered for our test setup.
- Board level device placement was as uniform as possible to facilitate an A/B comparison of test results.

Section II- Test process:

Objective:

The JEDEC Cosmic Ray test specification JESD89 gives general guidelines on how to perform the tests, but it is up to the test personnel in general to achieve the desired results. Methodologies vary widely from vendor-to-vendor, but various QDR vendor input was considered for this test. The basic direction of the test process was to achieve an upset rate of around a 50 to 100 errors per device for a given time. This amount of time this takes will be considered a “test cycle” for a given DUT. This was performed several times in order to record a baseline for a device. The basic test flow included the following order of events:

- 1) Setup and check out the system and device under test. This included the following steps:
 - a) Setup system, power on and boot Manufacturing diagnostics.
 - b) Do initial voltage checks on system with a DVM and record power plane values.
 - c) Perform an initial diagnostic test to insure hardware functionality and to check for any stray “location effects” of the site.
- 2) Initial neutron beam setup and test check using a baseline DUT. This was mostly to establish what initial neutron flux (beam energy) and beam fluence (beam density) will achieve the desired 100 upsets for a given device. The test was repeated 3 to 5 times to get test cycle results for 50 errors in each test cycle. Cycle results were summed to get the 100 upset goal.
- 3) Performed initial tests for DUTs outlined in Section-I above. Other devices were tested in the same manner noted in #2 above, for 3 to 5 test cycles each. Most of this testing was performed using a modified version of BIST tests running under Manufacturing code. This test loops indefinitely and record errors against a given QDR interface. This test also recorded error information, and start/finish times of the 100 error goal.
- 4) Some test consideration was given to various ASICs and CAMs using the same method in #2 and #3 above. Steps 2 and 3 were also repeated aiming the beam from the back side of the QDR device as recommended by NEC. NEC noted that a different soft error rate was obtained when aiming the beam at the bottom of the QDR package.

Section II- Test process con't:

- 5) An attempt was made to enable ECC correction on the IKE ASIC during packet memory tests to see if there is any adverse affect on the SER rate for the IKE ECC circuits. Test method was the same as outlined in #2 and #3 above.
- 6) BIST and register tests were run on various ASIC devices to see if they are affected by cosmic ray soft error testing and latch-up.

Data Collection and Final Test:

- 1) Data was recorded for the various devices during the test. Parameters like the beam neutron count, beam energy, exposure time, error count, and chip location were recorded. This data will be used to calculate a Soft Error FIT rate for the various devices.
- 2) A final device level check was performed using the Huron QDR/ASIC group. This was done as a baseline consistency check, and to verify that the device has not experienced any “total dose” effect from the neutron bombardment. This is similar to a device saturation effect.
- 3) Data was collected and analyzed to determine a soft error FIT rate. The results were checked to see if the Boron 11 in the NEC QDR provides any significant improvement in SER protection. An A/B comparison of results between the Samsung and NEC QDR's may not be significant, due to the small Samsung population of QDR. We could not test the 512KX36 18M QDR part, because of the vendor design issues. Bit position failures will be evaluated for any relationships and correlation's between locations on devices. This may indicate areas of concern on the chip for SER susceptibility.

Data analysis and SER FIT rates:

The data was analyzed and Soft Error FIT rates were calculated. The preliminary results are listed below by vendor. NEC has provided us with a simulation result of 400 FITs per megabyte.

Cartman ASIC QDR group:	Upper QDR	Lower QDR
NEC Boron 11 based QDR SRAM	= 127.65 FIT/Mb	121.01 FIT/Mb
NEC Boron 10 based QDR SRAM	= 142.16 FIT/Mb	160.78 FIT/Mb
Samsung (unrefined) QDR SRAM	= 129.32 FITM/b	132.56 FIT/Mb

IKE Packet Memory QDR group:

NEC Boron 11 based QDR SRAM	= 355.76 FIT/Mb
NEC Boron 10 based QDR SRAM	= 458.07 FIT/Mb
NEC QDR Simulation of FIT rates	= 400.00 FIT/Mb

NOTE: results are in FIT per megabit of memory.

Data Collection observations:

NEC

- The NEC Boron 10 based part had a very bad habit of developing hard-like bit errors when exposed to the beam. This happened on almost every ASIC group that was tested. They were usually bit failures that behaved like stuck-at faults. The errors would usually go away when the beam was removed, but two chips turned into hard fails that would not go away- even with a power cycle. We will review these failures with NEC after the board has been re-tested back here at Extreme.
- The NEC Boron 11 QDR ram held up better than the Samsung QDR, or the NEC Boron 10 QDR ram, but only 4 were tested. (about 18% better FIT in NEC Cartman QDR, 23% better FIT in NEC IKE packet memory QDR) No evidence of stuck-at faults in the diag captures for the B11 part.
- NEC stated that they noticed the SER rate is higher when the neutron beam strikes the bottom of the device. That effect was not noticed when testing in a clamshell group in 4 locations. Initial observations of focusing the beam on the backside of the QDR for the IKE packet memory rams, shows no evidence of this effect.

Samsung

- The Samsung QDR had just slightly less performance than the NEC Boron 11. Only two could be tested though. (NEC Boron 11 was about 5% better)
- There was slight evidence of “bit dependence” in some of the Samsung captures. This means the same bit would be affected for a few locations for a few different addresses. Not sure if this is a multibit strike limited to one data pin or array structure. The affect was minimal and random in most cases.

General QDR observations:

Almost all bit failures seen in Cartman QDR testing occur when the rams are written with all 1's This is apparent across both QDR vendors, and it did not matter if I used Cartman 8 or 6. The only other time different patterns would fail is when the NEC QDR with Boron 10 developed hard fails. The IKE QDR failures are all random patterns, and I did not see evidence of any fault trending.

- An attempt was made to run the Kenny CPU based packet memory loopback tests with ECC turned on. This board already had a multibit failure on Ike 2. I ran it for a few minutes with the neutron beam on, and looked at the data mismatches. I only saw the known ram corruption show up in the mismatch data. The IKE ASIC held up well in all the BIST memory tests. No multi-bit errors on QDRs noted.

Netlogic CAM observations:

- The Netlogic CAM could not be properly SER tested with our diagnostics. We need to turn the parity scan logic off to test the core array for single bits. The parity logic errors were overriding the diagnostics capability to check core array memory. There needs to be a diag switch to turn off parity scan during memory testing.

ASIC / CPU observations:

- The ASICs held up very well in this test. This was a major area of concern in the mainframe/server industry- even more than the SRAMs, because soft-LSI strikes could cause a CPU to hang, or the system to crash. I ran well over 10,000 passes of register tests to various IKE and Kenny ASICs with no failures. I also ran internal BIST memory tests to the Kenny ASIC for over 15 minutes with no failures noted. I tried every BIST test I could run on the various ASICs, and had no problems.
- The CPU sub-system on the Huron board was also exposed to this neutron beam. In one case, the beam was close enough that the CPU was mostly in its path. No unusual behavior or failures were noted. I was impressed after hearing talk from the scientist, how some vendors test boards will not even work in this beam.

Data Collection issues:

There were several issues encountered that affected the outcome of the tests. Usable test results were still obtained, but some of these issues should be considered for any future test planning:

- The Los Alamos site experienced a massive power outage just before we started tests. This pushed the start time out a day, and the beam was unstable for the first few test shifts. The beam instability is reflected in the first two shifts of test results.
- The Boron 10 rams were getting hard-like bit failures described in the observation section that made it very hard to get even 50 hit count samples on other devices. This could be fixed in diag code to disable the QDR interface, but not onsite.
- The Mariner I/O blade had the management port fail due to cable side force on the connector. All testing was accomplished on the Huron CPU blade.
- The most consistent test results came from the Cartman clamshell QDR tests. This test did not have chip location decoding in the diag tests, so I had to manually decode almost 900 upsets. We need to add this capability to any diag used for LANL SER testing, since it took almost a week to manually decode all upsets. The IKE QDR tests were perfectly modified for data collection.
- CAM tests would not work correctly when the CAM was exposed to the neutron beam. The background parity error logic gets checked in the diagnostics, and the errors misrepresent the actual count of upsets. This needs a switch in the code to disable parity logic during tests.
- The Wendy init problem kept showing up on power on. Unplugging the system was the only way to boot it behind the shield wall. I believe this is fixed now.
- We only had small population of Samsung rams to check out due to the 512KX36 part design issue and population.

REPORT ON EXPERIMENT (Please Type)

Submit all experiment reports to:

LANSCCE User Office, MS H831, Los Alamos National Laboratory, Los Alamos, NM 87545

Experiment was carried out at: Local Contact Proposal #LANSCCE Use Only Manuel Lujan Jr. Neutron Scattering Center
Fotiadis 2003503 Report Rcdx Weapons Neutron Research Facility FP/Instrument Used 6/1/04 WNR/Blue Room 4FP60R

Title Investigation of ^{197}Au via the $(n,n\gamma)$ reaction

Authors and Affiliations

N. Fotiadis LANL
R.O. Nelson LANL
M. Devlin LANL
J.A. Becker LLNL
L.A. Bernstein LLNL
W. Younes LLNL
P.G. Garrett LLNL
Experiment Report

States of ^{197}Au with up to ~2 MeV excitation energy have been studied using the $^{197}\text{Au}(n, n'\gamma)$ reaction.

The data were taken using the GEANIE spectrometer and the neutron beam of the Los Alamos Neutron Science Center's WNR facility.

Partial γ -ray cross sections have been measured for a total of 92 transitions of ^{197}Au and the deduced excitation functions combined with $\gamma\gamma$ -coincidence information were used to extend the previously known level scheme of ^{197}Au (see the level scheme obtained in the present work in Fig. 1).

The structure above the previously known $11/2^-$ isomer of ^{197}Au was established for the first time.

A total of 52 new γ -rays and 32 new levels were established.

The first excited states of the decoupled band built on the $h_{11/2}$ proton hole configuration were established and can be compared with the sequence of states calculated previously using a particle-plus-symmetric-rotor model [1].

A possible candidate (the 1836 keV state) for the coupling of the aligned $h_{11/2}$ proton hole with the 5^- state of the core was also observed.

The states originating from the “intruder” $f_{7/2}$, $h_{9/2}$, and $i_{13/2}$ orbitals were not observed.

Au has also been used as a rad-chem diagnostic and these data provide new information on the excitation of the isomeric levels.

References:

[1] P. O. Tjøm, M. R. Maier, D. Benson Jr., F. S. Stephens, and R. M. Diamond, Nucl. Phys. **A231**, 397 (1974). Experiment Report (continued)

IMPORTANT! List or attach a list of publications resulting from this experiment (published or in press).

Submit all experiment reports to:
 LANSCE User Office, MS H831, Los Alamos National Laboratory, Los Alamos, NM 87545

Experiment was carried out at:		Local Contact	Proposal #	<i>LANSCE Use Only</i>
<input type="checkbox"/>	Manuel Lujan Jr. Neutron Scattering Center	John Ullmann	2003504	Report Rc'd 9/10/04
<input checked="" type="checkbox"/>	Weapons Neutron Research Facility	FP/Instrument Used		
<input type="checkbox"/>	WNR/Blue Room	4FP15R		

Title

Cross section measurements for cosmic ray studies using neutrons

Authors and Affiliations

Janet Sisterson, Northeast Proton Therapy Center, Massachusetts General Hospital
John Ullmann, LANSCE, Los Alamos National Laboratory

Experiment Report

We were scheduled beam time from 7 am October 18 – 7 am November 1 2003.

Aim of the experiment

The primary goals were to measure average cross sections for the production of ^{10}Be , ^{14}C , ^{22}Na and ^{26}Al from Si and Al targets using a white neutron beam with energies in the range of $\sim 0.1 - 750$ MeV. Si and Al are found in both the lunar surface and meteorites and we need these cross sections to better understand the interactions of cosmic rays with extraterrestrial materials. Dr. Tim Jull will measure ^{14}C using Accelerator Mass Spectrometry (AMS) at the AMS facility at the University of Arizona. A new beam line is under construction that will be able to make this measurement in these large mass active targets. Dr Marc Caffee will measure ^{10}Be and ^{26}Al at PRIME Lab, Purdue University, once upgrades to that facility are complete. Janet Sisterson will measure ^{22}Na (and other relevant gamma-emitting short-lived products) in all targets and monitor foils using non-destructive gamma-ray spectroscopy. Dr Kuni Nishiizumi of the University of California, Berkeley will make the necessary chemical preparations before the ^{10}Be and ^{26}Al measurements. An additional target was included in the 9-day irradiation (described below) to try and measure cross sections for the production of Ar isotopes from Ca. This target was provided by the University of California and was a Ca-containing compound.

Experimental conditions

Each irradiation is designed to produce the optimum number of product atoms that are required to get a good AMS measurement. For ^{14}C this is 1×10^7 ; for ^{10}Be and ^{26}Al 2×10^8 atoms are required. Irradiation times are calculated using these figures and estimated cross sections for the reactions. Practically this meant that for the beam conditions in 2003, where we had 3.6 micro-sec spacing, that a 3-day irradiation was suitable for ^{14}C production; a 9-day irradiation was required for ^{10}Be . ^{26}Al is usually measured in the same target as ^{10}Be . However, because of the much higher cross sections for the production of ^{26}Al from Si and Al compared to those for ^{10}Be production meant that far too many ^{26}Al nuclei would be produced in these targets, probably requiring significant dilution of the aliquots before the ^{26}Al could be measured using AMS. Therefore, a 1-day irradiation was included specifically to irradiate targets to give yields of ^{26}Al better suited to the AMS determination. In all irradiations, a fission chamber continually monitored the beam.

Targets: Each Al target stack was made up of 1 mm thick 50 x 50 mm Al targets and each Si target stack was made up of 1 mm thick 50 mm diameter Si targets, all of high purity. For the 1-day irradiation, each target stack contained 1 target, for the 3-day and 9-day irradiations, each target stack contained 4 of these targets. In each irradiation, monitor foils of Au, Al, Ni and Cu were included. The target stacks were wrapped in Al foil for irradiation.

Experiment Report *(continued)*

After irradiation each individual target was placed in a separate small plastic bag to prevent contamination with modern concentrations of the isotopes of interest.

The U. of California target was made up of an Al holder with many pits in it, which contained the Ca-containing compound.

Beam Line: 4FP15R was used with essentially the same experimental configuration as was used in 2002. 2 inches of polyethylene was placed well upstream to eliminate low energy neutrons. ~2.5 feet of donuts each with a 2 inch diameter hole were used to collimate the beam to give a size that was greater than the maximum target size at the irradiation position.

Irradiation set-up: The existing target stack holder was placed in 4FP15R about 2 meters downstream of the fission chamber, which was located as far upstream as possible in the room. The beam pipe downstream of our target position was removed to reduce the neutron background downstream. The upstream stand that normally supported this section of beam pipe was used as a target holder for the U. of California target. Additional monitor foils were included on the downstream surface of this target.

Irradiations: Image plates were used to align the target holder, and so the target stacks, with the beam. To align the U. of California target, an image plate was exposed at that location and after computer analysis, a picture of the beam spot was taped in place at the irradiation position and then the target placed on top of that. For the period of our experiments, the beam was relatively stable but corrections are made for all periods of no beam that are greater than ~10 minutes. These corrections are obtained from the CCR logs. These corrections are particularly important for the short-lived radioactive products produced. The three runs lasted for 6.52 hours, 73.2 and 196 hours respectively.

Shipping of targets: For many reasons, it took nearly 6 weeks before the targets were shipped back to MGH. This was not ideal and I hope this can be expedited better in future irradiations.

Experimental results:

Fluence calculations: These are still in progress but using our previously measured cross sections in the monitor foils we can estimate the total fluences for each irradiation, which appear to be lower than anticipated.

Yield of short-lived radionuclides: The Ge detector is now located at MGH and counting of the targets and monitor foils is in progress. To date only a few measurements have been made due to the long delay in shipping the targets from LANSCE back home.

Publications:

Sistersen JM, Kim KJ and Reedy RC. (2004) Revised production rates for ^{22}Na and ^{54}Mn in meteorites using cross sections measured for neutron-induced reactions. In Lunar and Planetary Science XXXV, Abstract #1354, Lunar and Planetary Institute, Houston (CD-ROM).

IMPORTANT! List or attach a list of publications resulting from this experiment (published or in press).

REPORT ON EXPERIMENT (Please Type)

Submit all experiment reports to:

LANSC User Office, MS H831, Los Alamos National Laboratory, Los Alamos, NM 87545

Experiment was carried out at: Local Contact Proposal #LANSC User Only Manuel Lujan Jr. Neutron Scattering Center B. Takala 2003 507 Report Rc'd X Weapons Neutron Research Facility FP/Instrument Used 6/29/04 WNR/Blue Room 4FP30L-A

Title

MEASUREMENTS OF NEUTRON INDUCED SINGLE EVENT EFFECTS IN LOW POWER AND HIGH DENSITY INTEGRATED CIRCUITS

Authors and Affiliations

Dr. D.B.S. King, BAE SYSTEMS, Warton, England

Dr. T. Granlund, AerotechTelub AB, Linköping, Sweden

Simon N. Clucas, QinetiQ, Farnborough, England

Andrew M. Chugg, MBDA UK Ltd, Filton, England

Adrian Shipley, Smith Aerospace, Cheltenham, England

Experiment Report

Five different companies; AerotechTelub AB, QinetiQ, BAE Systems, MBDA UK Ltd, and Smith Aerospace performed experiment in the ICE House during week 47 year 2003. Each of the participants had their own test set for testing. AerotechTelub tested for Single Event Upsets (SEUs) and Latch-ups (LU) of various numbers of static random access memories (SRAMs). QinetiQ tested SRAMs for SEU and LU. BAE Systems tested power supplies, a FLASH memory device, a small quantity of SRAM's, a CCD camera and an Active Pixel Sensor for SEU and LU. MBDA UK Ltd tested a CCD camera for the purpose of analyzing the tracks of the secondary recoils in the CCD detector. Smith-aerospace tested for SEU in a F16 Engineering ISIS unit containing potential susceptible devices.

Figure 1 shows all test sets lined up in the neutron beam. First in the beam are AerotechTelub's test set for testing SRAMs. They tested six different types of SRAMs and each type were represented by 3 to 8 devices giving in total 30 devices. All devices were of industrial standard, commercial SRAMs and of the same technology, i.e., 0.13 μ m gate length and bulk SRAMs. The SEU result clearly shows that the trend continues for bulk SRAMs when the gate length is shrinking, i.e., the devices get more susceptible to neutrons resulting in an increase of the SEU when decreasing the gate length. This trend was established from tests, done by them in year 2002 at WNR, on SRAMs of different gate length. SRAMs; SEU starts to increase when the gate length reaches below 0.25 μ m [1]. This data were also used for comparative studies between WNR and a Quasi mono-energetic neutron source [2]. The recent test on 0.13 μ m technology gave an upset rate of around 3E-10 errors per hour at normal flight altitude depending on the supply voltage and geographical location. This is almost a 50% increase compared to 0.16 μ m technology. AerotechTelub need to do more testing in WNR in order to get more information to see for example how large the multiple bit upset contribution is to the total SEU. During this test the SRAMs were also heated up to 70°C showing an increase in SEU rate between 2-30% depending on the type of SRAM. These latest results will probably be presented next year at NSREC.

Figure 1. Test set-ups from all companies. First in the beam line are AerotechTelub,

second QinetiQ, third BAE Systems, fourth MBDA UK and at the end are Smith Aerospace.

Experiment Report (continued)
QinetiQ tested static RAMs. These were mostly 4Mbits devices and also some older 1Mbits parts. Plenty of SEU statistics were gained. Some devices suffered latch-ups, but recovered after power cycling. Excellent use was made of the beam time with shift working throughout the night.

MBDA acquired a total of around 10,000 image frames from E2V technologies CCD02-06 and CCD62-06 devices in the neutron beam, for example see **Figure 2**. In excess of a hundred neutron events were discernible in each 0.6 second frame (see montage of 5 frames in the figure below). A general analysis of the events will be given in a paper accepted for presentation at NSREC2004 (poster paper PF-1). The results show the highest resolution histories of RTS in neutron-induced dark current spikes yet reported. These results are also used to illustrate and validate a new technique for determining the proportion of multiple bit upsets (MBU's) in SEE test data by monitoring the MBU-induced broadening of the variance of the number of affected pixels in a frame (or bits flipped in a memory read-cycle) relative to its mean value. This has been accepted for presentation at NSREC2004 as oral paper I-4.

MBDA also tested the Austin MT5C1008 1Mbit SRAM, which had previously been investigated using MBDA's SEE laser facility (SEREEL). The main purpose of this exercise was to begin work on calibrating the SEE effects of laser pulses against those induced by high energy neutrons. Significant numbers of SEU's were seen during WNR testing of 6 samples (three different date codes and at least two different dies).

Figure 2. Picture showing the tracks from secondary recoils produced from neutron silicon spallation reaction in a CCD camera.

BAE Systems tested two types of switch mode power supply intended to power Field Programmable Gate Arrays (FPGA's). There were no observed effects on the National Semiconductor LM2653MTCADJ (two parts tested). A Xilinx FLASH based memory device was tested. It failed to communicate with its JTAG interface after approximately a day of exposure (far more fluence than would be seen in the life of an aircraft). After power cycling the device behaved normally and no problems were experienced programming the device at a later date. An elementary trial using an Active Pixel Sensor device to capture neutron induced events was highly successful – plenty of good data was obtained. A trial using a CCD failed due to a fault in the recording equipment. The nature of the fault has not yet been determined. Some SRAMs were also tested – some were found to be very sensitive, they latched up and burnt out before the power supplies could be removed.

Smith Aerospace tested the F16 Engineering ISIS unit. The aim of these initial tests for the SPAESRANE programme was to measure a baseline performance for the ISIS unit as it stands, against which future updates, which implement SEE mitigation techniques can be compared.

The testing showed that the unit was generally relatively immune to cosmic radiation effects with the exception of the Power Supply Unit, which repeatedly caused the unit to fail. This type of failure is most probably due to the optical feedback architecture used, since optical components are known to be disrupted when subjected to

neutron radiation.

The other main area in the unit that was likely to be susceptible was the processor, which contains SRAM Cache and the SDRAM memory devices. The processor cache did not fail once throughout the tests, while the SDRAM proved to be quite robust, giving only one soft error after 15 minutes and 2 soft errors after 75 minutes. Moreover, the three ACTEL FPGA devices embedded in the unit showed no signs of induced errors.

This team of companies will during the following two years concentrate on testing SRAMs and FPGAs for SEUs and Latch-ups on separate devices and in larger systems. Fault tolerant measures will be taken to evaluate their efficiency. **IMPORTANT! List or attach a list of publications resulting from this experiment (published or in press).**

[1] T. Granlund, B. Granbom, and N. Olsson, "Soft Error Rate Increase for New Generations of SRAMs", *IEEE Transactions on Nuclear Science*, vol. 50, no. 6, December 2003.

[2] T. Granlund, B. Granbom, and N. Olsson, "A Comparative study between two Neutron facilities regarding SEU", *IEEE Transactions on Nuclear Science*, to be published in year 2004.

Submit all experiment reports to:
LANSCE User Office, MS H831, Los Alamos National Laboratory, Los Alamos, NM 87545

Experiment was carried out at:	Local Contact	Proposal #	LANSCE Use Only
<input type="checkbox"/> Manuel Lujan Jr. Neutron Scattering Center	Bruce Takala	2003508	Report Rc'd
<input checked="" type="checkbox"/> Weapons Neutron Research Facility	FP/Instrument Used		11/6/03
<input type="checkbox"/> WNR/Blue Room	4FP30L		

Title Single Event Characterization of Very High Performance Memories for National Critical Infrastructure
Authors and Affiliations John S. Browning, Sandia National Laboratories; Mike Tucker, Alpha Sciences Inc.; Jerry Hausner, ElectroScience Technologies LC.

<p>Experiment Report</p> <p>We performed accelerated single event rate (ASER) characterization of eleven CMOS SRAM device types, some of which are embedded applications of new technology. The tests were designed and executed to comply with the requirements and procedures for soft-error rate testing of the JEDEC Standard, "Measurement and Reporting of Alpha Particles and Terrestrial Cosmic Ray-Induced Soft Errors in Semiconductor Devices," JESD89, dated August 2001. The broad energy spectrum neutron beam, available at the LANSCE ICE House, was used to characterize the single event susceptibility to secondary cosmic rays of six samples of each SRAM device type. Each sample was tested at four bias voltages: maximum, minimum, nominal, and data retention. The test hardware was custom designed to accommodate large package sizes (~600 FCBGA) and radio frequency signal test conditions (100 MHz to 1 GHz clock cycles). Two types of devices were tested: 1) Very High-speed Memory Devices for Data Networking Applications, and 2) a Single Event Hardened CMOS SRAM for implantable pacemakers and cardioverter defibrillators. (St. Jude Medical Cardiac Rhythm Management Division has entered into a cooperative research and development agreement to assess the threat of alpha-emitters in packaging materials and secondary cosmic rays to the reliability of their 0.18 micron bulk CMOS SRAM memory under development.) The basic procedure was to mount each of the various memory chips, or devices under test (DUTs), onto a tester board, or test vehicle (TV), in a manner in which they can be written to and then read while exposed to the neutron beam. The test to measure the soft error rate and check for latch ups included writing a predetermined pattern to the DUTs, and then reading the memory locations at short specific intervals. Typical cycle time between readings was less than 16 seconds. The host test system would poll the DUTs, with a typical read time of about 2 seconds. If all 8 slots were filled, then a specific DUT would be read every 16 seconds. Prior to beam exposure, each DUT was subjected to a cold test. A 60 second test was conducted with no beam exposure to ascertain that the DUT was working error free under benign conditions. The duration of a test was predetermined to be either a specific number of errors, a number of latch ups, or a unit of time. The dedicated program allowed such a selection and sounded an alarm when the end-of-test condition was satisfied. Figure 1 shows the GUI associated with the software generated to run these tests. A specialized test fixture was designed that consists of a mother board which contains a single board Z-World processor to write to and read from the TVs, see Figure 2. The mother board can hold up to 8 TVs (1 DUT per TV) connected via two separate busses. Each bus has a terminator board that contains pull up resistors on each data line. The mother board is mounted in an aluminum frame which allows the up to 8 TVs to be plugged in and held in place by card guides. A bank of four fans is provided to cool the DUTs. Each TV also contains a bank of Altera programmable logic devices (PLDs) to permit rapid, on-site programming of the routing of the signals to each of the different DUTs. Power to the DUTs is brought in through separate connectors on the top of each TV to allow varying of the</p>

Experiment Report (continued)

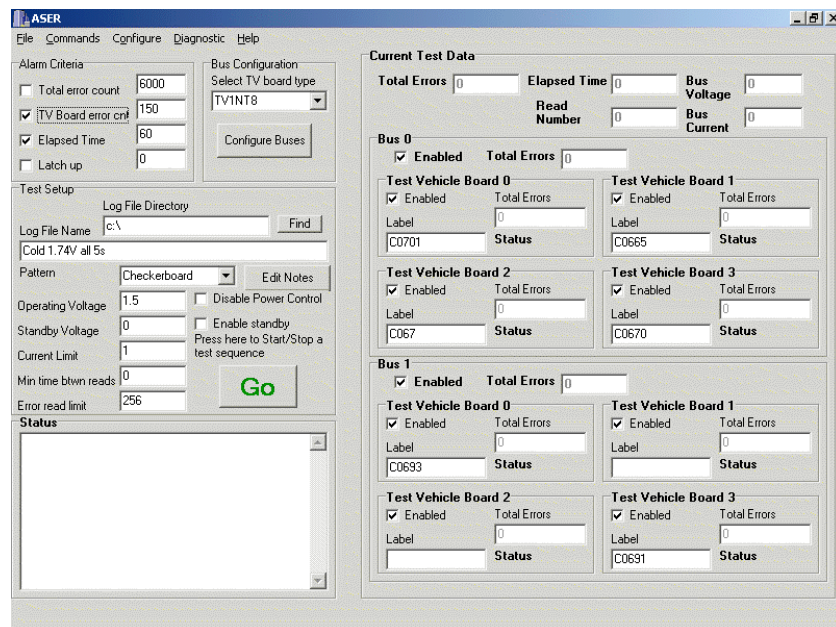


Figure 1. Graphic User Interface designed for ASER Testing

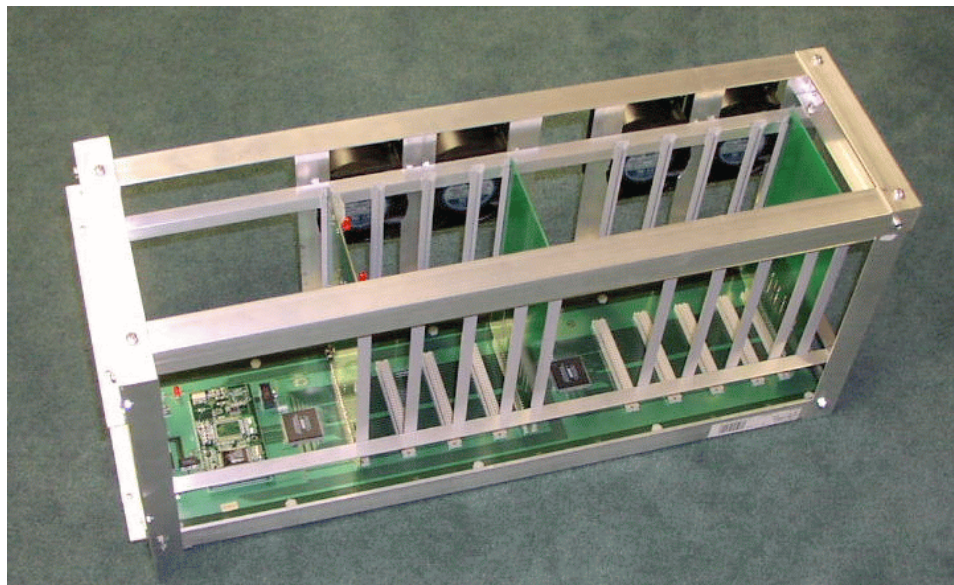


Figure 2. Main test fixture showing the mother board, card slots, Z-World computer, Altera bus controllers and cooling fans.

IMPORTANT! List or attach a list of publications resulting from this experiment (published or in press).



REPORT ON EXPERIMENT
(Please Type)

Submit all experiment reports to:
 LANSCE User Office, MS H831, Los Alamos National Laboratory, Los Alamos, NM 87545

Experiment was carried out at:	Local Contact	Proposal #	<i>LANSCE Use Only</i>
<input type="checkbox"/> Manuel Lujan Jr. Neutron Scattering Center	Olivier Lauzeral	2003509	11/12/03
<input type="checkbox"/> Weapons Neutron Research Facility	FP/Instrument Used		
<input checked="" type="checkbox"/> WNR/Blue Room	WNR 30L		

Title	Cosmic Ray Soft Error Rate Testing
--------------	------------------------------------

Authors and Affiliations

Olivier Lauzeral, iRoC Technologies, Director of Operations

Experiment Report

During this experiment several types of state of the art electronic devices were tested on behalf of different companies:

Content Addressable Memories (CAM) for NetLogic (US)
SRAM and FCRAM for Toshiba (Japan)
SRAM for Agilent (US)

The purpose of these tests is to bring more and more companies and more and more new technologies to be tested for Soft Errors and Single Event Latch Up.

Since most independent device manufacturers (IDM) firms are now entering into the deep submicron technologies (.13 μm and beyond), the threat of soft errors is becoming a real issue. Publications and conferences on the topic are more frequent now, like the need to test on these effects.

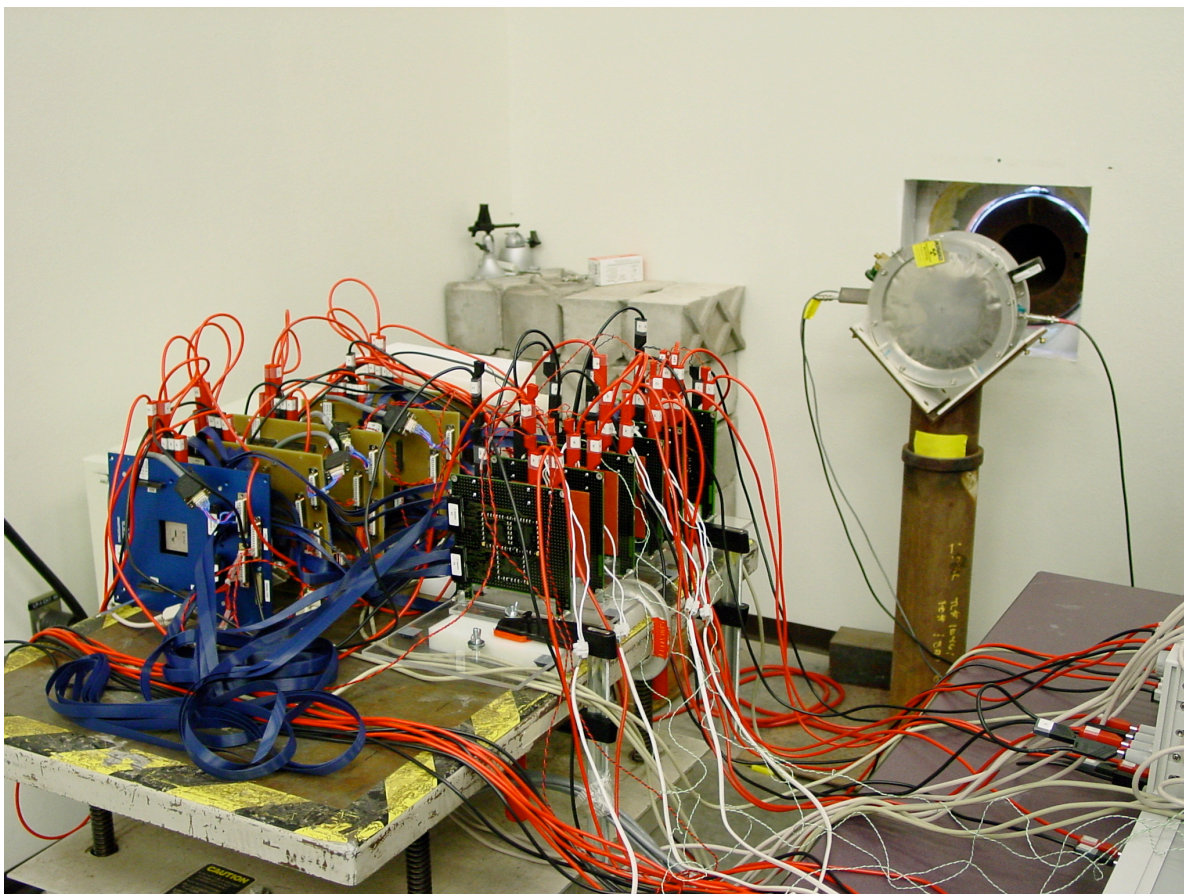
Throughout the different test campaign run at Los Alamos, iRoC is able to define trends in the new technologies and to bring a better awareness of the threat to the whole industry. Usually tests are performed with different combinations of parameters like voltage, temperature, test pattern for memories and orientation towards the beam. The count of test conditions for one single chip can sometimes be more than 50. According to the sensitivity of the device one condition can last from 10 minutes to few hours.

The WNR neutron beam is the preferred facility for accelerated Soft Errors testing, because its spectrum is so closely matched to the terrestrial environment.

The results of the tests run during this campaign are proprietary of NetLogic, Toshiba and Agilent respectively, and cannot be displayed.

Experiment Report *(continued)*

The following figure shows the experimental set-up. Six different devices are stacked-up and tested in parallel to make the most effective use of the beam resource. The campaign duration was 72 hours and the beam was used during the entire available time.



IMPORTANT! List or attach a list of publications resulting from this experiment (published or in press).

REPORT ON EXPERIMENT (Please Type)

Submit all experiment reports to:

LANSC User Office, MS H831, Los Alamos National Laboratory, Los Alamos, NM 87545

Experiment was carried out at: Local Contact Proposal #LANSC User Only Manuel Lujan Jr. Neutron Scattering Center Bruce Takala #2003510 Report Rc'd Weapons Neutron Research Facility FP/Instrument Used 6/1/04 XWNR/Blue Room – ICE House

Title

"Neutron-Induced Soft Error and Latch-up Sensitivity in 0.09um SRAM Memories and Logic Devices" Authors and

Affiliations

Robert Baumann	Texas Instruments
Vivian Zhu	Texas Instruments

Experiment Report

During the WNR 2004 Winter/Spring run cycle, Texas Instruments used the LANL facilities to examine SEU trends in our most advanced 90nm CMOS technologies, which are of extreme interest to the computer and communications industries. Also new, we performed our first n-ASER measurements on a pure logic device test structure in addition to the usually tested pure memory SRAM devices. Although we have never seen neutron induced latch-ups in TI parts we also looked for this failure mode as well. Finally we did neutron tests on a full product DSP chip built in 0.13um CMOS technology.

This set of experiments included the following:

1.)

Verification of SRAM neutron SEU models using 0.09um 24.1 Mbit SRAM test chips in the neutron beam.

2.)

Searched for signs of neutron induced latch-ups (LU).

3.)

First neutron data from dedicated logic (flip-flop and latch) test structures at the 0.09um node.

4.)

First neutron results from a 0.35um DSP product (JANUS chip) including SRAM and logic tests.

Detailed results are TI confidential but we can say that the testing for each of these components was successful. The 90nm SRAM studies revealed the expected result that SRAM per bit SEU rate is now decreasing as a function of technology scaling and the magnitude of the SEU actually was quite close to our simulation results of 90nm technology. We observed a few LU-like events but further tests eliminated all but a few events as being LU related. The remaining LU-like events could not be separated from circuit/tester artifacts and thus more controlled data from more mature devices will have to be repeated to verify whether or not LU was observed at all. Tests revealed that logic SEU sensitivity is increasing relative SRAM sensitivity. While it is still lower than the SRAM SEU rate (on a per bit basis), Logic SEU is becoming a bigger issue – particularly in devices that use error correction in the memory. Finally, results from the DSP product tested in the neutron beam agreed well with SRAM predictions based on SRAM test structures and simulation. Evaluation of the DSP results are still in progress particularly in the FF/latch SEU observed. Final results will probably be reported in IEEE IEDM presentation (if accepted). **IMPORTANT! List or attach a list of publications resulting from this experiment (published or in press).**

Some neutron results will be disclosed in IEEE IEDM 2004 (pending acceptance)

Submit all experiment reports to:
LANSCCE User Office, MS H831, Los Alamos National Laboratory, Los Alamos, NM 87545

Experiment was carried out at:	Local Contact	Proposal #	LANSCCE Use Only
<input type="checkbox"/> Manuel Lujan Jr. Neutron Scattering Center	Dr. Bruce Takala	2003511	Report Rc'd
<input checked="" type="checkbox"/> Weapons Neutron Research Facility	FP/Instrument Used		
<input type="checkbox"/> WNR/Blue Room	FP30L		

Title

Validation of (Quasi-) Mono Energy Neutron Beams as a Probe of Single Event Effects of Semiconductor Devices by Using the WNR White Neutron Beam

Authors and Affiliations

Yasuo Yahagi, Eishi Ibe, Production Engineering Research Laboratory, Hitachi, Ltd.
Yukiaki Yoshino, Shigehisa Yamamoto, Yasuhiko Takahashi, Hideaki Kameyama, Renesas Technology Corp.
Atsushi Saito, Mitsumori Hidaka, Elpida Memory Inc.

Experiment Report

Single event upset (SEU) of semiconductor devices induced by terrestrial neutrons is one of the most crucial issues for the leading-edge devices, particularly after the publication of the JEDEC Standard JESD89 [1]. It describes how to evaluate soft-error rate (SER) of a specific device in the field, including errors by alpha particles. In JESD89, WNR is recommended as a preferred facility of estimation of the SER by accelerated neutron irradiation test. Although the spectrum of WNR is seen to match the terrestrial neutron spectrum in JESD89, there is wide variation of calculated or measured energy spectra of terrestrial neutrons as shown in Fig. 1[2-4] and the calculated value of SER can include a wide range of errors. On the other hand, the authors have investigated the estimation method for SERs by using (quasi-) mono energy neutron beams in FNL (Fast Neutron Laboratory) and CYRIC (Cyclotron and Radioisotope Center) of Tohoku University, Japan, RCNP (Research Center for Nuclear Science) of Osaka University, Japan, and TSL (Theodor Svedberg Laboratory) of Uppsala University, Sweden. SER can be estimated by using the following formula:

$$\text{SER [FIT]} = 3.6 \times 10^{12} \int_{E_{th}}^{\infty} \sigma_{SEU}(E_n) \frac{\partial \phi(E_n)}{\partial E_n} dE_n \quad (1)$$

where E_n [MeV] is the neutron energy, $\phi(E_n)$ [n/cm²/s] the flux of terrestrial neutron, E_{th} [MeV] the SEU threshold energy and $\sigma_{SEU}(E_n)$ [cm²] the energy dependence SEU cross-section of the device[5,6]. An estimated value of SER strongly depends on a used spectrum as the formula (1) and the wide variation of terrestrial neutrons as shown in Fig. 1 makes the value of SER ambiguous. From the viewpoint of the validation of SER-estimation method by using (quasi-) mono energy neutron beams, the well-defined white neutron spectra in WNR instead of terrestrial neutron spectra are very useful. Instead of SERs, SEU cross-sections directly obtained by experiments in WNR, $\sigma_{SEU}(WNR)$ [cm²] are compared in this report.

The SEU cross-section data acquired by using (quasi-) mono energy neutron beams can be described as a function of energy. Several functions, such as the Bendel function [7], are proposed for fitting of proton and heavy ion irradiation data. The authors select the Weibull function of 4 parameters [8]. With the best fitted Weibull function $\sigma_{Weibull}(E_n)$ and the double differential spectrum of white neutron beam in WNR, estimation of SEU cross-section by neutron irradiation test in WNR is carried out as following:

$$\sigma_{SEU}(WNR) = \frac{\int_{E_{th}}^{800\text{MeV}} \sigma_{Weibull}(E_n) \frac{\partial \phi_{WNR}(E_n)}{\partial E_n} dE_n}{\int_{E_{th}}^{800\text{MeV}} \frac{\partial \phi_{WNR}(E_n)}{\partial E_n} dE_n} \quad (2)$$

$$\sigma_{Weibull}(E_n) = \sigma_{\infty} \left[1 - \exp \left\{ - \left(\frac{E - E_{th}}{W} \right)^S \right\} \right] \quad (3)$$

where $\phi_{WNR}(E_n)$ [n/cm²/s] is the flux of white neutron beam in WNR, σ_{∞} [cm²] a saturated value of SEU cross section, W a width factor and S a shape factor of the Weibull function, respectively.

The irradiated devices were SRAMs of 0.18μm, 0.15μm and 0.13μm and a DRAM of 0.25μm. The spectra of neutron beams (Fig.2) were varied by setting polyethylene-shield (2", 4" and 8" -thick) in the flight path of FP30L. The test results are summarized in Table 1 and Fig.3, in which SEU cross-sections per Mega-bit are shown as relative values. The measured values were obtained by using neutron fluence both for $E_n > 1.5\text{MeV}$ and $E_n > 10\text{MeV}$. The errors (%)

Experiment Report (continued)

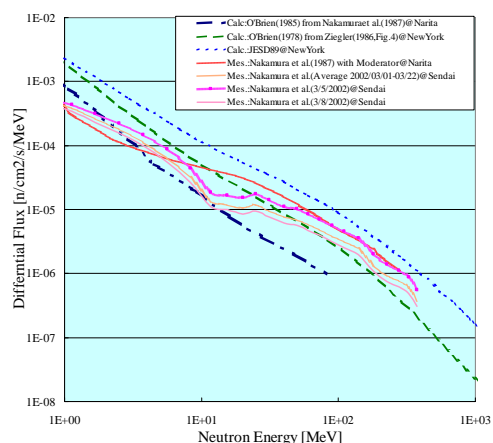
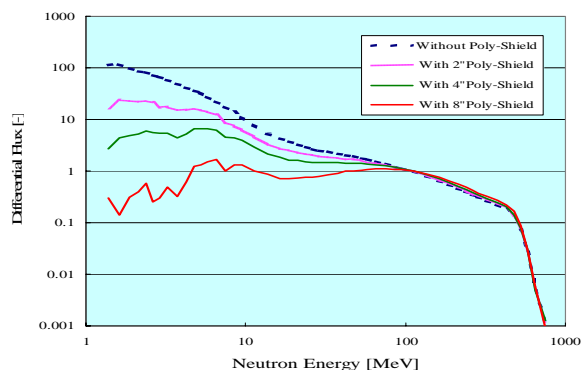
shown in Table1 were calculated by

$$\text{error (\%)} = \frac{(\text{Estimated } \sigma) - (\text{Measured } \sigma)}{(\text{Estimated } \sigma)} \times 100.$$

The measured value of $\sigma_{\text{SEU}}(\text{WNR})$ for $E_n > 10\text{MeV}$ shows relatively good agreement with estimated one, compared with that for $E_n > 1.5\text{MeV}$. This means that SERs under any conditions of white neutron irradiation, including field tests [5,6], can be precisely estimated by using basic SEU cross section data acquired by (quasi-) mono energy neutron beams.

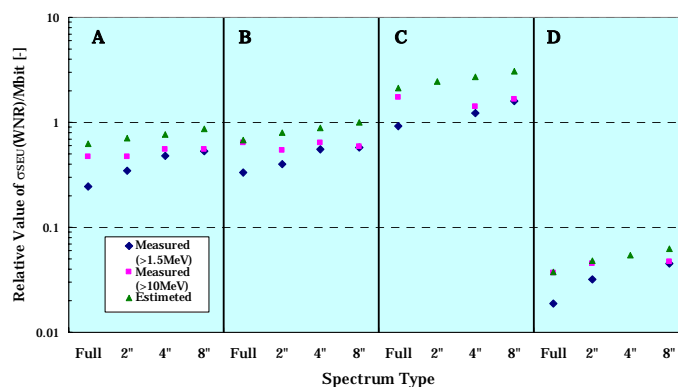
References

- [1] JEDEC, "JEDEC Standard No.89: Measurement and Reporting of Alpha Particles and Terrestrial Cosmic Ray-Induced Soft Errors in Semiconductor Devices", JESD89 (2001).
- [2] Ziegler, J.F., "Terrestrial Cosmic Rays", IBM J. Res. Develop., Vol.40, No.1, pp.19-39(1996).
- [3] Nakamura, T., Y. Uwamino, T. Ohkubo and A. Hara, "Altitude Variation of Cosmic-ray Neutrons", Health Physics, Vol.53, No.5, pp.509-517 (1987).
- [4] Nakamura, T., Private Communication (2002).
- [5] Yahagi, Y., E. Ibe, Y. Saito, A. Eto, M. Sato, H. Kameyama, M. Hidaka, K. Terunuma, T. Nunomiya, T. Nakamura, P.-U. Renberg and A. Prokofiev, "Self-Consistent Integrated System for Susceptibility to Terrestrial-Neutron Induced Soft-error of Sub-quarter Micron Memory Devices", in Final Report of IEEE 2002 International Integrated Reliability Workshop, Stanford Sierra Camp, S. Lake Tahoe, Oct. 21-24, 2002, pp.143-146 (2002).
- [6] Ibe, E., Y. Yahagi, F. Kataoka, Y. Saito, A. Eto, M. Sato, H. Kameyama and M. Hidaka, "A Self-Consistent Integrated System for Terrestrial-Neutron Induced Single Event Upset of Semiconductor Devices at the Ground", IEEE 1st International Conference on Information Technology & Applications, Bathurst, Australia, Nov. 25-28, 2002, Paper No.273-21 (2002).
- [7] Goka, T., H. Matsumoto and N. Nemoto, "SEE Flight Data from Japanese Satellites", IEEE Transactions on Nuclear Science, Vol.45, No.6, pp.2771-2778 (1998).
- [8] Petersen, E. L., J. C. Pickel, J. H. Adams, Jr. and E. C. Smith, "Rate Prediction for Single Event Effects", IEEE Transactions on Nuclear Science, Vol.39, No.6, pp.1577-1599 (1992).

**Fig.1 Variation of Terrestrial Neutron Spectra****Fig.2 Variation of Neutron Spectra in WNR****Table 1 Test Devices and Results**

Device ID	Type	Process (μm)	Density (Mbit)	Spectrum	$\sigma_{\text{SEU}}(\text{WNR})/\text{Mbit}$			
					Measured (>1.5MeV)	Measured (>10MeV)	Estimated*	% error (>1.5MeV)
A	SRAM	0.18	8	Full	2.46E-1	4.72E-1	6.32E-1	61.1
				2"	3.48E-1	4.72E-1	7.05E-1	50.6
				4"	4.78E-1	5.49E-1	7.61E-1	37.3
				8"	5.32E-1	5.49E-1	8.69E-1	38.7
B	SRAM	0.13	16	Full	3.33E-1	6.38E-1	6.73E-1	50.5
				2"	3.98E-1	5.41E-1	7.96E-1	50.0
				4"	5.54E-1	6.36E-1	8.77E-1	36.8
				8"	5.72E-1	5.90E-1	1.00E+0	42.8
C	SRAM	0.15	2	Full	9.14E-1	1.74E+0	2.12E+0	56.8
				2"	-	-	2.47E+0	-
				4"	1.23E+0	1.42E+0	2.71E+0	54.5
				8"	1.60E+0	1.65E+0	3.07E+0	47.9
D	DRAM	0.25	64	Full	1.89E-2	3.65E-2	3.75E-2	49.4
				2"	3.18E-2	4.53E-2	4.75E-2	33.2
				4"	-	-	5.42E-2	-
				8"	4.53E-2	4.67E-2	6.26E-2	92.8

*Estimated with SEU Weibull function obtained from quasi-mono energy experiments

**Fig.3 Test Devices and Results**

IMPORTANT! List or attach a list of publications resulting from this experiment (published or in press).

Submit all experiment reports to:
LANSCE User Office, MS H831, Los Alamos National Laboratory, Los Alamos, NM 87545

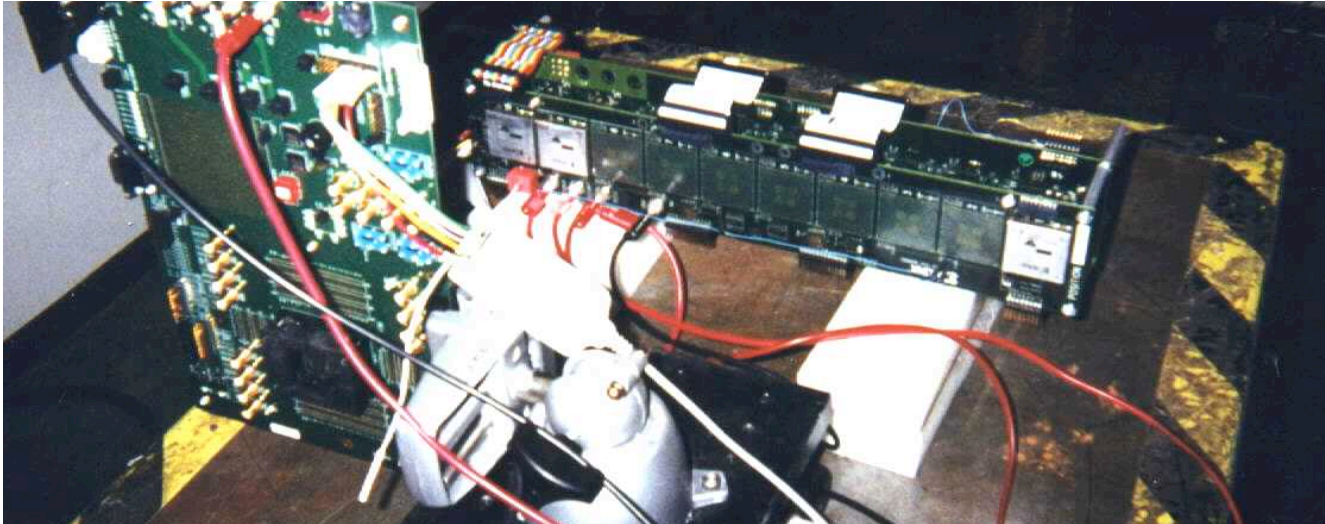
Experiment was carried out at:		Local Contact	Proposal #	LANSCE Use Only
<input type="checkbox"/>	Manuel Lujan Jr. Neutron Scattering Center	Bruce Takala	2002512	Report Rc'd 11/20/03
<input checked="" type="checkbox"/>	Weapons Neutron Research Facility	FP/Instrument Used		
<input type="checkbox"/>	WNR/Blue Room	FP30L-A		

Title Atmospheric Neutron Sensitivity Measurements of Advanced Silicon Sub-Micron CMOS Technologies
Authors and Affiliations Joseph J Fabula Xilinx Corporation

Experiment Report

Our neutron experiments, which were performed over a 48 hour period, evaluated the effects of accelerated exposure to a neutron flux which approximated the energy spectrum of the neutrons seen in the atmosphere (Hess spectrum). During this 48 hour period we experienced better than 98% beam availability and the experiment was successfully completed.

The experiment utilized the 30L beam line at the LANSCE facility, and the data taken was compared with data taken previously at this facility on earlier versions of our products, and with data taken by other researchers in reactor neutron sources. It is necessary to periodically evaluate such data to maintain the accuracy of our neutron modeling efforts. The reactor data had been previously published. All data taken at the LANSCE facility remains proprietary to Xilinx Corporation and cannot be disclosed externally without the written consent of Xilinx Corporation and/or its representatives.



REPORT ON EXPERIMENT (Please Type)

Submit all experiment reports to:

LANSCCE User Office, MS H831, Los Alamos National Laboratory, Los Alamos, NM 87545

Experiment was carried out at: Local Contact Proposal #LANSCCE Use Only Manuel Lujan Jr. Neutron Scattering Center R.C.

Haigh 2003513 Report Rcd Weapons Neutron Research Facility FP/Instrument Used 6/28/04x WNR/Blue Room

Title

Preliminary Beam Characterization in Preparation for W76-1/Mk4A Piece-Part Annealing Studies

Authors and Affiliations:

Larry Posey—Sandia National Labororotory

Lee Ziegler—Bechtel Nevada

Mark B abineau—Ktech Inc.

Experiment Report

This experiment evaluated the use of LANSCE as a source of short-duration pulsed neutrons, and associated gamma-rays, for the testing of weapon-system electronic components. Of primary importance was the determination of the maximum useable neutron fluence, the time history of the pulse and the associated gamma environment; i.e., magnitude and time history. Of secondary importance was a detailed knowledge of the neutron energy spectrum. This initial characterization went so well that experiments to measure the displacement damage, and subsequent annealing, for bipolar junction transistors were started during the initial operating period in January and were completed during the operating period in March. MCNPX was used to predict the raw neutron fluence at the exposure plane available from a tungsten target with graphite reflector plates. This was done at computing facilities at the University of Nevada, Las Vegas The raw neutron

Experiment Report *(continued)*

fluence was then used to determine the 1-Mev neutron fluence. 2N2222 dosimetry transistors were used to measure the 1-Mev neutron fluence and the results are compared in Figure 1. The measured results are seen to be somewhat low and additional calculations are being carried to address this difference. In addition to the proton-beam diagnostics and spectral information provided by the LANSCE staff, our experimental team brought some of its own diagnostic equipment (i.e., (1) activation analysis using praseodymium foils, (2) p-i-n detectors, (3) photoconductive detectors (PCDs), (4) scintillation type. detectors), and the electronic equipment needed to measure the electrical performance of the transistors and diodes. Neutron time-of-flight measurements were made to compare with the calculated raw neutron spectrum. This data is presently being analyzed to obtain the energy spectrum of the raw neutron environment.

The displacement damage, and subsequent annealing, experiments were carried out for three types of bipolar transistors; two of the types were from two different manufacturers. These discrete semiconductor devices are quite small and, as a result, could be placed quite close to the converter. As a result, the required 1-Mev neutron fluence per pulse could be realized. Ten samples of each transistor type from each manufacturer were exposed which required two test boards per type and manufacturer combination. One of the primary objectives of the transistor exposures was to look at the dependence of inverse transistor gain upon cumulative 1-Mev

neutron fluence; i.e., was the dependence linear or not for multiple LANSCE pulses. Of the data analyzed to date the dependence was found to be linear for the On Semiconductor MMBT2369 transistor type. The slope obtained from this linear dependence at a various times after the LANSCE proton pulse can be plotted as a function of time in order to obtain the damage constant versus time as shown in Figure 2. This is the final form of the experimental results needed for all the transistor types irradiated at LANSCE. This data analysis is presently underway.

IMPORTANT! List or attach a list of publications resulting from this experiment (published or in press).

The results of these experiments will be published in the development report for W76-1/Mk4A Refurbishment Project.

Submit all experiment reports to:
LANSCE User Office, MS H831, Los Alamos National Laboratory, Los Alamos, NM 87545

Experiment was carried out at: <input type="checkbox"/> Manuel Lujan Jr. Neutron Scattering Center <input checked="" type="checkbox"/> Weapons Neutron Research Facility <input type="checkbox"/> WNR/Blue Room	Local Contact	Proposal # 2003518	LANSCE Use Only Report Rc'd <div>6/28/04</div>
	Bruce Takala		
	FP/Instrument Used 4FP30L		

Title

Measurement of the Neutron-Induced Soft Error Rate of the SRAMs on UltraSPARC-IIIi Microprocessors of Sun Microsystems

Authors and Affiliations

Steven R. Boyle, Staff Engineer, Sun Microsystems
 Raymond A. Heald, Distinguished Engineer, Sun Microsystems

Experiment Report

LANSCE scheduled 5 days of neutron beam time for us from 0800 November 13 through 0800 November 18, 2003.

Our objective was to measure the soft error rate of Sun's UltraSPARC-IIIi CPUs in the LANSCE neutron beam so that we could calculate the expected soft error rate of these CPUs as they are bombarded by cosmic background neutrons. We believe that our experiments were successful and that the soft error data that we generated is useful and accurate. We are pleased with the LANSCE and WNR facilities and with the services provided by the people with whom we interacted. We hope to return to the LANSCE WNR center in the foreseeable future to run more experiments of this nature on other UltraSPARC CPUs of state of the art designs and wafer fabrication processes.

We ran 42 experimental runs during our 5 days of beam time. In most experimental runs three CPUs mounted in three Sun servers were located in sequential order in the path of the beam. Delays of our experiments due to beam downtime were insignificant and we made reasonably efficient use of the neutron beam while it was available. We recorded data during more than 95 hours of the 120 hours of facility use time we were allocated. During this 95+ hours of data recording time the neutron fluence caused 13,688,881 counts. We stopped most of our runs when the WNR Ortec-871 counter displayed about 120,000 counts. Such runs typically took about 50 minutes. Some of the experiments ran longer or overnight. The CPUs in one overnight run were subjected to nearly 2,000,000 counts.

The variables in our experiments were, CPU operating voltage, specific CPU and its CMOS feature size, specific server containing the CPU, choice of specific CPU site in the server, sequential position of the server and its CPU in the neutron beam, test pattern for exercising various particular structures or test routine for the CPU, beam path direction through the CPU, beam attenuating material if any, and neutron fluence as recorded by the Ortec-871 counter in the beam. A daily report of the energy distribution of the neutron beam and the number of neutrons per count was provided to us by Bruce Takala of LANSCE.

Experiment Report *(continued)*

The UltraSPARC-IIIi CPUs caches we tested were made with CMOS processes with feature sizes of .13 microns and .09 microns. Soft error data was collected from memory cells of different design serving various functions. The soft errors in the various types of memories were recognized and reported in particular test routines. As expected, memory cells of different design showed different soft error rates. We believe that our data shows that the historic trend of decreasing SER/Kbit with scaling down of the memory cell size continues but the rate of decrease appears to be flattening out. We continue to study this soft error data for additional insight.

The soft error data from the SRAM memories on the CPU showed more clearly than ever before that several memory cells can be upset by a single neutron strike. A large amount of test data is necessary to get a statistically significant number of such multiple-cell soft errors because they are only a small percentage of the total SRAM soft errors generated. We recorded over 1,000 multiple-cell errors in the 1-MByte SRAM during almost 70 CPU hours of test time. We believe that this number of multiple-cell errors is statistically significant. We continue to study the nature of these multiple-cell soft errors.

Soft errors in a particular type of logic circuitry built with flip flops on the CPU also were generated and recorded. The soft error test results from this logic circuitry confirmed previous estimates.

As of June of 2004 we have not published any of the data we recorded or any of the conclusions drawn from it although we hope to do so. We will notify LANSCE of any such publication.

For the record it should be noted that Dave Wilkins and Rutger Vrijen of Sun participated in these experiments at the LANSCE 4FP30L site.

Steve Boyle
June 24, 2004

IMPORTANT! List or attach a list of publications resulting from this experiment (published or in press).

Experiment Report (continued)

Impact of Angle of Incidence on SEU/SEL Characteristics

The bulk of the experiments were focused on studying the impact of angle of incidence on SEU/SEL rates in commercial SRAMs. Recent research published at the NSREC has indicated that there are differences in neutron SER between front and back-side irradiation. These differences have been attributed to different neutron reaction rates in the mostly SiO₂ overlayers over the active silicon device (front-side irradiation) vs. reaction rates in the Si substrate (back-side irradiation). However, these differences have not always been consistent between various technologies. In our experiments, SEU and SEL rates were characterized in three different commercial SRAMs as a function of angle of incidence from 0 degrees (front-side irradiation) to 180 degrees (back-side irradiation). Characteristic results are shown in Figure 2. For the devices tested here, no significant impact of angle of incidence was measured for either SEU or SEL. In general, part-to-part variation was as large as any variation noted with irradiation angle.

Neutron Effects in High-K Dielectrics

Due to extreme scaling of the gate dielectric in modern IC technologies, classical SiO₂ gate dielectrics are reaching fundamental limits on physical thickness. To reduce leakage currents through ultra-thin gate dielectrics, several alternate dielectric materials have been proposed, notably hafnium oxides and aluminum oxides. These “high-k” alternate dielectrics (so termed because of their increased dielectric constant k) can achieve electrical performance equivalent to SiO₂ dielectrics at larger physical thickness. However, the reliability of these new materials systems is largely unknown. In this experiment, we hoped to irradiate high-k dielectrics to various neutron fluences and perform electrical reliability testing to quantify their reliability in terrestrial neutron environments. Unfortunately, the available test structures were research-grade dielectrics, and lacked sufficient uniformity and repeatability to allow the experiment to be performed.

Publications

[1] J. R. Schwank, P. E. Dodd, M. R. Shaneyfelt, J. A. Felix, G. L. Hash, V. Ferlet-Cavrois, P. Paillet, J. Baggio, P. Tangyunyong, and E. Blackmore, “Issues for Single-Event Proton Testing of SRAMs,” accepted for publication in *IEEE Trans. Nucl. Sci.*, vol. 51, no. 6, Dec. 2004.

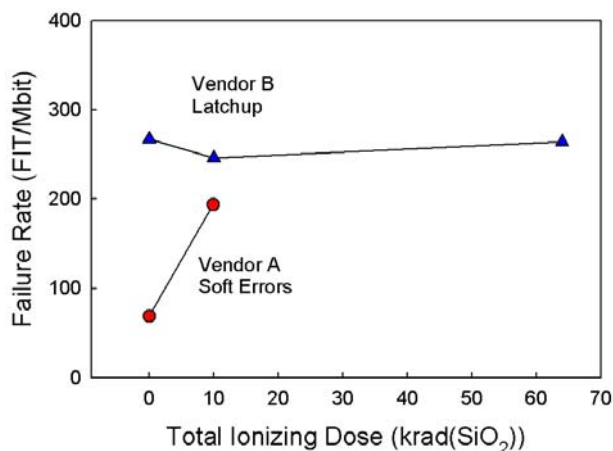


Figure 1. Neutron-induced soft error and latchup rate as a function of dose in commercial 4 Mb SRAMs.

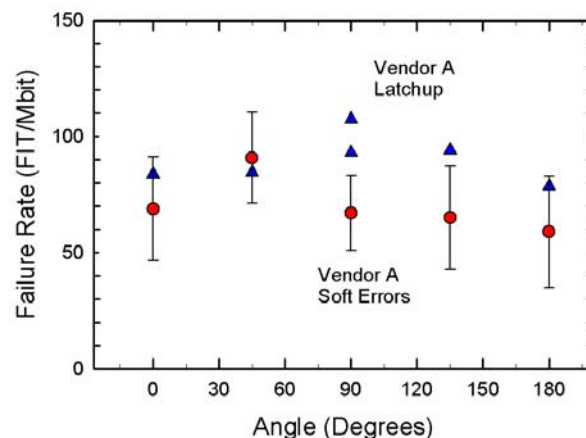


Figure 2. Neutron-induced soft error and latchup rate as a function of irradiation angle in commercial 4 Mb SRAMs.

IMPORTANT! List or attach a list of publications resulting from this experiment (published or in press).

REPORT ON EXPERIMENT
(Please Type)

Submit all experiment reports to:

LANSCe User Office, MS H831, Los Alamos National Laboratory, Los Alamos, NM 87545

Experiment was carried out at: Local Contact Proposal #LANSCe Use Only Manuel Lujan Jr. Neutron Scattering Center S.
Wendler 2003525/584 Report Rc'd x Weapons Neutron Research Facility FP/Instrument Used 7/1/04 WNR/Blue Room FP415R

Title

Feasibility study for a measurement of the neutron-induced deuteron breakup cross section **Authors and Affiliations**

J. L. Matthews, T. Akdogan, W. A. Franklin (MIT)

M. A. Kovash (U. Kentucky)

M. Yuly (Houghton College)

Experiment Report

In the summer of 2003 we set up an array of CsI (proton) and plastic or liquid scintillator (neutron) detectors to carry out a feasibility study for observing non-quasifree neutron-deuteron breakup. The object of the measurement was to observe this process – $d(n, np)n$ – in kinematic regions where large sensitivities to three-nucleon forces have been predicted.

Data taken in autumn 2003 indicated that background events and random coincidences were dominant, making it essentially impossible to extract the small breakup cross section.

An improved setup was implemented in spring 2004, with more extensive shielding and better placement of the detectors. These data are currently being analyzed. **Experiment Report** (continued)

IMPORTANT! List or attach a list of publications resulting from this experiment (published or in press).

Submit all experiment reports to:
 LANSCE User Office, MS H831, Los Alamos National Laboratory, Los Alamos, NM 87545

Experiment was carried out at:		Local Contact	Proposal #	<i>LANSCE Use Only</i>
<input type="checkbox"/>	Manuel Lujan Jr. Neutron Scattering Center	Robert C. Haight	2003532	Report Rc'd
<input checked="" type="checkbox"/>	Weapons Neutron Research Facility	FP/Instrument Used		7/14/04
<input type="checkbox"/>	WNR/Blue Room	4FP15L		

Title
Inclusive (n,xn) Double-Differential Cross Section Measurement (III)

Authors and Affiliations

Kenji Ishibashi, Nobuhiro Shigyo, Satoshi Kunieda, Takehito Watanabe, Department of Applied Quantum Physics and Nuclear Engineering, Kyushu University, Fukuoka, Japan
Robert C. Haight, LANSCE-3, Los Alamos National Laboratory, Los Alamos, NM, USA

Experiment Report

The recoil proton method was tested for measuring the continuous-energy neutron-incident (n, xn) reaction cross section. The flight-path length between the target and each recoil proton detectors was about 50 cm. The detection angles were 15 degrees. Phoswich-type scintillators were used as the recoil proton detectors to discriminate the full-energy deposition events in the scintillator from the partial-energy deposition ones. To subtract the influence from carbon in the radiator, we also made measurement by the use of dummy carbon disks. The sample-target was an iron disk 4 cm thick and 5 cm in diameter. To eliminate the charged particle events coming from the iron target, plastic scintillators were set between the target and the radiators. Since partial energy deposition events might take place by high-energy recoil protons fully-penetrating the phoswich scintillator, they were redundantly checked by a plastic scintillator set behind the phoswich detector. In addition to the charge signal of the scintillators, the flight time data between the accelerator signal and the phoswich detectors were also taken to obtain the incident neutron energy. In order to increase effective detection efficiency of emitted neutron below 100 MeV, we used the NE213 liquid organic scintillators instead of the recoil proton method. The emitted neutron energy was obtained by unfolding the light output data of liquid organic scintillator. The dimension of each liquid organic scintillator was 125 mm thick and 125 mm long. The detection angles were 15, 30, 60, 90, 120 and 150 degrees. The flight path between sample and each scintillator was about 50 cm. We also irradiated the NE213 scintillators with collimated neutron beam directly to get the light output for higher energy neutrons of the scintillators.

The goals of this experiment were as follows:

- To get response functions of the liquid organic scintillators and phoswich detectors.
- To compare the recoil proton method and using the liquid organic scintillator for emitted neutron detection.
- To measure the continuous energy (n, xn) reaction cross sections for the iron and the lead sample.

In a current analysis we found that

Pulse-shape discrimination of the events in the NaI region from ones in the plastic scintillator was clear for the phoswich detectors.

Experiment Report *(continued)*

Event rate by fully-penetrating protons (above 400 MeV) was rather low for the large size detectors.

The energy calibrations of the large size phoswich detectors were difficult, where the standard gamma ray sources such as ^{60}Co or Pu-Be were used.

Pulse-shape discrimination of the neutron and gamma-ray events in the liquid organic scintillators were good.

In preliminary analysis, contribution of elastic scattering is large at the forward direction. It is difficult to distinguish between elastic scattering and reaction components. Fig. 1 shows the double-differential cross sections for an iron sample. The LA150 data underestimate the experimental values at 15 degrees.

Our further analysis will include;

Correction of the detection efficiency of the phoswich detectors for proton incidence.

Subtraction of carbon effects in the polyethylene radiator.

Unfolding the light output of the liquid organic scintillators to obtain the energy of emitted neutron.

Deduction of the (n, xn) cross sections after all correction.

Comparison between the experimental cross section and the calculated values by simulation codes as the preequilibrium (GNASH), the intranuclear-cascade-evaporation (NMTC/JAM, PHITS), and the quantum-molecular-dynamics models (JQMD)

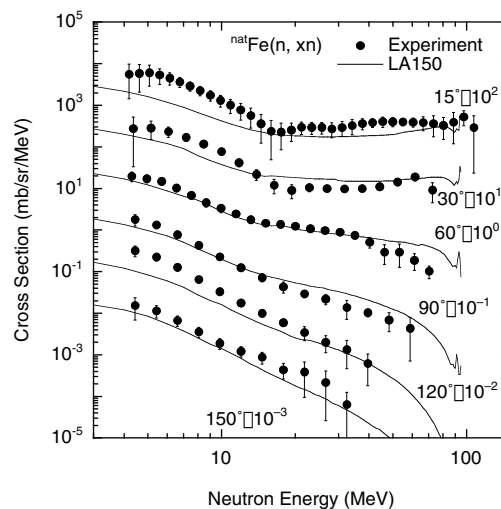


Fig. 1 Neutron-incident neutron-emission double-differential cross sections for an iron sample. The incident energy is 100 MeV. Marks and lines stand for present experimental values and calculation results of LA150, respectively. The experimental data were taken by the liquid organic scintillators.

IMPORTANT! List or attach a list of publications resulting from this experiment (published or in press).

T. Watanabe, et al., Proc. 2nd iTRS Int. Symp. on Radiation Safety and Detection Technology (ISORD-2), *J. Nucl. Sci. Tech.*, Suppl. 4, pp. 34 - 37, (2004).

S. Kunieda, et al., Proc. 2003 Symposium of Nuclear Data, JAERI-Conf. 2004-005, pp. 65 - 70 (2004).

Submit all experiment reports to:
LANSCCE User Office, MS H831, Los Alamos National Laboratory, Los Alamos, NM 87545

Experiment was carried out at:	Local Contact	Proposal #	LANSCCE Use Only
<input type="checkbox"/> Manuel Lujan Jr. Neutron Scattering Center	Bruce Takala	2003534	Report Rc'd 4/1/04
<input checked="" type="checkbox"/> Weapons Neutron Research Facility	FP/Instrument Used		
<input type="checkbox"/> WNR/Blue Room	Target 4, Flight Path 30L		

Title Evaluation of Neutron Accelerated Soft Error Rates of SRAMs with Various Structures
Authors and Affiliations Tatsuya Fujii, Ryosuke Fujio, NEC Electronics America Inc.; Koichi Kumagai, Muneaki Matsushige, Hiroshi Yamamoto, Takashi Yamada, NEC Electronics Corp.; Masami Hane, Yukiya Kawakami, NEC Corp.

Experiment Report 1. Introduction: Neutron-induced single event upset becomes a serious problem for reliability of semiconductor memory devices in deep sub-micron technology due to more number of memory cells per chip and lower supplied voltage. Joint Electron Device Engineering Council (JEDEC) standard, JESD89 recommends WNR as a facility for neutron accelerated tests, especially in its energy spectrum similar to that of the typical New York at sea level. Just in terms of intensity of neutron beam, WNR is outstanding as well. More flux is indispensable to more experiments. In last year's proposal No. 2002543, we obtained soft error rates (SERs) of single- and dual-port static random access memories (SRAMs) of 150nm-technology-node semiconductor. The results showed good agreement with those by our in-house simulator [1]. This year, we used SRAM chips of different technology nodes from 150nm to 90nm processes. We also compared error rates of different SRAM cell structures, such as SOI (silicon on insulator) devices. 2. Goals of experiment: 1) Understanding trend in neutron-induced SER among different technology nodes. 2) Measurement of dependency of SER on various SRAM cell layout and device structure such as deep N well or SOI. 3) Further improvement of in-house soft error simulator's accuracy by correlation with the above experiments. 3. Experimental apparatus: Fig. 1 shows the experimental apparatus for neutron-accelerated tests. Fig. 2 is the photograph of the motherboard and the daughter boards. We used the same general-purpose computers and the main board as last year, and several different daughter boards.

Experiment Report *(continued)***4. Experimental items:**

We evaluated SER's dependence upon the following parameters for various SRAM cell types:

- 1) Retention voltage: Nominal \pm tolerance for normal operation and even lower voltages only for data retention.
- 2) Beam direction: From the front to the back in Fig. 2 (from device's top to bottom), opposite and side.
- 3) Test pattern: Data patterns used in write operation including checkerboard, its complement, all 0, all 1, and so on.
- 4) Process deviation: The samples are also prepared with intentional deviation in process of fabrication.

5. Conclusion:

We got enough data to characterize the error rate of various technology nodes, and dependency on operating conditions. The data indicates some dependency of error rates on technology nodes. We confirmed advanced process technology such as SOI process improves error rate. We have not confirmed meaningful difference in error rate by using deep N well process. Error rate is clearly different depending on beam direction.

We found good correlation between actual measurement and simulation in 130nm and 90nm processes as well as 150nm process of last year.

Future work will be measurement of flip-flop and combinational logic's error rate.

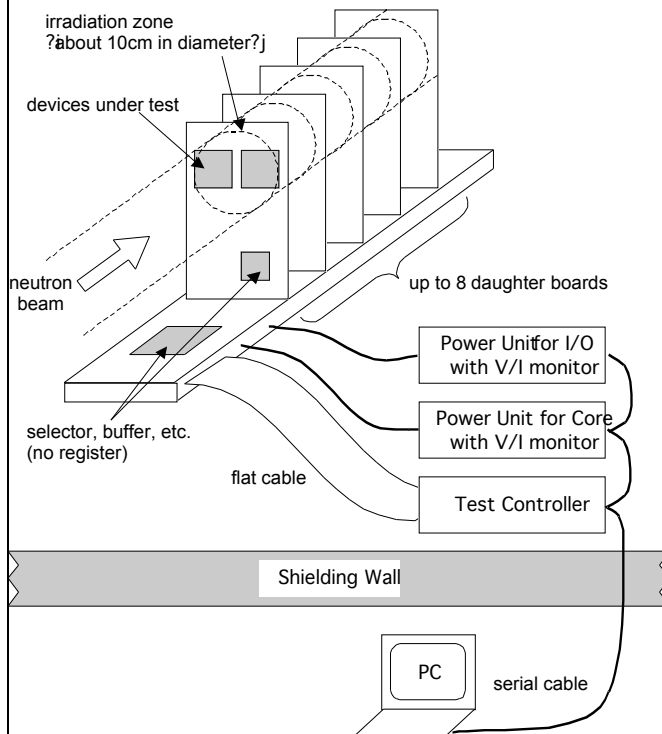


Fig. 1 The experimental apparatus

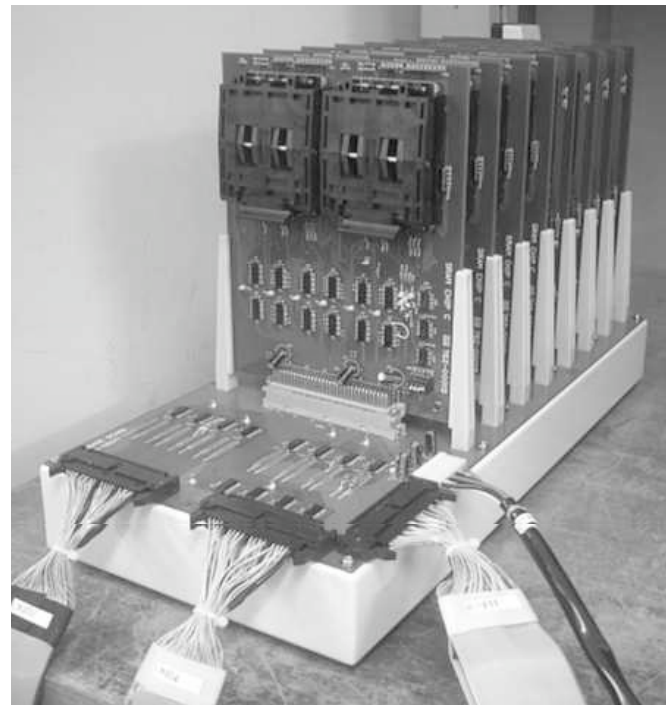


Fig. 2 The mother board and daughter boards

Reference:

- [1] M. Hane, et al., SISPAD (International Conference on Simulation of Semiconductor Processes and Devices) proceedings pp.239-pp.242 (2003)

IMPORTANT! List or attach a list of publications resulting from this experiment (published or in press).

Now under consideration

Los Alamos Laboratories (LANSCE)
Cosmic Ray latch up and Soft Error Rate Test results

2003536

Objective:

The objective of this experiment was to determine the effects of accelerated cosmic ray bombardment at the system level, on Extreme Networks next generation and current generation products. This will help determine an accelerated cosmic ray soft error rate, and cosmic ray latch-up susceptibility. A special evaluation of one SRAM vendor's device (NEC) will include a comparison test of a device where the BPSG layer in the chip has been replaced with a Boron 11 material, as opposed to a Boron 10 material. The Boron 11 material is supposed to improve the neutron soft error rate and cosmic ray latch up susceptibility. Another SRAM vendor with the same type of device (Samsung) was evaluated at the same time to determine a soft error rate and cosmic ray latch up exposure, and an A/B comparison of the two devices. The Netlogic CAM and select ASIC devices will also be tested in the same manner..

Purpose:

The purpose of this test is to evaluate the effects of cosmic ray soft error rates and latch up effects on current and future product lines. The primary focus of the test will be to evaluate CMOS SRAM and ASIC devices, and the effects of cosmic ray events with various vendors. The purpose of this test on next generation product is to evaluate specific vendor performance, the effects of long term system reliability, and calculate accelerated Cosmic Ray Soft Error FIT rate. A special consideration will be given to one vendor that offers a Boron 11 BPSG layer to help combat cosmic ray effect. It is hoped to establish the benefits of this enhancement when comparing the performance to the same device the vendor manufactures with a Boron 10 BPSG material. This information may be used to convince other vendors to establish this process change, or to migrate away from Boron based BPSG layers altogether.

The purpose of this test for current generation products, is to determine what our current cosmic ray exposure might be on two of our most popular product lines. The reason for this is two fold: to establish a current risk assessment, and to establish a base line comparison between current generation and future generation product lines. Data collected from both current and future product lines, will be used to compare against current and future vendor device level cosmic ray test data.

Extreme Network's current concern on cosmic ray exposure has been developed from various white papers on the subject, and discussions with SRAM vendors Micron, Sony, Samsung, and NEC that have or will be performing cosmic ray testing at Los Alamos Labs. Some of the presented material was from a presentation given at the 2001 International Reliability Physics Symposium by Robert Baumann. Supporting evidence gathered from mainframe industry field data for soft error rates, also shows a correlation of soft error rates and the effects of altitudes on RAM devices. LANL staff personnel have also recommended this testing, to determine the effects of these phenomena on Extreme Networks equipment used at LANL.

Section I-Test Setup

The test setup and procedure will follow the guidelines of JEDEC specification JESD89 for Cosmic Ray-Induced Soft Error testing. Since the QDR device can not be voltage margined at the system level due to internal voltage regulators, section 5.4.2.2 of JESD89 will be performed at nominal voltage. The physical orientation of all units and devices are listed below:

Section I-Test Setup cont.

- All CPU and I/O blades were positioned vertically in the chassis/test fixture so the neutron beam strikes at a 90 degree angle in reference to device under test. (DUT) The area under test was fit within the 8.5 cm Neutron beam. The systems were positioned about 2 meters from beam source.
- An adjustable table provided by the LANSCE ICE house allowed the chassis/test fixture to be positioned to strike various ASIC/QDR/CAM/SRAM locations on the CPU and I/O blades.
- Initial test setup information (beam flux, beam fluence, incidence angle, exposure time, ect...) were collected from Netlogic and NEC from their experiments at LANL. These parameters were considered for our test setup.
- Board level device placement was as uniform as possible to facilitate an A/B comparison of test results.

Section II- Test process:

Objective:

The JEDEC Cosmic Ray test specification JESD89 gives general guidelines on how to perform the tests, but it is up to the test personnel in general to achieve the desired results. Methodologies vary widely from vendor-to-vendor, but various QDR vendor input was considered for this test. The basic direction of the test process was to achieve an upset rate of around a 50 to 100 errors per device for a given time. This amount of time this takes will be considered a “test cycle” for a given DUT. This was performed several times in order to record a baseline for a device. The basic test flow included the following order of events:

- 1) Setup and check out the system and device under test. This included the following steps:
 - a) Setup system, power on and boot Manufacturing diagnostics.
 - b) Do initial voltage checks on system with a DVM and record power plane values.
 - c) Perform an initial diagnostic test to insure hardware functionality and to check for any stray “location effects” of the site.
- 2) Initial neutron beam setup and test check using a baseline DUT. This was mostly to establish what initial neutron flux (beam energy) and beam fluence (beam density) will achieve the desired 100 upsets for a given device. The test was repeated 3 to 5 times to get test cycle results for 50 errors in each test cycle. Cycle results were summed to get the 100 upset goal.
- 3) Performed initial tests for DUTs outlined in Section-I above. Other devices were tested in the same manner noted in #2 above, for 3 to 5 test cycles each. Most of this testing was performed using a modified version of BIST tests running under Manufacturing code. This test loops indefinitely and record errors against a given QDR interface. This test also recorded error information, and start/finish times of the 100 error goal.
- 4) Some test consideration was given to various ASICs and CAMs using the same method in #2 and #3 above. Steps 2 and 3 were also repeated aiming the beam from the back side of the QDR device as recommended by NEC. NEC noted that a different soft error rate was obtained when aiming the beam at the bottom of the QDR package.

Section II- Test process con't:

- 5) An attempt was made to enable ECC correction on the IKE ASIC during packet memory tests to see if there is any adverse affect on the SER rate for the IKE ECC circuits. Test method was the same as outlined in #2 and #3 above.
- 6) BIST and register tests were run on various ASIC devices to see if they are affected by cosmic ray soft error testing and latch-up.

Data Collection and Final Test:

- 1) Data was recorded for the various devices during the test. Parameters like the beam neutron count, beam energy, exposure time, error count, and chip location were recorded. This data will be used to calculate a Soft Error FIT rate for the various devices.
- 2) A final device level check was performed using the Huron QDR/ASIC group. This was done as a baseline consistency check, and to verify that the device has not experienced any “total dose” effect from the neutron bombardment. This is similar to a device saturation effect.
- 3) Data was collected and analyzed to determine a soft error FIT rate. The results were checked to see if the Boron 11 in the NEC QDR provides any significant improvement in SER protection. An A/B comparison of results between the Samsung and NEC QDR's may not be significant, due to the small Samsung population of QDR. We could not test the 512KX36 18M QDR part, because of the vendor design issues. Bit position failures will be evaluated for any relationships and correlation's between locations on devices. This may indicate areas of concern on the chip for SER susceptibility.

Data analysis and SER FIT rates:

The data was analyzed and Soft Error FIT rates were calculated. The preliminary results are listed below by vendor. NEC has provided us with a simulation result of 400 FITs per megabyte.

Cartman ASIC QDR group:	Upper QDR	Lower QDR
NEC Boron 11 based QDR SRAM	= 127.65 FIT/Mb	121.01 FIT/Mb
NEC Boron 10 based QDR SRAM	= 142.16 FIT/Mb	160.78 FIT/Mb
Samsung (unrefined) QDR SRAM	= 129.32 FITM/b	132.56 FIT/Mb

IKE Packet Memory QDR group:

NEC Boron 11 based QDR SRAM	= 355.76 FIT/Mb
NEC Boron 10 based QDR SRAM	= 458.07 FIT/Mb
NEC QDR Simulation of FIT rates	= 400.00 FIT/Mb

NOTE: results are in FIT per megabit of memory.

Data Collection observations:

NEC

- The NEC Boron 10 based part had a very bad habit of developing hard-like bit errors when exposed to the beam. This happened on almost every ASIC group that was tested. They were usually bit failures that behaved like stuck-at faults. The errors would usually go away when the beam was removed, but two chips turned into hard fails that would not go away- even with a power cycle. We will review these failures with NEC after the board has been re-tested back here at Extreme.
- The NEC Boron 11 QDR ram held up better than the Samsung QDR, or the NEC Boron 10 QDR ram, but only 4 were tested. (about 18% better FIT in NEC Cartman QDR, 23% better FIT in NEC IKE packet memory QDR) No evidence of stuck-at faults in the diag captures for the B11 part.
- NEC stated that they noticed the SER rate is higher when the neutron beam strikes the bottom of the device. That effect was not noticed when testing in a clamshell group in 4 locations. Initial observations of focusing the beam on the backside of the QDR for the IKE packet memory rams, shows no evidence of this effect.

Samsung

- The Samsung QDR had just slightly less performance than the NEC Boron 11. Only two could be tested though. (NEC Boron 11 was about 5% better)
- There was slight evidence of “bit dependence” in some of the Samsung captures. This means the same bit would be affected for a few locations for a few different addresses. Not sure if this is a multibit strike limited to one data pin or array structure. The affect was minimal and random in most cases.

General QDR observations:

Almost all bit failures seen in Cartman QDR testing occur when the rams are written with all 1's This is apparent across both QDR vendors, and it did not matter if I used Cartman 8 or 6. The only other time different patterns would fail is when the NEC QDR with Boron 10 developed hard fails. The IKE QDR failures are all random patterns, and I did not see evidence of any fault trending.

- An attempt was made to run the Kenny CPU based packet memory loopback tests with ECC turned on. This board already had a multibit failure on Ike 2. I ran it for a few minutes with the neutron beam on, and looked at the data mismatches. I only saw the known ram corruption show up in the mismatch data. The IKE ASIC held up well in all the BIST memory tests. No multi-bit errors on QDRs noted.

Netlogic CAM observations:

- The Netlogic CAM could not be properly SER tested with our diagnostics. We need to turn the parity scan logic off to test the core array for single bits. The parity logic errors were overriding the diagnostics capability to check core array memory. There needs to be a diag switch to turn off parity scan during memory testing.

ASIC / CPU observations:

- The ASICs held up very well in this test. This was a major area of concern in the mainframe/server industry- even more than the SRAMs, because soft-LSI strikes could cause a CPU to hang, or the system to crash. I ran well over 10,000 passes of register tests to various IKE and Kenny ASICs with no failures. I also ran internal BIST memory tests to the Kenny ASIC for over 15 minutes with no failures noted. I tried every BIST test I could run on the various ASICs, and had no problems.
- The CPU sub-system on the Huron board was also exposed to this neutron beam. In one case, the beam was close enough that the CPU was mostly in its path. No unusual behavior or failures were noted. I was impressed after hearing talk from the scientist, how some vendors test boards will not even work in this beam.

Data Collection issues:

There were several issues encountered that affected the outcome of the tests. Usable test results were still obtained, but some of these issues should be considered for any future test planning:

- The Los Alamos site experienced a massive power outage just before we started tests. This pushed the start time out a day, and the beam was unstable for the first few test shifts. The beam instability is reflected in the first two shifts of test results.
- The Boron 10 rams were getting hard-like bit failures described in the observation section that made it very hard to get even 50 hit count samples on other devices. This could be fixed in diag code to disable the QDR interface, but not onsite.
- The Mariner I/O blade had the management port fail due to cable side force on the connector. All testing was accomplished on the Huron CPU blade.
- The most consistent test results came from the Cartman clamshell QDR tests. This test did not have chip location decoding in the diag tests, so I had to manually decode almost 900 upsets. We need to add this capability to any diag used for LANL SER testing, since it took almost a week to manually decode all upsets. The IKE QDR tests were perfectly modified for data collection.
- CAM tests would not work correctly when the CAM was exposed to the neutron beam. The background parity error logic gets checked in the diagnostics, and the errors misrepresent the actual count of upsets. This needs a switch in the code to disable parity logic during tests.
- The Wendy init problem kept showing up on power on. Unplugging the system was the only way to boot it behind the shield wall. I believe this is fixed now.
- We only had small population of Samsung rams to check out due to the 512KX36 part design issue and population.

Submit all experiment reports to:

LANSCCE User Office, MS H831, Los Alamos National Laboratory, Los Alamos, NM 87545

Experiment was carried out at:		Local Contact	Proposal #	<i>LANSCE Use Only</i>
<input type="checkbox"/>	Manuel Lujan Jr. Neutron Scattering Center	B. Takala	2003546	Report Rc'd <div style="border: 1px solid black; padding: 5px; text-align: center;">6/15/04</div>
<input checked="" type="checkbox"/>	Weapons Neutron Research Facility	FP/Instrument Used		
<input type="checkbox"/>	WNR/Blue Room	ICE House		

Title

Neutron Particle Effects on Flight Critical Systems

Authors and Affiliations

Celeste M. Belcastro, Ph.D., Kenneth Eure, Ph.D., Daniel Koppen, NASA Langley Research Center

Richard Hess, Honeywell International Inc.

Boyd Hill, Vigyan Inc.

Edward Hogge, Lockheed Martin

Steven Gray, Ph.D., Oscar Gonzalez, Ph.D., Linda Vahala, Ph.D., Old Dominion University

Experiment Report

Most Single Event Upset (SEU) studies performed to date have focused on specific integrated circuits but not on electronic systems. It is known, however, that SEU phenomena have affected the operation of aircraft electronic systems. NASA, Honeywell, and Old Dominion University, in collaboration with LANSCE and the FAA, are conducting research to investigate neutron particle effects on flight critical aircraft systems. The objectives of this research are to: (1) investigate the effects of SEU on closed-loop flight-control systems, (2) develop SEU closed-loop system test methods and capability, (3) develop design and analysis methods to mitigate and assess SEU closed-loop system effects, and (4) investigate the applicability of recoverable computing techniques to mitigate SEU effects. The expected benefit of this research will be the development of design and validation guidelines for the cost effective achievement of aircraft system performance in the atmospheric neutron environment that provides the degree of safety needed for critical aircraft functions.

The purpose of this experiment was to analyze the effects of neutron bombardment on avionics control systems operating at altitudes where single event effect rates on electronics are on the order of 100 to 1000 times greater than at sea level. The high intensity beam at LANSCE provides accelerated life tests that are representative of the actual neutron radiation that a Flight Control Computer (FCC) receives over a period of years. The specific FCC employed was a single-channel Recoverable FCC that was designed for robustness to transient disturbances. This computer uses a new approach to achieve fault tolerance called "rapid recovery". It uses a dual-lock-step processing architecture developed for the Aircraft Information Management System on the Boeing 777 airplane. The dual-lock-step computing platform monitors each processor and its memory on every CPU clock cycle to ensure lock-step operation of the processors.



Figure 1 *Recoverable FCC in neutron beam*

The FCC was placed in the neutron beam (see Figure 1) to form a closed-loop control system with a B737 simulation located outside the beam area. In this experiment, the Recoverable FCC executed B737 aileron and elevator control laws that closed the loop on a computer simulation of a B737 aircraft in level flight at 34,000 feet with the option of applying wind gusts. Real-time monitoring of the control commands was implemented and executed during exposure. Data was collected for each 50 ms calculation frame. Twelve beam alignment positions on the Recoverable FCC were selected to target specific regions within the FCC. The electronic targets included the CPU's, RAM, instruction memory, and scratchpad memory.

Experiment Report (continued)

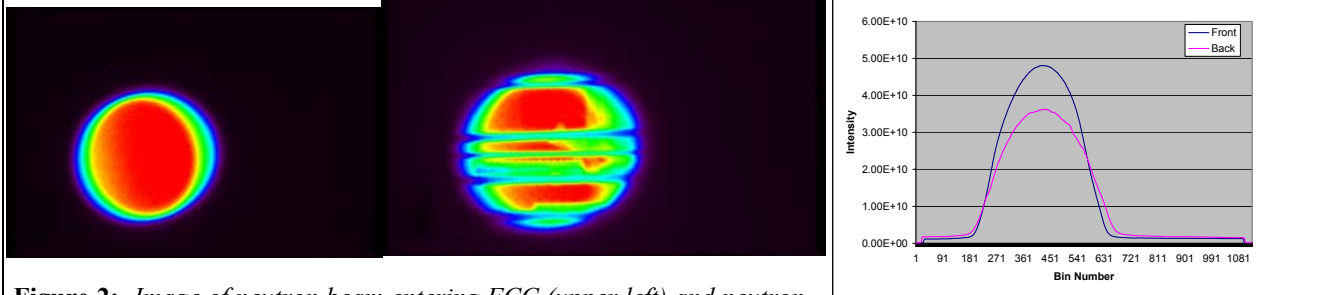


Figure 2: Image of neutron beam entering FCC (upper left) and neutron beam exiting FCC (upper center). Horizontal neutron beam profile (upper right). Vertical neutron beam profile (lower left).

Figure 2 shows neutron beam profiles before entering and after exiting the FCC for one of the targets denoted T2. The dips in the vertical distribution plot correspond to the horizontal lines in the beam profile after exiting the FCC. These result from neutron beam attenuation where the FCC boards are present. This particular targeting arrangement was centered on one of the CPUs.

Approximately 100 exposure runs were completed, exposing the FCC for about 56 hours. For most target positions there were recoverable fault events and occasionally an unrecoverable fault. For the unrecoverable faults, power was disconnected from the FCC and the system was restarted. Figure 3 shows some of the input-output signals being monitored for SEU effects. The upper left plot in Figure 3 shows 31 recoveries of the FCC before an unrecoverable SEU occurred, thus stopping this particular run. The center left figure shows recovery delay. The lower left figure shows supply voltages. The upper right figure shows neutron flux (blue) and the aircraft altitude in feet (green). The center right figure shows aircraft pitch and yaw. The lower right figure shows the aileron and elevator control commands. Part of the post experiment analysis is to characterize the SEU's, determine which electronic subsystem failed, and characterize closed-loop effects on aircraft performance. As can be seen from Figure 3, the FCC stopped communicating due to an unrecoverable event after completing approximately 75% of the 60 minute run.

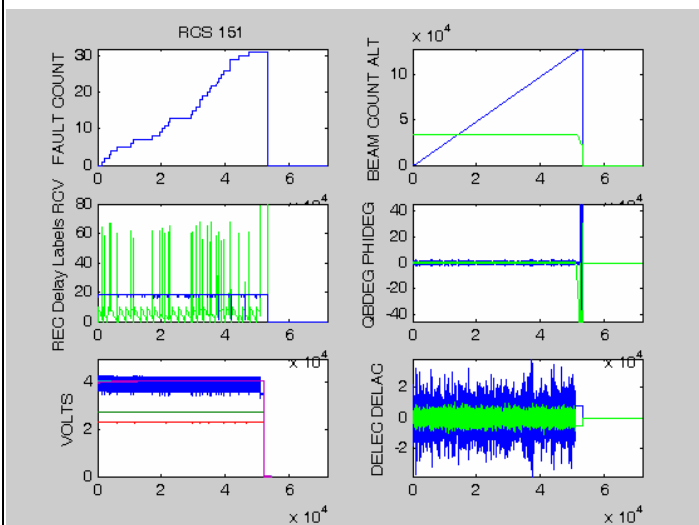


Figure 3 Input/Output signals of FCC

In summary, the rollback recovery mechanism was triggered during many runs where the FCC was exposed to the neutron beam. The rollback recovery technique appears to offer some robustness in the neutron particle environment. The data is currently being analyzed. The data from this experiment is also being used to validate theoretical models which predict the stability and performance characteristics of a closed-loop system with a recoverable controller. These models will help to demonstrate the effectiveness of this type of fault tolerance technique for SEU's.

IMPORTANT! List or attach a list of publications resulting from this experiment (published or in press).

Closed-Loop Neutron Particle Effects Testing on Flight Control Computers, Celeste M. Belcastro, Ph.D., Kenneth Eure, Ph.D., Richard Hess.

REPORT ON EXPERIMENT (Please Type)

Submit all experiment reports to:

LANSCCE User Office, MS H831, Los Alamos National Laboratory, Los Alamos, NM 87545

Experiment was carried out at: Local Contact Proposal #LANSCCE Use Only Manuel Lujan Jr. Neutron Scattering Center Bruce
Takala 2003547 Report Rc'd Weapons Neutron Research Facility FP/Instrument Used 6/8/04 WNR/Blue Room 4FP30L
Title

Experiments on the Effects of High Energy Neutrons on Processor Authors and Affiliations

Thane M. Larson - Hewlett-Packard

Experiment Report

With the evolution of the computer market, the large variety of processor families and types are consolidating into a few with the Intel Itanium family emerging as one of the most promising 64-bit capable processors. As HP and other vendors move away from proprietary architectures, the characterization of failures induced by secondary cosmic ray neutron flux needs to be compared between the Itanium family and the architecture that they will replace.

HP currently manufactures two families of servers, one based on the Itanium 2 processor, and the other on its proprietary PA-RISC architecture. Besides having fundamental logical and architectural differences, the Itanium and PA-RISC processors are manufactured by completely different processes. Consequentially, it is expected that the susceptibility to high-energy neutron flux will be drastically different.

There are three cases of neutron-induced bit flips that can be analyzed: detectable and recoverable, detectable and non-recoverable, and undetectable and non-recoverable. Thus, it is impossible to characterize every neutron-induced error down to the individual bit that flipped.

We tested both Itanium (rx26xx family) and PA-RISC (rp24xx) family. In addition, we performed two type of tests, the first a system level test and the second an intrusive firmware based test. Only the processors were examined for errors. Experiment Report (continued)

1) SYSTEM LEVEL TESTS

For these tests, each system used unmodified firmware and ran a low-level operating system with a proprietary HP system exerciser. These tests reflected the "normal" behavior of a system. The neutron flux was turned off during the boot to the OS/exerciser since the failures accumulate faster than the boot cycle of the computers. The time to event or crash was recorded by an external system. In some cases a register (PIM or MCA) dump of the crash was used for further analysis. The external system additionally spooled all console output to a log file (with a timestamp) to correlate the events to the neutron counts from failures.

Statistically, the different configurations were to be compared. However, upon test we found that the exerciser for the Itanium systems did not handle the multitude of errors accumulated in a typical cycle. However, the PA-RISC exerciser did, so we only have meaningful data for the PA-RISC machines. Further Itanium testing would be needed in the future to directly correlate to PA. The majority of events were single-bit in nature and occurred in the cache structures as anticipated. Normal auto-correction

routines would give adequate protection for the naturally occurring practical situation. Even so, without correction routines, the SYSTEM LEVEL TESTS show that the average time to an event that the customer would be aware of was dramatically longer than the lifetime of the system.

2) MODIFIED DIRECTED FIRMWARE

The SYSTEM LEVEL TESTS have the benefit of accurately representing the failure rates as would be seen under normal operating circumstances. However, since they do not exhaustively nor deterministically use the entire processor, there are neutron induced events that get discarded and are never seen by an application nor the customer. Thus we also used MODIFIED DIRECTED FIRMWARE to look at all processor structures looking for the latent events. As expected, these tests revealed more bit sites that were flipped in logic states than the SYSTEM LEVEL TESTS did.

For these tests, events came on the order of several / second due to the high neutron flux density of the beam. Such a high event rate created an excellent opportunity to flood the error recovery mechanisms of the processors to see how they perform under that extreme duress. As such, we validated theory on the relativistic differences between the processors and confirmed that the size of the caches was the primary contributor to the event rates. Like the SYSTEM LEVEL TESTS, console data was spooled to an external system. Unlike the SYSTEM LEVEL TESTS, a reboot was not always necessary so that more statistical data could be recorded in the same amounts of time.

Notes on WNR Facilities

We would like to do further comparisons of new processor structures to validate theoretical results. In addition, we suggest that we provide our monitoring station with a PCI card capable of monitoring the output of the pulse counter provided by WNR. We had to do this manually and it would have been better to do it automatically. Lastly, we had less than 50% beam uptime due to issues at WNR. Otherwise the facilities were excellent.**IMPORTANT!** List or attach a list of publications resulting from this experiment (published or in press).

NA

Submit all experiment reports to:
 LANSCE User Office, MS H831, Los Alamos National Laboratory, Los Alamos, NM 87545

Experiment was carried out at:		Local Contact	Proposal #	<i>LANSCE Use Only</i>
<input type="checkbox"/>	Manuel Lujan Jr. Neutron Scattering Center	Bruce Takala	2003549	Report Rc'd
<input checked="" type="checkbox"/>	Weapons Neutron Research Facility	FP/Instrument Used		
<input type="checkbox"/>	WNR/Blue Room	4FP30L		
				6/1/04

Title
Neutron-Induced Soft Errors in SRAM and Logic LSI

Authors and Affiliations

Hajime Kobayashi, Hiroki Usui, Akira Oyama, Hiroo Shoji ; Sony Corporation
Jun Kase ; Sony Semiconductor Company of America

Experiment Report

Soft errors of memory devices are becoming serious problem with downsizing of LSI. High energy neutron is the main cause of LSI soft error at present, because BPSG layer, which induces thermal neutron soft error, is no longer used [1]. As we described in the previous report (experiment report #2002513), we confirmed that the high energy neutron induced SER increases with downsizing of SRAM. Therefore, we tested the newest SRAM manufactured in 90 nm process this time. Recently, it was pointed out that the soft error in logic LSI could become more serious than memory devices with ECC [2]. Since enormous number of logic LSI are going to be related each other in the broadband network near future, SER in logic LSI will be a crucial problem that might cause fatal crush of network system. Therefore, we also measured SER of some simple logic LSI devices manufactured in 90 nm process.

The goals of the experiments were to:

- Evaluate the relationship between SER and process rules.
- Obtain the dependence on Vdd.
- Evaluate multi-bit error rate.
- Measure latch-up rate of 90nm devices.

The experiment was a success.

- Relationship between SER and process rule was obtained. As we concerned, SER/device increased with downsizing of devices.
- Vdd dependence was obtained. It is useful to estimate SER of future devices.

Experiment Report *(continued)*

- Multi-bit error rate was obtained. Adjacent cells upset with some probability. However, since physically adjacent cells are not in the same word, the probability of the multi-bit event was very small. It means that a simple ECC is effective to reduce SER even induced by high energy neutrons.
- No latch-up was observed at all in any devices.
- Reproducibility of the experiment was excellent thanks to the stable beam quality.

Acknowledgement

We would like to thank B. Takala, S. Wender and A. Bridge for their kind support.

References

- [1] H. Kobayashi et al, IEDM Tech. Dig. 13-3, p.337-340 (2002)
- [2] R. C. Baumann, IEDM Tech. Dig. 13-1, p.329-332 (2002)

IMPORTANT! List or attach a list of publications resulting from this experiment (published or in press).

Internal Test Report

Neutron Induced Soft Error Sensitivity Characterization

of the

Xilinx, Inc.

Spartan-3[™],
Virtex-II Pro[™] and Virtex-II[™]
Product Families

of

Field Programmable Gate Arrays (FPGA)

prepared
November 2003
Updated: May 2004

Executive Summary

Samples of **Spartan-3™** (90 nM), **Virtex-II Pro™** (130 nM), **Virtex-II™** (150 nM) FPGAs were tested for sensitivity to neutron induced upset. Neutrons exist in the atmosphere as the residue of cosmic ray showers which originate in deep space interacting with the upper atmosphere. As the atmosphere increases in density down toward sea level, nearly all cosmic rays are absorbed. However, there remains a spectrum of energetic neutrons present at all altitudes due to the nuclear reactions between these cosmic rays and the oxygen and nitrogen atoms in the air. While these neutrons have not been shown to be unsafe for humans, they do interact with matter as governed by the laws of physics. In silicon, they are able to generate charge (by elastic and inelastic collisions and the resultant scattering of atoms). The charge thus generated in silicon may be able to interfere with the operation of a semiconductor device. As technology has advanced, as feature sizes have continued to shrink and as the operating voltage has been necessarily reduced, the amount of charge that is stored in specific nodes in the circuitry has continued to decline, to the point where the charge generated by terrestrial neutron interactions with the silicon lattice may be sufficient to cause soft errors, referred to as Neutron induced Single Event Upset (NSEU). In a static-latch based FPGA these upsets could potentially interfere with device operation..

The objectives of this study were two fold. First, they included the determination of whether the Spartan-3, Virtex-II Pro and Virtex-II technologies could be upset by terrestrial neutrons and, if so, to measure the comparative sensitivity of these 90, 130 and 150 nM (respectively) feature size technologies to the results of similar measurements previously made on some of these and earlier technologies of 220 nM and greater feature sizes. Second, this study was intended to develop a calibration method for the accelerated testing methodologies utilized by comparing the results with actual applications testing (Rosetta Test) of these devices and to evaluate and chose the proper acceleration factors and models to apply to the results of accelerated testing to predict the real world effects of atmospheric neutrons on these devices.

A test capability was developed in-house at Xilinx to be able to remotely write a configuration bitstream to a device and then to read it back after irradiation in order to count the number of bits in a device that may have changed. Readback of the configuration data is a unique facility that has been built into all Xilinx FPGAs. Special software (FIVIT™) was developed to parse the resulting data files into specific categories. Finally, an application test (Rosetta) was developed to calibrate the accelerated neutron sources used to evaluate these devices against real world performance of the devices in a simulated application. Samples of the X3S1000 (Spartan-3 at 90 nM), the 2VP4 and 2VP7 (Virtex-II Pro at 130 nM) and the XC2V6000 (Virtex-II at 150 nM) were used for this evaluation. Accelerated testing was conducted at the high-energy Neutron Testing Facility at the Los Alamos Neutron Science Center (LANSCE). Application testing of the XC2V6000 was conducted in San Jose (sea level), in Albuquerque (5200 feet), at the White Mountain Research Facility (12,250 feet) in California and on Mauna Kea (13,500 feet)

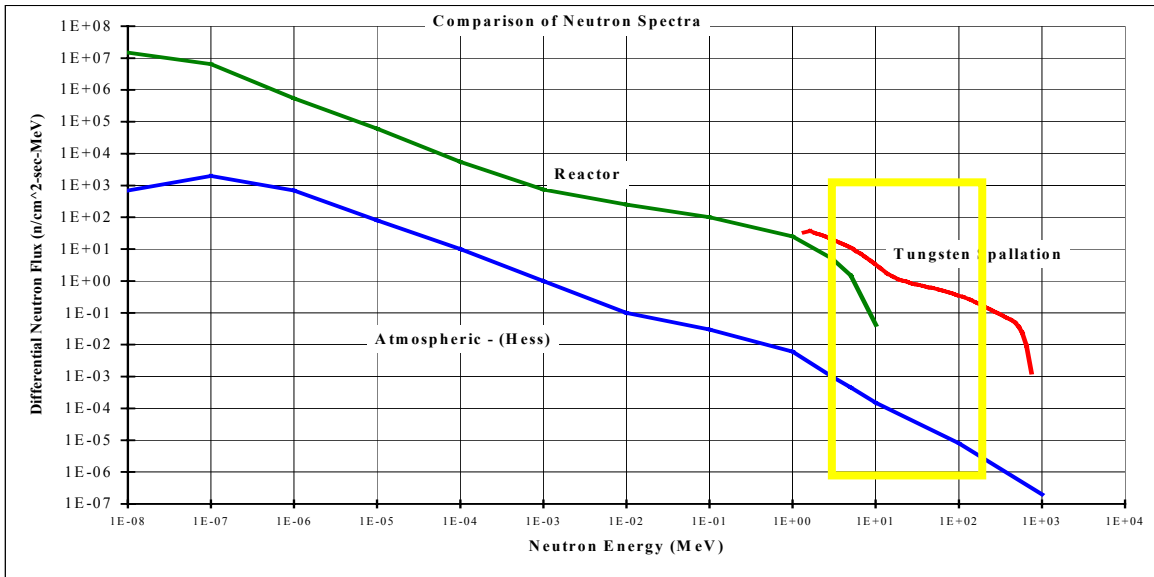
The results clearly showed that the effects of atmospheric neutrons on these technologies have often been over-stated by the inappropriate application of commercial SRAM upset data, and quantified the expected logic upset rates in actual simulated applications. Additionally the results confirmed the complete absence of any indication of neutron induced latch-up in all three device families.

This work has benefited from the use of the Los Alamos Neutron Science Center at the Los Alamos National Laboratory. This facility is funded by the US Department of Energy under Contract W-7405-ENG-36.

Accelerated Testing

The best resource currently available to simulate atmospheric neutrons is the high-energy Neutron Testing Facility at the Los Alamos Neutron Science Center (LANSCE). At LANSCE, high-energy neutrons are produced by spallation. A linear accelerator produces an 800-MeV pulsed proton beam that strikes a water cooled tungsten target. The impact produces a spectrum of neutrons whose energy distribution and intensity is precisely measured. The spectrum has energies in the range of 1 MeV up to approximately 600 MeV and is very similar in shape to the atmospheric (Hess) spectrum. A neutron flight path with a station (ICE House) at 20 meters from the neutron production target has been designed for accelerated neutron testing of semiconductor devices. The flight path consists of a small building for the irradiation which also encloses the testing equipment, isolated from the beam by a substantial concrete barrier. The devices to be tested are placed in the neutron beam line (in air) in the irradiation building. The experimenters control the neutron beam by opening and closing a shutter external to the irradiation building, and the number of neutrons on the sample is continuously monitored and recorded.

The integrated neutron flux (energies above 1 MeV) for the LANSCE beam is approximately 10^6 n/cm² with a beam spot size of approximately 10 cm. Uniformity across the beam is better than 5%. Since it was expected that between 10^{10} n/cm² and 10^{11} n/cm² would be required to provide a statistically significant number of upsets, long beam run times of 1 hour or more were usually needed for each data point.



The test configurations used often allowed several parts to be tested during each run. This is important in order to maximize the amount of data that could be collected in the long runs required for these tests. Because high-energy neutrons penetrate most materials easily, it was not necessary to decap the parts for exposure. We used an internal test system and software tool that utilized the JTAG test capability of the Spartan-3, Virtex-II Pro and Virtex-II architectures. Each device can be individually tested via the JTAG port. For the Virtex-II test we also utilized two additional parts that were not in the beam as controls. The Virtex-II test set-up was

an adaptation of the Rosetta fixture that normally required 10 samples on each board to complete the JTAG scan. On each of two PC boards, 2 devices would “stand-up” in the beam line while the third part was well outside the beam penumbra. The seven sockets on each board between the two parts under test and the single control at the end of the board were jumpered. For Spartan-3 and for Virtex-II Pro commercial performance boards, available from Xilinx, were used for the test. Each board was driven by a laptop PC in the control area over a 40-foot communications cable. The power supplies were also remotely located in the control room, with remote sense lines used to avoid voltage drops at the parts should high currents flow. The supplies were current limited to detect any possible latch. A set of voltage monitoring wires was used to make sure that the desired voltage levels were applied at each part. The test boards are shown below in Figures 1,2 and 3.

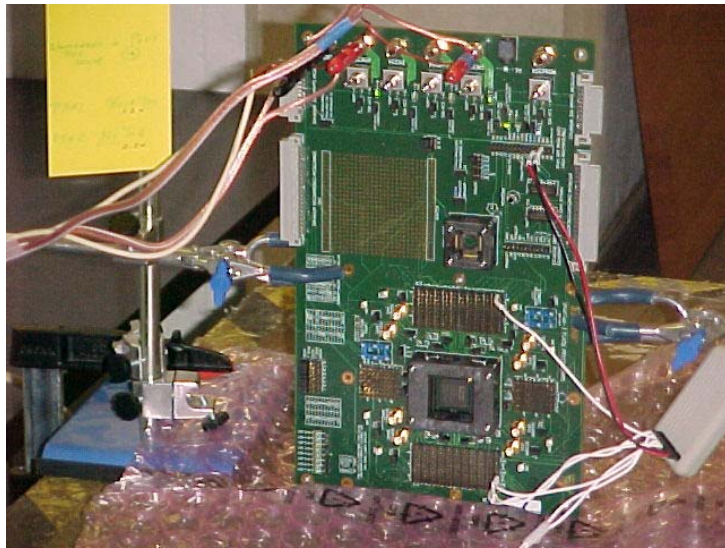


Figure 1
Spartan 3 Test Fixture

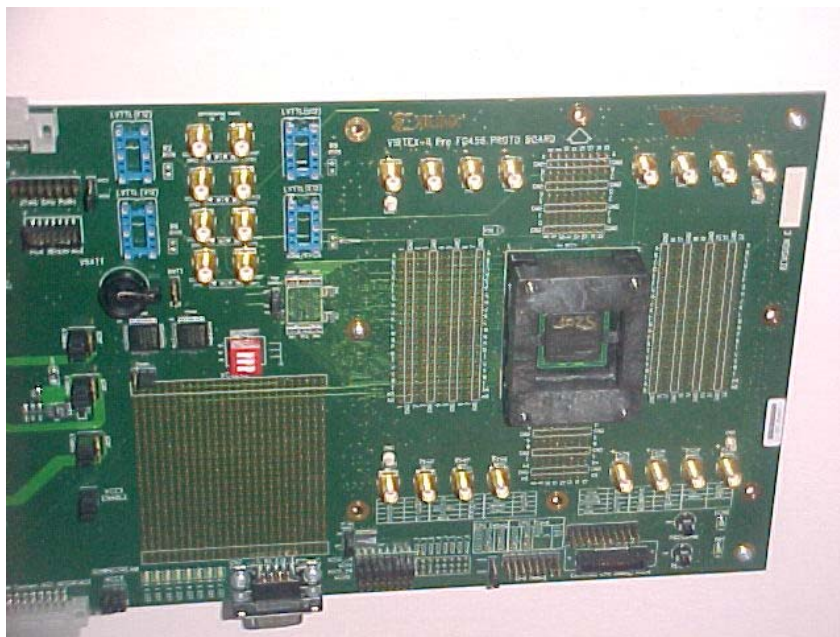


Figure 2
Virtex II-Pro Test Fixture

Figure 3
Virtex II Test Fixture

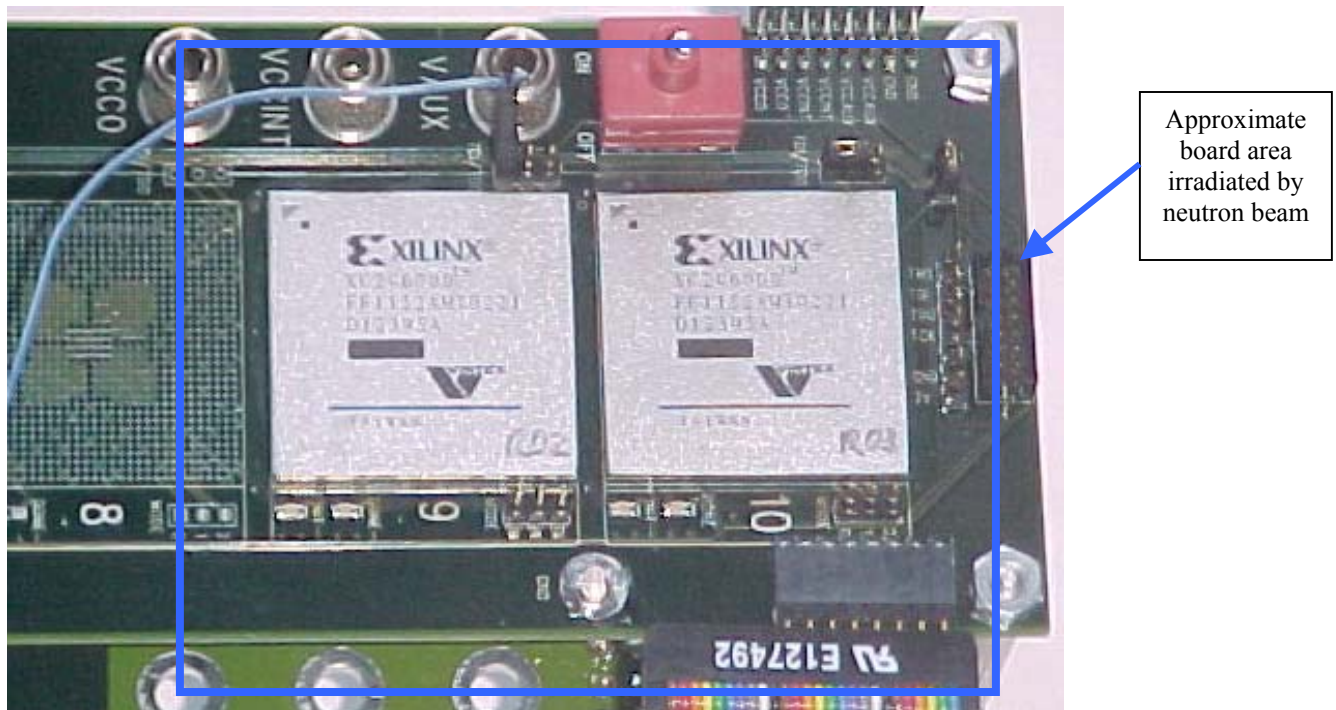
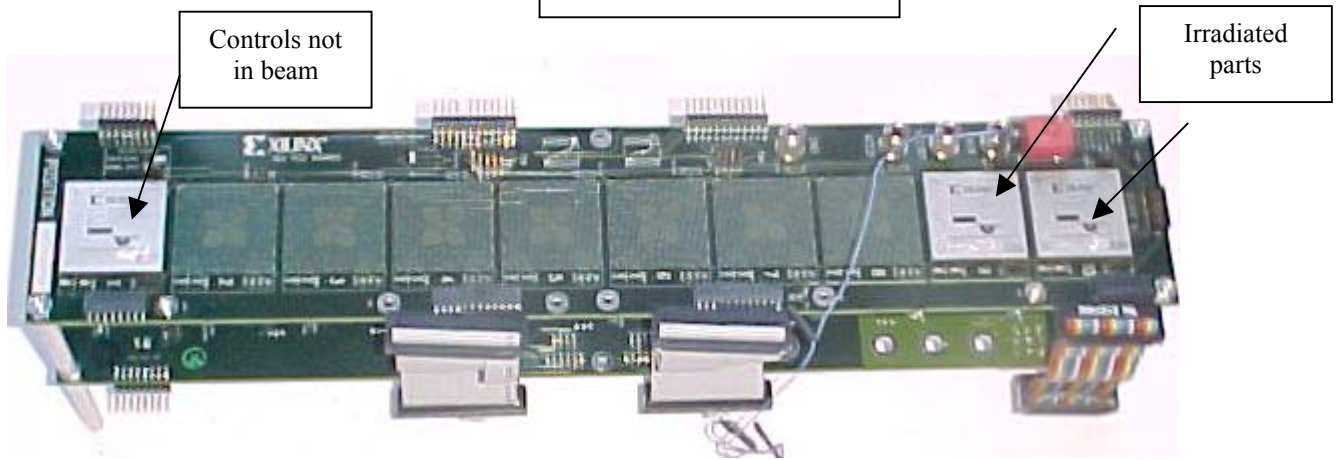


Figure 4. A close view of two of the four 2V6000s exposed to the neutron beam.

Many of these technologies had been previously tested in proton, neutron and/or heavy ion test environments, and both static and dynamic testing had been carried out to consider the issues of static mode vs. dynamic mode upset. Details of this testing have been published elsewhere and some of these publications can be

found on the Xilinx web site at “Xilinx.com”. Accordingly, the accelerated NSEU testing at LANSCE measured only the static mode upset sensitivity due to high-energy neutrons. Through the JTAG port of each device, the configuration bit stream was written and read. Test software (FIVIT) was developed that would write to the configuration bit stream of each part and parse the readback results. Because an arbitrary pattern could result in contention or violation of illegal conditions in an FPGA, previously documented patterns were selected for the static test. The test algorithm was implemented as follows:

1. Select the device to be programmed
2. Write configuration bit stream with the data pattern
3. Verify correct configuration with read back
4. Repeat for all samples
5. Pause while the neutron beam is applied (could be up to hours)
6. Verify post radiation configuration with readback
7. Compare data before and after radiation.
8. Record bit upsets including frame and location data
9. Reprogram to the original pattern to assure no stuck-bits
10. Run test long enough to accumulate up to 100 bit upsets per part for statistical validity.

Initial testing was done at room temperature and nominal power supply as appropriate. In the specific case of Virtex-II, the core voltage was varied from above the max operating voltage of the array (1.60 volts versus a maximum specification of 1.575 volts) to a voltage well below the minimum specification voltage of the array (1.20 volts versus a minimum specification of 1.425 volts) to investigate the robustness of the configuration latches. The test samples used included the XC3S1000, the XC2VP4, the XC2VP7 and the XC2V6000 . Icc was monitored throughout the testing in order to look for possible neutron induced latch-up. Neutron induced latch-up has not been seen for any of the devices in over 120 hours of beam exposure (equivalent to over 13,000 years of atmospheric exposure). Xilinx was allotted three slots at LANSCE of 48 hours each during the past year for this research.

Results for Virtex-II

Virtex-II testing has been performed at LANSCE on three different occasions: August 2002, December 2002 and September 2003. Each test utilized the 2V6000 devices. The following summarizes the test results from each date.

August 2002

Please note that Experimental Configuration B has one set of the Virtex-II samples (S/N 5 and 6) in the front of the beam line with the second set of Virtex-II samples behind them. Experimental configuration A has the position reversed. (i.e. S/N 2 and 3 are in front of the beam line) Experimental configuration C moved the location of the Virtex-II Pro board (results reported later) while position D rotated position A at a 45 degree angle to the beam in an attempt to investigate the effect of the neutron beam at a non-orthogonal incidence.

Table 1. Neutron Bit Cross Section Data for Virtex-II (8/02)

Run #	Part Position	Count	Fluence >10 MeV	CONTROL not in beam			CONTROL not in beam			Average Errors	Cross-Section >10MeV
				S/N 1	S/N 2	S/N 3	S/N 4	S/N 5	S/N 6		
1	B	156,697	2.62E+09	1	1644	1708	0	1377	1358	1368	3.15E-14
2	B	466,852	7.82E+09	2	4936	4875	1	4005	3981	3993	3.08E-14
3	B	1,293,428	2.17E+10	9	13643	13779	2	10886	10915	10901	3.03E-14
4	A	562,097	9.41E+09	1	5044	5045	4	6745	6424	5045	3.23E-14
5	A	1,953,857	3.27E+10	1	17604	17413	1	22618	22615	17509	3.23E-14
6	C	311,031	5.21E+09	0	2436	2446	1	3286	3203	2441	2.83E-14
7	C	996,496	1.67E+10	1	7934	7701	1	10328	9974	7818	2.82E-14
8	D	468,256	7.84E+09	1	3873	3733	1	1579	2474		
9	D	1,799,424	3.01E+10	5	14402	14121	5	6685	9633		

Note: Shaded areas represent results that were not included in the the cross-section calculation.

The table above summarize the measurements that were made on all of the Virtex-II parts. The upset averages of the first pairs of parts in the neutron beam were utilized to calculate the bit cross section. The difference between the first parts in the beam and the second parts averaged a ratio of 1.23, and the magnitude of this difference was not expected and has been shown to be the result of enhanced dose from the spallation products resulting from the flip chip solder mounting balls. More about this effect appears later in this paper in the discussion section. Therefore for this calculation, only the data from the front units was used in the calculation of the cross section.

December 2002 and Sept 2003 Results

Table 2. Neutron Bit Cross Section Data for Virtex-II (12/02 and 9/03)

Run	Vdd	Count	Fluence >10 MeV	Fluence >1.5 MeV	CLB Cross-section	
					Errors	>10 MeV
Neutron SEU Test Sept 1, 2003 (2V6000)						
14	1.50	74975	1.33E+09	2.55E+09	650	2.95E-14
Neutron SEU Test, December 2002 (2V6000)						
1	1.50	126013	2.14E+09	4.08E+09	1213	3.42E-14
	1.50	126013	2.14E+09	4.08E+09	1137	3.20E-14
5	1.50	98091	1.67E+09	3.17E+09	894	3.24E-14
	1.50	98091	1.67E+09	3.17E+09	858	3.11E-14
6 (60deg angle)	1.50	90780	1.54E+09	2.94E+09	906	3.54E-14
	1.50	90780	1.54E+09	2.94E+09	880	3.44E-14
7 (30deg angle)	1.50	95821	1.63E+09	3.10E+09	913	3.38E-14
	1.50	95821	1.63E+09	3.10E+09	873	3.24E-14

The average CLB Cross-Section (>10MeV) for the Virtex-II based on all runs is 3.18e-14.

Results for Virtex-II Pro

Virtex-II Pro testing has been performed at LANSCE on two different occasions: August 2002 and September 2003. The August 2002 test utilized a 2VP4 while the September 2003 test was on a 2VP7. The following summarizes the test results from each date

August 2002

Only one device was available for the Virtex-II Pro experiment. The fixture used to expose the part is shown below in figure 4 and the results of the test runs are summarized in Table 3. The part was similarly programmed and interrogated (as was done with the Virtex-II parts). In run 3 the 2VP4 part experienced a SEFI and control of the bit stream was lost. This run was excluded from the calculation of the bit cross section, as the error count was fallacious. However this one SEFI did allow a crude estimate of the SEFI Cross Section for the 2VP4. The calculated cross section for this SEFI was about 2.0E-18 and the SEFI cross section, based on this single data point, is estimated to be somewhere between 10E-17 and 10E-19.

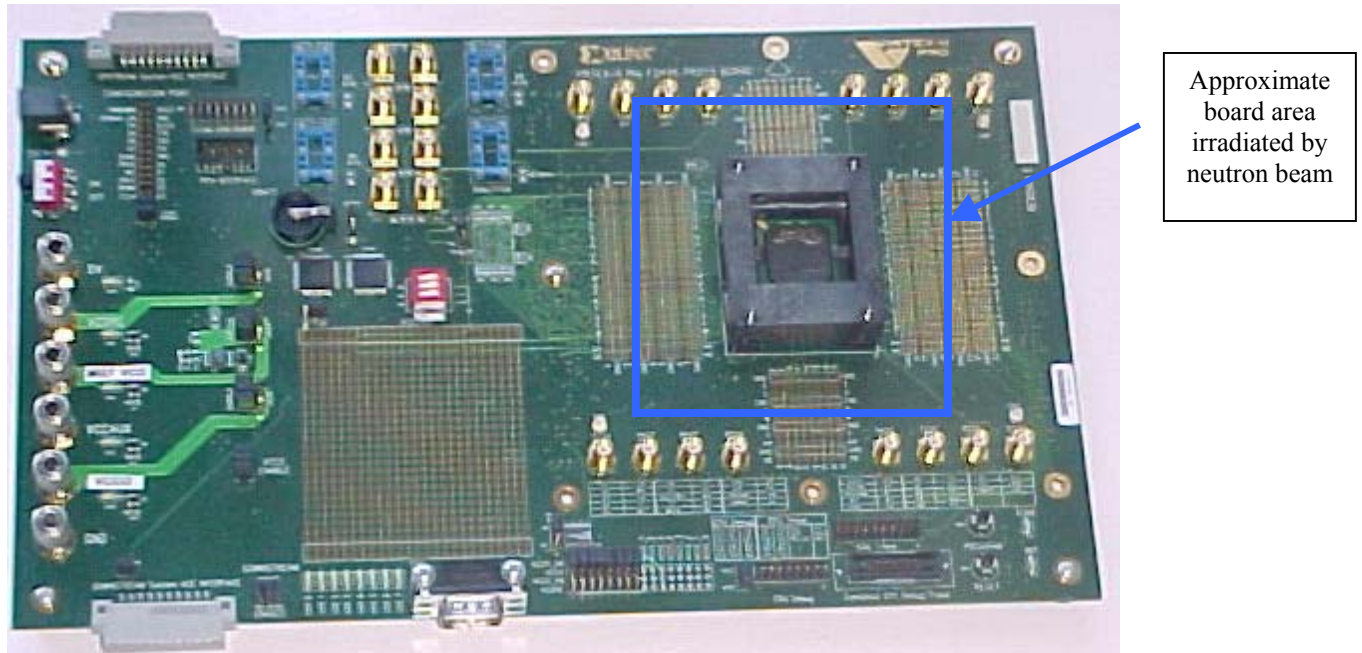


Figure 5. The performance board used to expose the 2VP4 to the neutron beam.

Calculation of the bit cross section was made using the neutron fluence estimates for the eight successful runs with an energy >1.5 MeV and again for an energy >10.0 MeV. The actual data taken on the Virtex-II Pro (2VP4) FPGA along with the calculation of the critical cross-section is shown below in table 3.

Table 3. Neutron Bit Cross Section Data for the Virtex-II Pro (8/02)

Run #	Experiment Configuration	Pulse Count	Counts per Minute	Run Time	Fluence >10 MeV	Fluence >1.5 MeV	Errors	Cross-section >10 MeV	Cross-section >1.5 MeV
1	A	156,697	3,561	44	2.62E+09	5.13E+09	142	2.19E-14	1.12E-14
2	A	466,852	3,112	150	7.82E+09	1.53E+10	367	1.90E-14	9.71E-15
3	A	1,293,428	3,804	340	2.17E+10	4.23E+10	174960		
4	A	562,097	3,386	166	9.41E+09	1.84E+10	515	2.21E-14	1.13E-14
5	A	1,953,857	3,428	570	3.27E+10	6.39E+10	1840	2.27E-14	1.16E-14
6	B	311,031	2,592	120	5.21E+09	1.02E+10	331	2.57E-14	1.31E-14
7	B	996,496	3,163	315	1.67E+10	3.26E+10	978	2.37E-14	1.21E-14
8	B	468,256	3,345	140	7.84E+09	1.53E+10	502	2.59E-14	1.32E-14
9	B	1,799,424	3,395	530	3.01E+10	5.89E+10	1844	2.47E-14	1.27E-14

A= part behind 2V6000s

B= part in front of beam

September 2003 Results

Table 4. Neutron Bit Cross Section Data for the Virtex-II Pro (9/03)

The average CLB Cross-Section for the Virtex-IIPro, based on the data above, is 2.98×10^{-14} for neutrons $>10\text{MeV}$. This figure (for a 0.13 micron technology) is lower than the cross section calculated for Virtex-II (a 0.15 micron technology). Due to the number of bit upsets that went into these calculations, the value arrived at has a high confidence of being correct. This implies that, while the Virtex II-Pro technology is fabricated on a tighter technology than the Virtex-II and hence has a lower Q-crit, the geometry factor predominated and resulted in a lower cross section calculation. The effect is believed to be real and a consequence of the lower probability of a neutron striking a critical area in the Virtex-II Pro technology.

Results for Spartan-3

Spartan-3 testing has been performed at LANSCE on two different occasions: September 2003 and November 2003. All tests utilized the 3S1000. The following summarizes the test results from both dates.

September 2003 and November 2003

The fixture used to expose the part was shown previously in figure 1 and the results of the test runs are summarized below in Table 5. The part was similarly programmed and interrogated (as was done with the Virtex-II and Virtex-II Pro parts). In this case, custom software (FIVIT) was used to interrogate the parts and to calculate average cross sections.

Table 5 Spartan-3 Test Results

Run	Vdd	Count	Time (min)	Fluence >10 MeV	Fluence >1.5 MeV	CLB Cross-section			BRAM Cross-Section		
						Errors	>10 MeV	>1.5 MeV	Errors	>10 MeV	>1.5 MeV
S-3 Testing (Sept 1, 2003) 3S1000											
1	1.20	73206	25	1.30E+09	2.49E+09	106	3.08E-14	1.60E-14	28	4.89E-14	2.54E-14
2	1.20	39755	15	7.04E+08	1.35E+09	57	3.05E-14	1.58E-14	18	5.78E-14	3.00E-14
3	1.20	78584	30	1.39E+09	2.68E+09	96	2.60E-14	1.35E-14	35	5.69E-14	2.95E-14
4	1.20	120305	45	2.13E+09	4.10E+09	160	2.83E-14	1.47E-14	47	4.99E-14	2.59E-14
5	1.20	160103	60	2.83E+09	5.46E+09	202	2.68E-14	1.39E-14	65	5.19E-14	2.69E-14
6	1.20	311946	120	5.52E+09	1.06E+10	412	2.81E-14	1.46E-14	126	5.16E-14	2.68E-14
7	1.20	300332	120	5.32E+09	1.02E+10	417	2.95E-14	1.53E-14	111	4.72E-14	2.45E-14
8	1.20	160020	85	2.83E+09	5.45E+09	213	2.83E-14	1.47E-14	54	4.31E-14	2.24E-14
9	1.20	161337	60								
10	1.20	30743	14	5.44E+08	1.05E+09	31	2.15E-14	1.11E-14	10	4.15E-14	2.16E-14
11	1.20	211320	90	3.74E+09	7.20E+09	254	2.56E-14	1.33E-14	87	5.26E-14	2.73E-14
12	1.20	87320	30	1.55E+09	2.98E+09	112	2.73E-14	1.42E-14	40	5.85E-14	3.04E-14
13	1.20	233173	90	4.13E+09	7.94E+09	356	3.25E-14	1.69E-14	100	5.48E-14	2.85E-14
27	1.20	201972	100	3.57E+09	6.88E+09	235	2.48E-14	1.29E-14	75	4.74E-14	2.46E-14
28	1.20	132054	50	2.34E+09	4.50E+09	173	2.79E-14	1.45E-14	43	4.16E-14	2.16E-14
29	1.20	97026	25	1.72E+09	3.31E+09	111	2.43E-14	1.26E-14	43	5.66E-14	2.94E-14
S-3 Testing (Nov 11, 2003) 3S1000											
10A	1.20	157176	60	2.78E+09	5.36E+09	244	3.30E-14	1.72E-14	59	4.79E-14	2.49E-14
11A	1.20	157473	60	2.79E+09	5.37E+09	253	3.42E-14	1.78E-14	76	6.16E-14	3.20E-14
17A	1.20	2031744	725	3.60E+10	6.92E+10	3537	3.70E-14	1.92E-14	539	3.39E-14	1.76E-14

Run #9 was not used in the calculations of cross sections because of a cockpit error which resulted in the loss of data. Note that there was negligible current increase during the dosing and absolutely no indication of single event latch in any of the testing. The cross sections were calculated based on the results from FIVIT and are consistent with earlier data taken on these same devices. The effects of process migration and improvements in the design of the configuration latches (to enhance latch stability) are detailed later in this report.

The average CLB Cross-Section (>10MeV) for the Spartan-III based on all runs is 2.87e-14.

Rosetta Results

The calculation of the neutron cross section for the Rosetta experiments (a Rosetta Board is shown below in figure 6) requires an assumption of the local neutron flux at each of the experimental sites. The data for this value (and for the resultant calculations of the various Rosetta cross sections) were taken from various publications, including the works of Zeigler and Norman. The Rosetta data results in upset rate that scaled with the theoretical altitude distribution of neutron flux, but demonstrated a factor of “x” robustness above measurements made at the LANSCE facility. This increase in robustness of the latches is referred to as the “Rosetta” factor and provided guidance in the selection of the proper energy model for calculating upset rates for Xilinx FPGAs. The results are summarized below in table 6.

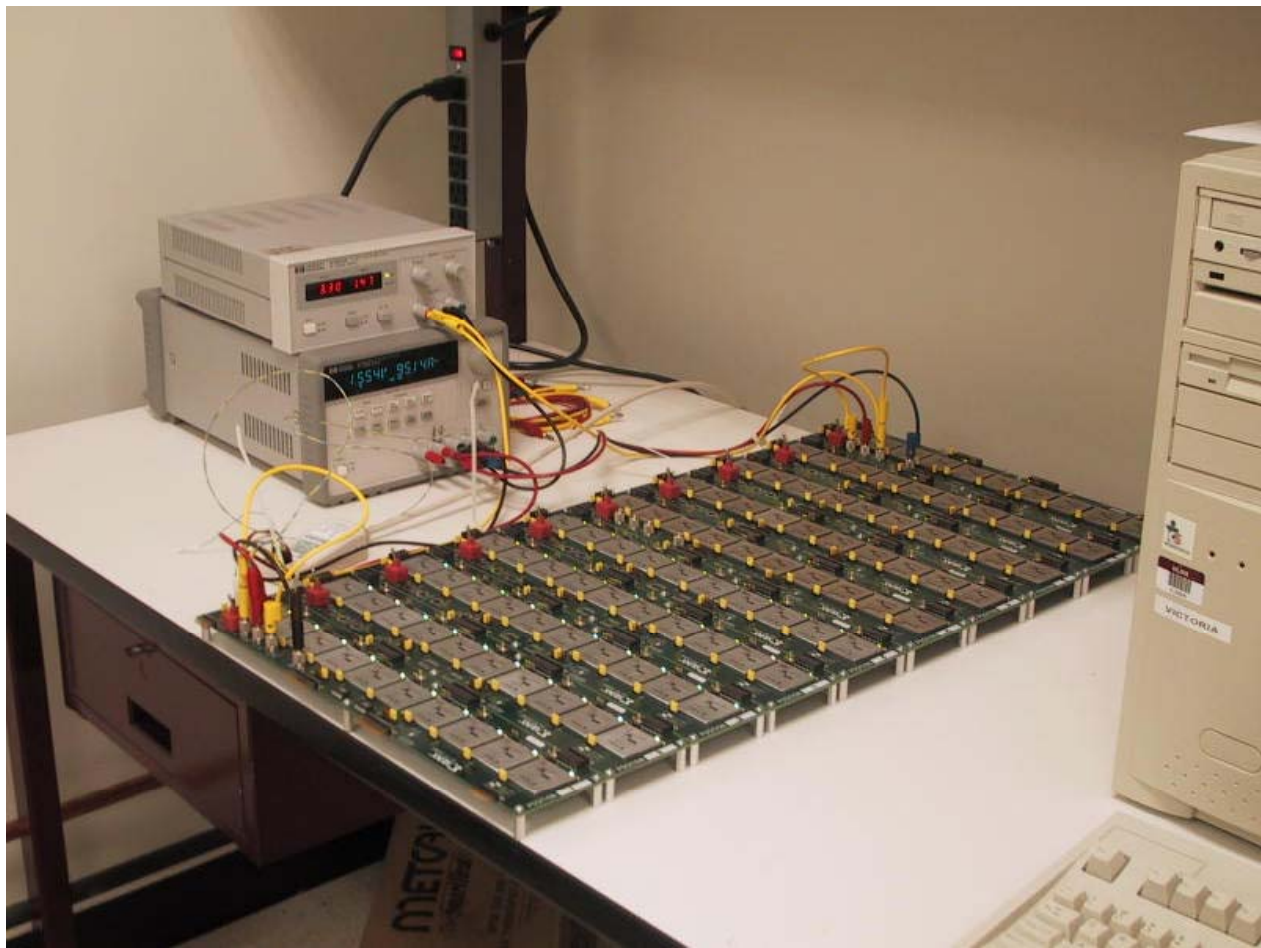
Table 6 The Rosetta Factor

Location	Days	Hours	Upsets	Device Hours	Bits	>10MeV Flux (n/cm2- hr)	>10MeV Fluence	>10MeV Cross-Section
San Jose	457	10968	6	1.10E+06	1.96E+09	14.40	157,939	1.94E-14
ABQ	577	13848	34	1.38E+06	1.96E+09	53.28	737,821	2.35E-14
WM	242	5808	72	5.81E+05	1.96E+09	338.40	1,965,427	1.87E-14
MK	104	2496	19	2.50E+05	1.96E+09	229.57	573,017	1.69E-14
Average Cross- Section								1.96E-14
LANSCE 2V6000								3.18E-14
Rosetta Factor								1.62

Previous publications on these results had used the >1.5 MEV energy distribution model proposed by Fuller et al. However JESD89 allows the choice of model based on real world demonstrations of the atmospheric error rates. LANSCE results using the flux >10.0 MEV allows correlation between real world results and the Rosetta results with a Rosetta Factor of only 1.62. This tells us that the accelerated NSEU testing performed at LANSCE is a close match to the Rosetta Results when the >10.0 MEV model is employed. This is very important in calculating the logic MTBF of FPGAs and is one of the errors that have been promulgated in the application of commercial SRAM data to the calculation of logic upset rates of a static latch based FPGA.

The Rosetta factor applied to other process geometries (Virtex-IIPro and Spartan-3) will have a small error associated with it since the Rosetta data presented was taken on Virtex-II (2V6000s). Rosetta testing has begun for VIIPro and S-3.

Figure 6: A Rosetta Implementation



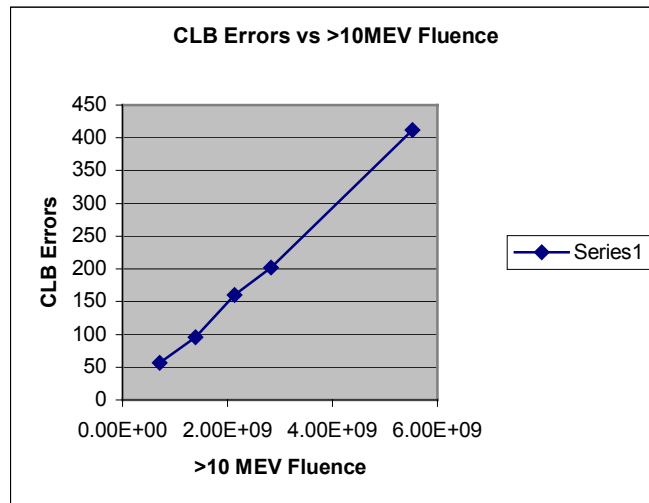
Discussions

There are several observations that can be made from the data that has been obtained.

First (and simplest), the upset rates were relatively linear with fluence. This indicated that the statistics of upset were relatively random in nature, and that the effects were not synergistic.

Second, since the total number of upsets was kept to a small percentage of the configuration file size, there was no need to correct the data for the possible effect of flipping a disturbed bit back to its initial value. This is illustrated in the curves below (figure 7) for data taken on the Spartan-3 samples:

Figure 7 Upset Linearity



Third, care must be taken in the directionality of the beam, especially for flip chip packaged devices. The reason for this is illustrated below. A Virtex-II part was rotated in the beam in 15 degree increments and a measure of the cross section was made as a function of beam angle. This was originally proposed to look for multiple bit errors from a single particle at low angles (evidence of multiple bit errors was not seen), which is consistent with the distributed nature of the configuration latches used to program Xilinx FPGA. However, there is a very definite effect of flux enhancement by the flip chip solder balls used to connect the die to the substrate. This effect is

not seen in wire bonded devices. While the same effect is occurring from radiation from the back of the die, the range of the spallation products produced from the backside is inadequate to affect the device operation. However, when the beam is incident from the top of a flip chip die, the spallation products are within range of the active area of the device and do affect the measured cross sections. The fortunate outcome of the effect is that the local dose enhancement is only a factor of two or less. See the following illustrations (figure 8) for details on this effect.

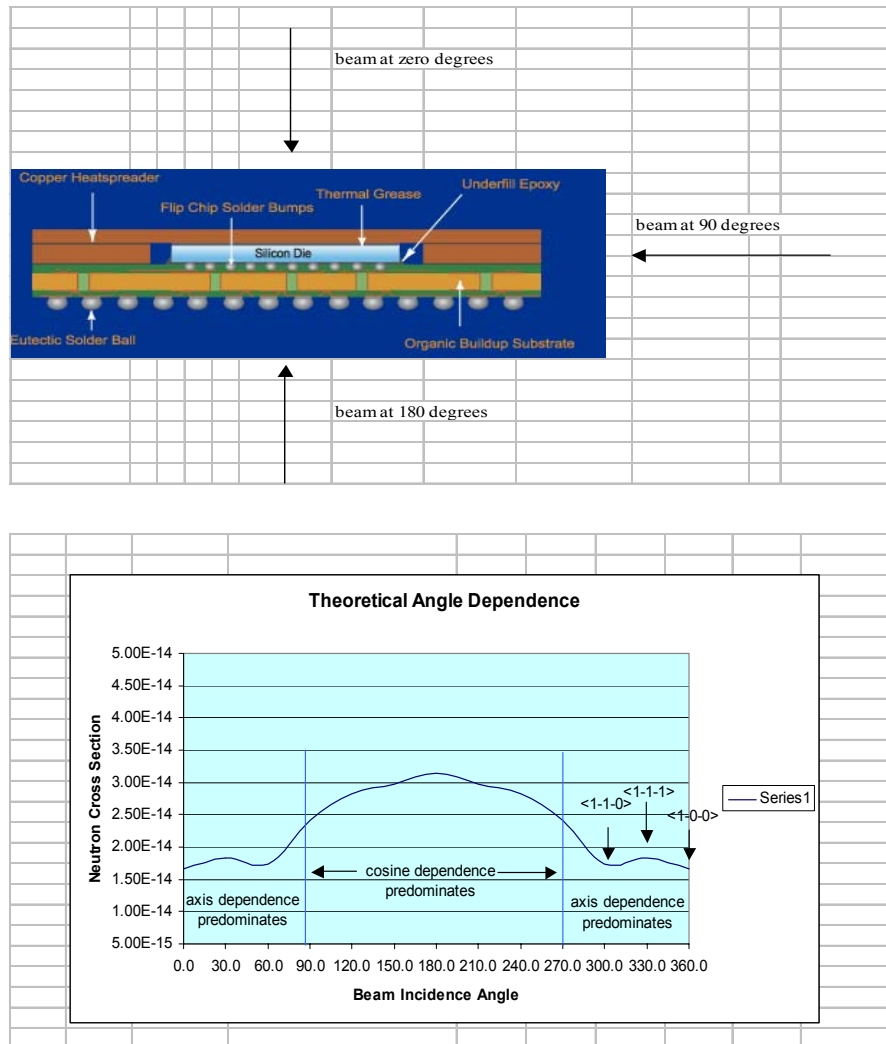


Figure 8 Beam Angle Effects on Flip Chip Devices

Fourth, the static latches that are used to configure an FPGA are not the same as the flip flops used in a commercial SRAM. The flip flops in a commercial SRAM are designed with three criteria, namely size, ability to quickly write, and ability to quickly read. Hence commercial SRAM cells have been shown to be relatively sensitive to NSEU effects. This is illustrated by the sensitivity of the upset rate of a commercial SRAM to operating voltage. This is not the case for the static latches used to program an FPGA. The design criteria for these static latches have historically been and continue to be stability, stability and stability. The size of an FPGA is dominated by interconnect, not by the configuration latches. Also, these latches are typically written to once and hold that data, they do not have to be particularly fast or easy to write to. What they have to be and have been historically designed to be is stable. This is well illustrated by the plot of cross section versus operation voltage for a 150 nm latch used in Virtex-II. The cross section was measured over the range of 1.20 volts to 1.60 volts, well outside the published operating voltage range of the device (1.50 +/- 5%) and the results are illustrated below in figure 9. This is one proof of the stability of these static latches.

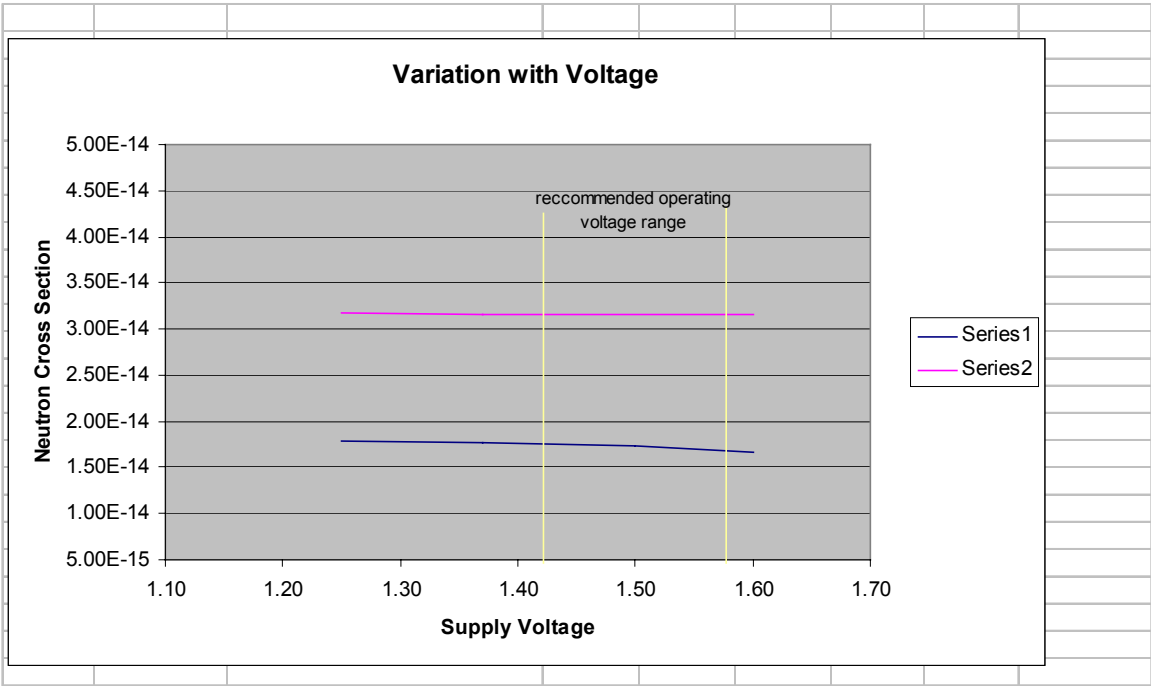
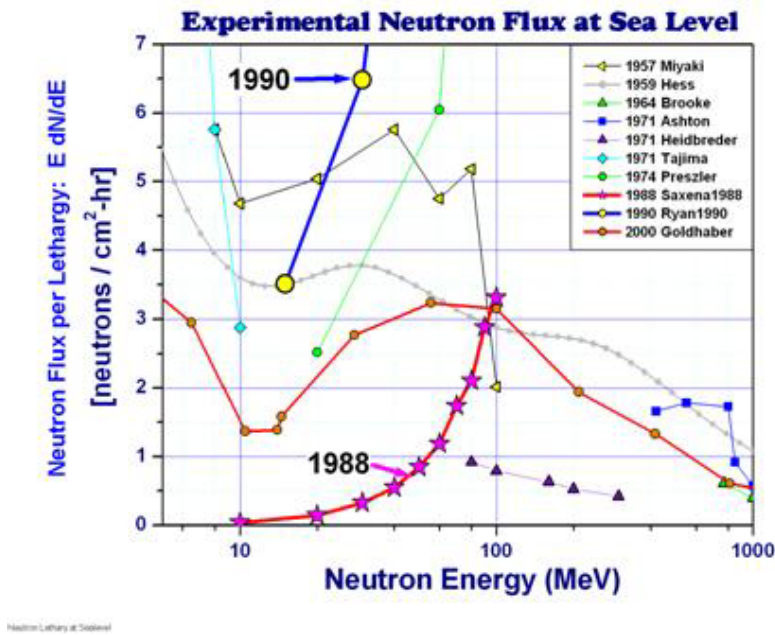


Figure 9: Static Latch Stability

Fifth, the Xilinx Rosetta experiments (performed on large quantities of FPGAs at three different altitudes) have demonstrated that the correct energy model to use for the calculation of FPGA upset rates from LANSCE data (the >10.0 MEV model) and is different from the extrapolations of >1.5 MEV commercial SRAM data that others have used to calculate these effects. The clear need to do Rosetta-like experiments to calibrate results from accelerated NSEU testing was illustrated by Zeigler in recent presentations and is illustrated below in figure 10. The choice of a flux and energy distribution to use in accelerated upset calculations is not possible based on the published literature over the past forty years, and must be determined for each specific technology by Rosetta-like experiments.

Figure 10: Effects of Terrestrial Cosmic Rays, J.F. Zeigler,



Sixth, A failure in a configuration memory cell statistically does not cause a functional failure. Research by BYU and LANL using their bit corrupter on a V1000 device has shown the multiplier to be between 25 and 100. SEUPI analysis of specific customer applications has shown SEUPI factors from 10 to 80 with a mean of 42. The conclusion is that a multiplier of 10 can be used conservatively.

Seventh, and finally, the projections of ever worsening neutron cross section and upset rates as technology has shrunk through the 220 nM, the 180 nM, the 150 nM and now the 90 nM range have not been shown to be correct. Rather the decreased size of the shrinking latches combined with robust design efforts have stabilized the critical neutron cross sections of state of the art static latches and reversed this trend. Indeed the MTBF that can be calculated for a million logic gate FPGA fabricated with 90 nM technology is no worse (and often better) than the MTBF of a similar complexity array fabricated in 150 or 130 nM processes. This is illustrated by the table below which illustrates the fact that the neutron cross section (and hence the upset rate) for 90 nM product is actually lower than the neutron cross section of similar 150 nM product.:

Technology	Cross-Section >1.5MeV	Cross-Section >10MeV
150nm	1.65e-14	3.18e-14
130nm	1.54e-14	2.98e-14
90nm	1.49e-14	2.87e-14

Conclusions

The latest LANSCE and Rosetta data have been measured and presented. From this data it is possible to calculate the logic upset rate of the recently production released 90 nM Xilinx FPGAs. Similar calculations on 220 nM, 180 nM, 150 nM and 130 nM have been published in the past and earlier reports are available. The data in this report demonstrated a couple of key points which lead to the calculation of the logic MTBFs presented below:

1. The neutron cross section of the static latch used to program Xilinx FPGAs has not tracked the neutron cross section of commercial SRAMs, and this is precisely because this static latch cell is not a commercial SRAM cell. Greatly different design goals are pursued during the design of a static configuration latch and an SRAM cell.
2. Calibration of the LANSCE accelerated neutron test results with actual applications test data was established with large numbers of devices operating continuously at three different altitudes and have confirmed the altitude factors first published by Zeigler and Norman for the atmospheric neutron flux, but have also established a “Rosetta Factor” to be applied to the accelerated data, which factor is dependent on the choice of an energy model.

3. The neutron energy model for neutrons >10.0 MEV shows a close correlation with the results of the Rosetta experiment (Rosetta factor is only ~ 1.51) versus a much larger factor if the earlier >1.5 MEV model is used. This represents good agreement between accelerated testing and applications testing.
4. The static latches used to configure Xilinx FPGAs are relatively insensitive to neutrons in the 1.5 to 10.0 MEV range, but do exhibit measurable and correlatable cross sections for neutrons whose energy is > 10.0 MEV. This confirms earlier data taken by Saab Avionics (report available on Xilinx.com).

APPENDIX A: Examples of MTBF Calculations

Calculated Spartan-III FPGA Logic MTBFs

Spartan-III MTBFs at Sea Level

Device	# Config Bits	Neutron Cross-Section	Config Upset (Hrs)	Config Upset (Yrs)	Config Upset Rosetta (Yrs)	Logic Upset (Yrs)
XC3S50	4.39E+05	2.87E-14	5.51E+06	629	1019	10187
XC3S200	1.05E+06	2.87E-14	2.31E+06	264	427	4271
XC3S400	1.70E+06	2.87E-14	1.42E+06	163	263	2634
XC3S1000	2.66E+06	2.87E-14	9.11E+05	104	169	1685
XC3S1500	5.21E+06	2.87E-14	4.64E+05	53	86	858
XC3S2000	7.67E+06	2.87E-14	3.15E+05	36	58	583
XC3S4000	1.13E+07	2.87E-14	2.14E+05	24	40	395
XC3S5000	1.33E+07	2.87E-14	1.82E+05	21	34	337

The Configuration Upset in hours is calculated by the following equation:

$$1 / (\text{Configuration Bits} * \text{Neutron Cross-Section} * \text{Flux}).$$

In the table above the flux was assumed to be 14.4n/cm²-hr (sea level – 45deg latitude), the Rosetta factor is 1.62 and the SEUPI factor 10.

Spartan-III MTBFs at Various Altitudes

Device	Logic Upset Sea Level (Yrs)	Logic Upset ¹ 5K ft (Yrs)	Logic Upset ² 10K ft (Yrs)	Logic Upset ³ 40K ft (Yrs)
XC3S50	10187	2845	1047	33.96
XC3S200	4271	1193	439	14.24
XC3S400	2634	736	271	8.78
XC3S1000	1685	471	173	5.62
XC3S1500	858	240	88	2.86
XC3S2000	583	163	60	1.94
XC3S4000	395	110	41	1.32
XC3S5000	337	94	35	1.12

¹ 5K feet reduction factor of 3.58 applied per IBM-Method, JEDEC-89

² 10K feet reduction factor of 9.73 applied per IBM-Method, JEDEC-89

³ 40K foot reduction factor of 300 applied per JEDEC-89



REPORT ON EXPERIMENT
(Please Type)

Submit all experiment reports to:
 LANSCE User Office, MS H831, Los Alamos National Laboratory, Los Alamos, NM 87545

Experiment was carried out at:		Local Contact	Proposal #	<i>LANSCE Use Only</i>
<input type="checkbox"/>	Manuel Lujan Jr. Neutron Scattering Center	Ron Nelson	2003-555	Report Rc'd
<input checked="" type="checkbox"/>	Weapons Neutron Research Facility	FP/Instrument Used	60RGEANIE	
<input type="checkbox"/>	WNR/Blue Room			

Title	Measurement of $^{191}\text{Ir}(n,n'\gamma)$, Cross Sections Populating Isomeric States
-------	--

Authors and Affiliations

R.O. Nelson, N. Fotiades, M. Devlin
 LANSCE-3, LANL
 P. E. Garrett, W. Younes, J.A. Becker
 N-Division, LLNL

Experiment Report

The two stable iridium isotopes, ^{193}Ir (63% abundance) and ^{191}Ir (37% abundance) provide unique neutron flux detectors. There are long-lived ground states or isomeric states suitable for drill-back sampling and diagnostics in all of the isotopes from $^{188-194}\text{Ir}$, except for ^{191}Ir . Previously, we studied ^{193}Ir that has a unique isomer with a 10.5 d half life populated by inelastic scattering.¹ This is the only neutron flux detector used that is primarily sensitive to fission neutrons. Other detectors are sensitive to higher energy fusion neutrons (using the (n,2n) reaction) or lower energy thermal neutrons (using the capture reaction). Having obtained good results for ^{193}Ir that are proving useful in better interpreting archival data, we are now concentrating on ^{191}Ir .

In 2002 we obtained some $\gamma\gamma$ coincidence data to help validate the structure of ^{190}Ir that has only recently been studied in detail.¹ The statistical accuracy of this data set appears to have been limited by an undetected problem in the electronics during data acquisition. With these data we were able to confirm some of the levels and γ rays in ^{190}Ir . In 2003 we successfully acquired singles γ -ray data on ^{191}Ir . These data and results are discussed below.

Experiment Report *(continued)*

Experiments on $^{191}\text{Ir}(n,x\gamma)$ were carried out from October 17 – November 1, 2003 using the GEANIE spectrometer, configured with both LEPS and coaxial Ge detectors. The sample was 2 grams of Ir 98.23% enriched in ^{191}Ir . A total of 15 days of beam time with 3.6 μs beam spacing was used with 80% of maximum availability. The beam pulse interval was longer than the usual 1.8 μs to avoid frame-overlap of lower-energy neutrons that populate the low-lying states in inelastic scattering in ^{191}Ir . Discrete gamma-ray spectra were measured for nuclei populated in $^{191}\text{Ir}(n,xn\gamma)$ reactions, with $x \leq 7$, as a function of incident neutron energy using neutrons from the “white” neutron source at the Los Alamos Neutron Science Center's WNR facility. The energy of the neutrons was determined using the time-of-flight technique.

The data have been analyzed and preliminary results were reported by Nikolaos Fotiades at the Nuclear Data Conference for Science and Technology in October 2004 in Santa Fe, NM.² The cross sections for emission of gamma-rays of $^{183-191}\text{Ir}$ were determined for neutron energies in the range $1 \text{ MeV} < E_n < 100 \text{ MeV}$, and a comparison with model calculations using the GNASH reaction model, was made. These cross sections were also compared with older GEANIE results from similar $^{193}\text{Ir}(n,xn\gamma)$ reactions. For some of the reactions the similarities are striking.

With GEANIE we also acquire data between proton macro pulses that can provide information on the lifetimes of long-lived (100 μs to 10 ms) states. An example of this is the ^{175}Lu data where the lifetime of the known $19/2^+$ isomer with a lifetime of 984 μs was measured.³ This type of data has proven useful in determining the lifetime of a low-lying isomeric state in ^{190}Ir as described below. Improvements to the beam-off electronics are planned to make these data even more useful by allowing good timing in observing prompt coincidences following a delayed decay, and in studying delayed coincidences.

IMPORTANT! List or attach a list of publications resulting from this experiment (published or in press).

Experiment Report *(continued)*

Results useful for radiochemical diagnostics interpretation, for nuclear structure, and for nuclear reactions have been obtained: [1] Cross sections as a function of incident neutron energy have been obtained for the (n,3n) reaction populating states in ^{189}Ir . These data can help constrain models of the $^{190}\text{Ir}(n,2n)^{189}\text{Ir}$ reaction cross section, and provide information on the population of the 372-keV 13.3 ms $11/2^-$ isomeric state in ^{189}Ir . [2] Beam-off (between proton macro pulses) data were used to determine the lifetime of a 36.2 keV state that is most likely a previously unknown isomer in ^{190}Ir . This state recently was identified in the work of Garrett *et al.*⁴, as having spin/parity $(4)^+$, but with only a lower limit for the lifetime of 2 ns. In the present work we obtain a lifetime of 1.4 ± 0.4 ms. [3] By γ -ray feeding we measure a part of the population of the 1^- , 1.12-hour isomer at 26.1 keV in ^{190}Ir . [4] A number of new levels and gamma rays have been identified in ^{191}Ir , adding to our knowledge of the structure. And we obtained data on the population of the 4.9s $11/2^-$ isomer in ^{191}Ir .

The observed levels and γ -rays in ^{190}Ir are shown in Fig. 1 and the excitation functions for populating the isomeric states and the ground state are shown in Fig. 2. In total we observe about 34% of the (n,2n) channel cross section populating states in ^{190}Ir . While a larger fraction is desirable, it is encouraging that we can do this well in an odd-N, odd-Z nucleus that is relatively heavy and far from closed shells, thus having a high level density. The information we obtain on isomer populations is new and can affect the interpretation of radiochemical diagnostics.

Figures 3 and 4 show the observed levels and γ -rays and the excitation functions for transitions populating the isomeric level in ^{189}Ir . In Fig. 5 we compare data from ^{193}Ir and ^{191}Ir for inelastic scattering and the (n,3n) reaction. Figure 6 displays representative excitation functions for each (n,xn) reaction from inelastic scattering to (n,9n).

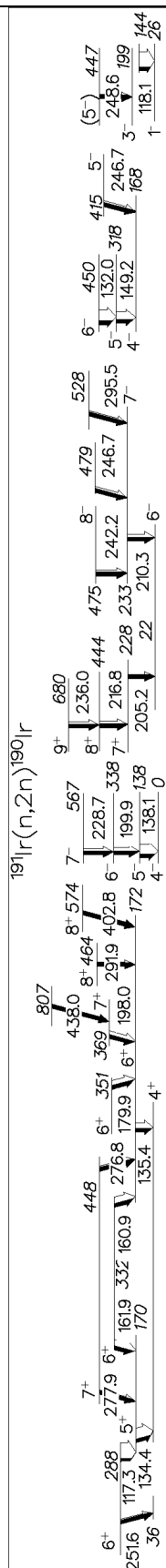


Figure 1. Observed levels and γ rays in the $^{191}\text{Ir}(n,2n)^{190}\text{Ir}$ reaction. The 6⁺, 22-keV level and the 4⁺, 168-keV level decay promptly to the ground state through highly-converted transitions that are not observed in our experiment. The 1⁺, 26-keV level has a 1.12 h half life, and the (4)⁺, 36-keV level has a half life of about 1 ms that was first measured in the present work.

Experiment Report (continued)

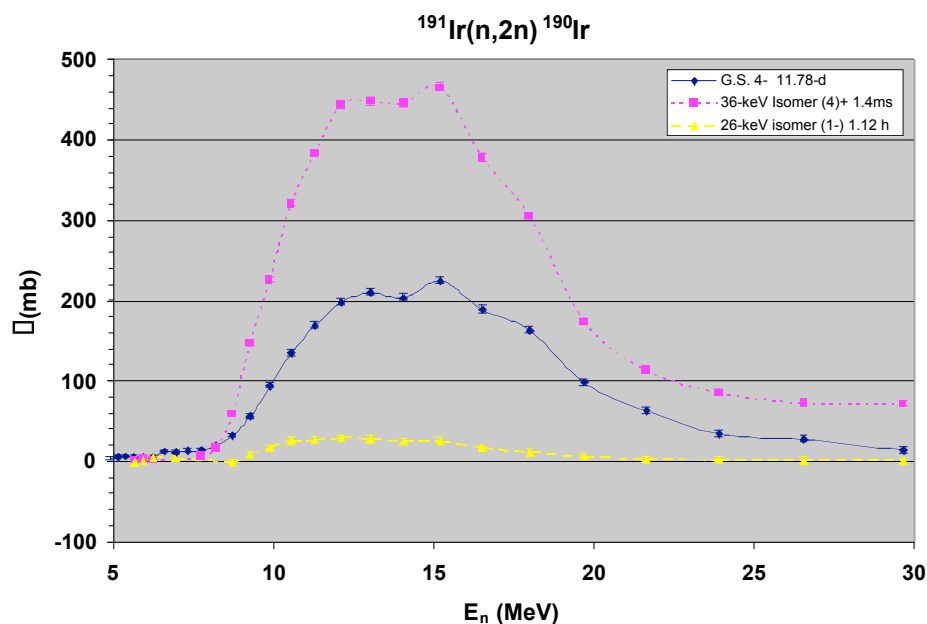


Figure 2. Cross sections for ^{19}F ground state are shown. The (2000 mb.

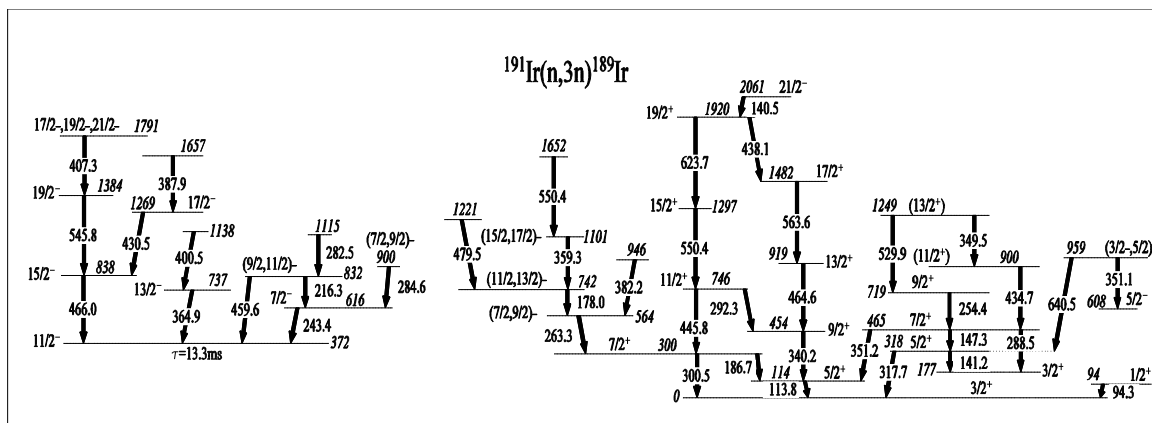


Figure 3. Observed γ -rays and levels in ^{189}Ir following the $^{191}\text{Ir}(n,3n)$ reaction. Decays populating the 13.3 ms $11/2^-$ isomer are shown on the left. Decays to the $5/2^+$ ground state are on the right. The structure and decays are very similar to those observed previously in $^{193}\text{Ir}(n,3n)^{191}\text{Ir}$.

Experiment Report (continued)

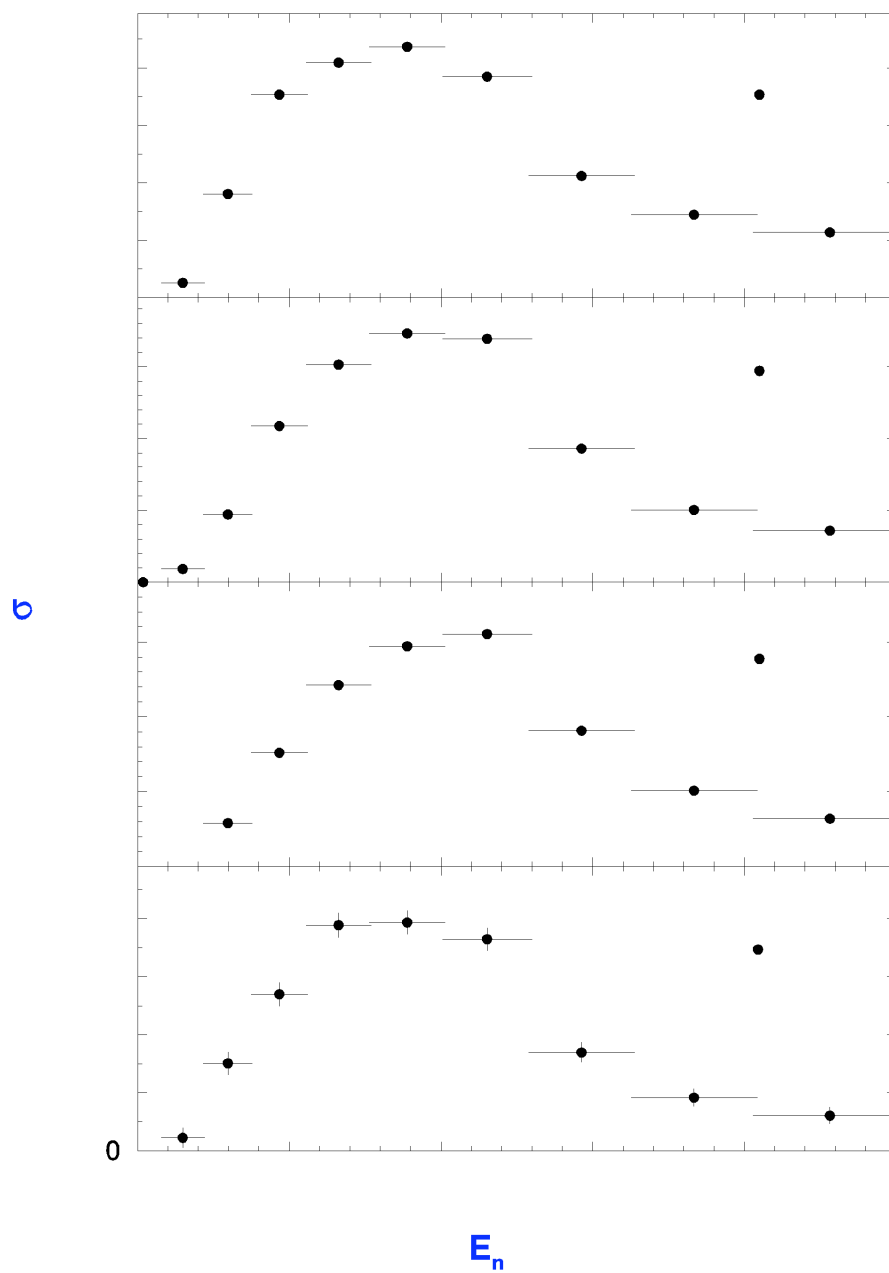


Figure 4. Excitation functions for the four independent γ rays populating the $11/2^-$ isomer in ^{189}Ir .

Experiment Report (continued)

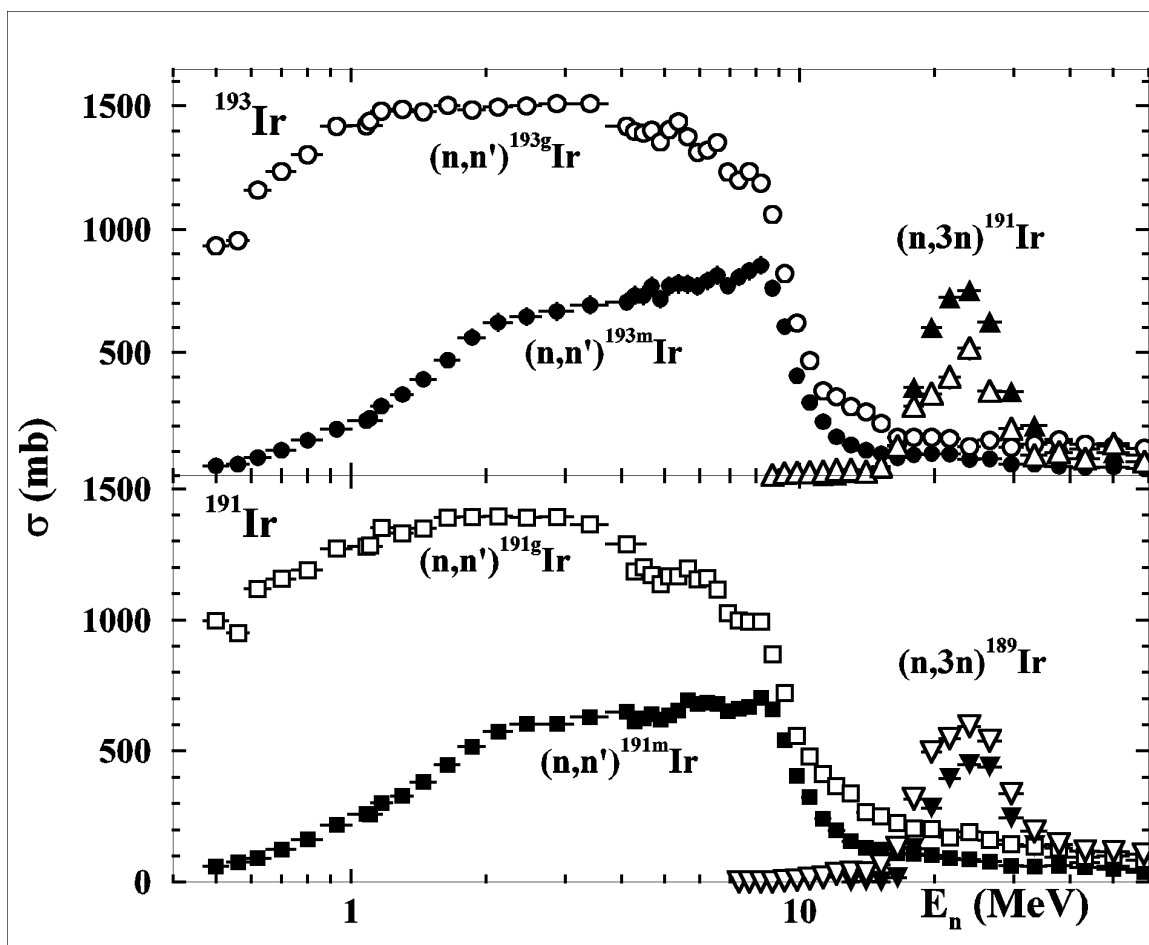


Figure 5. Cross sections of the observed (i.e. uncorrected for unobserved decays) inelastic scattering and (n,3n) reactions for ^{193}Ir and ^{191}Ir . Filled symbols indicate decay to the isomeric level, open symbols indicate decay to the ground state. Differences in the (n,3n) case may be due to the differing energies of the isomeric levels.

Experiment Report (continued)

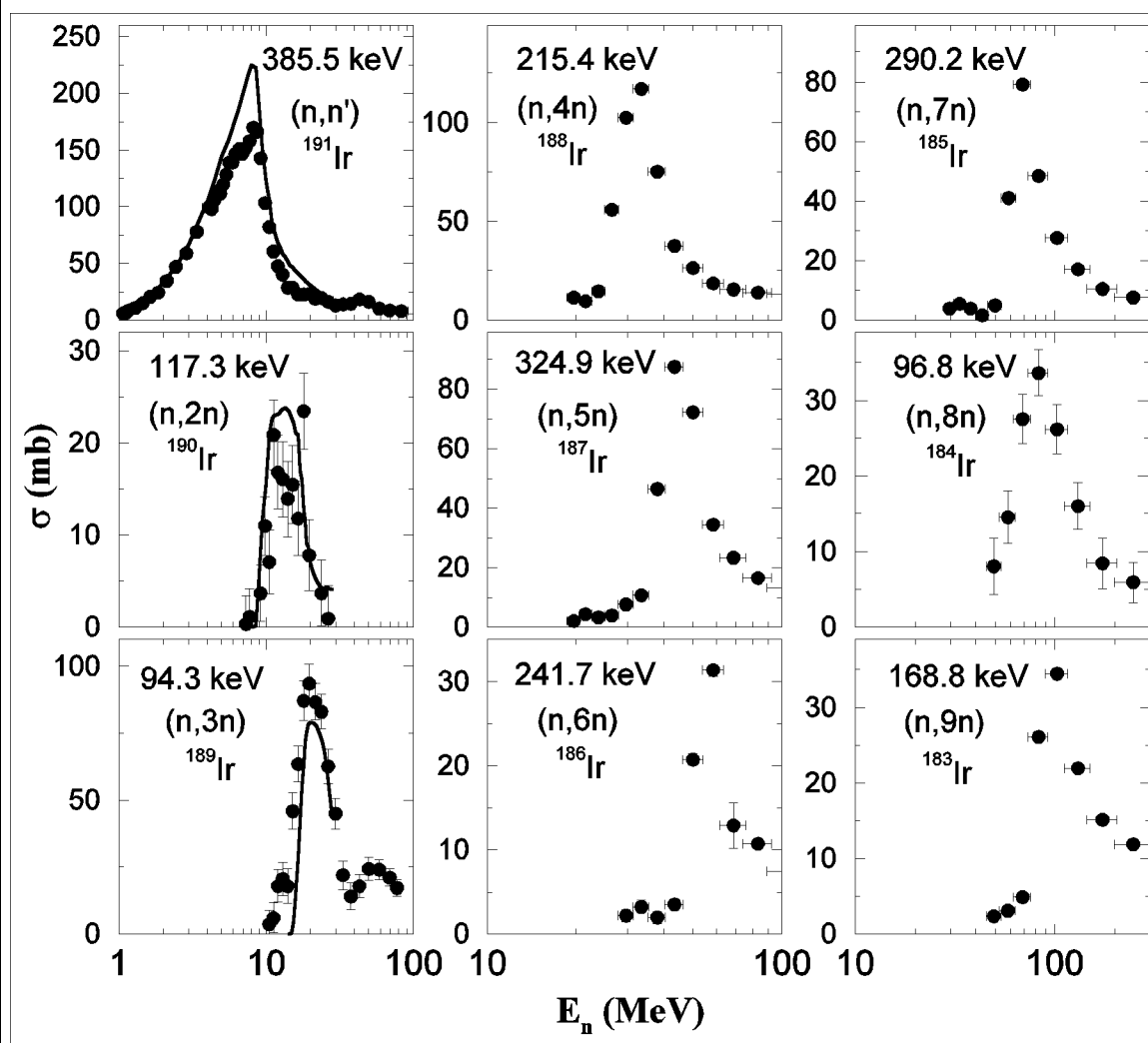


Figure 6. Representative excitation functions for the inelastic through (n,9n) reactions on ^{191}Ir . The solid lines are preliminary GNASH reaction model calculations.

References

- (1) R. O. Nelson, N. Fotiades, M. Devlin, P. Talou, M. B. Chadwick, R. MacFarlane, H. R. Trellue, A. C. Hayes, G. Jungman, M. C. White, S. C. Frankle, P. E. Garrett, W. Younes, and J. A. Becker, "New $^{193}\text{Ir}(n,n')^{193\text{m}}\text{Ir}$ Evaluated Nuclear Cross Sections for Radchem", NEDPC 2003, October 20 – 24, 2003, Los Alamos, NM, Proceedings of the Nuclear Explosives Design Physics Conference, in press (2004). LA-UR-04-0387 & LA-CP-04-0038.
- (2) N. Fotiades, R. O. Nelson, M. Devlin, M. B. Chadwick, P. Talou, J. A. Becker, P. E. Garrett, and W. Younes, "Cross Sections for Gamma-Ray Production in the $^{191}\text{Ir}(n,xn)^{\square}$ Reactions," International Conference on Nuclear Data for Science and Technology, Santa Fe, NM Sept. 26 - Oct. 1, 2004. LA-UR-04-6798
- (3) P.E. Garrett *et al.*, Phys. Rev. C **69**, 017302 (2004).
- (4) P.E. Garrett, *et al.*, Nucl. Phys. A **611** 68 (1996); P.E. Garrett, *et al.*, Nucl. Phys. A **662**, 235 (2000).



REPORT ON EXPERIMENT
(Please Type)

Submit all experiment reports to:
LANSCCE User Office, MS H831, Los Alamos National Laboratory, Los Alamos, NM 87545

Experiment was carried out at:	Local Contact	Proposal #	LANSCCE Use Only
<input type="checkbox"/> Manuel Lujan Jr. Neutron Scattering Center	Bruce Takala	2003556	Report Rc'd 6/8/04
<input checked="" type="checkbox"/> Weapons Neutron Research Facility	FP/Instrument Used		
<input type="checkbox"/> WNR/Blue Room	40FP30L-A		

Title

Neutron Soft Error Sensitivity of Advanced FPGAs

Authors and Affiliations

Bruce Euzent, Cheng Huang, Chih-Ching Shih, and Bill Kwong; Altera Corp, San Jose, CA

Experiment Report

The neutron soft error rate of various 130nm Altera's devices (Stratix, HardCopy Stratix, and Cyclone) and a 90nm SRAM test chip were characterized to investigate:

- 1) the factors affecting multiple-bit error of SRAM in advanced technologies,
- 2) the ratio between configuration SRAM (CRAM) and function soft error rate because not every CRAM bit error causes a functional error and
- 3) the effect of critical charge on soft error rate.

The power supply voltage was varied for the effect of critical charge on soft error rate and multiple-bit error. Bitmap data were recorded to analyze the SRAM multiple-bit error of different cell designs.

By comparing the neutron soft error rate at sea-level and alpha soft error rate from the accelerated soft error tests, we found the alpha soft error rate can be significant for advanced technologies depending on the packaging materials.

The results show that the occurrence of single strike 2-bit error of neutron will become significant for advanced technologies as cell size continues to shrink.

The ratio of soft error rate between CRAM and function was verified with a model. The ratio is calculated based upon the usage of CRAM and accelerated soft error rate data. Will collect more data with various designs for calibrating the model.

Customer Information

Soft Errors of SDRAMs

Creation	Status:	Version D
	Date / Version:	30.3.2004
	Author:	Günter Schindlbeck
	Approver:	Hans-Peter Klein
Contact	Department:	MP QM
	Address:	Balanstrasse 73 81541 München, Germany guenter.schindlbeck@infineon.com
Summary / Keywords	<ul style="list-style-type: none">• Soft Error Rate• Single Event Upset• Alpha Particle Test• Neutron Beam Test• Cosmic Radiation• Accelerated Soft Error Test• System Soft Error Test	

Content

1	DEFINITION OF SOFT ERRORS	3
2	SOURCES OF SOFT ERRORS.....	3
3	NOMENCLATURE	3
4	SOFT ERROR TESTS	4
4.1	Accelerated Tests	4
4.1.1	ASER Tests	4
4.1.2	NSER + TSER Tests	4
4.2	System Test.....	5
5	CONCEPT FOR LOW SOFT ERROR RATE	6
6	SOFT ERROR MODEL.....	7
6.1	Relative Comparison of the Susceptibility of Components to Ionizing Radiation	7
6.2	Low Level Alpha Counting	7
6.3	Evaluation of the SER	7
7	RESULTS	8
7.1	SSER Test with 256M S17 SDRAMs.....	8
7.2	SER Calculated from ASER Tests.....	8
7.3	SER Calculated from NSER Tests.....	9
7.4	Complete Soft Error Situation	9
8	EFFECTS ON THE SER	10
8.1	Comparison of Design Steps Via ASER Tests	10
8.2	Effect of Cycle Time on ASER and NSER Results	12
8.3	Effect of the Alpha Source.....	13
8.4	Range of Alpha Particles in Si.....	13
8.4	Effect of Elevation on Neutron Flux from Cosmic Radiation	14
9	HISTORY OF ASER VALUES OF DRAMS	15
10	REFERENCES	15

This work has benefited from the use of the Los Alamos Neutron Science Center at the Los Alamos National Laboratory. This facility is funded by the US Department of Energy under Contract W-7405-ENG-36.

1 Definition of Soft Errors

Soft errors are non-destructive disturbances of information in integrated circuits induced by ionizing radiation. In order to highlight the difference from “Total Dose Defects” (TDD), the term “Single Event Upset” (SEU) is also used. Most TDDs are soft errors. Sometimes latch-up, gate rupture, etc. also occur as single-event defects, but usually they are several orders of magnitude less frequent than soft errors.

Soft errors are temporary, not permanent malfunctions. They do not affect the long-term reliability of devices.

2 Sources of Soft Errors

Soft errors are produced by radiation with a sufficiently high ionization rate. In terrestrial applications there are three main sources of soft errors. One source is alpha particles from traces of uranium and thorium with their daughter products, which are present in most IC materials. Two other sources are high-energy neutrons from cosmic radiation and thermal neutrons from cosmic radiation and terrestrial sources.

3 Nomenclature

SER	Soft error rate in the field (for operational conditions of components in systems)
ASER	Proportion of the SER from alpha particles (tested in accelerated tests with alpha sources)
NSER	Proportion of the SER from cosmic radiation (tested in accelerated tests with high-energy neutrons)
PSER	Proportion of the SER from cosmic radiation (tested in accelerated tests with high-energy protons)
TSER	Proportion of the SER from thermal neutrons (from cosmic radiation and terrestrial sources, tested in accelerated tests with thermal neutrons)
SSER	Result of non-accelerated tests with components where all possible sources of soft errors are active (usually called “system soft error rate”)

4 Soft Error Tests

4.1 Accelerated Tests

Accelerated tests are performed in accordance with JESD 89.

A greatly increased flux of ionizing radiation enables rates and signatures of soft errors to be evaluated and the effects of test conditions and radiation parameters assessed in reasonable time.

4.1.1 ASER Tests

We test the ASER using a Radium-226 alpha source. The flux of alpha particles at the surface of this source is $1.2 \times 10^{12} \text{ m}^{-2} \text{ h}^{-1}$. Compared to the alpha flux of our standard mold compound of $52 \text{ m}^{-2} \text{ h}^{-1}$, the Radium source creates an acceleration of about 2.2×10^{10} for measurements.

In accelerated tests, devices are irradiated during dynamic operation. For tests with alpha particles, it must be ensured that the particles are not shielded from the active regions of the DUT (device under test). This is necessary because of the relatively short range of alpha particles in matter (see 8.4). During measurements the alpha source is therefore placed directly on top of an open device. If devices use special packaging technologies such as "lead on chip", the dies have to be mounted in lidless ceramic packages for tests.

We use ASER tests to evaluate the relative susceptibility of components to ionizing radiation after major changes in process or design.

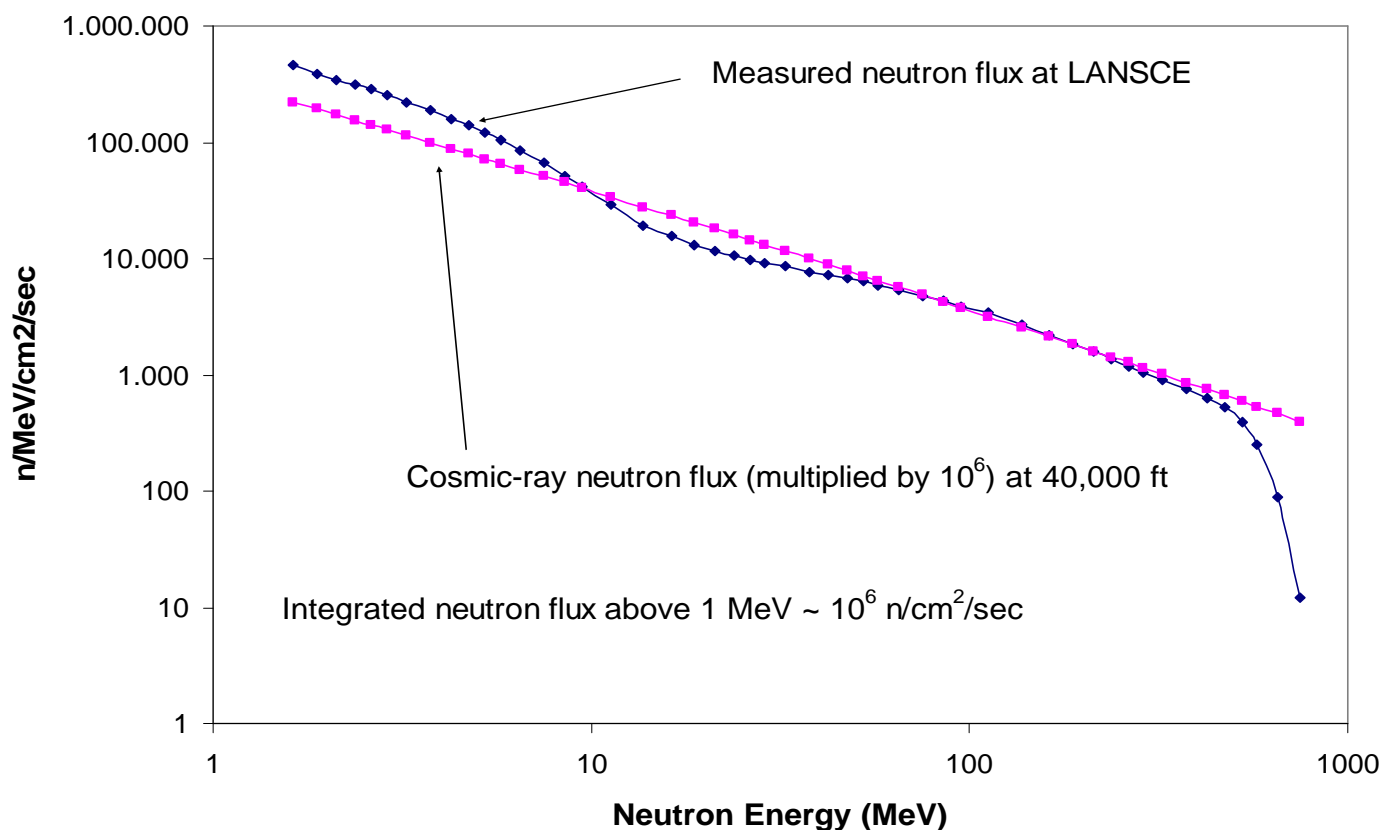
4.1.2 NSER + TSER Tests

We perform combined NSER +TSER tests with the LANSCE neutron beam at the Los Alamos National Laboratory (LANL). The energy spectrum of the neutrons of the LANSCE neutron beam is comparable to that of neutrons from cosmic radiation at sea level (see next page) which leads to simple and reliable evaluations of the measurements.

Tests are performed at the minimum specified Vcc voltage level at room temperature. Various data patterns and cycle times are used, but standard conditions are logical checkerboard plus inverted logical checkerboard and the minimum possible core cycle time.

A WORM ("Write Once, Read Many") test pattern is used to ensure that no "escapes" can occur during testing and all soft errors are detected.

We perform NSER tests once for every new generation of DRAMs to calculate the SER of our components from cosmic radiation.



4.2 System Test

In system tests, all sources of soft errors are active (alpha particles from IC materials, high-energy neutrons and thermal neutrons). The devices under test are operated under well-defined conditions. Several thousand devices have to be operated in parallel for several weeks (e.g. 5 million device hours). The result simulates the soft errors which occur during dynamic operation of devices in the field.

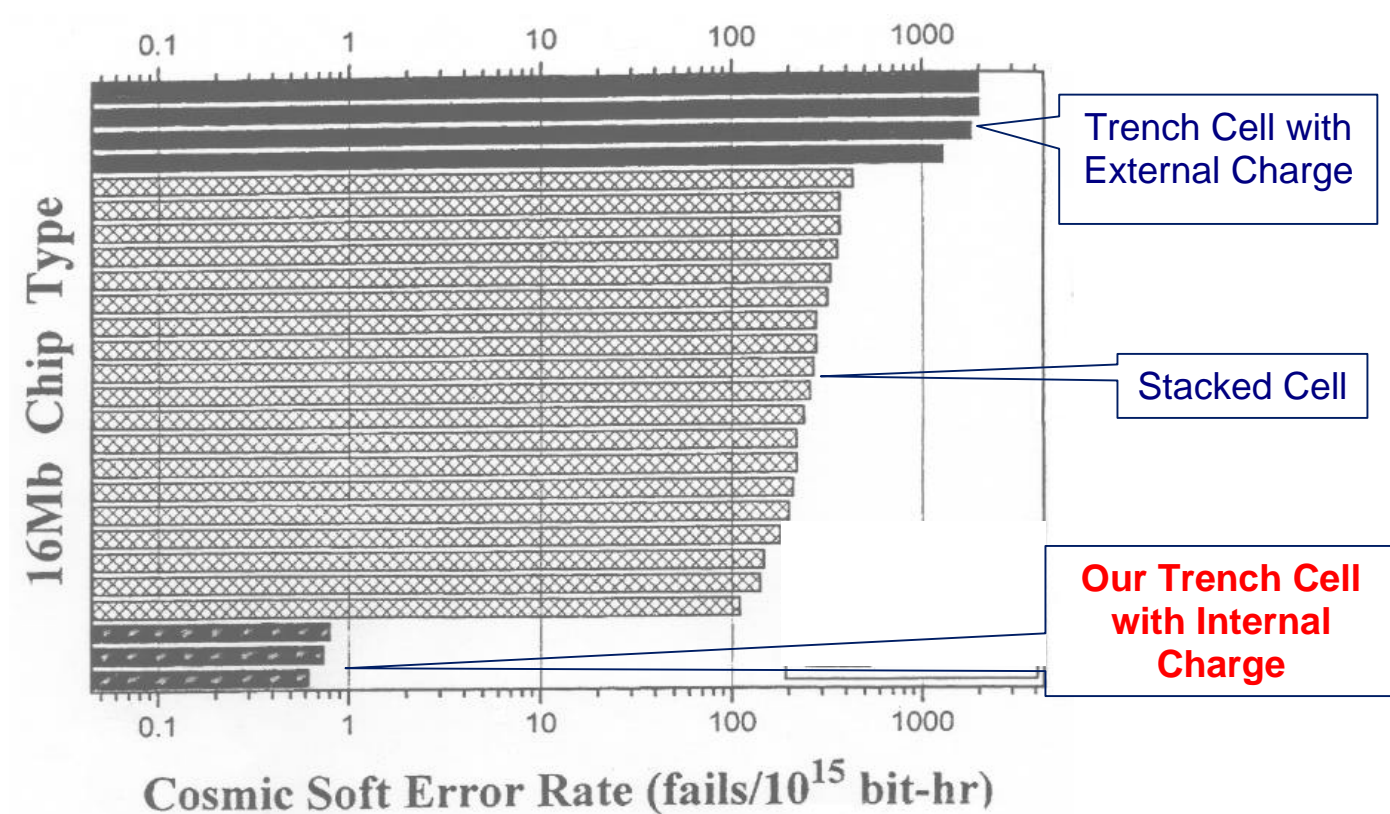
Special test patterns and test routines have to be used to ensure that all soft errors are detected and that system errors can be separated from soft errors due to ionizing radiation.

Usually logical checkerboard and inverted logical checkerboard are used for tests. For Vcc, the minimum specified voltage level is applied. Ambient temperature in the test chamber is 70°C. The cycle time (activate + write/read + precharge) is 300 ns. The test pattern is WORM.

SSER tests are both expensive and time-consuming but produce a detection limit which is about 5 to 6 orders of magnitude worse than that of accelerated tests. The value might be adequate for SRAMs but is far too poor for DRAMs. Consequently we no longer use SSER tests as a standard for DRAM qualification.

5 Concept for Low Soft Error Rate

Infineon uses special techniques to reduce the susceptibility of its SDRAMs to ionizing radiation. One reason for the low SER of our devices is the concept of the storage cell. We use “trench cells with internal charge”, which are extremely resistant to ionizing radiation.



/2/

A second method of reducing the SER is employed in the layers of the silicon substrate. A positively charged “buried n-well” is located below the negatively charged “deep p-well”. Ionizing radiation generates electron-hole pairs. Electrons from this charge are collected by the buried n-well so that they do not affect the charge in active areas near the surface of the semiconductor.

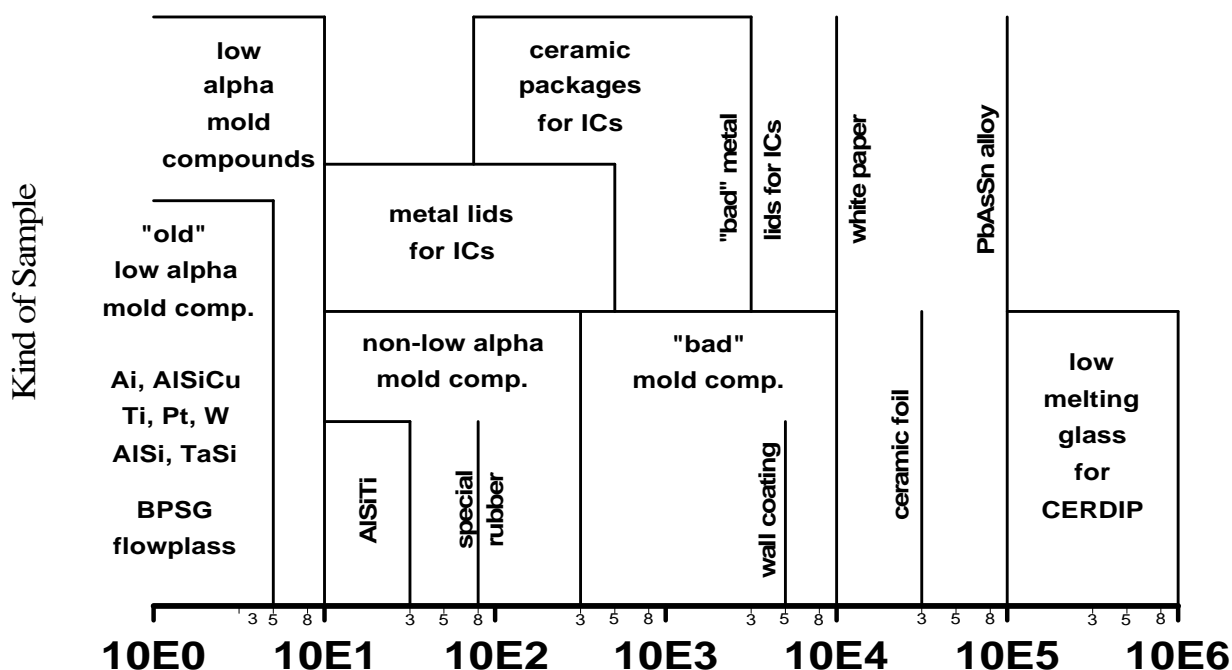
6 Soft Error Model

6.1 Relative Comparison of the Susceptibility of Components to Ionizing Radiation

Following any major changes in design or process, we use ASER tests to compare our components with their predecessors.

6.2 Low Level Alpha Counting

We measure the alpha flux of our IC materials to estimate the SER of our components from alpha particles. New materials are selected for agreeable alpha radiation.



Alpha Flux at the Surface of Samples in Counts per m²·h

Own results from Low Level Alpha Counting

6.3 Evaluation of the SER

We perform accelerated ASER and NSER tests and calculate the SER of our components from these results.

7 Results

7.1 SSER Test with 256M S17 SDRAMs

7012 components from 5 lots were tested in two SSER tests amounting to a total of 14.14 million device hours. No soft error was detected during these two runs. This corresponds to a

SER < 65 FIT (60% C.L.).

Test conditions were also 300 ns for complete write/read operations (activate, write/read, precharge), ambient temperature of 70°C, Vcc = 3.0 V, physical checkerboard and inverted checkerboard data pattern, and WORM test pattern. The tests were performed in Malacca/Malaysia (longitude = 103° east, latitude = 2° north, elevation = 0 = sea level).

In spite of the extremely high expense for this test it could only ensure a SER below 65 FIT (60% C.L.) and 163 FIT (90% C.L.). However, we knew from accelerated tests that the real SER of the 256M S17 is below 17 FIT. This comparison confirms the decision stated in section 4.2 to perform no further SSER tests for DRAMs.

7.2 SER Calculated from ASER Tests

For a rough calculation of the SER we divide the ASER value by the ratio of the alpha fluxes during accelerated testing and in the natural environment of the die, thus estimating the acceleration factor.

Alpha flux of the Ra-source = $1.2 \times 10^{12} \text{ m}^{-2} \text{ h}^{-1}$. Alpha flux of the mold compound (CEL 9200SI) = $52 \text{ m}^{-2} \text{ h}^{-1}$. Acceleration factor = $1.2 \times 10^{12} / 52 = 22 \times 10^9$. SER 256M S17) = ASER / Acc.Fct. = $4.0 \times 10^9 / 22 \times 10^9 = 0.2 \text{ FIT}$:

For 150 ns core cycle time (complete read/write operation), Vcc = 3.0 V, logical checkerboard data pattern, room temperature, 60% C.L.

256M SDRAM Design Step	S17	S14	D11
Calculated SER	< 0.2 FIT	< 0.02 FIT	< 0.73 FIT

7.3 SER Calculated from NSER Tests

The neutron flux from cosmic radiation equals $14 \text{ cm}^{-2} \text{ h}^{-1}$ in New York City ($E = 10 \text{ MeV}$; JESD89; nominal conditions). For estimating the acceleration factor of measurements in the LANSCE neutron beam we have to divide the total neutron fluence (given by LANSCE; $E = 10 \text{ MeV}$) by 14 (fluence in 1 hour N.Y.C.).

For nominal conditions (New York City, sea level, PC 133 timing with 60 ns core cycle time, $V_{cc} = 3.0 \text{ V}$, logical checkerboard data pattern, room temperature, 60% C.L.

512M SDRAM Design Step	D14	D11
Calculated SER	< 0.70 FIT	< 0.62 FIT

7.4 Complete Soft Error Situation

For comparison purposes, all SER values were standardized to the value of the cosmic radiation at **New York City**, a core cycle time of **60 ns**, 60% C.L., $V_{cc} \text{ min.}$, R.T., WORM test pattern, and logical checkerboard data pattern.

Components	256M	256M	512M	512M
Design Step	S17	S14	D14	D11
	= SDR	= SDR	= DDRI	= DDRI
SER from Alpha Particles	0.36	0.04	0.36	1.12
SER from Neutrons	20	13	0.70	0.62
Total SER	21	13	1.1	1.7

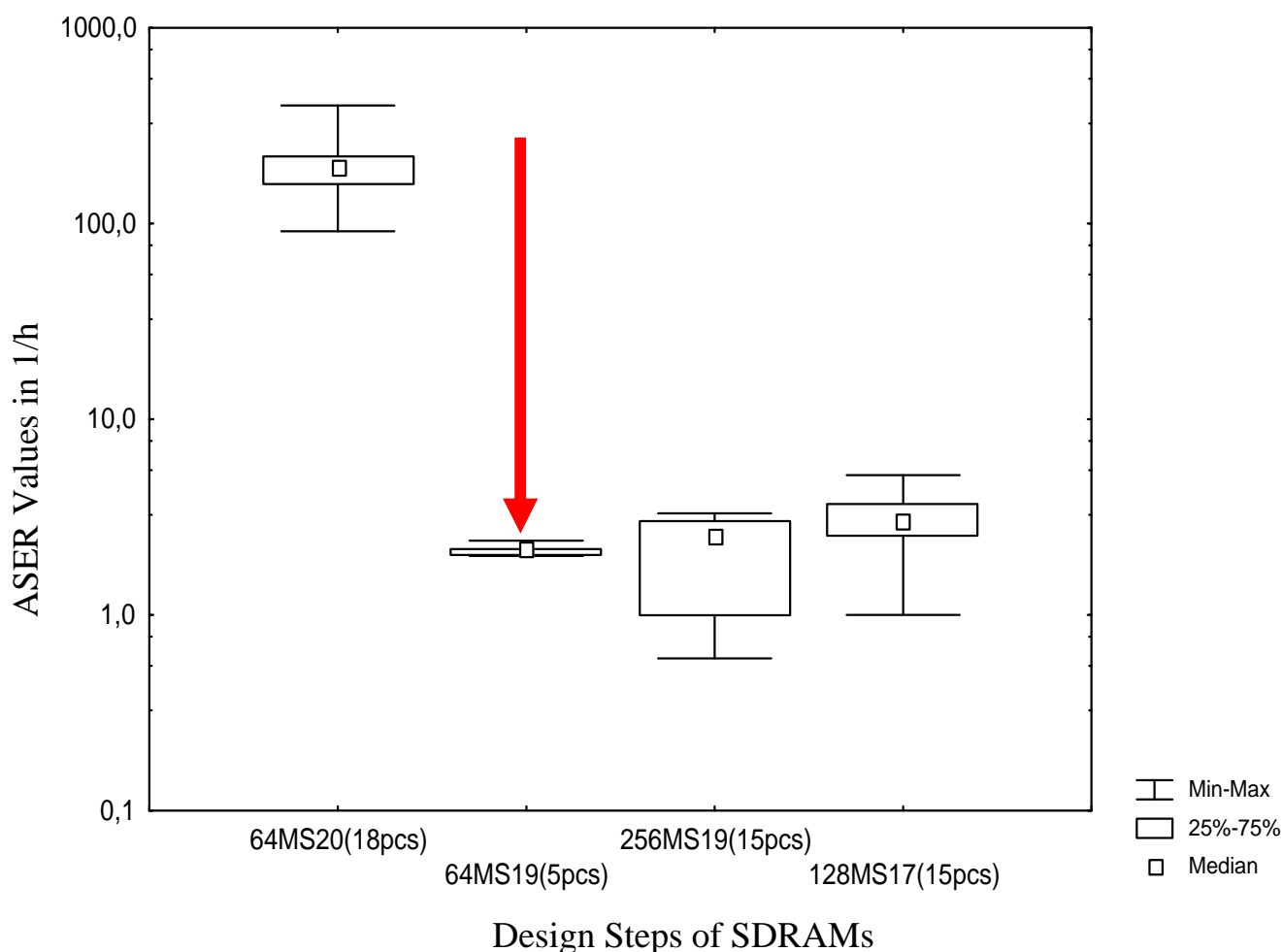
8 Effects on the SER

8.1 Comparison of Design Steps Via ASER Tests

The comparison showed that all subsequent design steps (64M S19, 128M S17, 256M S19) are significantly less susceptible to ionizing radiation than the 64M S20.

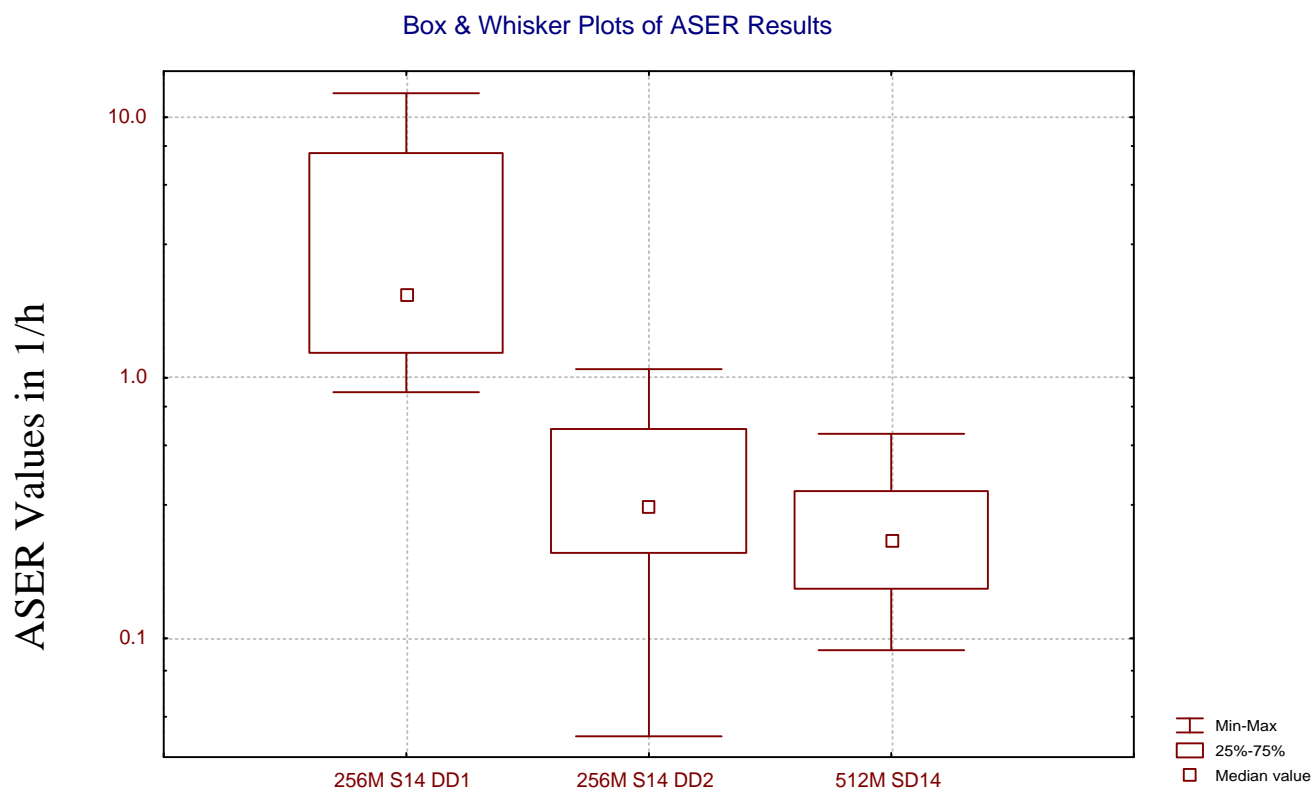
This is mainly due to the optimized geometry of the sense amplifiers.

“Box and whisker” plot of ASER results for different design steps of SDRAMs.



Test conditions:	Core cycle time	150 ns
	Data pattern	Phys. checkerboard + inverted ph. Ch.
	Vcc	3.0 V
	Ambient temperature	20°C
	Test pattern	WORM (Write Once, Read Many)

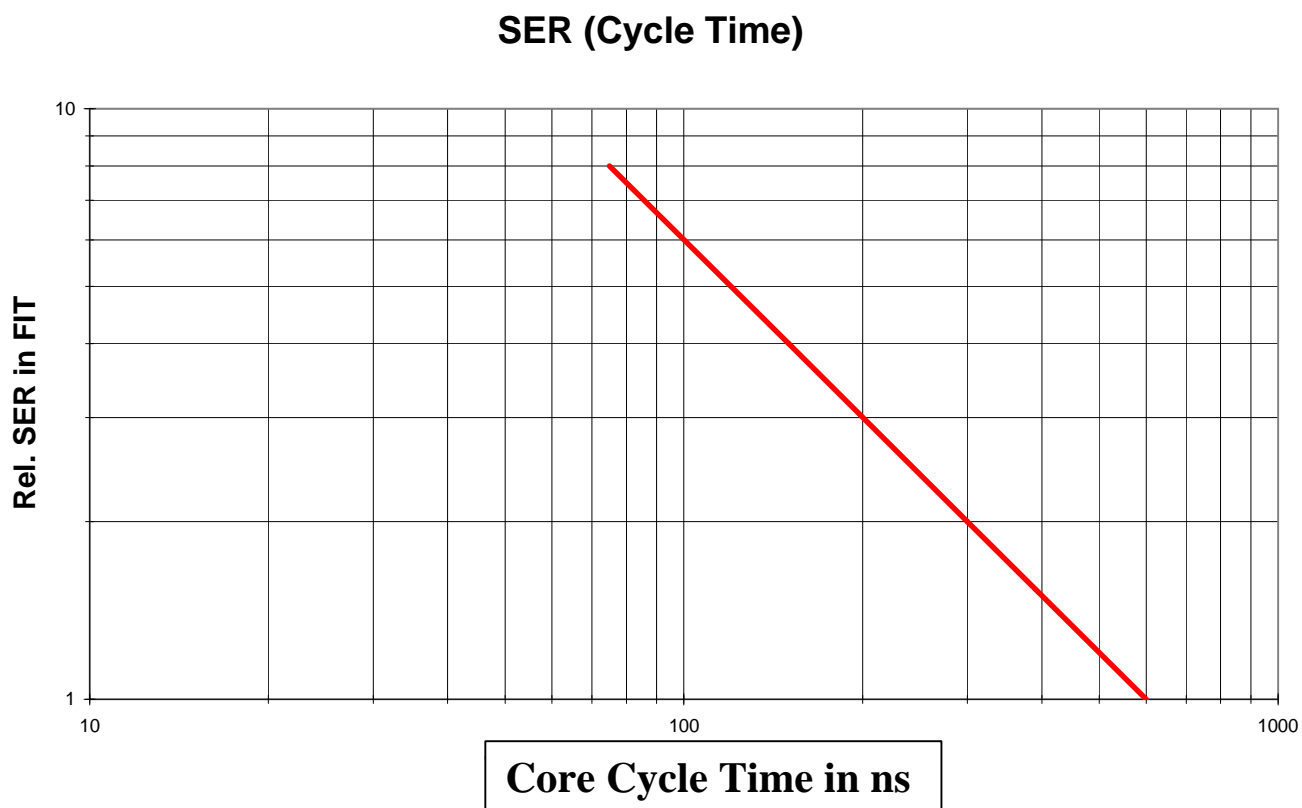
Comparison of ASER values of 3 design steps of components show the enhancement of the S14 DD2 and the SD14 (double data rate) compared to the previous step S14 DD1 (attributable to design improvements).



Design Steps of SDRAMs

Test conditions as before but logical checkerboard instead of physical checkerboard for data pattern.

8.2 Effect of Cycle Time on ASER and NSER Results



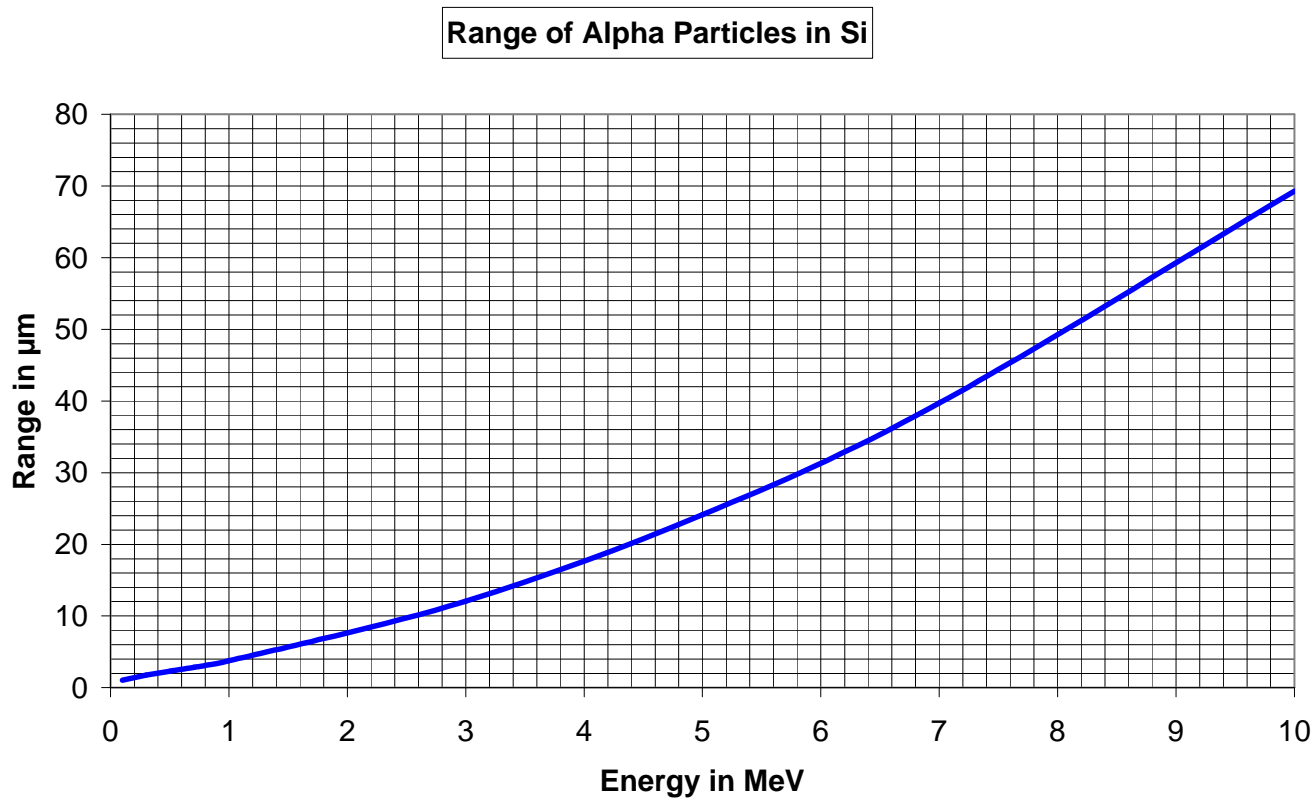
The strong dependence of ASER and NSER values on cycle times indicates that bit line / sense amplifier hits are chiefly responsible for soft errors. Cell hits and hits in peripheral circuits are of minor influence.

8.3 Effect of the Alpha Source

Tests showed that our Ra-226 source produces ASER values which are slightly more than 300 times higher than natural Th-232. This helps us keep the duration of ASER tests in the order of hours rather than weeks.

8.4 Range of Alpha Particles in Si

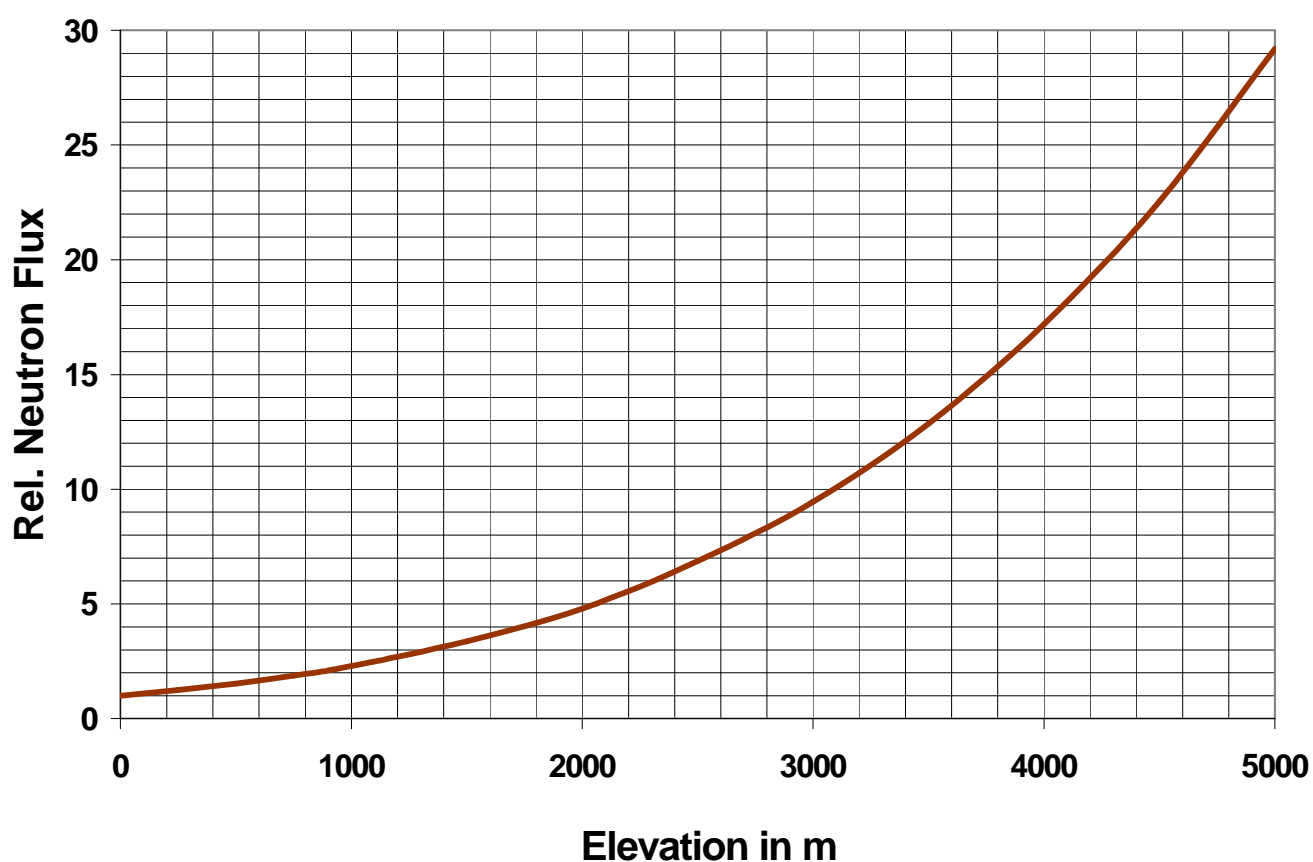
(Source: /4/)



8.4 Effect of Elevation on Neutron Flux from Cosmic Radiation

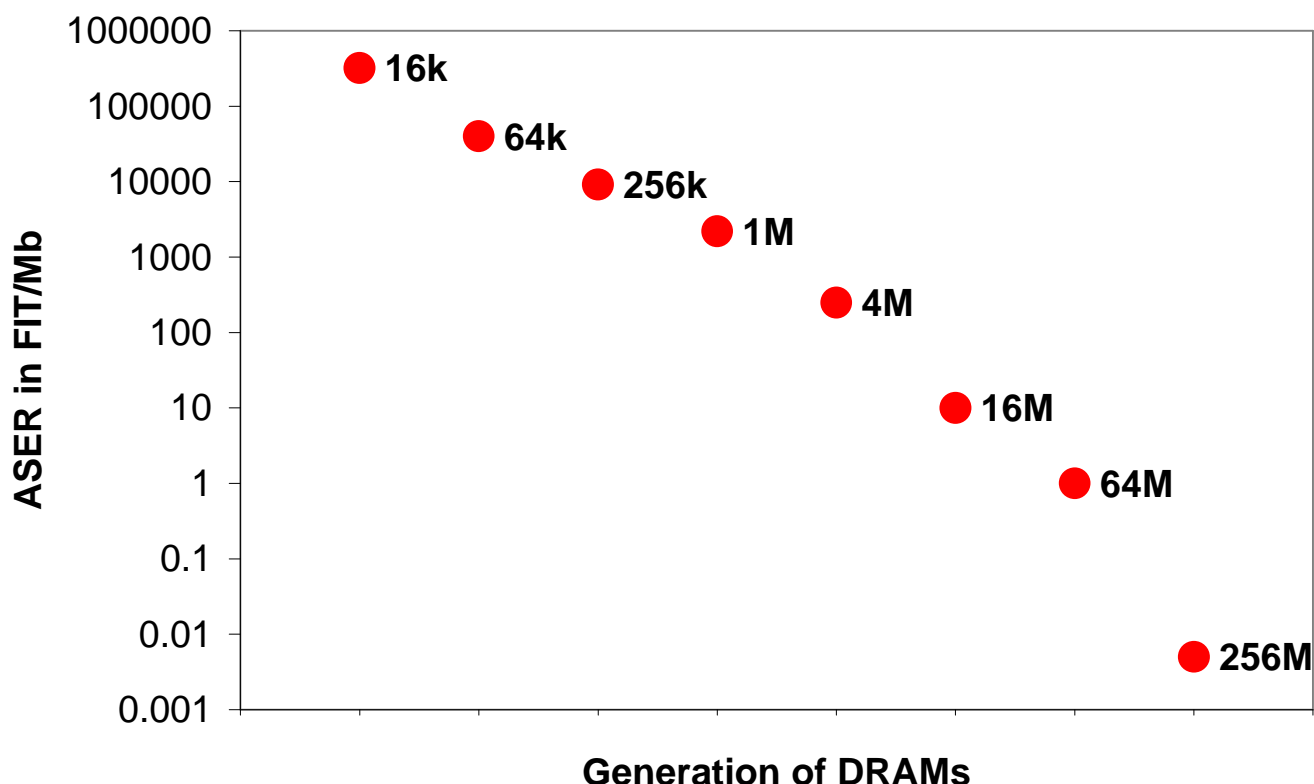
The neutron flux from cosmic radiation increases with elevation. The proportion of the SER from cosmic radiation is proportional to this neutron flux.

Shown here is the relative neutron flux from sea level to an elevation of 5000 m above sea level, calculated using the "IBM method" /1/.



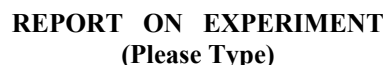
9 History of ASER Values of DRAMs

The ASER per Mb dropped about 8 orders of magnitude in 7 steps from 16M to 256M DRAM. The main reason for this improvement is the ever-decreasing area of the storage cells with a nearly constant storage capacity of about 30 fF. The remaining improvement was due to improved designs and processes.



10 References

- /1/ JEDEC Standard JESD 89, August 2001
- /2/ James F. Ziegler et al, IBM, "Cosmic Ray Soft Error Rates of 16Mb DRAM Memory Chips", IEEE Journal of Solid State Circuits, Vol.33, No.2, Feb. 1998
- /3/ Graph from Bruce Takala, LANSCE (measurements by Eugene Normand)
- /4/ TVDG LET Calculator)



Experiment was carried out at:		Local Contact	Proposal #	<i>LANSCE Use Only</i>
<input type="checkbox"/>	Manuel Lujan Jr. Neutron Scattering Center	Olivier Lauzeral	# 2003558	<div style="border: 1px solid black; padding: 5px; text-align: center;">6/8/04</div>
<input type="checkbox"/>	Weapons Neutron Research Facility	FP/Instrument Used		
<input checked="" type="checkbox"/>	WNR/Blue Room	WNR 30L		

Cosmic Ray Soft Error Rate Testing

Olivier Lauzeral, iRoC Technologies, Director of Operations

During this experiment several types of state of the art electronic devices were tested on behalf of different companies:

Actel : ProASIC Plus, Axcelerator
Xilinx : Virtex-II, Spartan-3
Altera : Cyclone
Starc : Latches .13 μ m, Latches 90nm
Alliance : SRAM 3 generations 4Mb, 9Mb, 18Mb
IDT : SRAM 2 generations, 4Mb 0.25 μ m, 4Mb 0.20 μ m
Toshiba : 1 test chip with SRAM, Register, Flip-flops
Mindspeed : logic gate probes
Samsung : SRAM for beam uniformity study

This campaign allowed us to test many devices in parallel, thanks to our multiple tester solution. We also used for the first time a device that measures the uniformity of the beam at each device level. Plots of the results are presented hereafter.

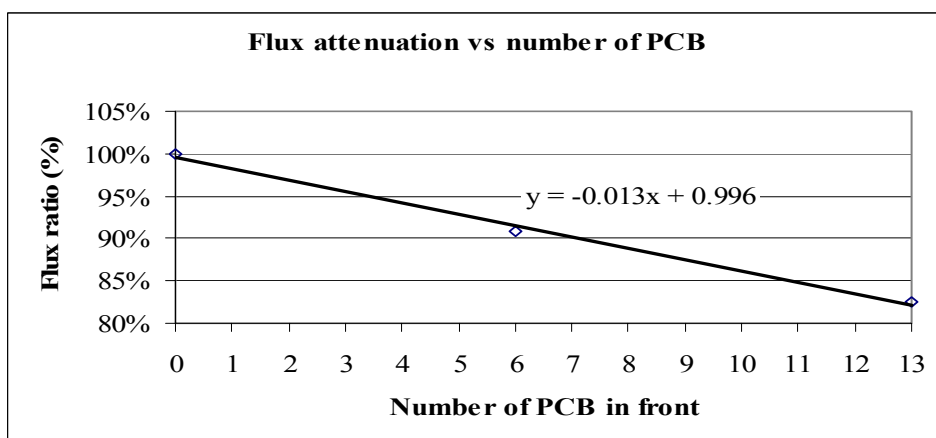
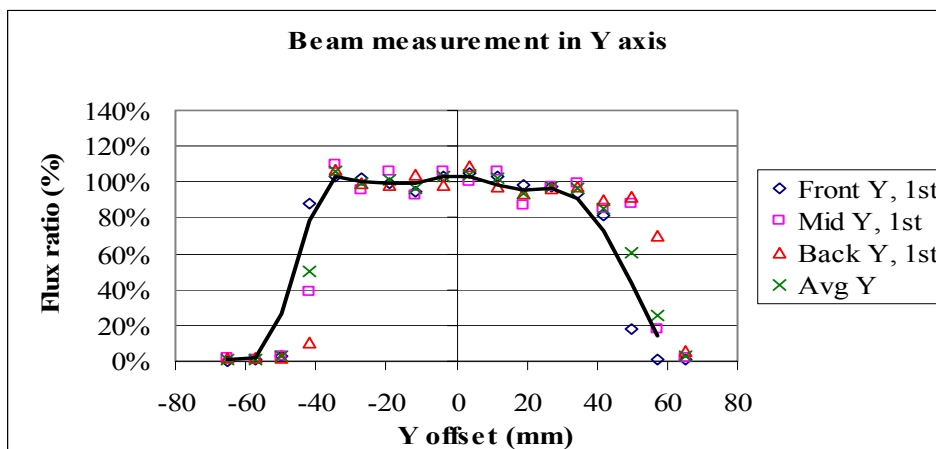
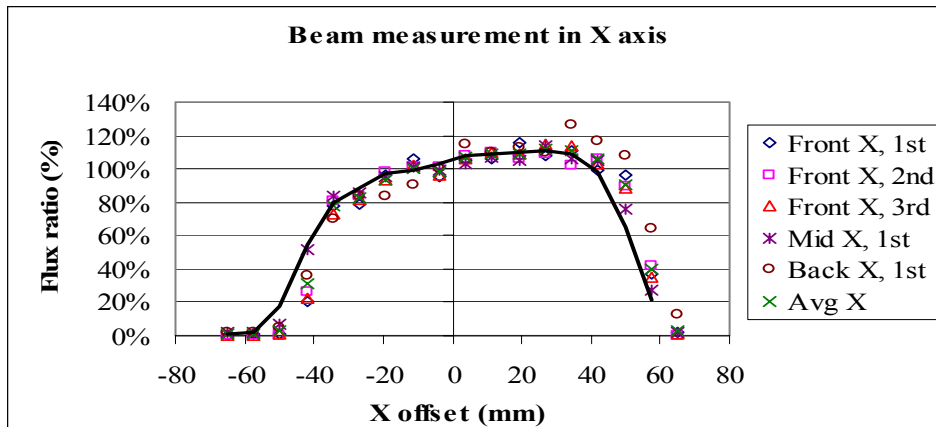
Throughout the different test campaigns run at Los Alamos, iRoC was able to define trends in the new technologies and to bring a better awareness of the Soft Error threat to the whole industry. Usually tests are performed with different combinations of parameters like voltage, temperature, test pattern for memories and orientation towards the beam. The count of test conditions for one single chip can sometimes be more than 50. According to the sensitivity of the device one condition can last from 10 minutes to few hours.

The results of the tests run during this campaign are proprietary of Starc, Toshiba and Mindspeed respectively, and cannot be displayed. Actel report on FPGA sensitivity is available online at: <http://www.actel.com/documents/RadResultsIROCreport.pdf>

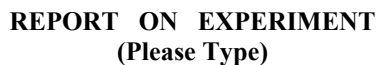
The report on our internal beam uniformity study has been sent to WNR. Few results are shown hereafter.

Experiment Report (continued)

The following figures show the measurement from our specific device of the beam flux wrt the center line given by the laser pointer. X axis (local horizontal) and Y axis (local vertical) are given here, as well as the attenuation effect of a stack of PCB in front of the beam. Front position is 1.94m away from the fission chamber, Mid position is 2.91 m away and Back position is 3.87 m away.



IMPORTANT! List or attach a list of publications resulting from this experiment (published or in press).



Experiment was carried out at:		Local Contact	Proposal #	<i>LANSCE Use Only</i>
<input type="checkbox"/>	Manuel Lujan Jr. Neutron Scattering Center	Matt Devlin	2003561	Report Rc'd 6/7/04
<input checked="" type="checkbox"/>	Weapons Neutron Research Facility	FP/Instrument Used		
<input type="checkbox"/>	WNR/Blue Room	4FP60R GEANIE		

Authors and Affiliations
 Matt Devlin, LANSCE-3
 Ron Nelson, LANSCE-3
 Nikolaos Fotiadis, LANSCE-3
 Paul Garrett, LLNL
 Walid Younes, LLNL
 John Becker, LLNL

A freshly precipitated sample of ^{233}U was obtained from John Fitzpatrick of C-AAC, LANL, in the form of an oxide powder with approximately 380mg of ^{233}U . The activity of this sample was monitored from about 5 months, during which time the ^{232}U decay-chain activity grew by about a factor five. The sample was also put in the beam, with the resulting gamma-rays detected by the GEANIE array, for approximately three weeks. Some additional beam time was spent for a background run, with the sample placed just out of the beam in such a way that the glass vial was still in the beam; hence the background is intended to be the beam-induced reactions on the glass, plus the decay activity of the sample.

Data analysis is beginning now, though the “quick” data analysis done during the run showed the presence of a few candidate (n,n') lines as well as some prominent lines which can be assigned to F(n,n') from neutrons scattered by the target to F near the GEANIE detectors (this is a common background with thick samples). We hope to complete the analysis of this experiment this summer, and then to decide if more data is needed.



REPORT ON EXPERIMENT

(Please Type)

Submit all experiment reports to:
 LANSCE User Office, MS H831, Los Alamos National Laboratory, Los Alamos, NM 87545

Experiment was carried out at:		Local Contact	Proposal #	<i>LANSCE Use Only</i>
<input type="checkbox"/>	Manuel Lujan Jr. Neutron Scattering Center	B. Haight	2003564	Report Rc'd
<input checked="" type="checkbox"/>	Weapons Neutron Research Facility	FP/Instrument Used		7/15/04
<input type="checkbox"/>	WNR/Blue Room	4FP15L		

Title	Development of a High Energy Neutron Spectrometer
--------------	---

Authors and Affiliations

T.D. McLean, R.H. Olsher and L. Romero, HSR-4, Los Alamos National Laboratory.
Peter Grudberg and Anthony Fallu-LaBruyere, X-ray Instrumentation Associates, Newark, CA
Ted Clifford and Guy Jonkmans, Bubble Technology Industries, Canada

Experiment Report

This experiment was in support of a proposal to design a portable hand-held neutron spectrometer for radiological surveys at LANSCE and other high energy neutron facilities. Such an instrument would be a major advance over existing technologies.

The concept is to use the pulse shape discrimination properties of certain inorganic scintillators to segregate in real time gamma and neutron-induced light ion spallation products. The count rate and energy distribution of the charged particles would be used to calculate an estimated dose rate and allow “hot spots” to be readily located. Subsequent offline deconvolution of the data would reveal the neutron spectrum and enable a better estimate of dose. It may also prove feasible to make use of the gamma spectrum during radiation surveys. A more detailed discussion and a presentation of preliminary data obtained during an initial proof-of-principle experiment (2002570) can be found in reference 1.

The goals of the current experiment were to build upon the earlier work and to assess the performance of a BaF₂-based spectrometer system. This system was designed and constructed by Bubble Technology Industries (BTI). It consisted of a probe unit comprising the scintillator, PMT, preamplifier and associated power supplies as well as a spectrometer unit operated remotely in the 90m trailer. This analog-based spectrometer processed individual waveforms and calculated a particle identification index. This value was recorded along with time-of-flight data on an event-by-event basis to a hard drive for later analysis.

A CsI-based digital spectrometer designed by XIA and used in the proof-of-principle experiment was upgraded for this experiment to allow time-of-flight data recording and an on-line determination of particle identification. Unlike the BTI system, the individual waveforms were also stored so that a comparison of off-line and on-line particle ID was possible. Several different sized scintillators from a number of manufacturers were evaluated.

A fission chamber was also used to get a reliable estimate of neutron fluence.

The data analysis is not yet complete and has been hampered by equipment problems encountered during the experiment. Unfortunately, many of these problems were not apparent until after the experiment was complete. As a result, it will be necessary to repeat these measurements once the problems have been resolved. However, the experiment did serve to reaffirm the feasibility of the design concept and it was possible to reach some conclusions;

Experiment Report *(continued)*

- 1) CsI is the better choice of scintillator in the proposed instrument as
 - the pulse shape discrimination properties are superior to BaF₂.
 - the relatively slow decay time of CsI is not an impediment at fluence rates well above those expected in routine surveys. Therefore the nanosecond timing available with BaF₂ is not an advantage in this case.
- 2) The on-line pulse shape discrimination performance was not as good as the off-line analysis. The on-line algorithm is to be reworked and re-evaluated.
- 3) Not all CsI scintillators are created equal – system performance was degraded when low cost scintillators were used.
- 4) A 2"x2" scintillator will probably have to be used in a survey instrument in order to get the required sensitivity in neutron leakage fields likely to be encountered in the field.

References

1. T.D. McLean, R.H. Olsher and R.T. Devine, "Development of a portable high energy neutron spectrometer", accepted for publication in Radiation Protection Dosimetry.

Submit all experiment reports to:
LANSCE User Office, MS H831, Los Alamos National Laboratory, Los Alamos, NM 87545

Experiment was carried out at:	Local Contact	Proposal #	LANSCE Use Only
<input checked="" type="checkbox"/> Manuel Lujan Jr. Neutron Scattering Center	John Ullmann	2003573	Report Rc'd
<input type="checkbox"/> Weapons Neutron Research Facility	FP/Instrument Used		7/15/04
<input type="checkbox"/> WNR/Blue Room	FP14/DANCE		

Title
DANCE Development

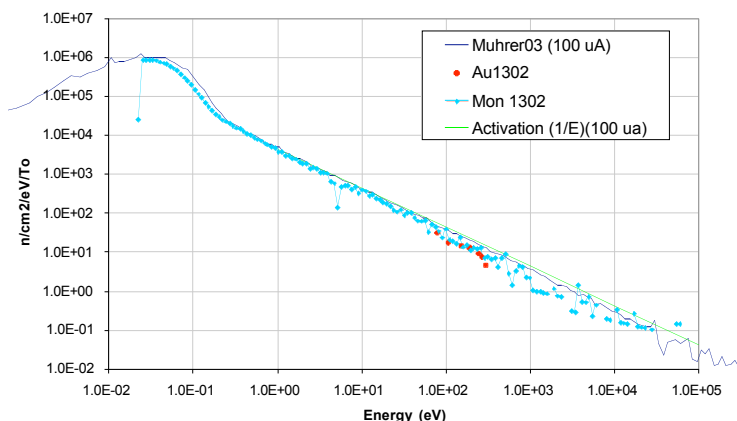
Authors and Affiliations

J.L. Ullmann, R. Reifarth, R.C. Haight, E.-I. Esch, J.M. O'Donnell, LANSCE-3, Los Alamos
R.S. Rundberg, T.A. Bredeweg, D.J. Vieira, A. Kronenberg, J.B. Wilhelmy, C-INC, Los Alamos
J.M. Wouters, IM-8, Los Alamos
U. Greife, A. Alpizar-Vicente, R. Hatarik, Colorado School of Mines, Golden, CO.

Experiment Report

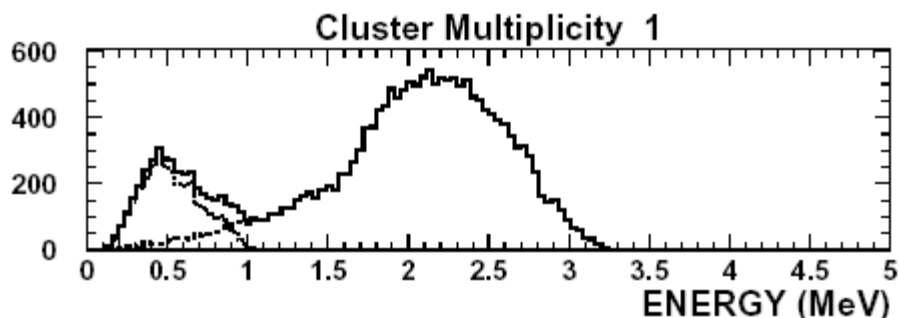
The Detector for Advanced Neutron Capture Experiments (DANCE) on FP14 is a 4 π calorimetric BaF₂ array designed for neutron capture measurements on small quantities of radioactive elements. During 2003/2003, a partial array (140 out of 160 crystals) was tested. The array was completed for the 2003/2004 run period, and the full array of 159 or 160 crystals (depending on configuration) was used. The proposals for DANCE development addressed understanding and testing several elements of data acquisition and detector operation.

The neutron flux at the target position in DANCE was measured using several methods, and compared to "as built" calculations of the flux made by Muhrer. Shown in the adjacent figure are measurements made by activating a thin (1 mg/cm²) foil with and without a Cd filter, using the ⁶Li(n,t) reaction (normalized to the Au activation), and by estimating the flux from Au resonance cross sections. The measurements and calculations are in reasonable agreement. The simulation has can be fit to a power law form AE^x with x = -1.01, while the measured value (using ⁶Li(n,t) is x=-1.08. Compared to earlier studies, the as-built simulation is about a factor of two lower than the previous simulation, and the flux measurements are about a factor of three higher, with a shape more similar to a thermal Maxwellian plus power law than observed in the earlier measurements. Since the reported measurements are based on several different techniques, we believe the actual shape of the spectrum may have changed when a new target-moderator system was installed.

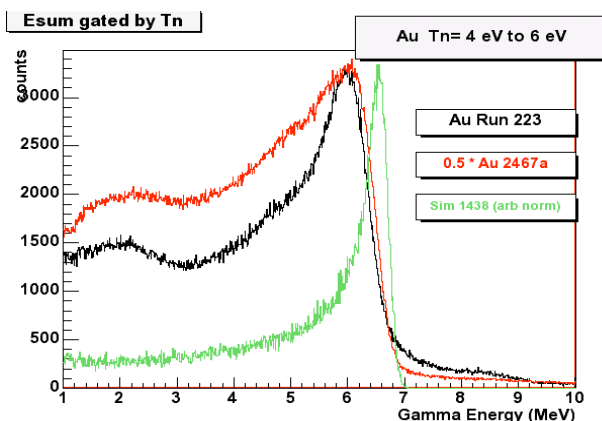


Experiment Report (continued)

Backgrounds are an important consideration in neutron capture experiments, and a very large background with gamma energy near 2.2 MeV was identified in the 2002/2003 test experiments. This background was tentatively identified as due to the $n+p \rightarrow d+\gamma$ reaction in the DANCE shielding. However, it was also observed with beam off, and simulations attribute it to the beta decay of ^{214}Bi ($Q_\beta=3.27$ MeV) and ^{214}Pb ($Q_\beta=1.03$ MeV), two isotopes in the ^{226}Ra decay chain that occurs naturally in the BaF_2 crystals. The figure below shows the detailed simulation for 10^5 decays of each isotope (See Publication 1). The peak at 2.2 MeV is due to the beta decay of ^{214}Bi . The typical alpha decay rate from the ^{226}Ra chain is about 200/sec in each crystal.



Another issue studied during development was the summed-energy resolution of the DANCE array. DANCE is a calorimetric gamma-ray detector, and an important parameter in identifying capture reactions is the sum of the gamma-ray energy over all of the gammas in the capture cascade. In the 2002/2003 run, the summed-energy resolution for Au was somewhat poorer than predicted by simulations. Simulations indicated that this could be due to a high single-gamma energy threshold coupled with energy "loss" due to using only 140 out of 160 crystals. The adjacent figure shows the summed-energy spectrum gated on the Au 4.92 eV resonance obtained with the full array and lower single-gamma thresholds. While the resolution has improved somewhat, it still does not meet expectations from the simulations. There are hints that similar discrepancies are seen in other 4pi arrays, and the problem is still being investigated.



Considerable experience with operating the DANCE array was gained during the 2003/2004 run cycle, and while there are still some problems that are not fully understood, it is well on its way to producing reliable and accurate data.

IMPORTANT! List or attach a list of publications resulting from this experiment (published or in press).

1. "Background identification and suppression for the measurement of (n,γ) reactions with the DANCE array at LANSCE. R. Reifarth, et al., submitted to Nucl. Instr. Meth.

Submit all experiment reports to:
LANSCÉ User Office, MS H831, Los Alamos National Laboratory, Los Alamos, NM 87545

Experiment was carried out at:	Local Contact	Proposal #	LANSCÉ Use Only
<input type="checkbox"/> Manuel Lujan Jr. Neutron Scattering Center	Ron Nelson	2003-574	Report Re'd
<input checked="" type="checkbox"/> Weapons Neutron Research Facility	FP/Instrument Used	FIGARO	
<input type="checkbox"/> WNR/Blue Room			

Title

**Fission gamma-ray measurements
with increased sensitivity**

Authors and Affiliations

R.O. Nelson, M. Devlin, R. C. Haight, J. M. O'Donnell, D. Rochman
LANSCÉ-3, LANL
T. Ethvignot, T. Granier
CEA, Bruyères-le-Châtel, France

Experiment Report

The goal of this proposal is to measure the gamma-ray energy spectrum and total prompt gamma-ray energy released in fission of $^{235,238}\text{U}$, ^{237}Np , and ^{239}Pu as a function of the incident neutron energy. This experiment was not performed during the 2003/2004 beam period because our CEA (Bruyères-le-Châtel) collaborators in France could not obtain the required permission to ship the necessary multi-foil fission chambers until the very end of the run cycle. We plan to pursue these important measurements now that we have the $^{235,238}\text{U}$ and ^{237}Np multi-foil fission chambers at LANL.



REPORT ON EXPERIMENT

(Please Type)

Submit all experiment reports to:
 LANSCE User Office, MS H831, Los Alamos National Laboratory, Los Alamos, NM 87545

Experiment was carried out at:		Local Contact	Proposal #	<i>LANSCE Use Only</i>
<input type="checkbox"/>	Manuel Lujan Jr. Neutron Scattering Center	Matt Devlin	2003580	Report Rc'd 6/7/04
<input checked="" type="checkbox"/>	Weapons Neutron Research Facility	FP/Instrument Used		
<input type="checkbox"/>	WNR/Blue Room	4FP60R GEANIE		

Title

Measurement of (n,xnypza) cross sections on fission products with GEANIE

Authors and Affiliations

Matt Devlin, LANSCE-3
Ron Nelson, LANSCE-3
Nikolaos Fotiadis, LANSCE-3
Paul Garrett, LLNL
Walid Younes, LLNL
John Becker, LLNL

Experiment Report

Isotopically enriched samples of both ^{130}Te (1.3g) and ^{100}Mo (1.25g) were obtained and put in-beam in the GEANIE array for approximately 10 days each. Preliminary analysis of the data suggests that both experiments were successful and an adequate amount of data was obtained to extract partial gamma-ray cross sections of numerous reaction channels. The data will be analyzed completely as soon as possible to extract the partial gamma-ray yields and hence the reaction cross sections for various reaction channels.

Submit all experiment reports to:
LANSCE User Office, MS H831, Los Alamos National Laboratory, Los Alamos, NM 87545

Experiment was carried out at:	Local Contact	Proposal #	<i>LANSCE Use Only</i>
<input type="checkbox"/> Manuel Lujan Jr. Neutron Scattering Center	Tony Hill	2003589	Report Rc'd
<input checked="" type="checkbox"/> Weapons Neutron Research Facility	FP/Instrument Used		
<input type="checkbox"/> WNR/Blue Room	FP90L		6/7/04

Title 237Np Fission Cross Section Measurement and Detector R&D in Support of the Advanced Fuel Cycle Initiative
Authors and Affiliations T.S. Hill, S.A. Wender; Los Alamos National Laboratory

Experiment Report 237Np fission cross section data was successfully taken on FP90L. These data will be normalized to 235U data that was taken in the same ionization detector simultaneously. This analysis is underway. First results should be available in the fall. In the course of running, the data acquisition system was successfully upgraded to minimize the dead-time and to remove dead-time correlations between samples in the same chamber.



REPORT ON EXPERIMENT
(Please Type)

Submit all experiment reports to:
LANSCCE User Office, MS H831, Los Alamos National Laboratory, Los Alamos, NM 87545

Experiment was carried out at:	Local Contact	Proposal #	LANSCCE Use Only
<input checked="" type="checkbox"/> Manuel Lujan Jr. Neutron Scattering Center	Tony Hill	2003592	Report Rc'd 6/7/04
<input type="checkbox"/> Weapons Neutron Research Facility	FP/Instrument Used		
<input type="checkbox"/> WNR/Blue Room	FP5		

Title

237Np Fission Cross Section Measurement and Detector R&D in Support of the Advanced Fuel Cycle Initiative

Authors and Affiliations

T.S. Hill, S.A. Wender; Los Alamos National Laboratory

Experiment Report

237Np fission cross section data was successfully taken on FP5. These data will be normalized to 235U data that was taken in the same ionization detector simultaneously. This analysis is underway. First results should be available in the fall. In the course of running, the data acquisition system was successfully upgraded to make time of flight measurements up to 30 milliseconds.

Submit all experiment reports to:
LANSCCE User Office, MS H831, Los Alamos National Laboratory, Los Alamos, NM 87545

Experiment was carried out at:	Local Contact	Proposal #	LANSCCE Use Only
<input type="checkbox"/> Manuel Lujan Jr. Neutron Scattering Center	Ron Nelson	2003-599	Report Re'd
<input checked="" type="checkbox"/> Weapons Neutron Research Facility	FP/Instrument Used	60RGEANIE	
<input type="checkbox"/> WNR/Blue Room			

Title <p align="center">Relative Measurements of Photon Production Cross Sections from Cr, Si, Fe, V, and Al for Standards</p>
Authors and Affiliations <p align="center">R.O. Nelson, N. Fotiades, M. Devlin LANSCCE-3, LANL P. E. Garrett, W. Younes, J.A. Becker N-Division, LLNL</p>

Experiment Report <p>This work was proposed in 2003 to be run as part of the GEANIE development time. The goal is to develop secondary cross section standards for neutron-induced photon production cross section measurements. By enabling accurate gamma-ray measurements relative to well-determined cross sections, the uncertainties involved in cross section measurements can be reduced in future experiments. There are many examples, such as $\text{Fe}(n,n'\gamma)$ $E_\gamma = 0.847$ MeV, where numerous measurements have been made, but the agreement between the various measurements is poor, or in the Fe case, extremely poor. See Fig. 1 that shows most of the measurements. The result of the large spread in cross section values is that different evaluations and data libraries also exhibit a large spread, and the resulting uncertainties afflict various measurements made relative to a particular "secondary standard".</p> <p>Cr appears to provide a fairly good secondary standard at $E_n = 14.5$ MeV. Five of six measurements of the cross section of the 1434-keV γ ray agree within errors as corrected and compiled by Simakov <i>et al.</i> The evaluated cross section has an accuracy of 3.8 %.</p>
--

Experiment Report *(continued)*

Some properties of useful neutron-induced gamma-ray cross section standards include:

- Large magnitude cross section - to minimize counting time and improve signal to background ratio.
- Cross section that is smooth and relatively constant vs neutron energy and detector angle.
- Samples with favorable physical and chemical properties and cost.

In selecting possible secondary standards, we have tried to balance the above considerations to choose samples that meet these criteria as much as possible.

For a number of years we have made both absolute cross section measurements using the well-determined $^{235}\text{U}(\text{n},\text{f})$ and $^{238}\text{U}(\text{n},\text{f})$ cross sections to determine our incident neutron fluence, and we have measured other gamma-ray cross sections relative to the $\text{Fe}(\text{n},\text{n}'\gamma)$ $E_\gamma = 847\text{-keV}$ cross section at 14.5 MeV. Because of inconsistencies in the Fe data base we relied upon our own measurements of this cross section to serve as our secondary standard. Due to the different requirements of experiments it is useful to have secondary cross section standards at several different γ -ray energies. The γ -rays we plan to use as secondary standards are given in the table below.

Active nuclide (Abundance)†	Primary γ -ray energy (keV) (approximate 14.5 MeV cross section in mb)*	Other useful energies (keV) (approximate 14.5 MeV cross section in mb)*
^{51}V (99.750%)	320 (310)	1609 (210)
^{56}Fe (91.754%)	847 (705)	1238 (400)
^{52}Cr (83.789%)	1434 (695)	935 (210)
^{28}Si (92.230 %)	1778 (400)	
^{27}Al (100%)	3000(110)	2211 (150)
^{12}C (98.89 %)	4439 (190)	
^{16}O (99.762%)	6129 (180)	

†Abundances from Nuclear Wallet Cards, J. Tuli, NNDC, Brookhaven National Laboratory, Jan. 2000.

*Approximate cross sections from S.P. Simakov, *et al.*, "Status of Experimental and Evaluated Discrete γ -Ray Production at $E_n = 14.5$ MeV", IAEA report INDC(CCP)-413, 1998.

Suitable samples include: High-purity metal foils of V, Fe, Cr, Si, and Al. Of these, Cr can be difficult to obtain with the desired thickness and good uniformity because the pure metal is rather brittle.

IMPORTANT! List or attach a list of publications resulting from this experiment (published or in press).

Experiment Report *(continued)*

Sintered samples of Cr can be used but must be well characterized. High purity Si wafers are readily available from the semiconductor industry. V, Fe, and Al can be rolled into sheets having good uniformity. Pyrolytic graphite is very pure and can be used if well characterized. SiO₂ is available with very high purity and uniform thickness and provides two standards in one material.

In 2003 from November 7-9, Fe + Cr were measured using thin foils of each to minimize corrections for neutron multiple scattering and reactions. Beam availability was about 65% for these three days. This was sufficient to obtain 1% statistics in a 1-MeV wide bin for both samples. These data were analyzed and reported at the International Conference on Nuclear Data for Science and Technology in Santa Fe, NM 2004. The results from the relative measurement agree with our absolute measurements for the Fe(n,n' γ) cross section within errors. In addition, we used available neutron total cross section data (accuracy of 1 – 2 %) on Fe and elastic scattering data to further validate our cross section value by demonstrating consistency of all the data. Figure 1 shows the cross section values from several data libraries and evaluations with our current results. Additional characterization of the samples and other minor corrections will allow us to reduce the uncertainties in these results.

Data were acquired on V + Cr for 6 days from November 22 – 28 with 79% beam availability. These data will be analyzed in soon. The lower cross sections for the V reactions, and the use of thin foils to reduce attenuation of the lower-energy γ ray in the samples required the increased beam time to obtain good statistical accuracy.

Future work will allow the extension of these measurements to SiO₂ and C samples that provide higher-energy γ ray standards. We expect to achieve 3 to 5% absolute accuracy in the final results.

Experiment Report (continued)

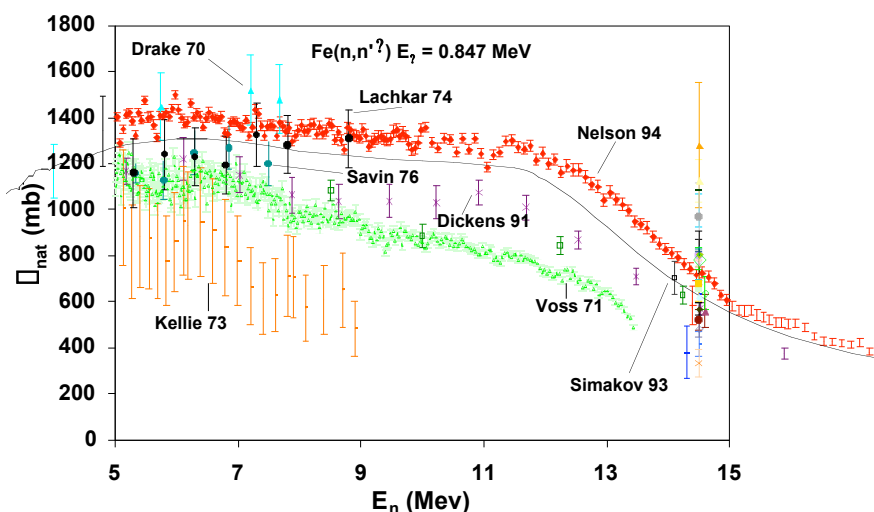


FIGURE 1. Absolute cross section measurements (most at 125 degrees) for the $^{nat}\text{Fe}(n,n') E_n = 0.847 \text{ MeV}$ γ ray. Authors are indicated for some of the 34 experimental results plotted. The black curve is the ENDF/B-VI evaluation for the ^{56}Fe inelastic channel cross section multiplied by the 91.8% abundance of ^{56}Fe to convert to the “natural” cross section for comparison.

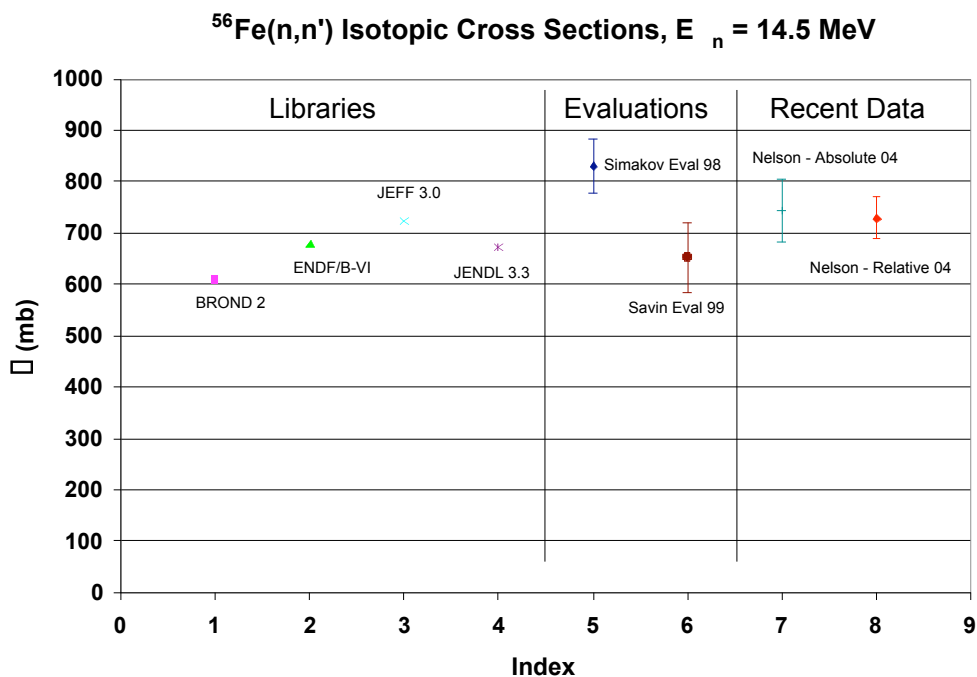


Figure 2. Isotopic $^{56}\text{Fe}(n,n')$ (evaluations and recent data) and inelastic channel cross sections (libraries) are plotted for $E_n = 14.5 \text{ MeV}$. Only the recent JEFF 3.0 library agrees well with the present results.

Search Instructions

Click the binocular icon in the Acrobat toolbar, this will bring up another window.

In the Find window, type the text you want to find in the Find text box, and click Find Again.

- Text can be a single word, number, a term, or phrase.**
- When you click Find Again the Finder will bring up the first page of the word or phrase you typed.**

To continue the search through the document for that word or phrase just click on Find Again and it will continue to look for the next time the phrase or word was used.

This report has been reproduced directly from the best available copy

It is available electronically on the Web
(<http://www.doe.gov/bridge>).

Copies are available for sale to U.S. Department of Energy employees and contractors from—
Office of Scientific and Technical Information
P.O. Box 62
Oak Ridge, TN 37831
(865) 576-8401

Copies are available for sale to the public from—
National Technical Information Service
U.S. Department of Commerce
5285 Port Royal Road
Springfield, VA 22616
(800) 553-6847



LANSCÉ

National User Facility

Los Alamos National Laboratory
is operated by the University of
California for the United States
Department of Energy under
contract W-7405-ENG-36.

